University of the Basque Country

PhD Thesis

ANALYSIS OF THERMOFLUIDS IN FLAMELESS (MILD) COMBUSTION

Assessment, improvement and development of combustion models by CFD

PhD candidate
Naiara Romero Anton

Supervisors
Dr. Koldobika Martín Escudero
Dr. Luis Alfonso del Portillo Valdés

October
2020

Abstract

Flameless combustion, also called MILD combustion (Moderate or Intense Low Oxygen Dilution), is a technology that reduces NO_x emissions and improves combustion efficiency. It is based on the aerodynamic recirculation of flue gas inside the furnace diluting air and/or fuel streams. Therefore, appropriate turbulence-chemistry interaction models are needed to address this combustion regime via computational modelling. In this Thesis the applicability of two different turbulence-chemistry interaction models, the Eddy Dissipation Concept (EDC) and the Flamelet Generation Manifold (FGM) models, are studied and then some extensions of both models are developed and implemented in ANSYS Fluent for better predict flameless combustion.

Overcoming the limitations of the standard EDC model, the New Extended Eddy Dissipation Concept model (NE-EDC) is developed. This model considers standard EDC's model coefficients space dependent as a function of the local Reynolds and Damköhler numbers, so that the existing dilution in flameless combustion is considered. Later, the Generalized NE-EDC model is developed, which includes the interaction among the reaction zones suggested by Direct Numerical Simulation (DNS) modelling. In the Generalized NE-EDC model the chemical time scale is calculated considering the reaction rates of CH_4, H_2, O_2, CO and CO_2, so that the interaction among the reaction zones is included by a global mechanism. However, detailed chemistry (smooke-25) is still used for temperature and species mass fraction calculation during modelling. Once the two EDC model's extensions are developed, they are implemented in ANSYS Fluent by User Defined Function (UDF) and User Defined Memory (UDM) and their modelling results (mean temperature and mean axial velocity at different heights of the furnace) are compared against experimental data. Additionally, a comparative study of the modelling results of (1) the EDC model with specific, fixed values of the model coefficients optimized for the current application, (2) the NE-EDC model and (3) the Generalized NE-EDC model is made. The mean temperature predictions by the Generalized NE-EDC model show the best agreement with experimental data at different heights of the furnace and it presents a slight improvement over the NE-EDC model.

Analysis of thermofluids in flameless (MILD)
combustion: assessment, improvement and
development of combustion models by CFD
Naiara Romero Anton

The flamelet based models, like the FGM model, present lower computational time than the EDC model using detailed chemistry, so that their suitability for flameless combustion is studied. The FGM model available in ANSYS Fluent generates flamelet tables based on pure fuel and pure air as boundary conditions, so that it does not consider the dilution effect existing in flameless combustion. Due to that, in this Thesis the Diluted Air Flamelet Generation Manifold (DA-FGM) model is for the first time implemented in ANSYS Fluent. This model includes the dilution effect during flamelets generation, and it has been implemented in ANSYS Fluent by generating the flamelet and Probability Density Function (PDF) tables outside ANSYS Fluent and loading and managing those tables by UDF. The DA-FGM model implementation methodology and ANSYS Fluent limitations for it are described and then the FGM and DA-FGM modelling results (mean temperature and mean axial velocity at different heights), are compared with experimental data.

The models are validated using experimental data of the Delft Lab Scale furnace (9kW) burning Natural Gas (T=446 K) and preheated air (T=886 K) injected via separate jets, at an overall equivalence ratio of 0.8.

It could be concluded that both models, the Generalized NE-EDC and the DA-FGM, are a good choice for Delft lab scale flameless combustion furnace modelling. It should be noted that the Generalized NE-EDC model provides better mean temperature results close to the burner and at the mid height of the furnace, and only, on the highest side of the furnace, where the dilution effect is more noticeable, the DA-FGM model shows better consistency with experimental data. Finally, it should be mention that the computational time of the DA-FGM model is around %28 lower than the Generalized NE-EDC model.

Acknowledgements

First, I would like to express my gratitude to my supervisors Koldobika Martin and Luis del Portillo for their dedication, support and trust throughout these years, as well as for giving me the opportunity to develop my research training with them. Even when on paternity leave, they have been there to guide me.

I also wish to thank Dirk Roekaerts for giving me the opportunity to do a three-month research stay at TU Delft university. His collaboration and guidance throughout these years have been essential for this Thesis to reach a good port. Once I was back in my country, he has shown interest and collaboration in my work and we continue working together.

Obviously, to my colleagues in the department for their day-to-day involvement and friendship, and for making it easier to get to work every day with a smile.

Finally, many thanks and a big kiss to my family and friends. Special mention to my parents (aita eta ama). Thanks for staying close to me always throughout these five years, even when the Thesis lost all sense for me… your support has always been priceless. I will never forget your short trip to Delft to visit me :). To my sister, Idoia, and her family Bengo, Goiuri and Oihan. They bore my long conversations on flameless combustion... without understanding anything, I love you all! And the family sages, my grandmothers Herme and Pili. Also, my friends, specially Unai, Amaia, Eider and Adrian, because they managed to distract me when everything seemed impossible. To finish, thanks to Mikel, my life partner who has been standing by me during these five years, thank you for your patience, understanding and support, and as a starting point of our next stage… will you marry me?

Table of contents

CHAPTER 1: INTRODUCTION AND THESIS OBJECTIVES

CHAPTER 2: FLAMELESS COMBUSTION IN FURNACES

Analysis of thermofluids in flameless (MILD)
combustion: assessment, improvement and
development of combustion models by CFD
Naiara Romero Anton

CHAPTER 3: EDC MODEL APPROACH AND VALIDATION FOR FLAMELESS COMBUSTION

CHAPTER 4: FGM MODEL APPROACH AND VALIDATION FOR FLAMELESS COMBUSTION

CHAPTER 5: EDC vs FGM APPROACHES IN ANSYS FLUENT

CHAPTER 6: CONCLUSIONS AND FUTURE RESEARCH

REFERENCES

ATTACHMENTS

Nomenclature

Nomenclature

A	[-]	turbulent flame speed constant
A_0	[-]	model parameter in realizable k-ε model
A_{fj}		pre-exponential constant of Arrhenius law
A_s	[-]	model parameter in realizable k-ε model
C_1	[-]	model parameter in realizable k-ε model
C_2	[-]	model parameter in realizable k-ε model
C_{D1}	[-]	model parameter in EDC model
C_{D2}	[-]	model parameter in EDC model
C_ξ	[-]	finite structure constant in EDC model
C_p	[J/(kg·K)]	mixture specific heat
C_τ	[-]	residence time constant in EDC model
C_μ	[-]	model constant for turbulent viscosity
C_y	[-]	PDF reaction progress variable based on species mass fraction
C_T	[-]	PDF reaction progress variable based on temperature
C	[-]	scaled progress variable
D	[m²/s]	diffusion coefficient between any two species
D_t	[m²/s]	turbulent diffusion coefficient
D_a	[-]	Damköhler number
$D_a{}^*$	[-]	Kolmogorov scale Damköhler number
D_{th}	[m²/s]	laminar thermal diffusivity
$D_{th,t}$	[m²/s]	turbulent thermal diffusivity
E_j	[kJ/kmol]	activation energy
f	[-]	passive scalar
H	[-]	pulsating function
H'	[J/kg]	enthalpy loss
h	[J/kg]	enthalpy
h_{ad}	[J/kg]	adiabatic enthalpy at local mixture fraction
$h_{\eta=0}^d$	[J/kg]	enthalpy with diluent with minimum enthalpy loss

$h_{\eta=1}^{d}$	[J/kg]	enthalpy with diluent with minimum enthalpy loss
K_{fj}		forward rate of reaction j
K_{rj}		backward rate of reaction j
K_{v}	[-]	flue gas recirculation rate
k	[m²/s²]	turbulent kinetic energy
k_{m}	[W/(m·K)]	laminar thermal conductivity of the mixture
L	[m]	turbulent length scale
L'	[m]	turbulent first cascade level length scale in EDC model
l_{t}	[m]	integral length scale
M_{k}	[-]	species k symbol
$\dot{m}$	[kg/s]	mass flow
$\dot{m}_{a}$	[kg/s]	air mass flow rates
$\dot{m}_{e}$	[kg/s]	recirculated flue gas mass flow rate, fuel and air
$\dot{m}_{f}$	[kg/s]	fuel mass flow rate
$\dot{m}_{ox}$	[kg/s]	oxidizer mass flow rate
P	[-]	probability function
P_{k}	[kg/(m·s³)]	the generation of turbulent kinetic energy in realizable k-ε model
q	[J/(kg·s)]	viscous energy dissipation at each energy cascade level
R	[kJ/(kmol·K]	Universal gas constant
$R_{k,j}$	[kg/(s·m³)]	net rate of production of species due to reaction j
R_{t}	[kg/(s·m³)]	reaction rate limited by turbulent mixing
Re	[-]	Reynolds number
Re_{t}	[-]	turbulent Reynolds number
r	[kg/kg]	stoichiometric oxidizer requirement of the fuel, mass based
S_{C}	[-]	scaled progress variable variance in DA-FGM
S_{L}	[m/s]	laminar flame speed (burning velocity)
S_{T}	[m/s]	turbulent flame speed (burning velocity)
$S_{Y_{c}}$	[kg/(m²·s)]	un-normalized progress variable source term
Sc	[-]	Schmidt number
Sc_{t}	[-]	turbulent Schmidt number
Sc_{kt}	[-]	turbulent Schmidt number for species k
S_{r}	[J/(m³·s)]	radiation source term

S_ξ	[-]	second mixture fraction variance in DA-FGM
s	[-]	stoichiometric mass ratio
T	[K]	temperature
T_{ac}	[K]	activation temperature
T_{in}	[K]	inlet temperature
T_{si}	[K]	self-ignition temperature
t'_{kj}	[-]	forward experimental concentrations' exponent
t''_{kj}	[-]	backward experimental concentrations' exponent
U^*	[-]	rate of rotation and deformation tensors
U_z	[m/s]	axial velocity
u	[m/s]	turbulent velocity
u'	[m/s]	first cascade level velocity
W	[kg/kmol]	Mixture molecular weight
W_k	[kg/kmol]	species k molecular weight
w	[m/s]	mechanical energy
w_{as}	[Hz]	antistoke frequency
w_p	[Hz]	pump beam frequency
w_{pr}	[Hz]	probe beam frequency
w_s	[Hz]	stoke beam frequency
$[X_k]$	[kmol/m³]	molar concentration
Y_c	[-]	un-normalized progress variable
Y_c^b	[-]	un-scaled progress variance in burnt reactant
$Y_c^{"2}$	[-]	un-normalized progress variable variance
Y_c^{eq}	[-]	un-normalized progress variable at chemical equilibrium
Y_c^u	[-]	un-scaled progress variance in unburnt reactant
Y_d	[-]	dilution variable
Y_d^b	[-]	dilution variable in in local burnt gases (at C=1 conditions)
Y_d^{Dil}	[-]	dilution variable at equilibrium and stoichiometric mixture conditions
Y_f	[-]	fuel mass fraction
Y_k	[-]	mass fraction of species k
Y_k^{eq}	[-]	kth species mass fraction at chemical equilibrium
Y_k^u	[-]	kth species mass fraction in unburnt reactant

Y_k^*	[-]	species mass fraction in EDC fine structure
Y_k°	[-]	species mass fraction of the incoming flow in EDC model
Y_{min}	[-]	Minimum mass fraction
Y_{ox}	[-]	oxygen mass fraction
$\widetilde{Y}_{pr}$	[-]	mean mass fraction of products
Z	[-]	mixture fraction
Z_{st}	[-]	stoichiometric mixture fraction
$Z^{"2}$	[-]	mixture fraction variance

Ancient Symbols

α	[-]	dilution factor
α_1	[-]	presumed β function parameter
α_k	[-]	constants in progress variable definition
β	[-]	presumed β function parameter
β_j	[-]	temperature exponent constant of Arrhenius law
γ	[-]	air dilution level (mass fraction of diluent in diluted air)
Δt	[s]	modelling time step
δ	[-]	diract delta function
δ_L	[m]	fine structure width
ε	[J/(kg·s)]	turbulent energy dissipation rate
η	[-]	enthalpy loss factor
η_k	[m]	Kolmogorov length scale
λ	[W/(m·K)]	laminar thermal conductivity of the mixture
λ_t	[W/(m·K)]	turbulent laminar thermal conductivity of the mixture
μ	[Pa·s]	dynamic viscosity
μ_t	[Pa·s]	turbulent dynamic viscosity
v	[m²/s]	laminar kinematic viscosity
v'_{kj}	[-]	reactants molar stoichiometric coefficient of species k in reaction j
v''_{kj}	[-]	products molar stoichiometric coefficient of species k in reaction j
v_r	[1/s]	mixing rate
v_t	[m²/s]	turbulent kinematic viscosity

ξ	[-]	second mixture fraction describing mixture between pure fuel and diluted air	
ξ^*	[-]	mass of fine structure divided by total mass in EDC model	
ξ_λ	[-]	mass of fine structure regions divided by total mass in EDC model	
ρ	[kg/m^3]	density	
σ_k	[-]	turbulent Prandtl number for turbulent kinetic energy	
σ_t	[-]	turbulent Prandtl number	
τ_c	[s]	chemical time scale	
τ_{ij}	[kg/(m·s^2)]	viscous tensor	
τ^*	[s]	residence time scale in EDC model	
τ_k	[s]	Kolmogorov time scale	
τ_t	[s]	flow time scale	
φ	[-]	reacting fine structure fraction	
Φ	[-]	Mixture properties	
Φ_f	[-]	pure fuel state	
Φ_{ox}	[-]	diluted air state	
χ	[-]	strain rate or scalar dissipation rate	
χ_{st}	[-]	Stoichiometric scalar dissipation rate	
ψ	[-]	equivalence ratio	
$\dot{\omega}_j{}'$	[kmol/m^3/s]	progress rate of reaction for the reaction pair	
$\dot{\omega}_k$	[kg/(m^3·s)]	chemical reaction rate of species k	
$\dot{\omega}_{Y_d}$	[kg/(m^3·s)]	dilution variable source term	
$\dot{\omega}_{Y_c}$	[kg/(m^3·s)]	un-scaled progress variable source term	
$\dot{\omega}_\Phi$	[kg/(m^3·s)]	reaction rate of mixture properties	

Abbreviations

CARS	Coherent Anti-stokes Raman Spectroscopy
CCS	Carbon Capture ad Storage
CFD	Computational fluid Dynamics
CSP	Computational Singular Perturbation
DA-FGM	Diluted Air Flamelet Generated Manifold
DFCB	Distributed and Flameless Combustion Burner
D-FPV	Diluted Flamelet Progress Variable

Analysis of thermofluids in flameless (MILD)
combustion: assessment, improvement and
development of combustion models by CFD
Naiara Romero Anton

DHR	Diluted Homogeneous Reactor
DJHC	Delft-Jet-in-Hot-flow burner
DNS	Direct Numerical Simulation
DO	Discrete Ordinate
DOE	Department of Energy
DTM	Discrete Transfer Method
DUT	Delft University of Technology
EBU	Eddy Break Up model
EDC	Eddy Dissipation Concept model
EDM	Eddy Dissipation model
E-EDC	Extended Eddy Dissipation Concept model
E-FPV	Extended Flamelet Progress Variable
EU	European Union
FGM	Flamelet Generated Manifold model
FLOX	Flameless Oxidation
FPV	Flamelet Progress Variable
FR	Finite Rate
GCI	Grid Convergence Index
Generalized E-EDC	Generalized Extended Eddy Dissipation Concept model
HCCI	Homogeneous Charge Compression Ignition
HiTAC	High Temperature Air Combustion
HR	Formylradical
IFRF	International Flame Research Foundation
IGCC	Integrated Gasification Combined Cycle
ILDM	Intrinsic Low Dimensional Manifolds
JHC	Jet-in-Hot-Coflow burner
KHT	Royal Institute of Technology
LDA	Laser Doppler Anemometry
LDI	Lean Direct Injection
LFM	Laminar Flamelet Model
LIF	Laser-Induced Fluorescence
LOHC	Liquid Organic Hydrogen Carriers

MILD	Moderate or Intense Low Oxygen Dilution
NECP	National Energy and Climate Plans
NE-EDC	New Extended Eddy Dissipation Concept
NKK	Nippon Kokan Kaisha
OECD	Organisation for Economic Co-operation and Development
PaSR	Partially Stirred Reactor
PDF	Probability Density Function
PFR	Plug Flow Reactor
PSR	Perfectly Stirred Reactors
P1	Simplest case of the more general P-N radiation model
RANS	Reynolds-Averaged Navier–Stokes equations
RSM	Reynolds-Stress-Model
SCR	Selective catalytic reduction
SLF	Steady Laminar Flamelet
SNCR	Selective non-catalytic reduction
SSLF	Standard Steady Laminar Flamelet
RWTH	Rheinisch-Westfälische Technische Hochschule
TFM	Turbulent Flame Model
TUI	Text User Interface
UDF	User Define Functions
UDM	User Define Memory
UDS	User Define Scalars
WSGGM	Weighted-Sum-of-Grey-Gases Model
WSR	Well Stirred Reactor
4D	4-dimension
6D	6-dimension

Superscript

$*$	Fine structure
$\bar{}$	Reynolds decomposition mean value
$\sim$	Favre averages mean value
$'$	Reynolds decomposition fluctuation

Analysis of thermofluids in flameless (MILD)
combustion: assessment, improvement and
development of combustion models by CFD
Naiara Romero Anton

´´   Favre averages decomposition fluctuation or variance

CHAPTER 1: INTRODUCTION AND THESIS OBJECTIVES

1 Energy Background

1.1 Energy framework in the European Union

Nowadays the European Union (EU) is facing a rise in energy demand, volatile prices and disruptions in supply. In order to overcome these situations, the EU is going ahead with new technologies and energy efficiency improvement. Consequently, three remarkable key items are defined on the EU energy framework; (1) Energy Efficiency in Industry, Transport and Buildings; (2) Climate Change and (3) Technology Research and Innovation. Having said this, in January 2014 EU launched the 7 year long research program "Horizon 2020" (1291/2013 Regulation, 2013), and later 2030 and 2050 climate and energy frameworks were defined (COM/2014/015 final, 2014). The 2030 energy framework covers from 2021 to 2030 and its key targets are:

- (1) Reduce at least 40% of greenhouse gas emissions with respect to 1990 levels.
- (2) Achieve at least 32% share of renewable energy in the electricity generation mix.
- (3) Achieve at least 32.5% improvement in energy efficiency.

Additionally, the climate change is beginning to be perceived in our daily live, thus it is the biggest challenge that the society is facing nowadays. In order to control environmental impact, the international community in 1997 adopted The Kyoto Protocol (Kyoto 2nd commitment period (2013–20).) with the aim of reducing greenhouse gas emissions, but

Analysis of thermofluids in flameless (MILD)
combustion: assessment, improvement and
development of combustion models by CFD
Naiara Romero Anton

it would have to wait until 2005 to enter into force. The first commitment period was from 2008-2012 and the second commitment period will remain in force until December 2020. In the meantime, it was in 2015 during Paris climate conference that the Paris Agreement was adopted (Agreement, 2015). The Paris Agreement is a separate instrument with the goal to control environmental impact of the energy production by limiting average ambient temperature rise to 2°C during this century.

Following the same goal as the Paris Agreement, recently the "Regulation on the governance of the energy union and climate action" (2018/1999/EU Regulation, 2018) entered into force in order to foster the achievement of 2030 energy target. This regulation stablishes that each Member State should prepare their own National Energy and Climate Plans (NECPs) for 2021 to 2030. Thus, the energy sector impact in the environment is another issue to be included in the energy framework.

Energy efficiency has always been a key component of the EU energy policy, so that since 1980's economic crisis, research on energy efficiency in Industry, Transport and Building has been a priority (Romero-Anton, N. et al., 2018). Some of the projects carried out in the industry sector with the goal to increase energy efficiency and reduce emissions are described in reference (Romero Anton et al., 2019).

1.2 Word Energy Consumption analysis

Our age now is really determined using energy. 20 years ago, the question was, how can we get more energy under the ground? But today there is nothing more important than trying to answer to the question, how can we get energy minimising the pollution of the environment?

According to the Department of Energy's (DOE) International Energy Outlook 2016, despite the effort that the society is doing, the total energy demand will increase from 2012 to 2040 a 48%, which is still too much (EIA, 2016). The energy consumption in the next years will increase mainly due to Non-OECD (Organization for Economic Cooperation and Development) countries (see Fig. 1. 1). Basically, India and China are responsible of that as OECD country energy consumption will be almost constant.
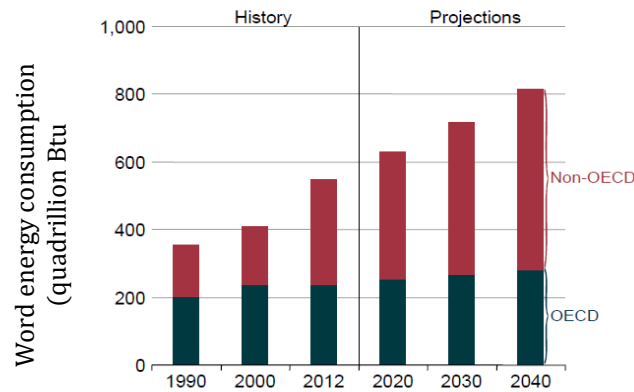
Fig. 1. 1 World energy consumption. 1990–2040 (quadrillion Btu). Source: (EIA, 2016)

Then, DOE's International Energy Outlook 2018 (EIA, 2018), on Fig. 1. 2, defined world energy consumption predictions by energy source in absolute values. It is appreciated that nowadays and in the foreseeable future, energy consumption will be mostly covered thanks to fossil fuels combustion.
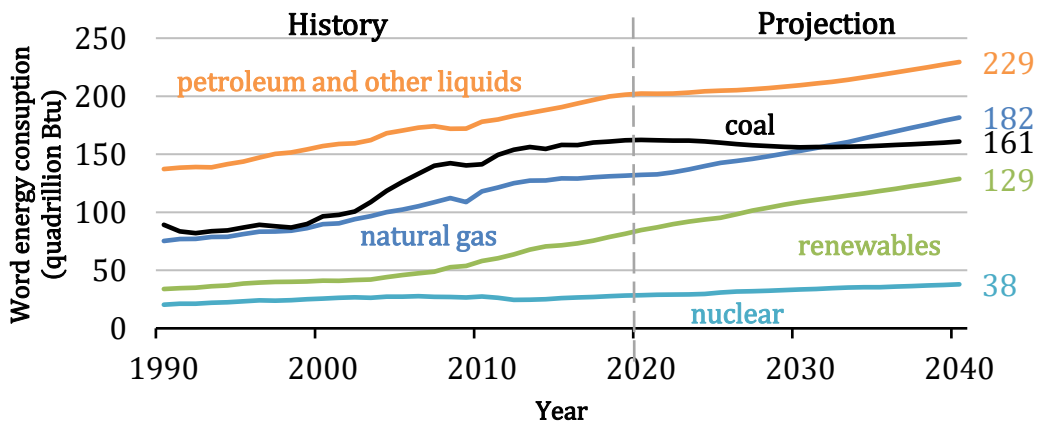

Fig. 1. 2 World energy consumption values by energy source. Source: (EIA, 2018)

Then, if the energy consumption values are displayed in percentages (Fig. 1.3), it can be concluded that in the coming years petroleum demand will go a bit down, coal consumption will go down a 3%, (which is not that much if the world wants to reduce CO_2 emissions), natural gas consumption will increase a 2% , renewable energy will increase a factor of 4% (which is not enough to reduce the emissions), and finally, after the nuclear source drop due to the Fukushima accident in 2011, the nuclear source is expected to maintain constant.
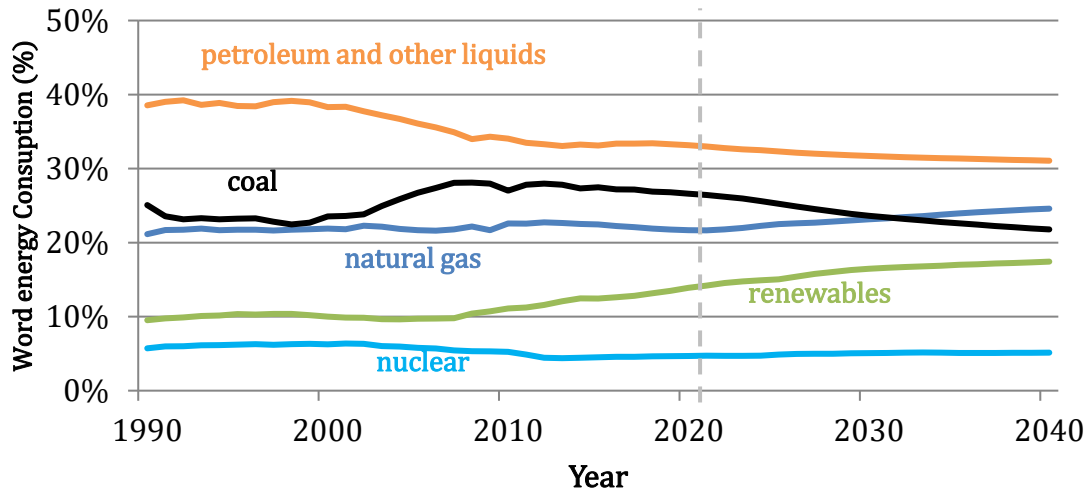
Fig. 1.3 World energy consumption % by energy source

Although renewable energy is very important and the new installed capacity is soaring, the energy demand is increasing faster, so that in 2040 only 23% of the energy demand will be covered by renewable and nuclear sources, while the rest will still be supplied by fossil fuels (EIA, 2018).

Having a look at today's situation, more than 80% of the energy produced on the earth comes from fossil fuels' and biofuels' combustion. Therefore, it can be concluded that today and in the near future, fossil fuels will be the primary energy source. Hence the vital importance of increasing combustion energy efficiency and reduce the greenhouse gases emissions in combustion systems. The EU is aware of this issue and they have put in place regulation on emissions (2010/75/EU Directive, 2010).

To better understand the challenge that energy efficiency improvement and emissions reduction implies, first, combustion science's mayor characteristics are going to be analysed and next, NO_x emissions from combustion are going to be evaluated.

1.2.1 Combustion and alternative technologies

Combustion research started many years ago as it is the oldest technology of humankind. Nowadays, combustion is the way that the human beings mostly transform primary energy sources into a different type of energy and it has several applications, such as

mobility and transport, power generation, industry and household. As of today, it is possible to say that the combustion is omnipresent.

What makes combustion special and complicated is the heat release during the process. The chemical reactions release heat and this increases temperature. When temperature increases, chemical reactions become faster and consequently there is a non-linear feedback. Besides, combustion combines the interaction of the flow (transport) and chemistry becoming on a multi-scale and multi-physics phenomenon. It is a multi-scale phenomenon as there are mixing time scale (τ_t) and chemical time scale (τ_c), and it is a multi-physics phenomenon as chemistry, radiation, flow and acoustics happens. Therefore, new dimensionless groups appear like Damköhler and Karlovitz numbers in order to "simplify" the combustion numerical calculation. These numbers have similar concept to Prandt, Grashoff and Reynolds numbers for the assessment of convection phenomena.

However, it is indeed important to calculate precisely the phenomenon that happens during combustion in order to 1) develop more efficient combustion chambers and 2) analyse combustion products impact on the earth like air pollution or atmospheric pollution (CO, SO_2, NO_2, O_3, particulates) and global warming (CO_2, CH_4, N_2O, halocarbons) (Sawyer, 2009). It was Fourier in 1824 who first proposed that gases in the atmosphere were responsible for raising the earth's temperature. Later, in 1896, it was estimated that doubling CO_2 emissions would provide a temperature rise of 5-6 °C (Arrhenius, 1896), remarkably close to recent estimations. But it was not until 1997 that the EU started thinking about regulations to try to stop the climate change, for example the Kyoto Protocol.

In order to reduce greenhouse gas emissions several approaches can be followed. One of them is the hydrogen economy (Fig. 1. 4) that proposes the hydrogen as an alternative fuel for the transport sector (Baroutaji et al., 2019; Shin et al., 2019) and home heating (Lopez-Ruiz et al., 2019). It also considers hydrogen as a storage and transport mean of electricity from intermittent renewable energies by Liquid Organic Hydrogen Carriers (LOHC) or by hydrogen electrolysis (Barbir, 2005).
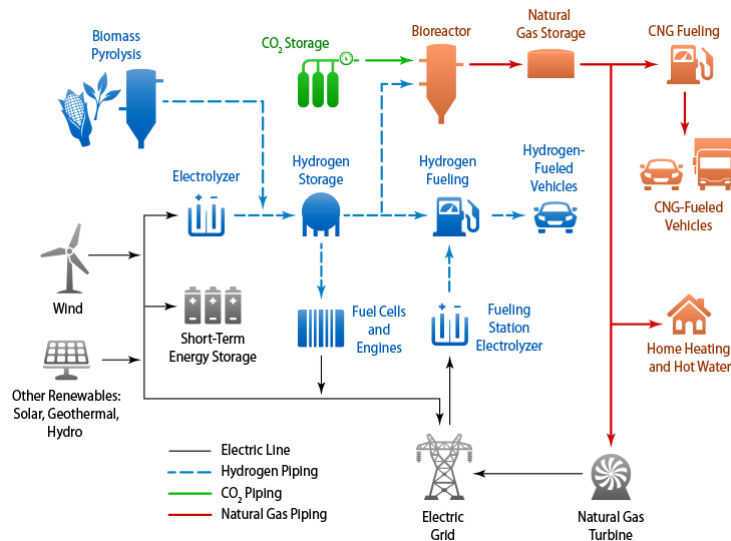
Fig. 1. 4 Renewable hydrogen and electricity production. Source:(NREL)

Carbon Capture and Storage (CCS) is another alternative to reduce greenhouse gases in the atmosphere (Fig. 1. 5). The three main technologies currently proposed are; post-combustion with a wet scrubbing (Favre, E., 2007), pre-combustion capture (synthesis gas) (Cormos, 2012) and oxyfuel capture (Wall et al., 2009).

Fig. 1. 5 Three main CO_2 capture technologies

The use of biofuels (mainly bioethanol and biodiesel) is apparently another climate friendly alternative as they replace conventional fossil fuels. Nevertheless, some biofuels

are produced from sugar, starch and vegetable oil, consuming farmland and indirectly contaminating water and soil resources by fertilizers and pesticides. Besides, some researchers concluded that they have higher cost than conventional fuels (Cherubini et a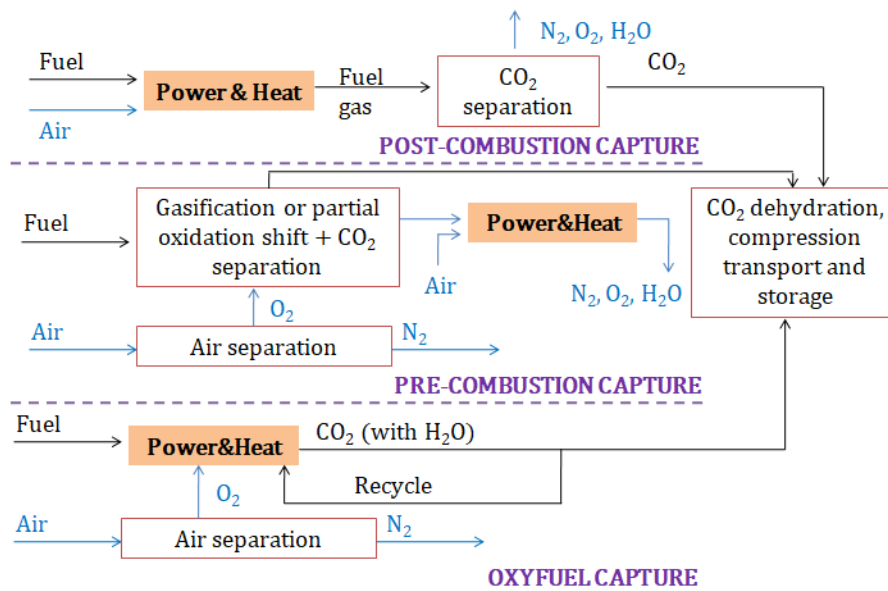l., 2009), so that in the long term they will replace relatively little fossil fuels. Despite its drawbacks, researchers are studying their application on internal combustion engines (Agarwal, 2007) and modelling (Lai et al., 2011).

Flameless combustion is another climate friendly combustion technology that reduces thermal NO_x emissions by reducing flame and furnace temperature thanks to the diluted reactants. In this combustion there is an internal flue gases recirculation diluting reactants.

Finally, the increase in combustion efficiency is another strategy to reduce greenhouse gases emissions. By increasing combustion efficiency fuel consumption is reduced, and therefore, CO_2 and NO_x emissions are reduced. Nevertheless, increasing efficiency on a combustion process is a challenge as other combustion aspects can be affected like stability, thermal NO_x emissions and cost. Therefore, there is a need for developing and understanting new combustion technologies in order to improve combustion efficiency. For example, depending on the studied field, different methods are studied that: Lean Direct Injection (LDI) technology for the aircraft turbines (Tacina et al., 2002), Homogeneous Charge Compression Ignition (HCCI) for car industry (Yao et al., 2009), oxy-coal Integrated Gasification Combined Cycle (IGCC) combustion for electricity generation (Buhre et al., 2005; Descamps et al., 2008) and finally, flameless combustion (Wünning & Wünning, 1997) for combustion chambers. Among the several available technologies able to reduce emissions and increase combustion efficiency, in this PhD Thesis flameless combustion technology is selected to study.

1.2.2   NOx emissions from combustion

The improvement of combustion efficiency to reduce fossil fuel and biofuels consumption and consequently reduce carbon dioxide emissions is a key issue in combustion research. One of the most used ways to improve energy efficiency is to preheat the combustion air through an external preheater by the energy coming from exhaust gas stream. But this

technique increases air temperature and leads to large thermal NO_x emissions, which are capped in many countries due to their negative impact in the environment (like climate change, acid rains and photochemical smog) (2010/75/EU Directive, 2010).

In combustion processes NO_x formation, there are mainly three sources: thermal NO_x, fuel NO_x (the conversion of fuel's nitrogen into NO_x) and prompt NO_x (attributed to the reaction of atmospheric nitrogen). Thermal NO_x formation is temperature dependent. The formation rate is primarily a function of high temperature (usually above 1873 K) and the residence time of nitrogen at that temperature (Wünning & Wünning, 1997). This explains why NO_x increases when preheated air has been used. Some experiments demonstrate that at 1800K the NO_x formation rate doubles for every 35K temperature rise (Beér, 1994). On Fig. 1. 6 thermal NO_x production depending on temperature is shown. It is appreciated that for temperatures higher than 1800K the thermal NO_x increases exponentially (N. A. Chigier, 1981).
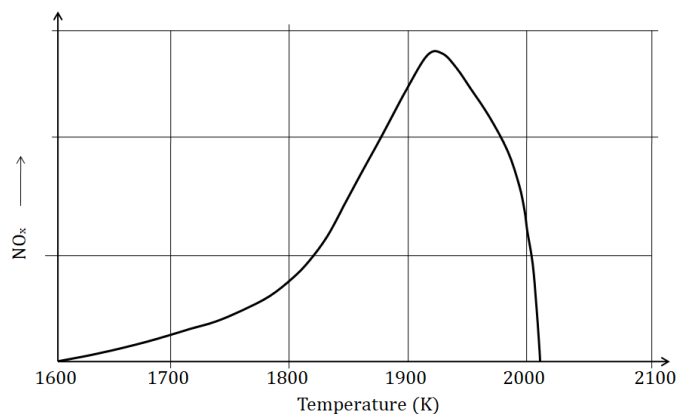
Fig. 1. 6 Relation between NO_x formation and Temperature

Considering NO_x temperature dependence, NO_x emissions reducing techniques are focusing on (1) avoiding peak temperatures, (2) reducing the residence time of air in high temperature areas and (3) avoiding high oxygen concentration in the reaction zone. Some of the proposed NO_x reduction techniques are staged combustion, selective non-catalytic reduction (SNCR), selective catalytic reduction (SCR) and a combination of them. The former has a NO_x reduction potential of 20-30% with a low economic impact. The other two techniques have 30-60% and 75-85% NO_x reduction capability, respectively, but the

economic impact and technology complexity increase drastically. As comented before, flameless combustion is another alternative to reduce NO_x emissions with a reduction potential of 35-55% and an affordable economic and technology impact (Franco & Diaz, 2009). Therefore, these characteristics make flameless combustion very attractive for industrial application, both technically and economically speaking.

2   State of the art

2.1   Flameless Combustion

Climate change is the biggest challenge that the society is dealing with and the burning of fossil fuels to release energy is the main responsible of greenhouse effect gases (Wünning & Wünning, 1997). Therefore, thermal efficiency of the combustion systems must be improved. When air is externally preheated by the heat release of the exhaust gases, better efficiency is achieved but it is well known that high air preheat temperatures will cause peak temperatures in the flame; hence, NO_x thermal emissions will increase.

Combustion technology must evolve to be more climate-friendly and less energy consuming, and flameless combustion is contributing to this goal. Flameless combustion is based on the aerodynamic recirculation of flue gas inside the furnace to dilute fuel and air stream, reducing O_2 concentration. At the same time, the efficiency is increased if flue gases heat is used to preheat reactants. As combustion takes place at low fuel and oxygen content with a flue gas mass taking part on the heat release from the reaction, flame temperature peaks are cut down reducing NO_x emissions. It can be concluded that by flameless combustion energy efficiency is increased, NO_x emissions are reduced and as fuel consumption is reduced, there are CO_2 formation savings.

Fig. 1. 7 shows the difference on temperature distribution in conventional (a) and in flameless(b) combustion furnaces.

a) Conventional combustion   b) Flameless combustion
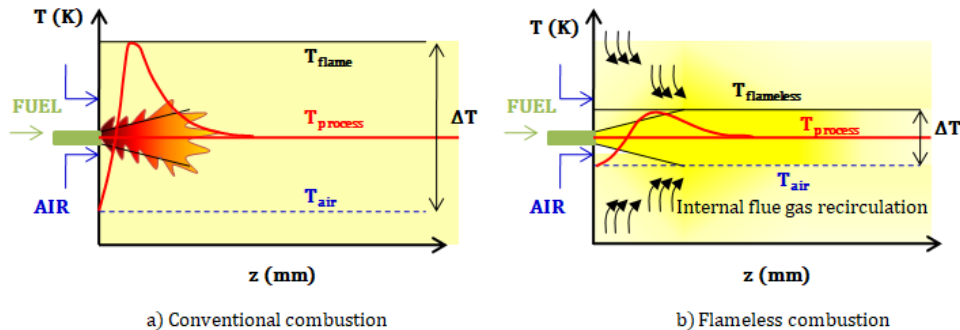
Fig. 1. 7 Temperature distribution of conventional combustion and flameless combustion

In conventional combustion Fig. 1. 7 a) there is a peak in flame temperature and flame front is distinguishes. On the other hand, in Fig. 1. 7 b), due to the internal flue gas recirculation, reactants are preheated (air in this example) and diluted, and consequently lower flame temperature is reached (≈1500 K). In those conditions, flame front disappears and there is not a visible flame. Thanks to flameless combustion efficiency increases, NO_x and noise emissions are reduced and a more stable flame is reached. On Table 1. 1 shows a summary of the characteristics of flameless and conventional combustion.

Table 1. 1 Conventional and flameless combustion characteristics

Characteristics	Conventional Combustion	Flameless combustion
Flame temperature	High (near adiabatic temperature)	Lower ≈ 1500K
Uniform temperature distribution	✗	✓
Recirculation of combustion products	✗	✓
Turbulence intensities and kinetic	⇊	⇈
Visible flame	✓	✗
Stable flame	⇊	⇈

Diluted reactants	✗	✓
Preheated reactants	✗	✓
O_2 concentration	⇈	⇊
Damköhler number (Da)	Da>1	Da ≈1
Noise emissions	⇈	⇊
NO_x emissions	⇈	⇊
Efficiency	⇊	⇈

After comparing conventional and flameless combustion, the latter presents some remarkable advantages; (1) uniform temperature distribution along the furnace, (2) more stable flame, (3) noise emissions reduction, (4) NO_x emissions reduction and (5) energy efficiency increase. One example of Flameless combustion capacity reducing NO_x emissions is shown on Fig. 1. 8 (Flamme, 2001). Experimental results showed that flameless burner (FLOX) presents lower emissions than both conventional burner and staged burner.
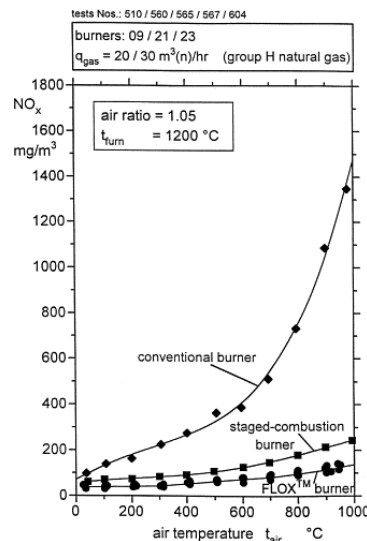
Fig. 1. 8 NO_x concentration expressed as NO_2 (dry, 8% O2) as a function of combustion air temperature t_{air}. Source:(Flamme, 2001)

The two basic characteristics to get flameless combustion are high temperature reactants and diluted reactants, which are obtained by flue gases internal recirculation into the

reaction zone. A recirculation rate parameter, K_v, was defined to analyse the necessary recirculation and furnace temperature to get stable flame (Wünning & Wünning, 1997).

$$K_v = \frac{\dot{m}_e}{\dot{m}_f + \dot{m}_a}$$

Eq. 1. 1

where $\dot{m}_e$, $\dot{m}_f$ and $\dot{m}_a$ are the mass flow rates of recirculated flue gas, fuel and air respectively. The recirculation rate and furnace temperature determine three reactions zone (Fig. 1.9).
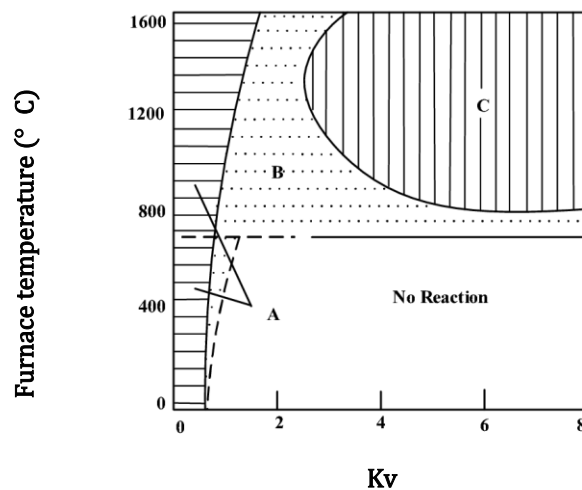
Fig. 1.9 Schematic diagram of the stability limits for different combustion modes.
Source: (Wünning & Wünning, 1997)

Zone A represents stable flames, which covered the entire range of combustion chamber temperatures but with a thin recirculation ratio value. For higher recirculation rates, there is zone B, where the flame can be unstable. But if recirculation rate and furnace temperature are relatively high, stable flames are reached, C zone, corresponding to flameless condition (Fig. 1.9). It is appreciated that it is not possible to operate on flameless combustion in a cold furnace, therefore, furnace need to be preheated before start operating in flameless mode. Usually conventional burners are used at the beginning to preheat the furnace and once the furnace is hot the burner operation mode is changed to flameless mode.

In the literature several names are used to refer to flameless combustion as it is still a lack of its boundaries definition. The first name, FLOX, was proposed applying flameless combustion technique in the context of industrial burners and furnaces (Wünning & Wünning, 1997). This name was proposed because during experiments the flame was invisible and inaudible. This name is quite close to flameless combustion but it adds oxidation word. It is true that combustion reactions are oxidation reactions, but there are also oxidation reactions that are not combustion reactions. Therefore, later High Temperature Air Combustion (HiTAC) name was proposed (Hiroshi Tsuji et al., 2002). It is based on the high inlet air temperature, but in flameless combustion high reactants temperature is required, therefore, not only air can be preheated but also fuel. Consequently, Moderate or Intense Low-Oxygen Dilution (MILD) name appeared (Cavaliere & de Joannon, 2004). It is the most used definition to refer to flameless combustion: "A combustion process is named MILD when the inlet temperature of the reactant mixture (T_{in}) is higher than mixture self-ignition temperature (T_{si}) whereas maximum allowable temperature increase with respect to inlet temperature (ΔT) during combustion is lower than mixture self-ignition temperature". Referring to MILD definition out coming graphic was developed (Fig. 1.10):
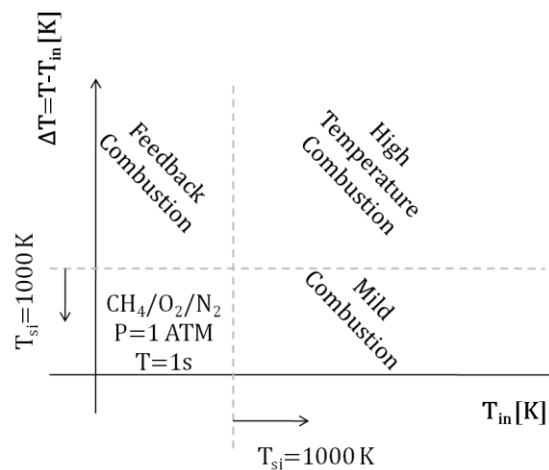

Fig. 1.10 Combustion modes for different inlet temperature and temperature change.
Source:(Cavaliere & de Joannon, 2004)

Nevertheless, this name is also confusing because it is not known whether the adjectives "medium" or "intense" refer to low oxygen or to dilution. Besides, MILD definition is based

on Well Stirred Reactor (WSR), which is easy to apply in premixed combustion but not for non-premixed combustion (Minamoto, Y. et al., 2013). Normally in non-premixed combustion, inlet temperature is lower than autoignition temperature, and during the mixing of flue gases and reactants autoignition temperature is reached. Consequently, along this work flameless combustion name is used.

Flameless combustion is applied in industrial boilers and furnaces as well as explored for gas turbines application. In order to establish the methodology for combustion chamber design to reduce fuel consumption and pollutant emissions, flameless combustion technology should be perfectly understood. To this end, lab-scale and semi-industrial scale experiments and Computational Fluid Dynamics (CFD) simulations have been carried out. Thanks to them, the knowledge of this promising combustion technology behaviour in industrial scale environments has increased.

A 3 dimension CFD modelling gives to the designer detailed information that it is complicated or expensive to get by experimental data. Additionally, the designer could get detailed information of the flow path and temperature in the whole domain. Due to that in this work ANSYS Fluent CFD modelling has been selected to study flameless combustion.

2.2 Experimental studies

Literature shows that flameless combustion has been experimentally analysed in lab-scale configurations due to the short dimensions and affordable environmental conditions. Experimental lab-scale setups are divided into two classes: unconfined and confined configuration. In the first class, most of the experiments concern Jet-in-Hot-Coflow (JHC) burners, mimicking the mixing by recirculated products via a controlled mixing in a secondary burner. The second class includes a few lab-scale furnaces with a single burner and a few of them with more burners approaching industrial and semi-industrial furnaces. The data of those experiments have been used to gain insight in the combustion process and to validate simulation results.

JHC burner is a non-enclosed flame with easily access for diagnostics and measurements. It has a jet containing fuel surrounded by a coflow preheated or diluted. A secondary burner usually generates the coflow, thus, the result is a jet flame easily accessible by laser diagnostics for velocity, temperature and species measurement, as well as, high-speed equipment for flame structure visualization.

The first set of experiments on a JHC flameless burner was made on Adelaide burner (B. B. Dally et al., 2002). The burner used a mixture of H_2 and CH_4 (equal in volume) as fuel and three different O_2 concentrations: 3, 6 and 9% (mass base). Point measurements were made for species concentration and temperature measurement. Later, using the same burner but changing the fuel composition, O_2 concentration impact on OH and formaldehyde (CH_2O) was analysed (Medwell et al., 2007). Laser-Induced Fluorescence (LIF) measured coflow velocity and temperature, OH and CH_2O distribution. Another JHC set up is Cabra burner or Dibble burner. It is based on H_2-N_2 mixture of hot coflow with H_2 lean combustion, O_2 concentration was 14.74% much higher than Adelaida burner (Cabra et al., 2002). The goal was to reproduce combustion with Damköhler numbers close to one. Then, a series of experiments were carried out on Delft-Jet-in-Hot-Coflow (DJHC) burner. Their goal was to analyse flameless burner flame stabilization (Oldenhof, E. et al., 2010; Oldenhof, E. et al., 2011). The general goal of JHC burners investigations was to improve the understanding of flameless combustion as later will be applied on large-scale furnaces. However, it was found that JHC burners were based on low Reynolds coflow (the maximum Reynolds value was achieved in Cabra burner and it was below 6000) (Oldenhof, Ernst et al., 2013). In order to analyse higher Reynolds numbers Distributed and Flameless Combustion Burner (DFCB) setup (Duwig et al., 2012) was developed, which has higher flue gases recirculation

The key findings of the works commented above were the consequences on auto-ignition and flame front extinction due to the decrease of O_2 concentration. The conclusions were obtained thanks to the easy optical access to measure temperature, OH and CH_2O. The results showed that low O_2 concentration leads to lower temperature peaks and less OH concentration while CH_2O levels figure out a zone similar to autoignition. Additionally, it was concluded that flame stabilization improvement in hot coflow flames was due to a

Analysis of thermofluids in flameless (MILD)
combustion: assessment, improvement and
development of combustion models by CFD
Naiara Romero Anton

combined effect of both auto-ignition and flame propagation. Note that in conventional flames the stabilization depends on the propagation of energy and radicals from the reaction zone to the incoming reactants.

Although JHC open-air setups are the most studied configurations for flameless combustion (due to their easy optical access), experiments in lab-scale furnaces are also carried out. Lab-scale furnace is a burner with an enclosure, limited optical access and more complex geometry and flow characteristics than JHC burner. However, it is still simple enough comparing to real applications (industrial furnaces). Comparing to JHC burner, the advantage of doing experiments on lab-scale furnace is that combustion gases internal recirculation is more similar to industrial furnaces. Therefore, for flue gases properties measurements non-intrusive methods, like laser diagnostic, are recommended so as not alter the flow path.

The first experiments on lab-scale furnaces were based on laser-optical measurements (Plessing et al., 1998a) and later, other series of experiments were carried out in parallelepiped furnace configuration (Cavigiolo et al., 2003; Lupant, D. et al., 2007; Lupant, Delphine & Lybaert, 2015; Szegö et al., 2008; Veríssimo et al., 2011; Veríssimo et al., 2013a; Veríssimo et al., 2015). On those investigations fuel type, equivalence ratio, air jet velocity, power input and air temperature impact on emissions and OH was studied. Additionally, experiments in setups with no optical access (Rebola et al., 2013) and different enclosures shape (Khalil & Gupta, 2014) were also made. Recently, a cyclonic combustion chamber with high residence time has being studied (Sorrentino, Giancarlo et al., 2015; Sorrentino, Giancarlo et al., 2016).
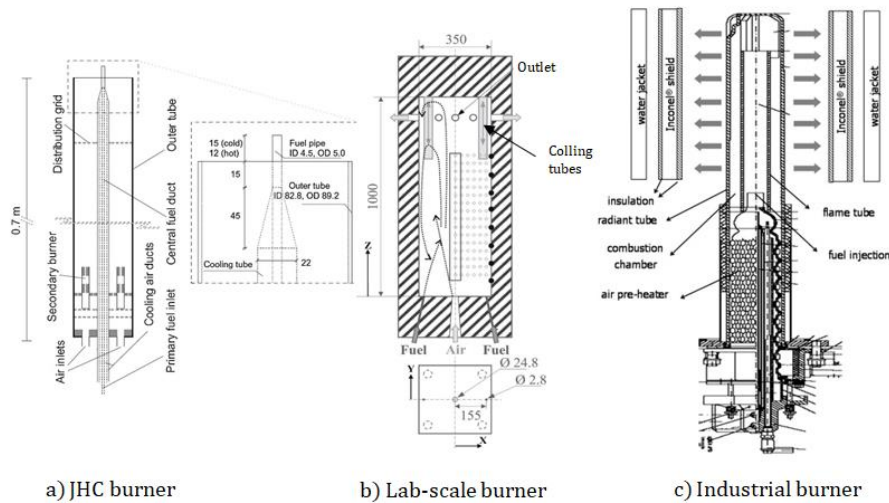
Fig. 1. 11 a) JHC burner. Source:(Oldenhof, E. et al., 2011) , b) Lab-scale burner. Source:(Lupant, Delphine & Lybaert, 2015) and c) Industrial burner. Source:(Parente, A. et al., 2008)

In confined configurations, the experimental target was to measure pollutants emissions, which depend on the residence time and recirculation ratio. Those values are more realistic in experiments with confined configurations rather than on JHC burner as they are not in an open-air atmosphere. Therefore, equivalence ratio, power input, inlet temperature and velocities were changed to analyse their impact on residence time and reaction intensity (only when OH distribution could be measured). In contrast to JHC burners, in enclosed devices, it is more difficult to measure the flow path of reactants and products due to the reduced optical access. Therefore, these setups are not appropriately to study auto-ignition or reaction progress. Finally mention that all the experiments were made at atmospheric conditions, as flameless combustion is still an immature field. It should be mention that in confined configuration some semi-industrial and industrial approaches can be found; a burner with a cylindrical combustion chamber (Galletti et al., 2007), an industrial burner fed with hydrogen (Parente, A. et al., 2008) and a multiburner combustion furnace (Cho et al., 2011; Danon et al., 2011a; Danon et al., 2011b). These devices have a more complex geometry and their operation conditions are harder, that is way only specific studies were made.

As a summary, it can be concluded that JHC burners are optimal for flameless combustion autoignition and reaction progress understanding, due to their excellent optical access. But enclosed setups have a more realistic residence time and recirculation values, so that,

they are used for flameless combustion emissions measurement. In this Thesis, experimental data of an optically accessible lab-scale furnace is used to validate modelling results.

2.3 Numerical modelling studies

Apart from the experimental approach, numerical modelling is an interesting tool to analyse what is happening in the furnace during flameless combustion. A good numerical modelling could give to the researchers' information that cannot be measured in the experiments. A review of the numerical models developed for flameless combustion is shown on Perpignan et al. work (Perpignan et al., 2018).

In this Thesis, a few of the most often used ones are named (see Table 1. 2). The simplest models are based on a rate limiting turbulent mixing time scale and an overall reaction rate; like Eddy Break Up (EBU) (Spalding, 1971) and Eddy Dissipation Model (EDM) (Magnussen & Hjertager, 1977). The micromixing model-based approaches are based on an assumed type of micromixing controlled by relevant turbulent time scales. The Eddy Dissipation Concept (EDC) model describes the micromixing as mass exchange between an ideal type of chemical reactor (fine structure) and non-reacting surroundings. The Partially Stirred Reactor (PaSR) model (Jerzy Chomiak, 1987) provides an alternative for the modelling of fine structure scales in the EDC model instead of Plug Flow Reactor (PFR) or Perfectly Stirred Reactors (PSR) (Aminian et al., 2016; Ferrarotti et al., 2019; Li et al., 2017; Li et al., 2018). The PaSR model considers both a mixing time scale and a chemical time scale factor and can cover various regimes. The transported Probability Density Function (PDF) model provides the most elaborate stochastic simulation of micromixing coupled to reaction (Christo & Dally, 2004). Finally, the flamelet models and their extensions, Intrinsic Low Dimensional Manifold (ILDM) (Maas & Pope, 1992), the Computational Singular Perturbation (CSP) (Lam & Goussis, 1989), the Flamelet Generated Manifold (FGM) model (Abtahizadeh et al., 2017; Göktolga et al., 2017; Huang, Xu, 2018; van Oijen et al., 2016) and the Flamelet Progress Variable (FPV) (Ihme & See, 2011; Lamouroux et al., 2014; Pierce & Moin, 2004), assume that information on local flame structure can be retrieved from canonical laminar flames. The computational time

required in flamelet based models is lower than micromixing based models, therefore, it is an interesting model to be applied in flameless combustion as well as on industrial scales furnaces.

Table 1. 2 Most often used turbulence-chemistry interaction models in non-premixed combustion

Simplest Models	Eddy Break Up (EDB) Eddy Dissipation Model (EDM)	Reaction rate is limited by turbulence mixing	$R_t = 1/\tau_t$
Micromixing Models	EDC PDF	PASR; PFR; PSR Stochastic simulation	
Flamelet based models	FGM	Combination of flamelet and ILDM	Mixture fraction (Z) and progress variable (Yc) defined flamelets
	FPV	Extension of ILDM	Mixture fraction (Z) and scalar dissipation rate χ defined flamelets

It should be noted that the computational cost demanded by the EDC combustion model depends directly on the chemical mechanism used, but it is still lower than the PDF model but higher than the Flamelet based models.

Simplest models presented in Table 1. 2 do not consider chemistry, therefore, they are neglected for flameless combustion modelling. Nevertheless, micromixing models have been applied on the research of flameless combustion from the beginning (Cabra et al., 2002; Christo & Dally, 2005; Tabacco et al., 2002). In all these works, however, the simulation results did not match well with flameless combustion experimental data, showing that combustion models developed for conventional combustion, like the standard EDC model, often do not accurately describe the consequence of the dilution by recirculated products, resulting in the overprediction of the temperature of the combustion gases (at least locally). As an example Fig. 1. 12 shows the results of the EDC

model in flameless combustion modelling (Christo & Dally, 2005). It is appreciated an overprediction of the maximum mean temperature by the EDC model (solid lines) comparing with experimental data (open symbols).
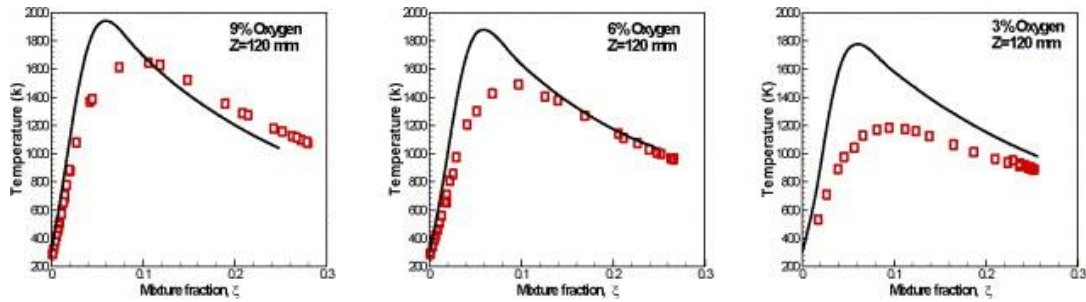
Fig. 1. 12 Mean temperature profiles comparison for different O_2 concentrations. Open symbols: experiment, solid lines: CFD model using EDC combustion model with GRI3.0 kinetics.

This issue happens in the EDC model because the EDC model constants values were empirically chosen for conventional combustion, so that it is not considered the reactants dilution of flameless combustion. Note that in flameless combustion, due to the dilution, the temperature of the furnace is reduced and consequently, chemical time scales (reaction region) are increased. These specific flameless combustion features are not considered in the standard EDC model, and due to that, the EDC model constants modification is proposed to improve modelling results (Aminian et al., 2012; De et al., 2011; Evans et al., 2015; Mardani, 2017; Rebola et al., 2013). Among the micromixing models the EDC model has been applied extensively as its computational cost is lower than the PDF model.

2.3.1   Extensions of EDC model in flameless combustion

As standard EDC model avoid diluted reactants consideration, the first approach to improve its modelling results was to change manually the finite structure constant C_ξ and the residence time constant C_τ values calibrating them with experimental data. Changing both model's constants flameless combustion predictions were improved (Aminian et al., 2012; De et al., 2011; Evans et al., 2015; Mardani, 2017; Rebola et al., 2013). However, other researchers concluded that C_τ had almost not influence in simulations results but C_ξ strongly influence on mean temperature, thus, they concluded that the latter constant

value should only be increased for flameless combustion modelling (Graça et al., 2013; Rehm et al., 2009). Recently, a systematic and complete review of these approaches, introducing modified values of model parameters has been given (Ertesvåg, 2019; Lewandowski & Ertesvåg, 2018). The review also benchmarks the proposed modifications with respect to the original principles and the consistency conditions of the EDC model formulation proposed in the works by Magnussen and co-workers (Magnussen & Hjertager, 1981; Magnussen, 2005). In order to reduce the dependency on experimental data and also make the EDC more widely applicable to flameless combustion systems, an important step was made by proposing an extension of the EDC model (here called E-EDC), where model constants depend on the local Reynolds and local Damköhler numbers (Parente, Alessandro et al., 2016). Nevertheless, the E-EDC model shows discrepancies with experimental data, so that it is a challenge to improve this model.

Additionally, the nature of the reaction zones in flameless combustion and the implications for modelling have been the subject of many studies (Perpignan et al., 2018). Turbulence-chemistry interaction models based on thin reaction zones (flamelet-based models) or models calibrated for conventional combustion conditions, such as the standard EDC models, fail to give accurate predictions. This is often attributed to the presence of distributed reaction zones in flameless combustion.

To provide a more fundamental understanding and possible explanations of the reasons why models have a certain performance, several Direct Numerical Simulations (DNS) studies were made of the special characteristics of the flame front structure under flameless combustion (Minamoto, Y. et al., 2013; Minamoto, Y. & Swaminathan, 2014; Minamoto, Y. et al., 2014; Minamoto, Yuki & Swaminathan, 2014). These studies concerned the evolution and interaction of flame fronts in initially homogeneous isotropic turbulence in a cubical volume bounded by symmetry or periodic boundaries. They used a skeletal mechanism with 16 species and 36 reactions and a non-unity Lewis number for species transport. The results revealed a complex flame structure. The PDF of the reaction progress variable based on temperature (C_T), presented a wide range of intermediate values between 0 and 1 suggesting distributed reaction zones. This finding contrast with

Analysis of thermofluids in flameless (MILD)
combustion: assessment, improvement and
development of combustion models by CFD
Naiara Romero Anton

the standard thin premixed reaction fronts in conventional combustion, where the probability of finding intermediate values between 0 and 1 is very small. However, the PDF of the reaction progress variable based on the fuel species mass fraction (C_y), provided a bimodal distribution suggesting thin reaction zones (as in conventional combustion). The experimental results (Dally et al., 2004; Duwig et al., 2012; Plessing et al., 1998b) and the DNS modelling results (Minamoto, Y. et al., 2013; Minamoto, Y. & Swaminathan, 2014; Minamoto, Y. et al., 2014; Minamoto, Yuki & Swaminathan, 2014), were found to be consistent with each other: OH-PLIF and C_y suggested thin reaction zones, while temperature images and C_T showed more similar distributed reaction zones. Therefore, it could be concluded that combustion structures in flameless regime can be described as small flamelets interacting with each other. The DNS modelling results also suggested that, depending on the dilution level, the interaction between the thin reaction zones varies; that is, sustained interaction between the thin reaction zones occurs at high dilution levels, while little interaction occurs at a low dilution level.

Minamoto and Swaminathan (Minamoto, Y. & Swaminathan, 2014) investigated in detail how good mean reaction rates in the DNS of MILD combustion are described by three 'paradigms': standard flamelets based on pure fuel and pure oxidiser, flamelets based on diluted streams ('mild flame elements'), and a PSR with the size of the laminar flame thickness. They concluded that the pure fuel and pure air flamelets are not suitable while the diluted flamelets give qualitative agreement, but the PSR-based model is the most appropriate. Here, the well stirred reactor was assumed to be the size of a representative laminar flame thickness (thermal thickness or Zeldovich thickness).

Considering that the DNS modelling results suggest interactions among the combustion reaction zones can invalidate the commonly used combustion assumption: infinity fast-chemistry and flamelets modelling (Swaminathan, 2019). Under this circumstance, a Generalized E-EDC model has been proposed(Evans et al., 2019), based on the model developed by Parente et al (Parente, Alessandro et al., 2016), but including detailed chemical kinetics for considering reaction zones interaction. Recently, it was discussed the necessary conditions for distributed reactions (Driscoll et al., 2020), leaving still

possibilities to the EDC model to be applied in MILD combustion (Minamoto, Yuki et al., 2014). In the Generalized E-EDC, the chemical time scale is calculated considering the reaction rates of CH_4, H_2, O_2, CO and CO_2 and not following the CH_4 one-step mechanism (as was done in the E-EDC). Additionally, Generalized E-EDC eliminates the proportionality factor in laminar flame velocity following the NE-EDC suggestion (Romero-Anton, Naiara et al., 2020). The model was applied in a JHC burner (with controlled coflow) and the results showed better agreement with the experimental data than the E-EDC model, but they are still some deviations with experimental data that can be improved.

2.3.2 Flamelet based models in flameless combustion

The application of flamelet based models like FGM or FPV in flameless combustion are of interest as the computational time required is lower than the EDC model. Due to that, it is an attractive model to be applied in LES simulation as well as in industrial scale devices. Fewer works can be found on the literature doing flameless simulation based on flamelet models (Christo & Dally, 2005; Shabanian et al., 2013). The results showed discrepancies between experimental data and simulations results, as dilution variable is not considered in flamelet tables generation. Therefore, it is a challenge to include the dilution effect on flamelet tables generation. In the literature extensions of the flamelet based models are found considering the dilution effect, for example, the extended FPV (E-FPV) model defined an additional conserved scalar to consider dilution effect (Ihme & See, 2011). The E-FPV model can be applied only when the diluted reactants composition is constant. This only happens in JHC burners as diluted reactants are controlled by the coflow burner. On industrial furnaces application, for example, the dilution is achieved due to the internal recirculation of the combustion gases (with not controlled diluted reactants composition), so that the E-FPV model cannot be applied for enclosed furnaces modelling. In order to overcome this weakness the Diluted FPV model (D-FPV) (Lamouroux et al., 2014), the Diluted Homogeneous Reactor (DHR) model (Locci et al., 2014; Locci et al., 2015) and the Diluted Air-FGM (DA-FGM) model (Huang, X. et al., 2017; Huang, Xu, 2018) were developed. The D-FPV model is based on steady flamelet equation and flamelet tables are generated as laminar counterflow flames considering diluted fuel, diluted air

streams and heat loss. A transport equation is used for dilution variable definition, but the weak point of this model is that during the tabulation the mixing between fuel and diluent is considered, while the reactions between fuel and diluent stream in lean combustion is not considered. On the other side, the DHR model is based on homogeneous reactor (not on flamelet equation) and tabulates auto-ignition trajectories. A transport equation is not used for dilution variable definition, instead, the dilution variable is defined divided into non-reactive and reactive parts. This methodology is less accurately than defining a dilution variable by a transport equation. In order to overcome those models' weak points, the DA-FGM model was developed, which is based on steady flamelet equation and flamelet table is generate considering laminar counterflow flames with fuel and diluted air (for more details go to chapter 4). The DA-FGM model has been only implemented in OpenFOAM package (its implementation in ANSYS Fluent is not found in the literature). Therefore, it becomes interesting to study the DA-FGM model implementation methodology in ANSYS Fluent and its modelling results.

2.3.3 Conclusions

The EDC and flamelet based models have been used for flameless combustion modelling at the level of mean properties as targeted in RANS. To better model flameless combustion extensions of them are proposed in the literature. A summary of extended EDC and flamelet based models is shown on Table 1. 3.

Table 1. 3 Turbulence-chemistry interaction models extension situation

Standard Models	Extensions
EDC	EDC modifying model constant: • Model constant are arbitrary change. • Calibration with experimental data is necessary.
	E-EDC

	• Model constant are calculated as a function of local Reynolds and local Damköhler numbers depending or arbitrary proportionalities. $$C_\xi \propto f_1(Re_T, Da^*)$$ $$C_\tau \propto f_2(Re_T, Da^*)$$
	Generalized E-EDC • Follows E-EDC model assumptions but eliminates the proportionality factor in laminar flame velocity following the NE-EDC suggestions $$C_\xi = f_3(Re_T, Da^*)$$ $$C_\tau = f_4(Re_T, Da^*)$$ • Chemical time scale is calculated considering CH_4, CO, H_2, O_2 and CO_2 species and not on CH_4 1-step global mechanism
FGM and FPV (Flamelet based models)	E-FPV • Additional conserved scalar is included to consider dilution • Only applicable with controlled dilution stream (JHC burners)
	D-FPV • Applicable with no controlled dilution stream • A transport equation is considered for dilution variable • Flamelet tables are generated as laminar counterflow flames considering diluted fuel, diluted air streams and heat loss • Only the mixture of fuel and diluent is considered in tabulated tables, the possible reaction of fuel and the air molecules in diluent when there is a lean combustion is not considered.
	DHR • It is based on Homogeneous Reactor

Analysis of thermofluids in flameless (MILD)
combustion: assessment, improvement and
development of combustion models by CFD
Naiara Romero Anton

| | Tabulates homogeneous auto-ignition trajectories Convective and diffusive effect of the flow are not considered A transport equation is not considered for dilution variable. The dilution level is divided in a non-reactive and a reactive part, which is less accurately than considering a transport equation for dilution variable. |
| | DA-FGM Applicable with no controlled dilution stream A transport equation is considered for dilution variable Flamelet tables are generated as laminar counterflow flames considering fuel and diluted air streams and heat loss Only implemented in OpenFOAM package |

3 Motivation and objectives

Climate and Energy framework commitment for 2030 rely on the energy efficiency improvement and greenhouses emissions reduction. After analysing DOE's word energy consumption data, it is concluded that today and in the future fossil fuels combustion will be the primary source energy consumption. Therefore, it is crucial to research in combustion techniques to reduce greenhouses emission and improve combustion efficiency.

Most industrial installations, such as, thermal power plants, refineries, chemical industry, ceramic, glass, cement and steel factories and paper mill have a combustion process along a furnace or a boiler furnace. Due to that, in this work there is a motivation towards understanding the fundamentals of flameless combustion by numerical modelling on a lab-scale furnace. This would lead new opportunities to improve furnace design, and consequently, increase combustion efficiency and reduce emissions in industrial scale

equipment. In this work, flameless combustion technology is selected due to its attractive characteristics of low NO_x emissions and efficiency improvement.

Flameless combustion is based on the aerodynamic recirculation of flue gas inside the furnace to dilute fuel and air stream, reducing O_2 concentration. The additional inert molecules of the diluent stream act as a heat sink reducing flame temperature, consequently thermal NO_x emissions are reduced. At the same time, if diluted stream is used to preheat reactants, the efficiency increases.

In this work ANSYS Fluent package is selected with the goal to contribute to the search for an accurate and computationally affordable turbulence-chemistry interaction model, which can be suitable for the accurate simulation of flameless combustion. The already developed turbulent-chemistry interaction models do not simulate flameless combustion accurately in their standard form, as they over predict combustion temperature. Therefore, extended models are needed. In order to take a compromise between computational time and detailed chemistry, in this work the EDC model (based on micromixing concept) and the FGM model (based on flamelet idea) are chosen for flameless modelling. There have been taken also as reference the cases in the literature where a good agreement was found between the predictions of these extended models and the experimental data (De et al., 2011; Huang, X. et al., 2017; Huang, Xu, 2018; Parente, Alessandro et al., 2016).

The extensions of the EDC model proposed in the literature are mainly three. The first one modifies the EDC model constants arbitrary for each application and calibrate them with experimental data (here called "EDC mod"). The second one, the E-EDC model, which calculates the EDC model constant as a function of local Damköhler and Reynolds number (improving the "EDC mod" model as model constant calibration is not necessary). Later, the Generalized E-EDC model was proposed to include the DNS findings which suggest interactions among the reaction zones. Both, the E-EDC and the Generalized E-EDC model, are applied to a JHC burner with controlled coflow.

Due to that, this work was motivated to develop and test, with Delft lab-scale furnace experimental data (an enclosed furnace without controlled coflow), a New-Extended EDC

Analysis of thermofluids in flameless (MILD)
combustion: assessment, improvement and
development of combustion models by CFD
Naiara Romero Anton

model, which can predict better flameless combustion. Following a similar analysis to that used in the E-EDC model, in the NE-EDC model, the model coefficients are calculated based on the local Reynolds and the Kolmogorov scale Damköhler numbers. Both, the E-EDC and the NE-EDC, introduce fine structures that characterize chemical conversion. They differ in the postulated length scale of the structures but agree in giving them the turbulent velocity as velocity scale. The E-EDC associates a length scale of the type laminar flame thickness, obtained as product of laminar flame speed and chemical time scale. On the other hand, the NE-EDC associates the Kolmogorov scale with the structures and avoids the need for a calibration of proportionality factor in an expression for laminar flame speed. Additionally, in this work the Generalized NE-EDC model is developed including the DNS modelling findings suggesting interaction among the reaction zones.

On the other side, the FGM model presents lower computational time than the EDC model using detailed chemistry. Therefore, it is an attractive model to be used on flameless combustion and analyse its accuracy for the current application. Among the extension of flamelet based models which considers dilution, the DA-FGM model presents more advantages than others do (see chapter 4), but this model is only implemented in OpenFOAM package. Therefore, there is a motivation to implement the DA-FGM model in ANSYS Fluent package and analyse its capabilities and limitations, as ANSYS Fluent is the most extended CFD simulation package in engineering companies.

Table 1. 4 Motivations of the work

Literature		Motivation of the Present work	
EDC mod	C_τ and C_ξ arbitrary change for each set up.	**EDC mod**	Parametric study for Delft lab-scale flameless furnace
E-EDC (Parente, Alessandro et al., 2016)	$C_\xi \propto f_1(Re_T, Da^*)$ $C_\tau \propto f_2(Re_T, Da^*)$	**NE-EDC** (developed)	$C_\xi = f_5(Re_T, Da^*)$ $C_\tau = f_6(Re_T, Da^*)$

Generalized E-EDC (Evans et al., 2019)	$C_\xi = f_3(Re_T, Da^*)$ $C_\tau = f_4(Re_T, Da^*)$ $\tau_c = \max\left[{Y_k}\Big/{\left(|\dot\omega_k|\big/\rho\right)}\right]$ $\dot\omega_k$ of CH_4, O_2, CO and CO_2	**Generalized NE-EDC** **(developed)**	$C_\xi = f_5(Re_T, Da^*)$ $C_\tau = f_6(Re_T, Da^*)$ $\tau_c = \max\left[{Y_k}\Big/{\left(|\dot\omega_k|\big/\rho\right)}\right]$ $\dot\omega_k$ of CH_4, O_2, CO and CO_2
DA-FGM	Implemented in OpenFOAM	**DA-FGM (develop implementation)**	First time implemented in ANSYS Fluent

Therefore, the following objectives, which are divided in main and secondary objectives, are pursued in this Thesis:

Main objectives:

1. State of the art analysis to detect weak points and limitations in the modelling of flameless combustion.

2. Study the applicability of two different turbulence-chemistry interaction models; the EDC model (based on local micromixing structure) and the FGM model (following flamelet approach).

3. Develop a methodology for the new extended EDC model (NE-EDC) in order to be able to better predict flameless combustion. The model coefficients are space dependent as a function of the local Reynolds and Damköhler numbers in order to consider the influence of the dilution on the reaction rate and temperature.

4. Update the NE-EDC model by the Generalized NE-EDC which includes the interaction among the reaction zones.

5. Implement in ANSYS Fluent the DA-FGM model in order to include the effect of recirculated products during flamelets generation. This generalization of the FGM model is not among the default options offered by ANSYS Fluent.

6. Obtain conclusions on the suitability of each model.

Analysis of thermofluids in flameless (MILD)
combustion: assessment, improvement and
development of combustion models by CFD
Naiara Romero Anton

Secondary objectives:

1. Experimental analysis of flameless combustion in a lab-scale furnace.

2. Analyse the EDC model's constants influence in flameless combustion on lab-scale-furnace, derived a parametric analysis of the EDC model coefficients optimized for Delft lab-scale furnace and compare modelling results with experimental data.

3. Check the accuracy of Flamelet Generated Manifold (FGM) model with pure fuel and air as boundary conditions for flamelet generation for Delft lab-scale furnace.

4. Compare different global reaction mechanism for a more accurate time scale calculation for flameless combustion.

5. Comparison between developed models and experimental data.

4 Outline of the Thesis

This Thesis is a contribution to the search for an accurate and computationally affordable turbulence-chemistry interaction model, which can be suitable for the accurate simulation of flameless combustion. Delft lab-sale furnace is chosen for numerical modelling of flameless combustion, as experimental data was available from a previous work (Huang, Xu, 2018). The availability of this data is a consequence of the close research collaboration between the PhD student of this Thesis and the Department of Process and Energy of the Delft University of Technology. The contributions of this Thesis are developed throughout the 6 chapters of the Thesis.

This chapter, **Chapter 1**, introduces the energy framework and current energy consumption and future predictions, outlining the motivation and objectives of this Thesis. The state of the art is analysed for flameless combustion; the experimental flameless combustion setups as well as the last extended EDC based models and the flamelet based models.

Chapter 2 explains the advantage of using flameless combustion in furnaces and then Delft lab-scale furnace is described. The experimental data available and measurement techniques used in Delft lab-scale furnace are briefly described. Then, a brief description

of the theories of computational modelling for turbulent non-premix combustion is introduced. Finally, the boundary conditions, physical models and computational domain used for the Delft lab-scale furnace modelling in ANSYS Fluent package are defined.

Chapter 3 introduces the basic concepts of the standard EDC model and analyses the influence of the model constant in reaction rate and temperature. A parametric study is carried out in order to optimize the EDC model coefficients for the Delft-lab-scale furnace. The NE-EDC model methodology is described with the entire mathematical process and then, the Generalized NE-EDC model is developed, which includes the interaction among the reaction zones suggested by the DNS numerical modelling. A comparative study of the four models is carried out: the E-EDC model, the NE-EDC model, the Generalized NE-EDC and the EDC model with specific and fixed values of the model coefficients optimized for the current application. The models are validated using experimental data of the Delft Lab Scale furnace (9kW) burning Natural Gas (T=446 K) and preheated air (T=886 K) injected via separate jets, at overall equivalence ratio 0.8.

Then **Chapter 4** introduces the basic concepts and theories of flamelet based models. The FGM model advantages comparing with the other models are discussed and its selection is justified. Then, the DA-FGM model implementation methodology in ANSYS Fluent is described, stressing the limitations of this modelling package. In ANSYS Fluent, it is not possible to generate flamelets and PDF tables considering the dilution variable, therefore, those tables are generated outside ANSYS Fluent and later, by User Define Function (UDF), those tables are implemented in ANSYS FLUENT. Several 4-dimension (4D) and 6-dimension (6D) tables are loaded into ANSYS Fluent, therefore index finding and 4D and 6D interpolation is coded inside UDF. Additionally, as dilution variable is not considered, its transport equation is included through User Define Scalar (UDS). Finally, modelling results of both models are compared with experimental data and the first conclusions are drawn

Chapter 5 is a summary of chapters 3 and 4, where the existing models in the literature are applied to Delft lab-scale furnace (Parente et al. for the E-EDC, and the FGM of Oijen) and modelling results are compared with experimental data. After checking the possible

advantages and disadvantages of existing models, developed models in this Thesis, the Generalized NE-EDC model and the implementation of the DA-FGM model, are compared with experimental data.

Finally, the main conclusions reached in the Thesis, the contributions made and the future research lines are made in **chapter 6**.

2 annexed are included at the end of the document:

- Annex A) Generalized NE-EDC model's UDF
- Annex B) DA-FGM model's UDF

CHAPTER 2: FLAMELESS COMBUSTION IN FURNACES

1 Introduction

The main goals of industrial furnace design are to achieve a controlled, in general homogeneous, temperature distribution in every furnace zone, efficient energy use, energy savings and low pollutant emissions. Flameless combustion is a key technology towards obtaining these goals. It is based on the dilution of fuel and air stream by aerodynamic recirculation of the flue gas. The mixing with recirculated products is responsible for the main characteristics, such as, namely, diluted reaction zones, uniform temperature distribution, non-visible or audible flames and low thermal NO_x emissions. Flameless combustion was first studied in high temperature furnaces in the 1990s in Japan (Hiroshi Tsuji et al., 2002) to reduce NO_x emissions, and later in Germany (Wünning & Wünning, 1997) in the context of recuperative and regenerative FLOX burners.

When flameless combustion technology is applied in a large-scale furnace, a first principle is to use heat from combustion products to preheat reactants (above autoignition temperature). Due to that, energy efficiency is increased and fuel savings are obtained. This feature already implies reduction of CO_2 and NO_x emissions but additionally, in flameless combustion reactants are also diluted (O_2 levels <15%) which implies lower flame temperature and homogeneous temperature distribution along the furnace reducing thermal NO_x emissions.

Experiments carried out in flameless combustion showed spatial temperature fluctuation of 15% while in conventional combustion it is a 50% (Kumar et al., 2002). Another advantage discovered of flameless combustion is its stability, and as reactants are preheated above auto-ignition temperature, high-velocity jets can be used (Cavaliere & de Joannon, 2004). These characteristics (high velocity jets and preheated reactants) make larger and more uniform heat flux (convective and radiative heat transfer increases) throughout the combustion chamber providing opportunities for energy savings.

As an example of energy savings, three combustion systems were compared using a CFD code with the objective of getting a net power of 160 kW (Wünning & Wünning, 1997). The first combustion system was a burner without preheated air, and the required burner capacity was 400 kW. Then, using a heat recovery unit the air was preheated (600°C) and the required power input was 245 kW. Finally, with a FLOX regenerative system (a flameless combustion burner) the air was preheated (950°C) and 200kW were required. Therefore, it was concluded that FLOX regenerative system provided more energy savings than the other systems.

Although the potential of flameless combustion in industrial application is large, the lack of soundly based validated models in large-scale furnaces has only been an obstacle for widespread the use of this promising technology. Due to that, a few simulations vs. experimental studies in industrial furnaces can be found in the literature, see Table 2. 1. The Royal Institute of Technology (KTH) simulated a semi-industrial furnace of 200 kW$_{th}$ (Weihong & Wlodzimierz, 2006) by STAR-CD CFD package in order to understand better the fundamentals of flameless combustion. The International Flame Research Foundation (IFRF) modeled in Fluent a 1000 kW$_{th}$ flameless furnace (Hekkens & Mancini, 2004). Researchers of Mons University made extensive studies of a 200kW$_{th}$ natural gas flameless combustion furnace, including Fluent modelling (Lupant, Delphine et al., 2006). The Nippon Kokan Kaisha (NKK) steel corporation in Japan (Ishii et al., 2002) also used the Fluent CFD package to simulate regenerative reheating furnaces with Low Calorific Value fuel. At Delft University of Technology (DUT), a detailed CFD simulation was carried out on a 300 kW$_{th}$ multi-burner flameless combustion furnace (Danon et al., 2011a)).

In those works, the used turbulence-chemistry interaction models were the simple models (EDM, Finite Rate (FR) and EBU) and micromixing based models (PDF and EDC). Simulation results showed that temperature was always over predicted with the use of those models in their standard mode. In order to improve mean temperature prediction extended turbulence-chemistry interaction models should be studied. One solution could be the use of a more detail chemistry mechanism in combination with a turbulence-chemistry interaction model considering it. Nevertheless, the required computational time in industrial modelling configuration will be too much higher than the 1 or 2 step mechanism and the simple models already used (see Table 2. 1). Therefore, lab-scale furnaces setups are becoming attractive for flameless modelling study. First because more detail chemistry mechanism can be used in these set ups. Second, extended and improved turbulence-chemistry interaction models can be used (due to the lower computational time required by them). Finally, in contrast with larger furnaces, lab-scale furnace configurations can be fully accessible for non-intrusive measurements, so that detailed statistics of velocity and temperature can be available for model validation.

Considering the advantages presented by the lab-scale furnace (compared to the industrial furnaces) in this Thesis, the Delft lab-scale flameless combustion furnace has been used for which detailed in-furnace velocity and temperature experimental data are available.

Table 2. 1 Industrial furnace numerical modelling

Ref.	Turbulence model	Chemical mechanism	Turbulence-chemistry Interaction	Radiation	Measurement Technique
KHT	Standard k-ε	2-step	ED/FR	DTM	Intrusive Probes & Thermocouple
IFRF	Standard k-ε	2-step	β-PDF equilibrium, B-PDF flamelet, EBU	DO	Intrusive Probes & Thermocouple LDA

MONS	Standard k-ε	1-step	β-PDF equilibrium, ED/FR	DO	Intrusive Probes & Thermocouple CCD camera for OH
NKK	Standard k-ε	15 species	β-PDF equilibrium	P1	Intrusive Probes & Thermocouple
DUT	Realizable k-ε	16 species	EDC	DO + WSGGM	Intrusive Probes & Thermocouple

In the literature, other lab-scale furnace can be found. The Rheinisch-Westfälische Technische Hochschule (RWTH) Aachen furnace (Plessing et al., 1998a), the Technical University of Lisbon furnace (Veríssimo et al., 2011; Veríssimo et al., 2013a; Veríssimo et al., 2013b; Veríssimo et al., 2015), the University of Adelaide furnace (Szegö et al., 2008), the University of Mons furnace (Lupant, D. et al., 2007; Lupant, Delphine & Lybaert, 2015) and the University of Federico II di Napoli furnace (Sabia et al., 2019; Sorrentino, G. et al., 2017; Sorrentino, Giancarlo et al., 2015). However, the advantages of the Delft lab-scale furnace over those mentioned above are that (1) the furnace is optically accessible via small windows in the sidewall, so that, detailed statistics of velocity and temperature are available for model validation, (2) it does not have cooling tubes inserted as heat sink into the furnace (like happens in Mons furnace) which could alter the flow path of recirculated products and finally, (3) Laser Doppler Anemometry (LDA) and Coherent Anti-stokes Raman Spectroscopy (CARS) experimental data are available. Table 2. 2 shows a summary of commented above lab-scale furnace shape, power and measurement techniques.

Table 2. 2 lab-scale furnaces features

Furnace	Shape	Power (kW)	Measurement Technique
Aachen	Parallelepiped	5-10 kW	OH-PLIF
Lisbon	Cylindrical	6-13 kW	Temp. point measurement

Adelaide	Parallelepiped	7.5-20 kW	Temp. point measurement
Mons	Parallelepiped	30 kW	Temp. point measurement Species point measurement
Napoli	Cyclonic Chamber	2 kW	Photography (OH) Temp. point measurement
Delft	Parallelepiped	9 kW	CARS LDA

In this work apart from turbulence predictions, several turbulence-chemistry interactions models are compared with the goal of finding an accurate and efficient model for flameless combustion modelling. Next, Delft lab-scale furnace configuration, description and measurement techniques are described (subsection 2) and later the computational modelling is explained (subsection 3).

2 Experimental Lab-Scale Furnace

The database used for model validation has been created by experimental measurements in the Delft lab-scale furnace performed by Huang (Huang, Xu, 2018). The burner and the furnace are first described and then the numerical setup.

2.1 Configuration

The geometry of the Delft lab-scale furnace is shown in Fig. 2. 1. The furnace can operate in flameless mode thanks to the recuperative burner injecting fuel and preheated air in separate high momentum jets.
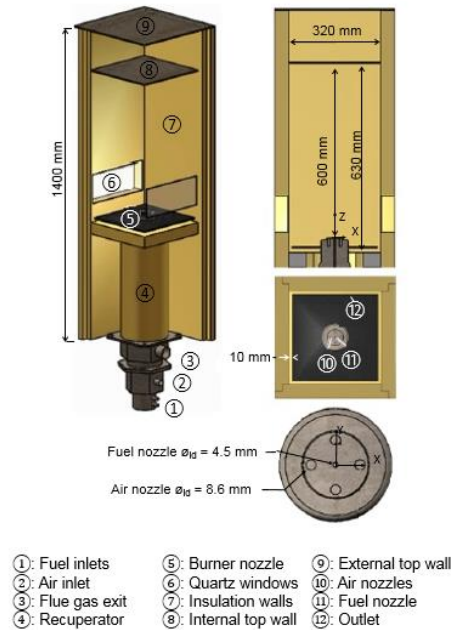
Fig. 2. 1. Delft Lab-scale furnace (Huang, Xu, 2018)

The internal dimensions of the furnace are 320 mm x 320 mm x 630 mm. The burner nozzle system is located at the bottom and consists of a central fuel nozzle ($\varnothing_{id}$ = 4.5 mm) surrounded by four air nozzles ($\varnothing_{id}$ = 8.6 mm). The nozzles protrude into the furnace by 30 mm, making the distance from the burner nozzle tip to the internal top wall equal to 600 mm. The flue gas outlet is a slit near the walls in the bottom plane, close to the burner (see point 12 of Fig. 2. 1). The start-up of the furnace is done using the injection of premixed fuel and air through the four outer nozzles. Once the furnace is preheated to 1123 K (850°C), the burner is switched to injection for flameless mode with a non-premixed fuel and air combustion (fuel in the centre and air in the outer nozzles). The combustion gases leaving the furnace are traversing a heat exchanger to preheat the air to a maximum temperature of 973 K (700°C).

The experimental measurements, which are used to validate modelling results, are obtained when the furnace operates with Dutch natural gas (mole fractions: CH_4 81.3%, C_2H_6 3.7%, N_2 14.4% and the rest 6%), which is injected into the furnace at 446 K, and the preheated air is injected at 886 K. The thermal input power of the burner is 9 kW. Experimental data was obtained for several equivalence ratios; 0.7, 0.8 and 0.9. The velocity and temperature measurements have been made, respectively, using LDA and

CARS (Table 2. 3 provides information on reported measurement accuracy). It should be noted that it is an optically accessible furnace via small windows in the sidewall (see Fig. 2. 1), with one window used for LDA in backscatter mode and two windows for CARS. A Testo 335 flue gas analyser was used for product composition measurement, which has a resolution of 1 ppm for both CO and NO_x while the inaccuracy for CO measurement is ± 10 ppm reading at 0-200 ppm for NO_2. The flow rates of fuel and air are measured using Bronkhorst mass flow controllers with an inaccuracy of $\pm 0.5\%$ reading plus $\pm 0.1\%$ full scale. Finally, super OMEGACLADTM XL sheathed ungrounded thermocouples type K were used for flue gas and wall temperature measurement.

Table 2. 3 Technique and reported accuracy of the measured variables

Variable	Technique	Reported Accuracy
Velocity	LDA	2-8%
Temperature	CARS	20 K

To enable a fixed position of the optical equipment, the burner and top wall of the furnace are moved vertically to the appropriate position for taking measurements at a specific height above the nozzle exit. The top wall of the furnace acts as a heat sink. The side walls are well insulated, thus minimizing heat losses.

The measured experimental profiles do not have the mirror symmetry that would follow from the furnace design. This is attributed to the asymmetry in the fuel and air supply system upstream of the furnace. To prepare for a fair comparison with the results of computations using perfectly symmetric inlets, all experimental mean profiles have been shifted in space in order to obtain close to symmetric results before comparing with the model results (chapter 3, 4 and 5). As an example of space shift see Fig. 2. 2, which illustrates the mean temperature profile at z=100 mm height for original and shifted experimental data.

Analysis of thermofluids in flameless (MILD)
combustion: assessment, improvement and
development of combustion models by CFD
Naiara Romero Anton
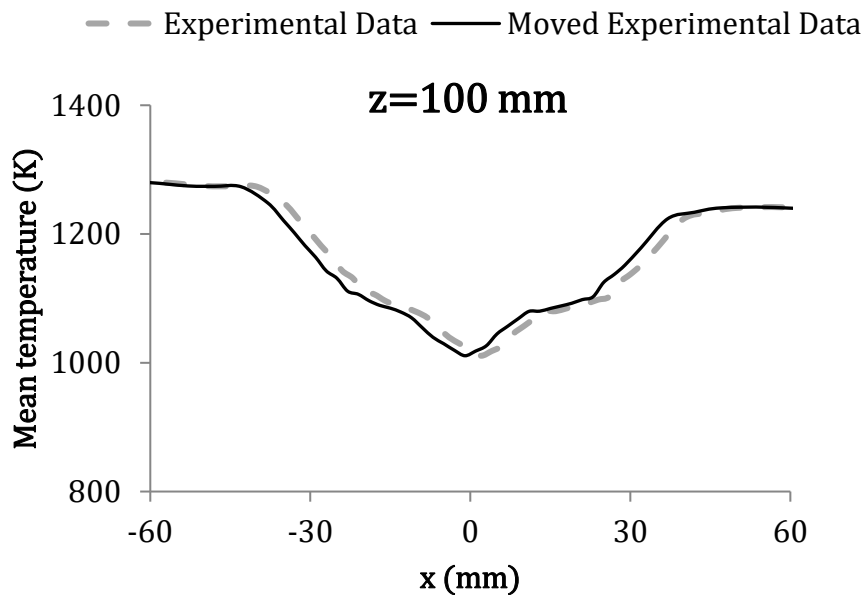
Fig. 2. 2 Experimental mean profiles shifting

2.2 Measurements techniques

The main goal of the data collection in Delft-lab scale furnace was to use non-intrusive techniques in order to not alter the flow path along the furnace height. Due to that, LDA for velocity measurement and CARS for flue gases temperature measurement were selected. It should be mention that comparing with the setups of Table 2. 2 Delft lab-scale furnace uses CARS for a more accurate temperature measurement and not thermocouples, except to Aachen with used LIF.

2.2.1 Laser Doppler Anemometry (LDA)

This measurement technique is widely accepted for turbulence flows velocity measurement since 1964 (Yeh & Cummins, 1964) and it is based on Doppler Effect. Small particles are introduced into the flow moving with it, so that particle velocity is the same as flow velocity. The velocity magnitude is measured by light scattered by the particles. Two lasers intersection provide a band with shiny and dark lights. When a particle goes through the band, the particle scatters light when is crossing the shiny line and does not scatter light through the dark line. Therefore, there is a shift in frequency (also known as Doppler frequency) related to the scattered light frequency. This Droppler shift is related with the particle velocity and with the flow velocity, providing the measurement of flue

gases velocity. Nevertheless, dropper efficiency tells us the scalar magnitude of the velocity but not the direction. In order to consider the direction, one beam frequency is shifted to a known value, thanks to that, particles frequency can be compared with known beam frequency and direction can be defined.

In the particle selection there are appreciated the low-cost particles with non-reactive and non-toxic characteristics, but specific optical and dynamic features are needed, for example, scattered light intensity. In Delft lab-scale furnace measurements, alumina oxide particles (Al_2O_3) of 1 μm diameter were added to the flow.

A sketch of the used LDA is shown on Fig. 2. 3. By a Doppler Power DPSS laser with 2x1W blue line (488 nm) and green line (514 nm) local instantaneous values of two velocity components (vertical and horizontal) were determined.
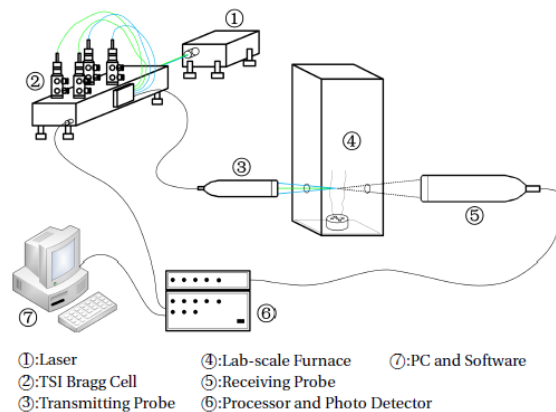
Fig. 2. 3 LDA setup (Huang, Xu, 2018)

The main advantages of LDA are that it is a non-intrusive technique and its capacity for flow direction detection. Thanks to that, the LDA enables the possibility to measure flow reversal, velocity magnitude and direction. It should be noted its simplicity for calibration, as one calibration factor is only needed. Nevertheless, it is a complex measuring technique which required experienced operator.

2.2.2   Coherent Anti-Stokes Raman Spectroscopy (CARS)

This method is based on non-intrusive diagnostic technique and it is practical for both temperature and species concentration measurement (Eckbreth, 1998). In addition, it can be also applied to measure temperature close to surfaces with quite good resolution (100

µm), that is way it is a recommended technique for closures devices. The advantages of CARS are the strong signal and the good temporal and spatial resolution in gas-phase flows.

CARS is a third-order nonlinear optical process comprised by three laser beams; pump beam (with w_p frequency), Stoke beam (with w_s frequency), and one probe beam (with w_{pr} frequency), which match in one probe volume generating a fourth beam (CARS beam) with an anti-stoke frequency $w_{as} = w_p + w_{pr} - w_s$. Anti-stoke frequency w_{as} is developed only when $w_p - w_s$ is equal to Raman allowed transition (see Fig. 2. 4 CARS energy level sketch).
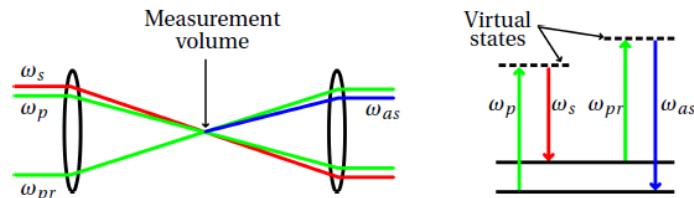
Fig. 2. 4 Coherent anti-Stokes Raman spectroscopy optical distribution (left) and energy level sketch. (Huang, Xu, 2018)

Signal generation depends on the concentration probe. In fuel-air flames, the N2 is chosen as probe molecule due to its huge concentration. Therefore, in Delft lab-scale furnace diagnostic analysis N2 has been chosen as probe molecule. The sketch of the used CARS system is shown on Fig. 2. 5.

N2-CARS was used for local instantaneous temperature measurements. An Nd: YAG Laser is used as pump laser, which a maximum pulse energy of 500 mJ at 532 nm and repetition rate of 10 Hz. The 80% of the pulse energy is used to pump a modeless dye laser (Mode-X ML-3). By Rhodamine 640 in methanol a Stoke beam is generated and the remaining 20% of pulse energy goes through a delay path where it is divided into two beams; pump and the probe beam. Then by the BOXCARS technique (Eckbreth, 1978), beams are matched. The beams pass a focus lens (300 mm) and enter the furnace, crossing in the probe volume. The outgoing beams, after passing through a receiving optics, go to the Spectrometer and finally the information goes to a PC where measured spectra are converted to temperature, for more details see (Huang, Xu, 2018).

①:Nd: YAG Laser ④:Focus Lens   ⑦:Spectrometer and CCD
②:Dye Laser   ⑤:Lab-scale Furnace ⑧:PC and Software
③:Delay path   ⑥:Receiving Optics
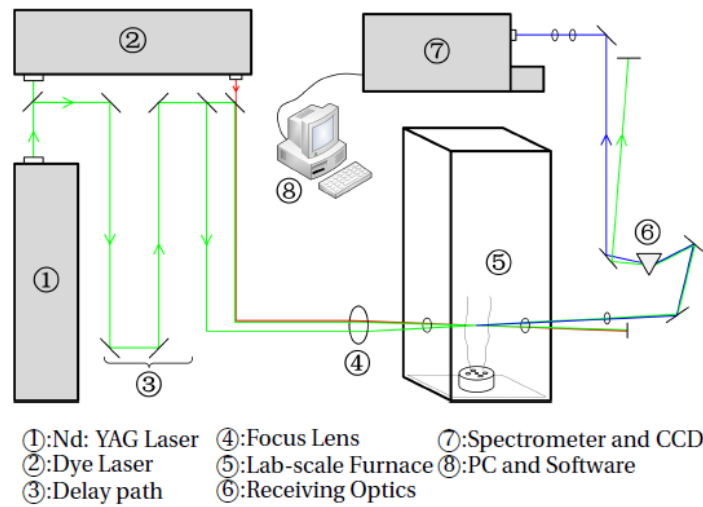
Fig. 2. 5 CARS layout used in Delft-lab scale furnace diagnostic analysis (Huang, Xu, 2018)

2.3 Measured temperature and velocity values

Diagnostic analysis was made in Delft lab-scale furnace burning Dutch natural gas (see composition in Table 2. 4), operating at 9kW and with three different equivalence ratios: case1 ψ =0.7, case 2 ψ =0.8 and case 3 ψ =0.9 (Huang, Xu, 2018)

Table 2. 4 Natural gas composition applied in this work

Species	CH_4	C_2H_6	N_2	Rest
Mole %	81.3	3.7	14.4	0.6

Temperature (see Fig. 2. 6) and velocity (see Fig. 2. 7) measurements were taken in the cross plane of fuel and air jets at different heights (z) of the furnace for the three equivalence ratio cases. The first plane of measurement is located at the exit of fuel and air nozzles. Velocity profiles were taken for z=3, 50, 100, 200, 300, 400 and 500 mm heights while temperature profiles were taken for z=3, 15, 100, 200, 300, 400 and 500 mm heights.
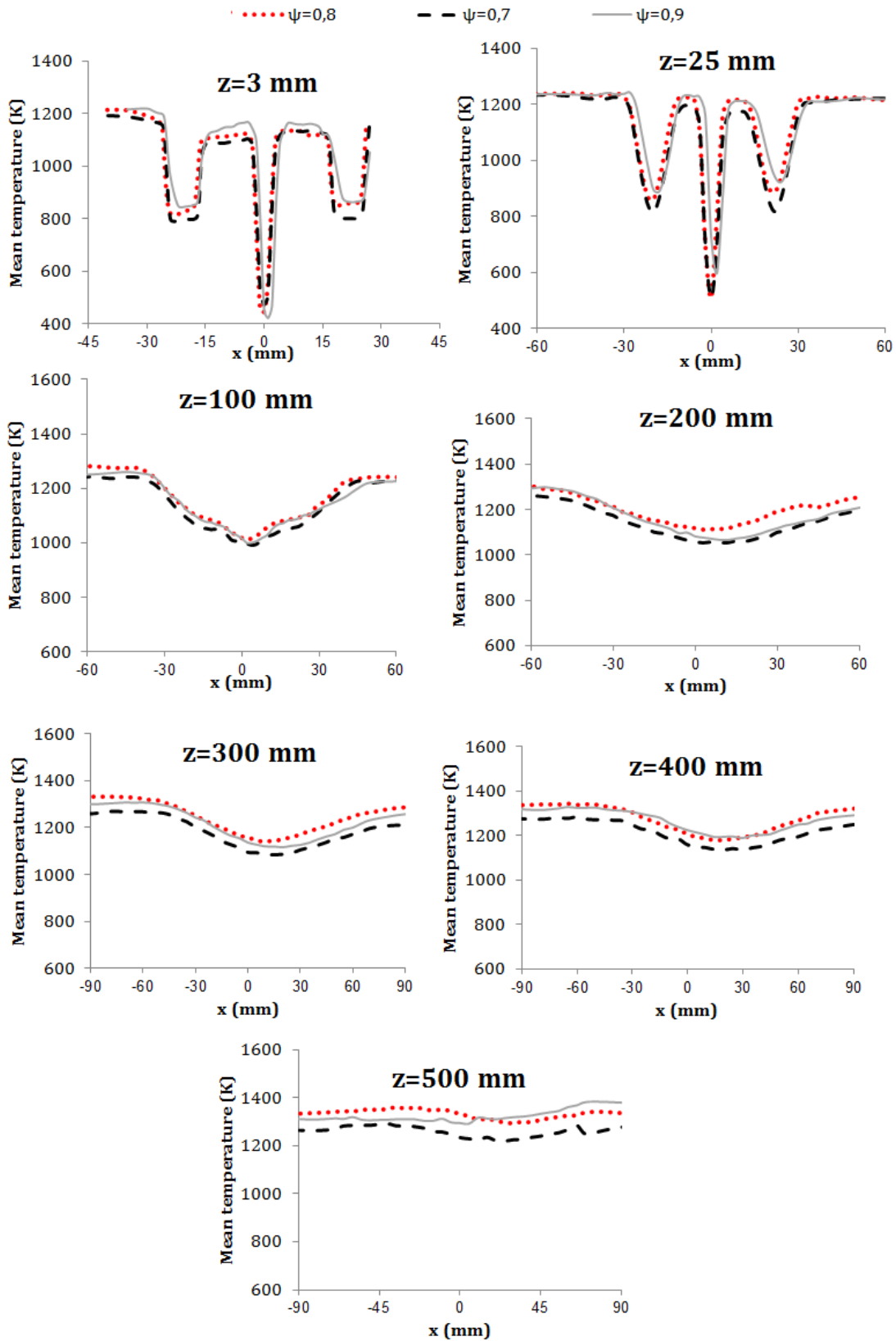
Fig. 2. 6 Measured mean temperature profile for different equivalence ration, ψ =0.7, 0.8 and 0.9
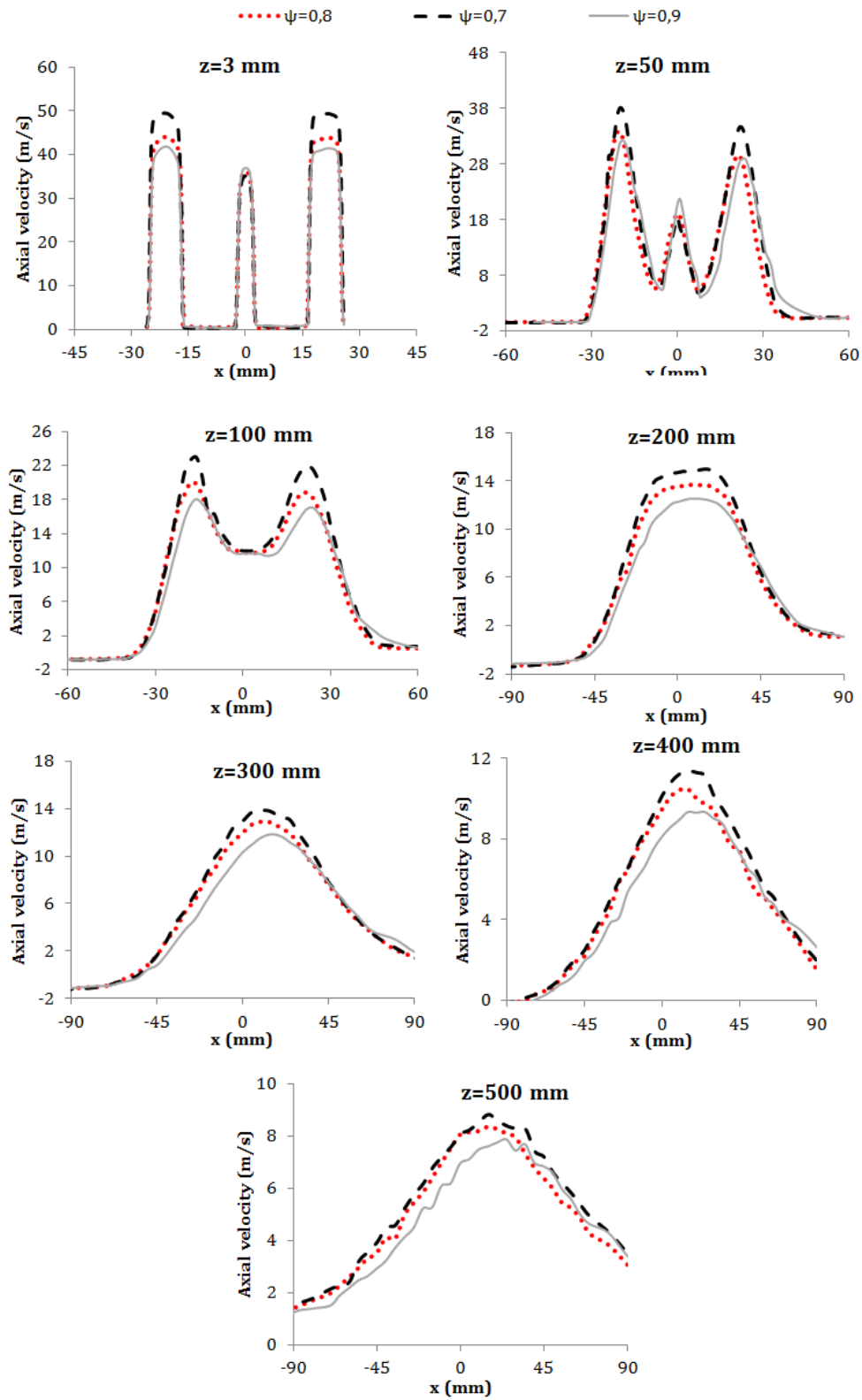
Fig. 2. 7 Measured axial mean velocity profile (U_z) for different equivalence ration, ψ =0.7, 0.8 and 0.9

It can be concluded that in both cases, peak temperature and velocity values are displaced some millimetres from the centre (x=0 mm) of the furnace. This is attributed to the asymmetry in the fuel and air supply system upstream of the furnace. To prepare for a fair comparison with the results of computations using perfectly symmetric inlets, all experimental mean profiles have been shifted in space in order to obtain close to symmetric results before comparison with the model results. The measured profiles of mean velocity, turbulent kinetic energy and mean temperature data, from z=100 to z=500 mm, have been moved by a distance of $z * tan(\theta)$ before comparing them with the predictions. The value of the angle θ is obtained considering that the shear stress has a value equal to zero on the centreline and is $\theta \approx 0.03$.

Mean temperature profile at z=3 mm shows the same behaviour for the three cases. This position is too close to the nozzles exit, due to that the values at this position has been considered as inlet boundary conditions for modelling. At z=25 mm air nozzles and fuel nozzles are differentiated. At this height temperature values are quite similar to the previous position, only a slight temperature increase can be appreciated. This can be because at this height flue gas recirculation starts diluting and preheating reactants, but the reaction has not happened yet. On the next height, z=100 mm, fuel and air jets start to disappear getting a more homogeneous temperature distribution but at z=200 mm they complete vanish. At this height, it is appreciated that there is a maximum temperature for case 2 and a minimum temperature for case 1. It was expected to have a higher temperature in case 3 but at this height it does not happen. As the flows develops (z=300 and z=400 mm) more homogeneous temperature is reached and case 2 is still the case with maximum temperature values. Finally, for the last measurement height, the temperature profile follows nearly a horizontal line and in the x positive side case 3 temperature value starts being above case 2 mean temperature value. This is related with the reaction zone location. According to the OH cheminulescense images (see Fig. 2. 8), for cases 1 and 2 the reaction rate zone is located between 450 mm and 550 mm above the burner nozzle while for case 3 the reaction zone is located at 510-600 mm above the burner nozzle. Due to that the heat release in case 3 starts in the last height of the furnace and that is way its temperature is below case 2 in the lower heights of the furnace.
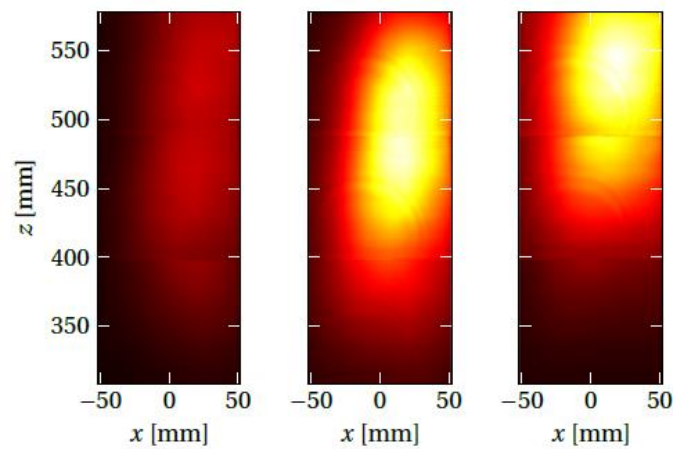
Fig. 2. 8 Mean OH* chemiluminescence intensity images. Left: case 1, middle: case 2, right: case 3. (Huang, Xu, 2018)

To finish with mean temperature analysis it can be said that the reaction rate influence on the mean temperature profile starts happening at z=200 mm, up to this height reactants are preheated and diluted by combustion gases recirculation (not by reaction rate).

Then, analysing mean velocity profiles, at z= 3mm, a peak value is observed for case 1, this is because in this case more air mass flow is introduced in the burner in order to get a leaner combustion. The data at this height is really close to nozzles exit, due to that the values at this position are considered as inlet boundary conditions. At z=50 mm air jets and fuel jets are still distinguished, this is because at this point air and fuel nozzles are still diluted by recirculating products, but reaction does not happen yet. At next height, z=100 mm, fuel jet disappears but air jets are still displayed. When the flows develop (z=200 mm) fuel and air jets disappear and a bell type velocity profile appears. In the next heights, z=300, z=400 and z=500, the velocity profile is maintained with the same shape.

Among the three cases, the modelling in this Thesis are carried out for the case with an equivalence ratio of 0.8.

Analysis of thermofluids in flameless (MILD)
combustion: assessment, improvement and
development of combustion models by CFD
Naiara Romero Anton

3 Computational modelling

Delft lab-scale furnace operates in flameless mode as non-premix turbulence combustion. The non-premixed turbulence combustion (also called diffusion) is widely used in industry systems as burner design is simpler (reactants mixing happens naturally outside of burner geometry) and also because it is a safer combustion technique (flame propagation is not possible as fuel and oxidizer are not mixed before entering the furnace).

Mixing of fuel and oxidizer inside the furnace is the most important characteristic in non-premix turbulence combustion system. Mixture fraction (Z) parameter is used to define reactants mixture as described fuel and oxidizer proportion, where Z=1 for pure fuel and Z=0 for pure oxidizer. It is defined by Bilger formulation, Eq. 2. 1, (Bilger et al., 1990):

$$Z = \frac{\dot{m}_f}{\dot{m}_f + \dot{m}_{ox}} = \frac{sY_f - Y_{ox} + Y_{ox}{}^0}{sY_f{}^1 + Y_{ox}{}^0} = \frac{f - f}{f_1 - f_0} \qquad \text{Eq. 2. 1}$$

Where $\dot{m}_f$ and $\dot{m}_{ox}$ are fuel and oxidizer mass flow rate, s stoichiometric mass ratio, Y_f and Y_{ox} fuel and oxidizer mass fraction, 0 denotes oxidizer inlet stream, 1 fuel inlet stream and β a passive scalar defined as $\beta = sY_f - Y_{ox}$.

In stoichiometric mixture, fuel and oxygen are not present in the products, therefore, the stoichiometric mixture fraction is calculated as:

$$Z_{st} = \frac{Y_{ox}{}^0}{sY_f{}^1 + Y_{ox}{}^0} \qquad \text{Eq. 2. 2}$$

It should be mention that when $Z < Z_{st}$ there is a lean mixture $\left(Z = \frac{-Y_{ox} + Y_{ox}{}^0}{sY_f{}^1 + Y_{ox}{}^0}\right)$ and at $Z > Z_{st}$ there is a rich mixture $\left(Z = \frac{sY_f + Y_{ox}{}^0}{sY_f{}^1 + Y_{ox}{}^0}\right)$.

In this work Delft lab-scale furnace's turbulence non-premixed combustion is simulated by the ANSYS Fluent package. A three-dimensional steady-state Reynolds Averaged Navier Stokes (RANS) modelling has been made. Different chemistry-interaction models

are compared in this work while keeping the other sub-models the same: the realizable two-equation $k - \varepsilon$ turbulence model, the Discrete Ordinates (DO) method solving the radiative transfer equation in combination with the grey weighted-sum-of-grey-gases model (WSGGM) for the absorption coefficient. The chemical mechanism used in the EDC modelling is the smooke-25 with 17 species (Peeters, 1997) while Grimech30 mechanism with 53 species is used with the FGM and the DA-FGM model (P. Smith et al.,).

3.1 Averaging of computational equations

Reynolds averaging splits any f quantity into a mean $\bar{f}$ and fluctuating f' component:

$$f = \bar{f} + f'$$

<div align="right">Eq. 2. 3</div>

On density variable flows, Reynolds averaging introduce unclosed correlations between f quantity and density fluctuations $\overline{\rho' f'}$ (Poinsot & Veynante, 2005). In order to avoid this difficulty, mass-weighted averages ($\tilde{f}$), also called Favre averages, are used (Favre, A., 1969; Kuo, K. K., 2005):

$$\tilde{f} = \frac{\overline{\rho f}}{\bar{\rho}}$$

<div align="right">Eq. 2. 4</div>

and any f quantity can be divided into a mean and fluctuation component

$$f = \tilde{f} + f'' \text{ with } \widetilde{f''} = 0$$

<div align="right">Eq. 2. 5</div>

Considering that, Favre averaging equations are defined as:

Mass:

$$\frac{\partial \bar{\rho}}{\partial t} + \frac{\partial}{\partial x_i}(\bar{\rho} \tilde{u}_i) = 0$$

<div align="right">Eq. 2. 6</div>

Momentum:

Analysis of thermofluids in flameless (MILD)
combustion: assessment, improvement and
development of combustion models by CFD
Naiara Romero Anton

$$\frac{\partial \bar{\rho}\tilde{u}_i}{\partial t} + \frac{\partial}{\partial x_i}\left(\bar{\rho}\tilde{u}_i\tilde{u}_j\right) + \frac{\partial \bar{p}}{\partial x_j} = \frac{\partial}{\partial x_i}\left(\bar{\tau}_{ij} - \bar{\rho}\widetilde{u_i''u_j''}\right)$$

Eq. 2. 7

Chemical species:

$$\frac{\partial \bar{\rho}\tilde{Y}_k}{\partial t} + \frac{\partial}{\partial x_i}\left(\bar{\rho}\tilde{u}_i\tilde{Y}_k\right) = -\frac{\partial}{\partial x_i}\left(\overline{\rho D \frac{\partial Y_k}{\partial x_\iota}} + \bar{\rho}\widetilde{u_i''Y_k''}\right) + \overline{\dot{\omega}_k} \qquad for\ k = 1, N$$

Eq. 2. 8

Enthalpy:

Eq. 2. 9

$$\frac{\partial \bar{\rho}\tilde{h}}{\partial t} + \frac{\partial}{\partial x_i}\left(\bar{\rho}\tilde{u}_i\tilde{h}\right) = \frac{\partial}{\partial x_i}\left(\overline{\rho D \frac{\partial h}{\partial x_\iota}} - \bar{\rho}\widetilde{u_i''h''}\right) + S_r$$

These equations are solved by ANSYS Fluent. Nevertheless, in RANS modelling there are some unclosed terms on the Favre averaging equations which need to be modelled, such as Reynolds stresses $\widetilde{u_i''u_j''}$, species and enthalpy turbulent fluxes $\widetilde{u_i''Y_k''}$ and $\widetilde{u_i''h''}$, mean laminar diffusive fluxes for species and enthalpy $\overline{\rho D \frac{\partial Y_k}{\partial x_\iota}}$ and $\overline{\rho D \frac{\partial h}{\partial x_\iota}}$, species chemical reaction rates $\overline{\dot{\omega}_k}$ and radiation source term S_r.

Those unclosed terms are closed with specific models. In this work ANSYS Fluent default models has been chosen for unclosed terms modelling (realizable two-equation $k - \varepsilon$ turbulence model, DO and WSGGM), except for the reaction rate $\overline{\dot{\omega}_k}$, where the turbulence-chemistry interaction models developed in this Thesis has been used for its closure. Chapter 4 describes developed extensions of the EDC model for $\overline{\dot{\omega}_k}$ modelling and chapter 5 describes the DA-FGM model implementation in ANSYS Fluent for $\overline{\dot{\omega}_k}$ modelling (including the dilution effect in flamelets table generation).

The realizable two-equation $k - \varepsilon$ turbulence model closed the Reynolds stresses $\widetilde{u_i''u_j''}$ terms. This model is selected because it presents some advantages comparing to standard model: (1) In turbulent viscosity calculation, C_μ value is not constant anymore (Eq. 2. 15) and (2) a modified transport equation is used for the dissipation rate (ε) calculation (Eq. 2. 14). Following Boussinesq's turbulent viscosity assumption (Pope, 2000) Reynolds stresses can be defined as:

$$\bar{\rho}\widetilde{u_i'' u_j''} = \overline{\rho u_i'' u_j''} = -\mu_t \left(\frac{\partial \tilde{u}_i}{\partial x_j} + \frac{\partial \tilde{u}_j}{\partial x_i} - \frac{2}{3} \delta_{ij} \frac{\partial \tilde{u}_k}{\partial x_k} \right) + \frac{2}{3} \bar{\rho} k \qquad \text{Eq. 2. 10}$$

Reynolds stresses depend on μ_t (the turbulent dynamic viscosity estimated by turbulent model) and k (turbulent kinetic energy), which are defined as:

$$k = \frac{1}{2} \sum_{k=1}^{3} \widetilde{u_k'' u_k''} \qquad \text{Eq. 2. 11}$$

$$\mu_t = \rho C_\mu \frac{k^2}{\varepsilon} \qquad \text{Eq. 2. 12}$$

and turbulent kinetic energy k and its dissipation rate ε are defined as:

$$\frac{\partial}{\partial t}(\bar{\rho}k) + \frac{\partial}{\partial x_i}(\bar{\rho}\tilde{u}_i k) = \frac{\partial}{\partial x_i}\left[\left(\mu + \frac{\mu_t}{\sigma_k}\right)\frac{\partial k}{\partial x_i}\right] + P_k - \bar{\rho}\varepsilon \qquad \text{Eq. 2. 13}$$

$$\frac{\partial}{\partial t}(\bar{\rho}\varepsilon) + \frac{\partial}{\partial x_i}(\bar{\rho}\tilde{u}_i \varepsilon) = \frac{\partial}{\partial x_i}\left[\left(\mu + \frac{\mu_t}{\sigma_\varepsilon}\right)\frac{\partial \varepsilon}{\partial x_i}\right] + \bar{\rho}C_1 S\varepsilon - C_2\bar{\rho}\frac{\varepsilon^2}{k + \sqrt{v\varepsilon}} \qquad \text{Eq. 2. 14}$$

Unlike standard k-ε model, C_μ coefficient is not constant and it is expressed as a function of mean flow and turbulence properties:

$$C_\mu = \frac{1}{A_0 + A_S U^* \frac{k}{\varepsilon}} \qquad \text{Eq. 2. 15}$$

U^* relates the mean rate-of rotation tensor with deformation tensor. The model constants used in the equations are set as $\sigma_k = 1.0$, $A_0 = 4.04$, $A_S = \sqrt{6} \cos \varrho$, C_1=max [0.43, η/(η] and $C_2 = 1.9$, for more details go to (Fluent Manual, 2017).

Then, species and enthalpy turbulent fluxes are closed by the classical gradient assumption (this assumption is considered in ANSYS Fluent default options).

$$\bar{\rho}\widetilde{u_i''Y_k''} = -\frac{\mu_t}{Sc_{kt}}\frac{\partial \widetilde{Y}_k}{\partial x_i}$$

Eq. 2. 16

$$\bar{\rho}\widetilde{u_i''h''} = -\frac{\mu_t}{\sigma_t}\frac{\partial \widetilde{h}}{\partial x_i}$$

Eq. 2. 17

Sc_{kt} is turbulent Schmidt number for species k and Pr_t is turbulent Prandlt number. The diffusive fluxes ($\overline{\rho D \frac{\partial Y_k}{\partial x_i}}$ and $\overline{\rho D \frac{\partial h}{\partial x_i}}$) are modelled in ANSYS Fluent as:
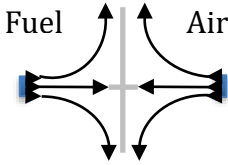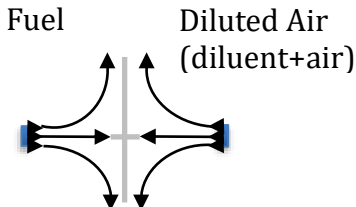
$$\overline{\rho D \frac{\partial Y_k}{\partial x_i}} \approx \bar{\rho}\bar{D}\frac{\partial \widetilde{Y}_k}{\partial x_i}$$

Eq. 2. 18

$$\overline{\rho D \frac{\partial h}{\partial x_i}} \approx \bar{\rho}\bar{D}\frac{\partial \widetilde{h}}{\partial x_i}$$

Eq. 2. 19

Finally, mean reaction rate closure for each specie k, $\overline{\dot{\omega}_k}$, is modelled according to the selected turbulence-chemistry interaction model. In this work, the default options of ANSYS Fluent are only used with the FGM model. The rest turbulence-chemistry interaction models applied in this Thesis follow a new developed closure term for the Delft lab-scale furnace application. As a starting point, the EDC model implemented in ANSYS Fluent is used, but with model constants modified for use in flameless combustion. For that, a parametric study has been made to get the appropriate EDC model constants values for the flameless Delft lab-scale furnace (chapter 3 section 2.3). Next, NE-EDC model is developed with model parameters depending on local Reynolds number and Kolmogorov scale Damköhler number. The NE-EDC model follows a similar analysis as the E-EDC model developed by Parente et al. (Parente, Alessandro et al., 2016). Nevertheless, the NE-EDC model assumes fine structure length scale (L^*) equal to Kolmogorov scale (η_k), following energy cascade concept, while the E-EDC model follows $L^* \neq \eta_k$ idea. Also, a different description of laminar flame speed is used in each model. Then, Generalized NE-EDC model is developed which incorporates the interaction among the reaction zones (chapter 3 section 3). Next, among the FGM models the default model implemented in ANSYS Fluent is used for simulation (chapter 4). The default FGM model

of ANSYS fluent does not consider the dilution effect. Therefore, the DA-FGM model has been for the first time implemented in ANSYS Fluent where dilution effect is considered in reaction rate and mixture fraction calculation (chapter 4). For a better understanding of the turbulence-chemistry interaction models applied in this thesis see Table 2. 5.

Table 2. 5 Used turbulence-chemistry interaction models summary

EDC mod	EDC C_ξ modified $\longrightarrow$	Parametric study for Delft lab-scale flameless furnace
E-EDC (Parente, Alessandro et al., 2016)	$C_\xi = f_1(Re_T, Da^*)$ **NE-EDC** $\longrightarrow$ $C_\tau = f_2(Re_T, Da^*)$ (developed) $$\tau_c = \frac{1}{8.3 \ 10^5 exp\left(-\frac{T_A}{T}\right)}$$ **Generalized NE-EDC** (developed)	$C_\xi = f_3(Re_T, Da^*)$ $C_\tau = f_4(Re_T, Da^*)$ $$\tau_c = \max\left[\frac{Y_k}{\left(\frac{|\dot\omega_k|}{\rho}\right)}\right]$$ $\dot\omega_k$ of CH_4, O_2, CO and CO_2 based on WD-2 constant
FGM (ANSYS Fluent default options)	Pure fuel and air as boundary conditions for flamelets generation	Fuel Air
DA-FGM (first time implemented in ANSYS Fluent)	Pure fuel and DILUTED air as boundary conditions for flamelets generation	Fuel Diluted Air (diluent+air)

As conclusions, two types of models are used in this Thesis: the EDC model and its extensions as representative of models assuming a local micromixing structure and the FGM model and its extension as representative of flamelet related tabulated chemistry models. For a review of the EDC models go to Ertesvåg (Ertesvåg, 2019) and for a review

on the FGM model go to van Oijen et al. (van Oijen et al., 2016). For more combustion models details go to reference (Poinsot & Veynante, 2005). For radiation source term closure go to reference (Coelho, 2007).

3.2 Computational Domain and Grid

In order to model the lab-scales-furnace of Delft University of Technology, the CFD code ANSYS Fluent, release 19.R2 (Fluent Manual, 2017), has been used. A three-dimensional steady-state RANS modelling has been made. Exploiting the furnace symmetry, a computational domain covering only half of the furnace domain is used. The domain starts upstream of the nozzle exit.

Fig. 2. 9 shows the computational grid used during the modelling. The mesh was made using a blocking strategy. Thus, a structured non-uniform mesh, with hexahedral cells and O-grid in the centre of each nozzle exit, is used.
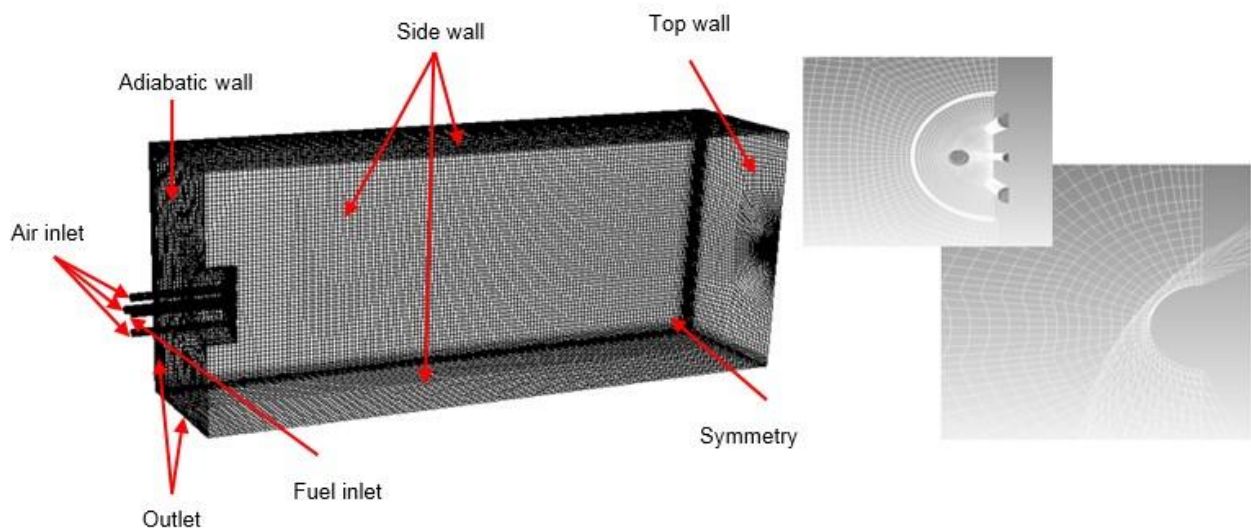
Fig. 2. 9 Three-dimensional view of the computational domain

In order to ensure a good mesh quality, a grid sensitivity analysis was carried out using the Fluent EDC model with constant values of the model. Results on three different mesh sizes were compared: a precise mesh with 1.78 million elements; a medium size mesh with 800,000 cells; and a coarse mesh with 350,000 elements. The Grid Convergence Index (GCI_{coarse}) method (based on Richardson extrapolation method) was chosen to quantify the discretization error (Celik et al., 2008; Roache, 1997). In the case under

study, the GCI$_{coarse}$ value was 3.1% for turbulence kinetic energy at the furnace outlet; using the base grid with about 800,000 cells (lower than the maximum recommended of 5%). Therefore, this was the selected grid size to carry out further modelling. It can be stated that the grid provides accuracy and consistency in the results on the one hand, and an acceptable CPU time on the other (run time for a 4 cores CPU@ 2.5 GHz is around 2 days, with a convergence level below 1e-5 for turbulence kinetic energy).

Finally, for the implementation of the E-EDC and the NE-EDC models, the reaction rates have been specified using User Defined Functions (UDF) and User Define Memory (UDM). And for the DA-FGM model implementation UDF, UDM and UDS have been used. These UDFs will be developed in the following chapters.

3.3 Boundary conditions

The boundary conditions are defined based on the experimental setup (Fig. 2. 10). For example, the air inlet is preheated air inlet, which comes from the recuperative burner. It is composed by %21 O$_2$ and 79% N$_2$ mole fractions. It is defined in ANSYS Fluent as mass flow type and introduced values are based on measured data (see Table 2. 6).
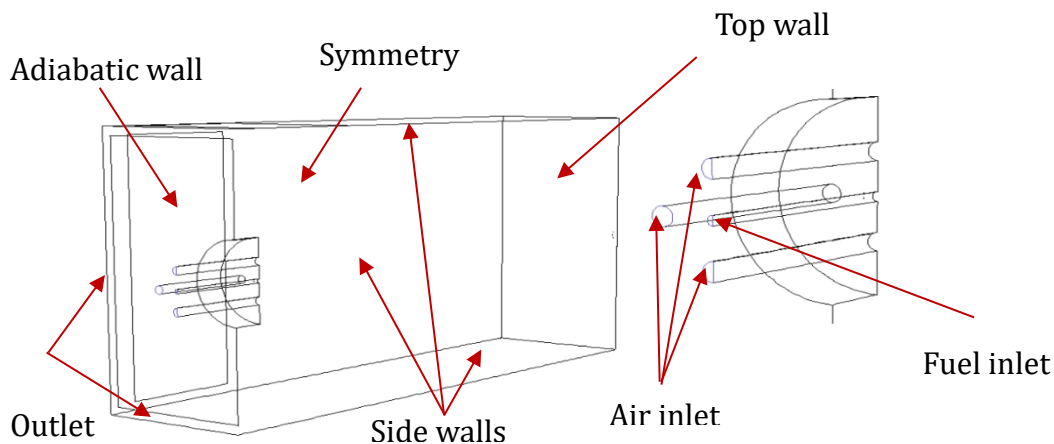
Fig. 2. 10 Geometry of the Delft lab-scale furnace

The fuel inlet is Dutch natural gas which is comprised of CH$_4$ 81.3%, C$_2$H$_6$ 3.7%, N$_2$ 14.4% and the rest 6% in mole fractions. Mass flow type boundary is also used for fuel inlet definition and measured data shown on Table 2. 6 are used. Then, the outlet in this furnace is in the same plane as the input streams (see Fig. 2. 10) and is composed by combustion

products. Combining the outlet stream with defined input streams, the boundary type selected in ANSYS Fluent for it is the pressure outlet.

The thermal boundary conditions at the walls are divided in three. First, the bottom wall of the furnace, which is on the same plane as the inlet streams, is defined as an adiabatic wall with a heat flux equal to 0 W/m^2. Second, the side walls of the furnace are defined in ANSYS Fluent by wall type boundary with a specified vertical temperature profile obtained through the interpolation of the measured data (see Table 2. 6). Finally, the top wall of the furnace is defined also as a wall type boundary but with a constant temperature equal to the measured value on that wall (see Table 2. 6).

Table 2. 6 Boundary conditions for simulations

Name	Type	Value
Air inlet	mass flow type	$\dot{m}_{full} = 9{,}67 * 10^\wedge - 4 \text{ kg/s}$ $\dot{m}_{half} = 4{,}84 * 10^\wedge - 4 \text{ kg/s}$ T= 843 K
Fuel inlet	mass flow type	$\dot{m}_{half} = 0.000118 \text{ kg/s}$ T= 446 K
Outlet	pressure outlet	-
Side Wall	wall type	T: piecewise linear $T(z) = \begin{cases} 300z + 1150 & 0 < z < 0.3\ [m] \\ 400z + 1120 & 0.3 < z < 0.4\ \ [m] \\ 1280 & \end{cases} K$
Top wall	wall type	T= 1280 K
Adiabatic wall		Heat flux 0 W/m^2

4 Conclusions

The simulation results will be compared with experimental data obtained in the Delft 9 kW lab-scale furnace during flameless operation with an equivalence ratio of 0.8 (Huang, X. et al., 2017; Huang, Xu, 2018). This furnace has several advantages compared to other experimental setups: (1) In contrast with Jet-in-Hot-Coflow burners (JHC) the setup includes both aerodynamic recirculation of products and important influence of radiative heat transfer. (2) In contrast with larger furnaces it is fully accessible for non-intrusive measurements. Detailed statistics of velocity and temperature are available for model validation (3) It does not have cooling tubes inserted as heat sink into the furnace (Lupant, Delphine & Lybaert, 2015), making the flow patterns more easy to compute.

Besides, RANS Favre average equations has been presented. It has been shown that unclosed terms will be closed by the models already implemented in ANSYS Fluent except for the turbulence-chemistry interaction model where the models developed in this Thesis are used for reaction rate closure: the EDC model and its extensions and the FGM model and its extension (the DA-DFGM first time implemented in ANSYS Fluent). The rest sub-models applied in this work are: the realizable two-equation $k - \varepsilon$ turbulence model which presents some advantages comparing to standard model: (1) C_μ value is not constant anymore (Eq. 2. 15) and (2) a modified transport equation is used for the dissipation rate (ε) calculation (Eq. 2. 14) and the DO model for radiation source term closure, as is the most accurate model integrated in ANSYS Fluent.

Finally, Delft lab-scale furnace computational domain and boundary conditions applied along this Thesis modelling are described.

CHAPTER 3: EDC MODEL APPROACH AND VALIDATION FOR FLAMELESS COMBUSTION

1 Introduction

This chapter presents the main characteristics of the extended EDC models and their modelling results. First, a short summary of the standard EDC model is provided and then the extensions of the EDC model applied to Delft lab-scale furnace are described.

The methodology for the extension of the EDC model development starts with the EDC model implemented in ANSYS Fluent but a parametric study has been carried out to get the appropriate values of the EDC model constants for flameless modelling. Thus, the influence of the correct selection for theses constant values is shown. Then the extended EDC models are described, first the E-EDC model of Parente et al. (Parente, Alessandro et al., 2016)) and next the new extended EDC (NE-EDC) model. The differences between both extended models are explained in detail. Next, the Generalized NE-EDC model development methodology is described stressing the changes against the NE-EDC model to incorporate the interactions among the reaction zones. Then, the predictions of velocity and temperature fields of the three models (the EDC model with specific and optimized fixed values of the model constants, the NE-EDC model and the Generalized NE-EDC model) are presented and compared with experimental data.

Finally, the NE-EDC model mean temperature profiles are compared against the E-EDC model results. Only the temperature profiles comparison is shown as velocity prediction of both models is almost identical, note that the same turbulence model is used for

modelling (realizable $k - \varepsilon$ model) and temperature deviance is not that big to change the velocity profile.

2 The Eddy Dissipation Concept (EDC) model

The original EDC model (Gran, Inge R. & Magnussen, 1996) assumes that the reactions are fast and occur in small zones that are modelled as a chemical reactor. The model conceptually divides every computational cell into two zones: the fine structures, where chemical reactions occur, and the surrounding fluid. The properties of the fine structures are denoted by a superscript '*', e.g. the length and velocity scales are denoted L^* and u^*. They are assumed to be of the same scale as the smallest scale of turbulence, the Kolmogorov scale. Both large and small turbulence scales are taken into account to set the residence time in the small reaction zones and the mass transfer to these zones. Therefore, EDC model consists of a cascade model and a reactor model. The cascade model links the fine structure with the mean turbulent field, normally resolved by RANS. This simplification makes the EDC model flexible and applicable to several flames' structures.

The EDC model was developed for conventional combustion and its constant were empirically selected ($C_\xi = 2.1377$ and $C_\tau = 0.4082$) for those specific combustion characteristics, so that they do not take into account the dilution effect of flameless combustion.

2.1 Basis of the model

Magnussen developed the EDC model (Gran, Inge R. & Magnussen, 1996) which is an extension of the EDM but with the difference that the EDC model allows the inclusion of detailed chemical mechanisms in turbulent flows. The reaction rate of the EDC is obtained by the mass balance of the fine-structure reactor (Fig. 3. 1). The inflow has surroundings' properties (defined by °) while interior and outflow has fine-structure properties (defined by *).

ENEDI Research Group
Energy Engineering Department
University of the Basque Country

enedi

Universidad   Euskal Herriko
del País Vasco Unibertsitatea

FACULTY
OF ENGINEERING
BILBAO
UNIVERSITY
OF THE BASQUE
COUNTRY

Surrounding fluid $\overline{(R_{k,j}}=0)$

$\rho^{\circ}, Y_k^{\circ}, T^{\circ}$

$\dot{Q}_{rad}$

$\dot{m}^*$

Fine structures
(reaction zone $\bar{R}_{k,j}$)
ρ^*, Y_k^*, T^*

ρ^*, Y_k^*, T^*
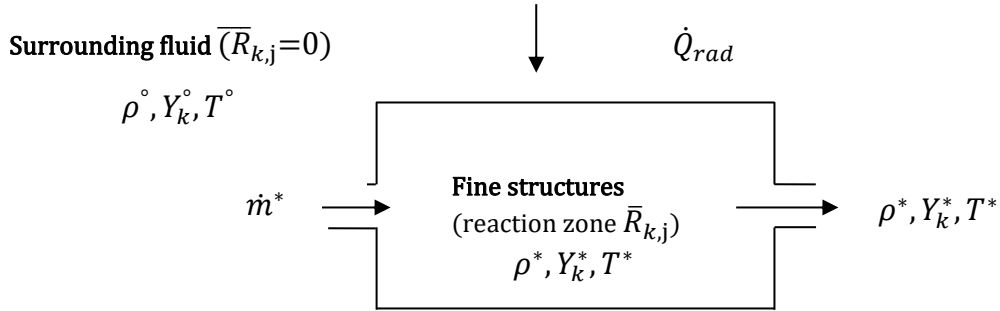
Fig. 3. 1 Fine structure reactor draft

After applying the mass balance on the reactor, the reaction rate is obtained (Eq. 3. 1):

$$R_{k,j}^* = \rho^* \dot{m}^* (Y_k^* - Y_k^{\circ})$$

Eq. 3. 1

The mass inflow rate divided by fine structures mass is defined as $\dot{m}^*$, which is the inverse of the fine structure residence time ($\tau^* = (\dot{m}^*)^{-1}$). The structure residence time is based on the mass transfer rate between the fine structures and the surroundings. Then, the mean reaction rate is displayed as:

$$\bar{R}_{k,j} = \frac{\bar{\rho}}{\rho^*} \xi^* \varphi R_{k,j}^*$$

Eq. 3. 2

The ratio of mass in the fine structure to the total mass is represented by ξ^* (the size of fine structure) and the fraction of the fine structure where reaction takes place is expressed as φ (the fraction of the fine structure that reacts). Combining Eq. 3. 1 and Eq. 3. 2 the mean reaction rate is given as:

$$\bar{R}_{k,j} = \frac{\bar{\rho} \xi^* \varphi}{\tau^*} (Y_k^* - Y_k^{\circ})$$

Eq. 3. 3

The mean mass fraction in the computational cell is the mass-weighted average over fine structure and surroundings (Eq. 3. 4):

$$\tilde{Y}_k = \xi^* \varphi Y_k^* + (1 - \xi^* \varphi) Y_k^{\circ}$$

Eq. 3. 4

Which can be expressed also as:

$$Y_k^* - Y_k^\circ = \frac{Y_k^* - \tilde{Y}_k}{(1 - \xi^*\varphi)}$$

Eq. 3. 5

Finally, combining Eq. 3. 3 and Eq. 3. 5 mean reaction rate is defined as:

$$\bar{R}_{k,\text{j}} = \frac{\bar{\rho}\xi^*\varphi}{\tau^*(1 - \xi^*\varphi)}(Y_k^* - \tilde{Y}_k)$$

Eq. 3. 6

During the years, Magnussen made several derivations defining ξ^* in order to improve the EDC model predictions by increasing the mean reaction rate space. In 1981 the mass of fine structures divided by total mass was defined as $\xi^* = (\xi_\lambda)^3$ (Magnussen & Hjertager, 1981), where ξ_λ is a fine structure length scale based on the ratio of the mass of regions containing fine structures and the total mass. Then, mean reaction rate is calculated as:

$$\bar{R}_{k,j} = \frac{\bar{\rho}(\xi_\lambda)^3\varphi}{\tau^*[1 - (\xi_\lambda)^3\varphi]}(Y_k^* - \tilde{Y}_k)$$

Eq. 3. 7

The fraction of fine structure which reacts, φ, was defined as:

$$\varphi = \frac{\tilde{Y}_{pr}/(1 + r)}{\xi_\lambda(\tilde{Y}_{pr}/(1 + r) + \tilde{Y}_f}$$

Eq. 3. 8

Later, on 1996 (Gran, Inge R. & Magnussen, 1996) the mass of fine structures divided by total mass was maintained ($\xi^* = (\xi_\lambda)^3$) but a factor of $(\xi_\lambda)^{-1}$ was introduced in Eq. 3. 7. With this change more non-reactive fluid goes into the fine structures, therefore mean reaction rate was expressed as:

$$\bar{R}_{k,j} = \frac{\bar{\rho}(\xi_\lambda)^2\varphi}{\tau^*[1 - (\xi_\lambda)^3\varphi]}(Y_k^* - \tilde{Y}_k)$$

Eq. 3. 9

In the 80s various formulations were tried for φ definition and the proposal of 1989 (Magnussen, 1989) was implemented in 1996.

$$\varphi = \varphi_1 \cdot \varphi_2 \cdot \varphi_3 \qquad \text{Eq. 3. 10}$$

$$\varphi_1 = \frac{\left(\tilde{Y}_{min} + \tilde{Y}_{pr}/(1+r)\right)^2}{\left(\tilde{Y}_f + \tilde{Y}_{pr}/(1+r)\right)\left(\tilde{Y}_{ox}/r + \tilde{Y}_{pr}/(1+r)\right)} \qquad \text{Eq. 3. 11}$$

$$\varphi_2 = \min\left\{\frac{1}{\xi_\lambda} \cdot \frac{\tilde{Y}_{pr}/(1+r)}{\tilde{Y}_{pr}/(1+r) + \tilde{Y}_{min}}, 1\right\} \qquad \text{Eq. 3. 12}$$

$$\varphi_3 = \min\left\{\frac{\xi_\lambda\left(\tilde{Y}_{pr}/(1+r) + \tilde{Y}_{min}\right)}{\tilde{Y}_{min}}, 1\right\} \qquad \text{Eq. 3. 13}$$

These equations (Eq. 3. 11, Eq. 3. 12 and Eq. 3. 13) can be formulated for a multi-step mechanism. However, on the 1996 EDC version (Gran, Inge R. & Magnussen, 1996) single-step global reaction of fuel and oxygen was formulated for a single φ value, which is applied for all species of a multi-step chemical mechanism.

And finally on 2005 (Magnussen, 2005) ξ^* was reformulated as $\xi^* = (\xi_\lambda)^2$ widen reaction space. Then, mean reaction rate is denoted as:

$$\bar{R}_{k,j} = \frac{\bar{\rho}(\xi_\lambda)^2 \varphi}{\tau^*[1 - (\xi_\lambda)^2 \varphi]}\left(Y_k^* - \tilde{Y}_k\right) \qquad \text{Eq. 3. 14}$$

And in this version, φ is calculated as:

$$\varphi = \frac{\tilde{Y}_{pr}/(1+r)}{(\tilde{Y}_{pr}/(1+r) + \tilde{Y}_{min}} \qquad \text{Eq. 3. 15}$$

The different expression for φ calculation where compared (Gran, I. R., 1994; Gran, Inge R. & Magnussen, 1996) with a detailed combustion and it was concluded that there was no difference between using Eq. 3. 11, Eq. 3. 12 and Eq. 3. 13 and the simplest form, where the reacting fine structure fraction is equal to one, $\varphi = 1$. Due to that, for simplicity, $\varphi = 1$ value is chosen for mean reaction rate calculation (Ertesvåg, 2019).

The fine structures were originally assumed to be PSR (chemical reaction in the presence of infinitely fast mixing) (P. Glarborg et al., 1986), but in some package the fine structures are represented as a PFR (chemical evolution in time, with no mixing) as mathematically are easier to handle. Therefore, PSR reactor model species are calculated by Eq. 3. 16, while for PFR Eq. 3. 17 is used.

$$\frac{dY_k}{dt} = v_r \cdot \left(Y_k^\circ - Y_k^*\right) + \frac{R_{k,j}}{\rho} \qquad \text{Eq. 3. 16}$$

$$\frac{dY_k}{dt} = \frac{R_{k,j}}{\rho} \qquad \text{Eq. 3. 17}$$

Where v_r is the mixing rate, Y_k° is the species mass fraction of the incoming flow and Y_k^* is the species mass fraction of the exit flow. In the PFR model the mass fractions Y_k^* are recalculated every computational time step by integrating the chemical kinetics starting from the current cell mean value up to a later time proportional to the Kolmogorov time scale.

The implication of the reactor model on the EDC has been discussed in detail (Ertesvåg, 2019; Tomasch & Ertesvag, April 2019) and it was concluded that the reaction type did not have impact on predicted values.

In the version implemented in ANSYS Fluent, the fine structures are represented as PFR. In addition, ANSYS Fluent follows 1996s mean reaction expression (Eq. 3. 9) with the simplest form of $\varphi = 1$. In Eq. 3. 9, turbulence-chemistry interaction is only taken into account via the estimates of the volume fraction of the fine structures and the transfer rates based on the energy cascade concept and not via fluctuations in local properties.

2.2 Energy cascade model

The influence of turbulence on the EDC model is considered by the energy cascade term. This cascade explains the energy distribution over eddies of different length scales present in the flow and which length scales carry enough energy to interact with the flame front.

ENEDI Research Group
Energy Engineering Department
University of the Basque Country

FACULTY
OF ENGINEERING
BILBAO
UNIVERSITY
OF THE BASQUE
COUNTRY

Universidad   Euskal Herriko
del País Vasco Unibertsitatea

Using an analysis of the energy-cascade concept, mechanical energy is transferred from large-scale eddies (the integral length scale l_t) to small eddies (the Kolmogorov length scale η_k). Large-scale eddies have the most part of kinetic energy while the small eddies whirl faster and therefore, they have largest viscous stress. Viscous dissipation is transformed to heat (q) but predominantly, it takes place in small eddies (see Fig. 3. 2).
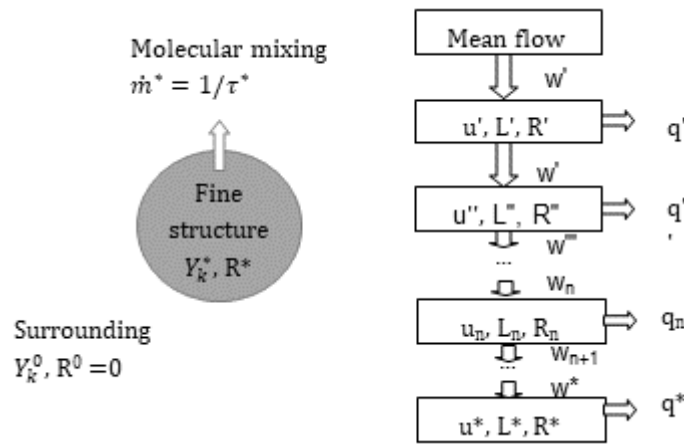
Fig. 3. 2 Fine structure and energy cascade model

The energy cascade concept is shown in Fig. 3. 2. There w refers to the mechanical energy transfer and superscript (') represents the cascade level. It is concluded that the dissipated turbulence energy (ε) is the same as the energy transfer along the cascade $\sum q = \varepsilon$. Besides, the first cascade level is characterized by a velocity $u' = \sqrt{2k/3}$, where k is turbulent kinetic energy. Considering a length scale of L', the eddy frequency is calculated by $R' = u'/L'$ (Ertesvag & Magnussen, 2000). This first cascade level represents the whole turbulence spectrum as smallest scales are also considered. Turbulent kinetic energy (k) and Eddy dissipation rate (ε) vary in space and time, thus they are defined by $k - \varepsilon$ turbulence model. Besides, another assumption of the energy cascade model is that eddy frequency is doubled at each cascade level, that is $w_n = 2w_{n+1} = u_n/L_n$ where n refers to the level. As it is shown on Fig. 3. 2, the last level is described by * superscript referring to the smallest scales which are assumed equal to Kolmogorov scale.

The mechanical energy (w_n) and viscous energy dissipation at each level (q_n) are described based on two models constants C_{D1} and C_{D2} (Magnussen & Hjertager, 1981) for the n-th level:

$$w_n = \frac{3}{2} C_{D1} R_n u_n{}^2 = \frac{3}{2} C_{D1} \frac{u_n{}^3}{L_n} \qquad \text{Eq. 3.18}$$

$$q_n = C_{D2} v R_n{}^2 = C_{D2} v \frac{u_n{}^2}{L_n{}^2} \qquad \text{Eq. 3.19}$$

After applying energy conservation there is:

$$w_n = q_n + w_{n+1} \qquad \text{Eq. 3.20}$$

Analysing the Kolmogorov scale level (n=*), mechanical energy at this level w* should be equal to the energy transfer (q) as there is not a smaller level, therefore:

$$w^* = \frac{3}{2} C_{D1} \frac{u^{*3}}{L^*} = q^* = C_{D2} v \frac{u^{*2}}{L^{*2}} \qquad \text{Eq. 3.21}$$

In the proposed energy cascade model (Ertesvag & Magnussen, 2000) the model constants value are defined as $C_{D1} = 0.135$ and $C_{D2} = 0.5$. These values are obtained considering that the dissipated turbulence energy (ε) is the same as the energy transfer along the cascade $\sum q = \varepsilon$

Besides, on the first level (n = ') viscous rate is really small compared to mechanical energy, thus, applying energy conservation (Eq. 3.20), on the first level mechanical energy can be considered equal to second level mechanical energy ($w' = w''$).

$$w' = w'' = \frac{3}{2} C_{D1} \frac{u'^3}{L'} \qquad \text{Eq. 3.22}$$

Considering that the dissipated turbulence energy (ε) is the same as the energy transfer along the cascade $\sum q = \varepsilon$, in the first level it can be concluded:

$$w' = \sum q = \varepsilon = \frac{3}{2} C_{D1} \frac{u'^3}{L'}$$

Eq. 3. 23

As mention before, the EDC model follows the assumption of fast chemical reaction, therefore the turbulence mixing control the reaction rate. Consequently, it is possible to relate C_{D1} constant with $k - \varepsilon$ turbulence model constant C_μ, by following turbulent viscosity v_t expression and $u' = \sqrt{2k/3}$ definition:

$$v_t = u' * L' = \frac{3}{2} C_{D1} \frac{u'^4}{\varepsilon} = \frac{2}{3} C_{D1} \frac{k^2}{\varepsilon}$$

Eq. 3. 24

As it was mention before, $w_n = 2w_{n+1}$, and after doing the sum of heat generation on each level it is concluded that $\varepsilon = \frac{4}{3} q^*$. Besides, considering Eq. 3. 19 it can be shown that the energy dissipation rate (ε) is related to the properties of the fine structures:

$$\varepsilon = \frac{4}{3} C_{D2} v \frac{u^{*2}}{L^{*2}}$$

Eq. 3. 25

Applying Eq. 3. 21

$$\varepsilon = 2 C_{D1} \frac{u^{*3}}{L^*}$$

Eq. 3. 26

The model constants were calibrated with experimental data on turbulent flows to the values $C_{D1} = 0.135$ and $C_{D2} = 0.5$ for conventional combustion modelling. Defining and evaluating the Reynolds number of the fine structure by Eq. 3. 27, it can be seen that the fine structures are indeed in the dissipative range since the Reynolds number is of order unity:

$$Re^* = \frac{u^* L^*}{v} = \frac{2 C_{D2}}{3 C_{D1}} \approx 2.5$$

Eq. 3. 27

The EDC model derivation based on the energy cascade concept defined the fine structure length ξ_λ and the residence time scale τ^* by Eq. 3. 28 and Eq. 3. 29.

$$\xi_\lambda \;=\; \left(\frac{3C_{D2}}{4C_{D1}^2}\right)^{1/4}\left(\frac{\nu\varepsilon}{k^2}\right)^{1/4} = C_\xi\left(\frac{\nu\varepsilon}{k^2}\right)^{1/4} \qquad \text{Eq. 3. 28}$$

$$\tau^* \;=\; \left(\frac{C_{D2}}{3}\right)^{1/2}\left(\frac{\nu}{\varepsilon}\right)^{1/2} = C_\tau\left(\frac{\nu}{\varepsilon}\right)^{1/2} \qquad \text{Eq. 3. 29}$$

The relation between the model constants C_ξ and C_τ and the model constants C_{D1} and C_{D2} is $C_{D1} = \frac{3}{2}\frac{C_\tau}{C_\xi^2}$ and $C_{D2} = 3C_\tau^2$, leading to $C_\xi = 2.1377$ and $C_\tau = 0.4082$. It should be noted that the EDC model values ($C_\xi = 2.1377$ and $C_\tau = 0.4082$) were empirically chosen considering conventional combustion characteristics.

Since the finite structure constant, C_ξ, is proportional to the EDC model fine structure length ξ_λ and the residence timescale, τ^*, is the product of the residence time constant, C_τ, and the Kolmogorov time scale, then the impact of the value of the constants on the mean reaction rate (Eq. 3. 19) and consequently on the products composition and temperature prediction is very direct.

2.3 EDC with modified constant model coefficient

In flameless combustion, the reaction zones seem to be more distributed and the temperature gradients in the mean profile significantly lower than in conventional combustion. It has been found that these differences lead to bad agreement between modelling results and experimental data when the EDC model with standard values of the model parameters C_ξ and C_τ are used. These constants modification can result in better predictions of flameless combustion during modelling (Ertesvåg, 2019; Lewandowski & Ertesvåg, 2018).

In the present work, an optimization of the spatially constant value of the model constants for the current lab-scale furnace is made. In some of the earliest studies, it was concluded that when selecting a different value for the model constants in flameless combustion

applications, the best results are obtained by leaving the residence time constant, C_τ, unchanged and increasing the value of the finite structure constant, C_ξ, (Graça et al., 2013; Rehm et al., 2009). Following this observation, in this work, the results of several simulations are presented, considering different values of C_ξ; C_ξ =2.1317 (original), C_ξ=2.4, C_ξ =2.9, C_ξ =3.7, C_ξ =4.5, and C_ξ =5 (see subsection 4.1). This range of variation is within the acceptable range of variation (Ertesvåg, 2019).

3 Improvement on the EDC by extension of the model

In the literature, it has been shown that the EDC model with the standard values of the model parameters $C_\xi = 2.1377$ and $C_\tau = 0.4082$ often over predicts furnace temperature. These constant values were empirically selected considering conventional combustion characteristics; therefore, they do not take into account the dilution effect present in flameless combustion. As a solution the EDC model with globally modified model constant was proposed, where constant values are selected by calibration with experimental data (they are case dependent and cannot be determined without empirical data). To overcome the limited generality of the EDC model with a globally fixed value of model constants, a new model is developed were model constants take values depending on local conditions. The first step was made by the E-EDC model proposed in reference (Parente, Alessandro et al., 2016). In this work, based on the E-EDC, alternative set of assumptions are proposed leading to the NE-EDC model. Next, both models and their differences are described.

3.1 Extended Eddy Dissipation Concept (E-EDC) model

On the E-EDC model, model constants C_τ and C_ξ are calculated depending on the local Reynolds and local Damköhler number. The first assumption of Parente et al. is that due to the high dilution in flameless combustion the size of the reacting structures can extend over a range of turbulent length scales and is in general larger than the Kolmogorov length scale (Poinsot & Veynante, 2005). Therefore, the length scale of the reacting fine structures L^* is chosen to be different from the Kolmogorov length scale ($\eta_k = \left(\frac{v^3}{\varepsilon} \right)^{1/4}$)

and its value is to be determined. The velocity of the reacting fine structure u^* is assumed to be equal to the turbulent flame speed S_T, ($u^* = S_T$). Since, in flameless combustion the Damköhler number is low and there is high intensity turbulence, the ratio of the turbulent flame speed to the laminar flame speed is calculated from the ratio of the turbulent thermal diffusivity $D_{th,t}$ to the laminar thermal diffusivity D_{th} using (Kuo, Kenneth Kuan-yun & Acharya, 2012):

$$S_T \approx S_L \sqrt{\frac{D_{th,t}}{D_{th}} + 1} \approx S_L \sqrt{\frac{v_T}{v} + 1} \approx S_L \sqrt{Re_T + 1}$$

Eq. 3. 30

Here, the laminar and turbulent Prandtl numbers have been assumed to be equal to unity, where Re_T is the turbulent Reynolds number and S_L is the laminar flame speed, which is estimated from (Kuo, Kenneth Kuan-yun & Acharya, 2012):

$$S_L \propto \sqrt{D_{th}K_{fj}} \propto \sqrt{v/\tau_c} \text{ (considering first order reaction)}$$

Eq. 3. 31

Combining the expression of turbulence flame speed with Eq. 3. 25 it is obtained:

$$\varepsilon = \frac{4}{3} C_{D2} v \frac{S_L^2 (Re_T + 1)}{L^{*2}}$$

Eq. 3. 32

Eq. 3. 32 shows that C_{D2} model constant depends on the Re_T and laminar flame speed. Using these assumptions, it follows that the ratio of the model constants C_{D2} and C_{D1} model is given by:

$$\frac{C_{D2}}{C_{D1}} = \frac{3}{2} \frac{u^* L^*}{v} = \frac{3}{2} \frac{S_L \sqrt{Re_T + 1}}{v} L^* \propto \frac{3}{2} \frac{L^* \sqrt{Re_T + 1}}{S_L \tau_c}$$

Eq. 3. 33

Assuming that the chemical reaction time scale is the time that a laminar flame needs to transverse the laminar flame and considering that in the EDC model the reacting fine structure is the flame, an estimate of the thickness of the reacting fine structure can be obtained as follows:

$$L^* = S_L \tau_c$$

<div align="right">Eq. 3. 34</div>

Using Eq. 3. 34 C_{D2} and C_{D1} model constant ratio becomes:

$$\frac{C_{D2}}{C_{D1}} \propto \frac{3}{2}\sqrt{Re_T + 1}$$

<div align="right">Eq. 3. 35</div>

Defining a Damköhler number based on the Kolmogorov time scale, $Da^* = \tau_k/\tau_c$, an expression where the C_{D2} constant depends on the Reynolds and Damköhler local values is obtained:

$$C_{D2} = \frac{3}{4}\frac{1}{(Re_T + 1)Da^*}$$

<div align="right">Eq. 3. 36</div>

C_{D2} and C_{D1} model constants are related via Eq. 3. 33 and it follows that:

$$C_{D1} \propto C_{D2} * \frac{1}{\sqrt{Re_T + 1}} \propto \frac{1}{(Re_T + 1)^{3/4} Da^*}$$

<div align="right">Eq. 3. 37</div>

Finally, using the relation between the model constants C_ξ and C_τ and the model constants C_{D1} and C_{D2}, expressions for C_ξ and C_τ depending on the Reynolds and Damköhler number values are obtained:

$$C_\tau = \left(\frac{C_{D2}}{3}\right)^{1/2} \propto \frac{1}{\sqrt{(Re_T + 1)Da^*}}$$

<div align="right">Eq. 3. 38</div>

$$C_\xi = \left(\frac{3C_{D2}}{4C_{D1}^2}\right)^{1/4} \propto \sqrt{(Re_T + 1)Da^*}$$

<div align="right">Eq. 3. 39</div>

The residence time constant is inversely proportional to Da^* whereas the fine structure constant is proportional to $\sqrt{Da^*}$. The value of the turbulent Reynolds number is obtained from the properties provided by the turbulence model. The determination of the value of Da^* also needs an estimation of the chemical time scale from chemical mechanism and local conditions. The E-EDC model (Parente, Alessandro et al., 2016) used the new expressions for the model constants in two ways. A first approach is to use simulation

Analysis of thermofluids in flameless (MILD)
combustion: assessment, improvement and
development of combustion models by CFD
Naiara Romero Anton

results to estimate the best global values of Re_T and Da^* and then to use these later values to identify the best global values of the model constants. A second approach is to evaluate Re_T and Da^* from local states and then use them locally varying values of C_ξ and C_τ.

The chemical time scale was obtained from a one-step reaction, using the temperature and main species concentrations coming from the detailed mechanism used for the gas phase reactions. Both approaches and the EDC with standard values of the model constants were applied to several cases of the Adelaide jet-in-hot-coflow experiments. It was found that the modification of the EDC model coefficients improves the predictions close to the burner whereas re-ignition phenomena farther away have not yet been reproduced. The latter was attributed to limitations of the RANS approach rather than the EDC model. In the application considered here the fuel and air jets are confined by the furnace walls and surrounded by products, while the downstream re-ignition present in the JHC configuration is absent. While preparing for the application of the extended EDC model to the application of the lab scale furnace the assumptions of the model were reviewed and an alternative formulation (here called NE-EDC) has been developed.

It should be noted that in a recent work (Evans et al., 2019) the approach of the E-EDC was extended, based on (Romero-Anton, Naiara et al., 2020), replacing the proportionality present in Eq. 3. 38 and Eq. 3. 39 by an equality with a constant coefficient, leading to Eq. 3. 40 and Eq. 3. 41, called here Generalized E-EDC model. In addition, the Generalized E-EDC included the interaction among the reaction zones calculating the chemical time scale considering CH$_4$, H$_2$, O$_2$, CO$_2$ and CO species reaction rates ($\tau_c = \max[Y_k/(\omega_k/\rho)]$):

$$C_\tau = \left(\frac{C_{D2}}{3}\right)^{1/2} = \frac{1}{2}\frac{1}{\sqrt{(Re_T + 1)Da^*}}$$

<div align="right">Eq. 3. 40</div>

$$C_\xi = \left(\frac{3C_{D2}}{4C_{D1}^2}\right)^{1/4} = \left(\frac{2}{3}\right)^{1/2}\sqrt{(Re_T + 1)Da^*}$$

<div align="right">Eq. 3. 41</div>

3.2 New Extended Eddy Dissipation Concept (NE-EDC) model

First, unlike in the E-EDC model by Parente et al., in the novel model proposed here the length scale of the reacting fine structure length is assumed to be the Kolmogorov length scale ($L^* = \eta_k$). This is consistent with the derivation of the EDC reaction rate derived from an energy cascade concept with an energy cascade extending to the Kolmogorov scale. But here it is proposed as a method to handle the fact that according the DNS results and the experimental OH*-luminescence observations by Huang (Huang, Xu, 2018), in flameless combustion there is not a collection of well-defined isolated reaction zones. Instead, a conglomerate of several flame fragments touching each other are present. This makes it hard to choose the size to define the fine structure of the system. Therefore, instead of basing the fine structure size on flame thickness, in this work the size is chosen based on the velocity field. A region smaller than the Kolmogorov scale is homogeneous in velocity and in all cases where chemical fronts are thicker than the Kolmogorov scale, a structure of that scale can be considered to be homogeneous and not disturbed by the flow field. This leaves the possibility open that significant variation in composition is only seen over a significantly larger scale than the Kolmogorov scale.

Secondly, the use of the expression for the laminar flame speed containing a proportionality factor (Eq. 3. 31) is avoided by eliminating the laminar flame speed from the equations. In this way a quantitative prediction for the model constant values is obtained without the proportionality factor. In the NE-EDC model (Romero-Anton, Naiara et al., 2020), as in the E-EDC it is assumed that the fine structure velocity scale (u*) is the characteristic speed of the turbulent mixture of multiple reacting fine structures ($u^* = S_T$). Here the turbulent flame speed is used because it is an overall measure of the conversion in a complex reacting flow. In flameless combustion, the reacting mixture consists of a conglomerate of local structures. Experimental data (Oldenhof, E. et al., 2010) indeed shows that ignition kernels are continuously forming and growing in size. Multiple developing and combining kernels represents the overall combustion. The conversion of reactants in the mix of local structures is characterised by the turbulent burning velocity (S_T) and this velocity is identified with the fine structure velocity (u*) and it is different from the Kolmogorov scale velocity. The NE-EDC model uses $u^* = S_T$

Analysis of thermofluids in flameless (MILD)
combustion: assessment, improvement and
development of combustion models by CFD
Naiara Romero Anton

and the same Damköhler expression for the ratio between turbulent flame speed and laminar flame speed : $S_T = S_L\sqrt{Re_T + 1}$.

Next, a fine structure chemical time scale is defined by $\tau_c^* = L^*/S_L$. Taking this equation into account, an alternative expression for Eq. 3. 33 is obtained, that does not contain the laminar flame speed:

$$\frac{C_{D2}}{C_{D1}} = \frac{3}{2}\frac{u^* L^*}{\nu} = \frac{3}{2}\frac{S_L\sqrt{Re_T + 1}}{\nu}L^* = \frac{3}{2}\frac{\sqrt{Re_T + 1}}{\nu}\frac{L^{*2}}{\tau_c^*}$$

Eq. 3. 42

As the fine structure length scale is assumed to be the Kolmogorov scale, the term $L^{*2}/\nu\tau_c^*$ is equal to the Kolmogorov scale Damköhler number

$$\frac{L^{*2}}{\nu\tau_c^*} = \frac{(\nu/\varepsilon)^{1/2}}{\tau_c^*} = \frac{\tau_k}{\tau_c^*} = Da^*$$

Eq. 3. 43

Then, the following final expressions for C_ξ and C_τ, are obtained:

$$C_\tau = \left(\frac{C_{D2}}{3}\right)^{1/2} = \frac{1}{2}\frac{1}{\sqrt{(Re_T + 1)Da^*}}$$

Eq. 3. 44

$$C_\xi = \left(\frac{3C_{D2}}{4C_{D1}^2}\right)^{1/4} = \sqrt{\frac{3}{2}(Re_T + 1)Da^{*3/4}}$$

Eq. 3. 45

In Eq. 3. 44 and Eq. 3. 45 the model coefficients are calculated as functions of the local Re_T and Da^* numbers. The difference with the E-EDC model is that the finite structure constant C_ξ is found to be proportional to $Da^{*3/4}$ and not to $Da^{*1/2}$. This difference arises because the definition of chemical time scale is different. The chemical time scale used in the NE-EDC is the time needed for a premixed flame to travel a distance equal to the Kolmogorov scale, while moving with the laminar flame speed. In this study this chemical time scale was obtained from the rate of a one-step mechanism. It has been evaluated as the inverse of an Arrhenius reaction rate as $\tau_c^* = \dfrac{1}{8.3\ 10^5 exp\left(-\frac{T_A}{T}\right)}$ with $T_A = 15,100\ K$.

3.3 Generalized New Extended Eddy Dissipation Concept (Generalized NE-EDC) model

In the NE-EDC model, a one-step global reaction rate of CH_4 is considered for chemical time calculation, $\tau_c = \frac{1}{8.3 \ 10^5 exp\left(-\frac{T_A}{T}\right)}$ where $T_A = 15,100 \ K$. Considering the interaction among the reaction rates suggested by DNS results, it would be interesting to study the impact of calculating the chemical time scale considering the reaction rate of other species of minor concentration. Accordingly, in this section the Generalized NE-EDC is proposed in order to consider also CH_4, H_2, O_2, CO_2 and CO species reaction rates in chemical time scale calculation.

The chemical time scale is calculated by UDF and then in combination with the flow time scale calculated by ANSYS Fluent the UDF calculates Da number. Later, Da number is applied in both Eq. 3. 44 and Eq. 3. 45.

3.3.1 Global reaction mechanisms

So as not to increase modelling computational time, global reaction mechanisms are proposed to calculate the chemical time scale (note that a detail mechanism, smooke-25, is used to calculate temperature and species concentration during modelling). Accurate and widely applied global mechanisms for CH_4 combustion are; Jones-Lindstedt (JL) mechanism (Jones & Lindstedt, 1988), Westbrook-Dryer mechanism (WD) (Westbrook & Dryer, 1984), Norbert-Peters 4 step mechanism (NP) (Peters, N., 1985) and Peters-Williams 3 (PW) step mechanism (Peters, N. & Williams, 1987).

NP and PW global mechanism were developed for conventional combustion, so as the Arrhenius coefficient are defined for that application. Nevertheless, JL and WD mechanism has being applied and adjusted for flameless combustion (Kim et al., 2008; Wang et al., 2012). Thus, in this work the adjusted global mechanisims with better consistency with flameless combustion experimental data are chosen to model Delft lab-scale furnace.

Analysis of thermofluids in flameless (MILD)
combustion: assessment, improvement and
development of combustion models by CFD
Naiara Romero Anton

- **Jones & Lindstedt adjusted global mechanism (JL1)**

This mechanism is based on the standard 4-step global mechanism of JL (Jones & Lindstedt, 1988). In flameless combustion O_2 concentration is reduced, so that the O_2 partial pressure is lower. Under this situation, the fuel oxidation rate become slower. Thus, the 4th mechanism of the standard 4-step global mechanism of JL is adjusted to this combustion system following Marinov et al. (Marinov et al., 1995) and Wang et al. (Wang et al., 2012) suggestions:

{C1} $CH_4 + 0.5O_2 \rightarrow CO + 2H_2$

{C2} $CH_4 + H_2O \rightarrow CO + 3H_2$

{C3} $CO + H_2O \leftrightarrow CO_2 + H_2$

{C4} $H_2 + 0.5O_2 \leftrightarrow H_2O$
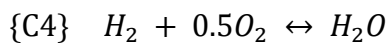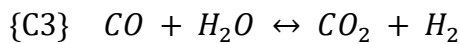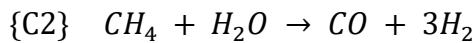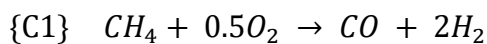
- **Westbrook & Dryer adjusted global mechanism (WD1)**

Westbrook and Dryer (Westbrook & Dryer, 1984) developed a 2-step global reaction mechanism. In the adjusted WD1 release, the CH_4 and CO oxidations rates are not changed to the original mechanism, but H_2 oxidation rate is added (C4) as happens in JL1:

{C5} $CH_4 + 1.5O_2 \rightarrow CO + 2H_2O$

{C6} $CO + 0.5O_2 \leftrightarrow CO_2$

{C4} $H_2 + 0.5O_2 \leftrightarrow H_2O$
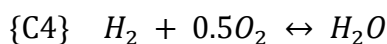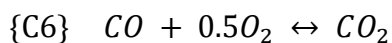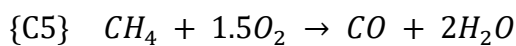
- **Westbrook & Dryer adjusted global mechanism (WD2)**

This mechanism maintains CH_4 and H_2 oxidation rates as WD1 but changed the CO oxidation rate. This change is made considering the CO dependency on the pressure equilibrium of [CO]/[CO2] following Andersen et al. (Andersen et al., 2009):

{C5} $CH_4 + 1.5O_2 \rightarrow CO + 2H_2O$

{C7} $CO + 0.5O_2 \leftrightarrow CO_2$

{C4} $H_2 + 0.5O_2 \leftrightarrow H_2O$
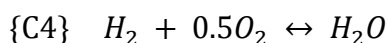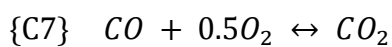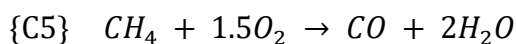
Table 3. 1 summarized the Arrhenius parameters defined for each global reaction mechanism:

Table 3. 1 Global mechanism's Arrhenius coefficient values and reaction orders

Nº	A	β	E_a/R	Reaction orders	Ref
C1	$4.4*10^{11}$	0	15095	$[CH_4]^{0.5}[H_2O]$	(Jones & Lindstedt, 1988)
C2	$3.0*10^8$	0	15095	$[CH_4][O]$	(Jones & Lindstedt, 1988)
C3$_f$	$2.75*10^9$	0	10065	$[CO][H_2O]$	(Jones & Lindstedt, 1988)
C3$_b$	$6.71*10^{10}$	0	13688	$[CO_2][H_2]$	(Wang et al., 2012)
C4$_f$	$7.91*10^{10}$	0	17609	$[H_2][O_2]^{0.5}$	(Marinov et al., 1995)
C4$_b$	$3.48*10^{13}$	0	47907	$[H_2O]$	(Wang et al., 2012)
	$5.03*10^{11}$	0	24056	$[CH_4]^{0.7}[O]^{0.8}$	(Westbrook & Dryer, 1984)
C6$_f$	$2.24*10^{12}$	0	20484	$[CO][O_2]^{0.25}[H_2O]^{0.5}$	(Westbrook & Dryer, 1984)
C6$_b$	$5*10^8$	0	20484	$[CO_2]$	(Westbrook & Dryer, 1984)
C7$_f$	$2.24*10^6$	0	5032	$[CO][O_2]^{0.25}[H_2O]^{0.5}$	(Andersen et al., 2009)
C7$_b$	$1.10*10^{13}$	-0.97	39452	$[CO][O_2]^{-0.25}[H_2O]^{0.5}$	(Andersen et al., 2009)

Units in kmol, m^3, K, s, kJ.

3.3.2   Implementation Methodology

The global reaction mechanisms described in section 3.3.1 have been implemented in ANSYS Fluent by User Define Functions (UDF) and User Define Memory (UDM).

Analysis of thermofluids in flameless (MILD)
combustion: assessment, improvement and
development of combustion models by CFD
Naiara Romero Anton

Considering the chemical kinetics of a system of N species reacting through M reactions we get:

$$\sum_{k=1}^{N} v'_{kj} M_k \leftrightarrow \sum_{k=1}^{N} v''_{kj} M_k \quad \text{for } j = 1, M$$

Eq. 3. 46

where M_k is species k symbol and v'_{kj} & v''_{kj} are the molar stoichiometric coefficient of species k in reaction j. It should be noted that reactions could proceed in one direction → (forward, f) or in both directions ↔ (forward, f, and backward, b). Considering the mass conservation, the progress rate of reaction for the reaction pair is defined as [kmol/m³/s]:

$$\omega'_j = K_{fj} \prod_{k=1}^{N} [X_k]^{v'_{kj}} - K_{rj} \prod_{k=1}^{N} [X_k]^{v''_{kj}}$$

Eq. 3. 47

where K_{fj} and K_{rj} are the forward and backward rates of reaction j. In this work they are calculated by Arrhenius law:

$$K_{fj} = A_{fj} T^{\beta_j} exp\left(-\frac{E_j}{RT}\right) = A_{fj} T^{\beta_j} exp\left(-\frac{T_{aj}}{T}\right)$$

Eq. 3. 48

where A_{fj} is a pre-exponential constant, β_j temperature exponent constant and E_j activation energy. The constants values used in this work are defined in Table 3. 1. The backwards rates K_{rj} are calculated considering the equilibrium constant (Poinsot & Veynante, 2005).

The progress rate of reaction, (Eq. 3. 47) theoretically is defined with the stoichiometric coefficients defined by the mass conservation law (v''_{kj} & v'_{kj}). In practice, instead of using stoichiometric coefficients as concentrations' exponent, other parameters (t'_{kj} & t''_{kj}) are used. These parameters are calculated based on experimental or detailed chemical numerical modelling. In this work, the exponents of Table 3. 1 are used (t'_{kj} & t''_{kj}).

Once the reaction rate of each specie k is calculated (Eq. 3. 47, Eq. 3. 48 and Table 3. 1), the next step is calculating the net molar production rate of each species k in reactions j [kmol/m³/s]:

$$R_{kj} = (\Gamma_j(v''_{kj} - v'_{kj})K_{fj}\prod_{k=1}^{N}[X_k]^{t'_{kj}} - K_{rj}\prod_{k=1}^{N}[X_k]^{t''_{kj}})$$

Eq. 3. 49

where $[X_k]$ is k species molar concentration. Then each k species net mass reaction rate is calculated:

$$\omega_k = W_k R_{kj}$$

Eq. 3. 50

where W_k is each species molecular weight W_k. Finally, chemical time scale is calculated

$$\tau_c = \max[Y_k/(|\omega_k|/\rho)]$$

Eq. 3. 51

where ω_k is the reaction rate in [kg/m³/s] of each specie (CH_4, H_2, O_2, CO and CO_2). The reaction rate below $\omega_k < 10^{-16}$ in kg/m³/s is excluded from the modelling.

Following this methodology, more species are considered for chemical time scale calculation. The UDF calculates chemical time scale following described methodology and in combination with the flow time scale calculated by ANSYS FLUENT, later, the UDF calculates Damköhler number, which is replaced in Eq. 3. 44 and Eq. 3. 45. However, this method maintains the efficiency of the NE-EDC model, as this method does not require the computational time of the method which calculates the eigenvalues of the Jacobian (Fox, 2003; Wartha et al., 2020). In this Thesis as CH_4, H_2, O_2, CO and CO_2 species are considered, the Arrhenius and reactions orders defined in section 3.3.1 are applied.

For a better understanding on the methodology, an example is shown for the JL1 global mechanism. First, the progress rate of reaction ω'_j are calculated [kmol/m³/s]:

$$\omega'_{C1} = 4.4 \cdot 10^{11}exp(\frac{-15095}{T[K]}) \cdot [CH_4]^{0.5}[O_2]^{1.25}$$

Eq. 3. 52

$$\omega'_{C2} = 3.0 \cdot 10^8exp(\frac{-15095}{T[K]}) \cdot [CH_4][H_2O]$$

Eq. 3. 53

$$\omega'_{C3_f} = 2.75 \cdot 10^9exp(\frac{-10065}{T[K]}) \cdot [CO][H_2O]$$

Eq. 3. 54

$$\omega'_{C3_b} = 6.71 \cdot 10^{10} exp(\frac{-13688}{T[K]}) \cdot [CO_2][H_2]$$

<div align="right">Eq. 3. 55</div>

$$\omega'_{C4_f} = 7.91 \cdot 10^{10} \exp(\frac{-17609}{T[K]}) \cdot [H_2][O_2]^{0.5}$$

<div align="right">Eq. 3. 56</div>

$$\omega'_{C4_b} = 3.48 \cdot 10^{13} \exp(\frac{-47907}{T[K]}) \cdot [H_2O]$$

<div align="right">Eq. 3. 57</div>

Then, the net molar production rate of each species k in reactions j [kmol/m³/s] are calculated by Eq. 3. 49:

$$\begin{bmatrix} R_{CH_4} \\ R_{H_2O} \\ R_{O_2} \\ R_{CO} \\ R_{CO_2} \\ R_{H_2} \end{bmatrix} = \begin{bmatrix} -1 & -1 & 0 & 0 & 0 & 0 \\ 2 & 2 & -1 & 1 & 1 & -1 \\ -\frac{1}{2} & 0 & 0 & 0 & -\frac{1}{2} & \frac{1}{2} \\ 1 & 1 & -1 & 1 & 0 & 0 \\ 0 & 0 & 1 & -1 & 0 & 0 \\ 0 & 0 & 1 & -1 & -1 & 1 \end{bmatrix} \cdot \begin{bmatrix} \omega'_{C1} \\ \omega'_{C2} \\ \omega'_{C3_f} \\ \omega'_{C3_b} \\ \omega'_{C4_f} \\ \omega'_{C4_b} \end{bmatrix}$$

<div align="right">Eq. 3. 58</div>

The parameters of the matrix represent the difference between the product and reactant stoichiometric coefficients for species k in reactions j. Next, Eq. 3. 50 is applied and the maximum chemical time scale is calculated. The chemical time scale calculation is carried out by UDF.

4   Results validation and discussions

This section presents the modelling results and validation. First, an appropriate C_ξ is determined for use in the EDC model with constant model parameters. Then, the predictions of velocity and temperature fields in two models (the EDC model with specific and optimized fixed values of the model constants and the NE-EDC model) are presented and compared with experimental data. Next, NE-EDC and Generalized NE-EDC models results are compared between them and with experimental data. Finally, the NE-EDC model mean temperature profiles are compared with the E-EDC model results.

4.1 C_ξ model constant value selection

To determine an appropriate C_ξ value to apply the EDC model to a flameless combustion furnace, the position of the zone with a high heat release, as known from the OH* measurements, is used as the criterion, so the degree of spatial homogeneity of the mean temperature, as known from the CARS measurements, is predicted correctly. As a numerical parameter representing the reaction zone, the product of the formaldehyde (CH2O) mass fraction and the OH mass fraction (Medwell et al., 2007) called formylradical (HR) is used. The mass fraction of CH2O indicates when the reaction starts while the latter indicates that a high temperature has been reached. Fig. 3. 3 shows the contour plot of the product of the two mass fractions for six values of the parameter C_ξ, from the standard value to higher values.
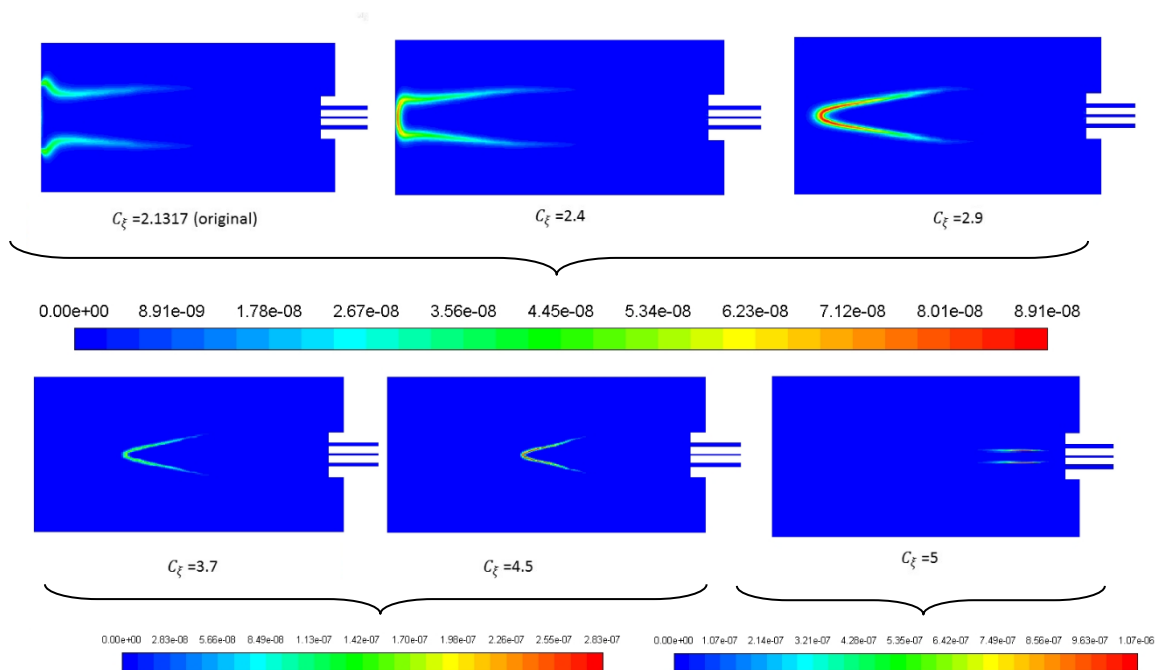
Fig. 3. 3 Predicted formylradical (HR) for different C_ξ values

According to the mean OH* chemiluminescence intensity distribution (Huang, Xu, 2018) for an equivalence ratio of 0.8 the reaction zone is located in the middle of the furnace between 450 mm and 550 mm above the burner nozzle. This is incompatible with the predictions for C_ξ=2.1317, 2.4 and 5. For the values C_ξ=2.1317 and 2.4, the reaction zone

Analysis of thermofluids in flameless (MILD)
combustion: assessment, improvement and
development of combustion models by CFD
Naiara Romero Anton

is too high, while for C_ξ=5 it is too low. For the choice between the other values the homogeneity of the mean temperature (see Fig. 3. 4) is used as the quality measure.
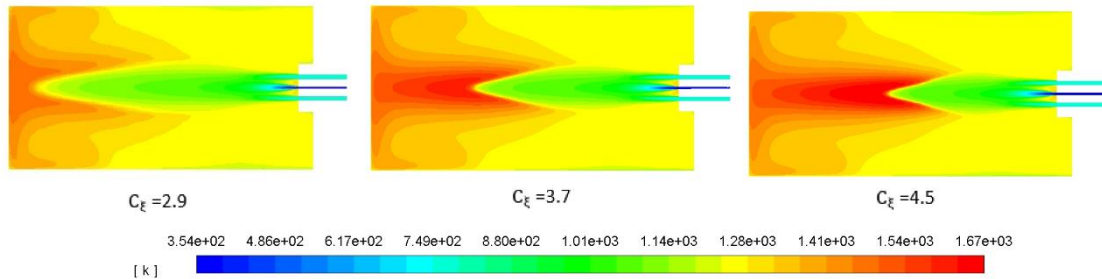
Fig. 3. 4 Temperature contour for several C_ξ values

One of the flameless combustion characteristics is the homogeneous temperature distribution along the furnace. The best temperature homogeneity for this case is found to be for the case C_ξ=2.9. Additionally, according to Fig. 3. 3, C_ξ=2.9 value matches better with the measured reaction zone (located in the middle of the furnace between 450 mm and 550 mm above the burner nozzle) than the other two cases. However, further analysis and a more detailed comparison with experimental data of velocity and temperature are necessary.

4.2   NE-EDC vs EDC modified

Before comparing predicted mean temperature to experimental measurements, flow field prediction is analysed, as the success of predicting combustion physics depends on the quality of the flow field.
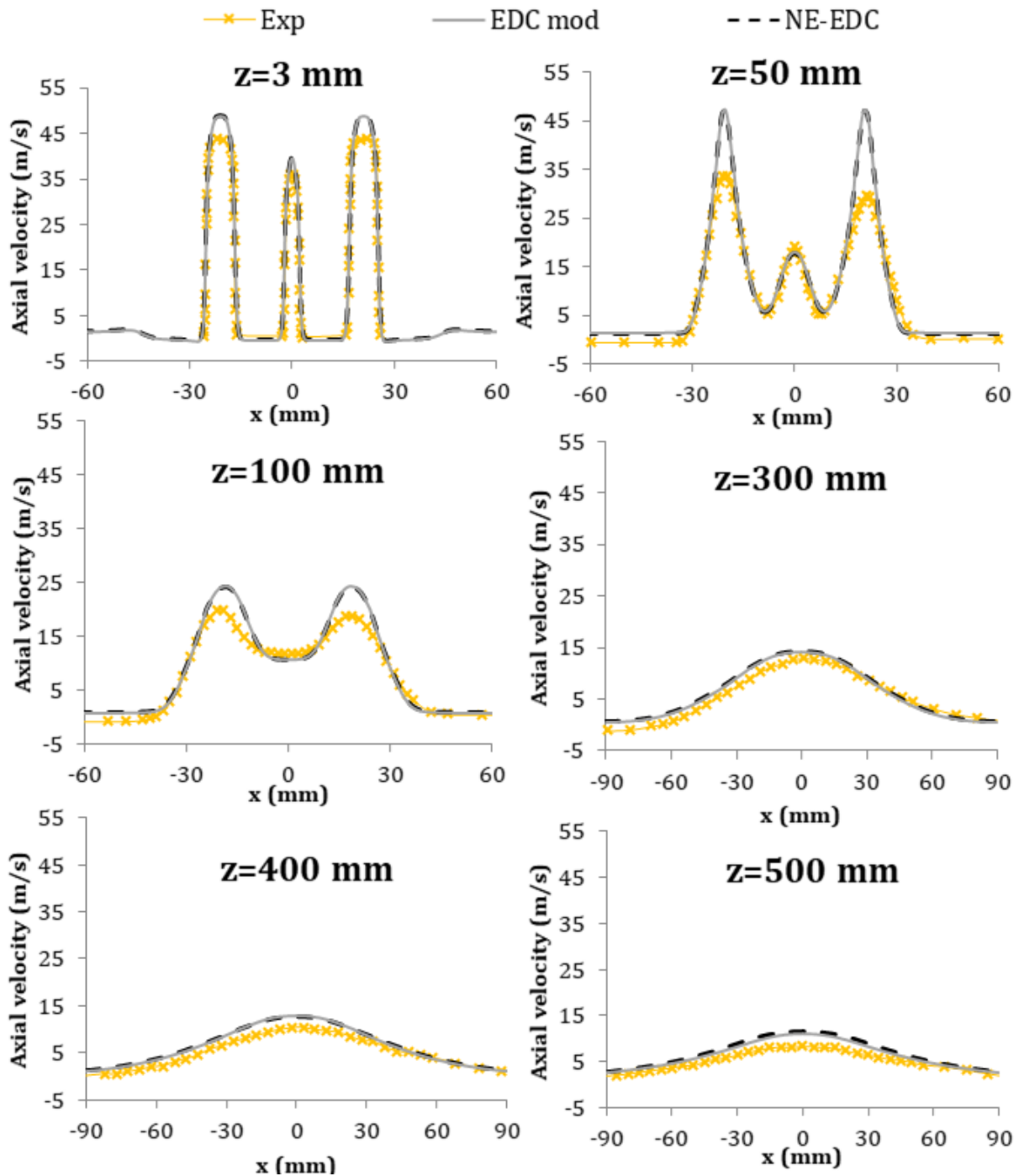
Fig. 3. 5 Comparison between measured and predicted radial profiles of mean axial velocity from simulations with EDC model with $C_\xi = 2.9$ and NE-EDC

In Fig. 3. 5, the radial profiles of the mean axial velocity ($\widetilde{U}_Z$) at different axial locations predicted by the two modified versions of EDC models, are compared with the experimental data. Experimental data is represented by yellow line while simulation

results are displayed as continuous lines for the EDC with global modification of model constant (called the EDC mod in the figures) and dash lines for the NE-EDC model. The mean velocity $\widetilde{U}_Z$ at the nozzle exit, by construction, agrees well with the experimental data but as the flows develop (z=50 mm and z=100 mm), the peak velocity on the centreline of the air jets is overpredicted. At the mid height of the furnace (z=300 mm), the two model results are in good agreement with the experimental data, showing acceptable performance of the realizable $k - \varepsilon$ model. At greater heights (z=400 and 500 mm) the predicted axial velocity is also in good agreement with the experimental data for the EDC model with model constant modification and the NE-EDC model.

Next, the mean turbulent kinetic energy predicted by the $k - \varepsilon$ model is analysed. Representative radial profiles are shown in Fig. 3. 6. At the inlet, the boundary condition for turbulent kinetic energy is derived from the measured data for the axial and radial directions and multiplying the contribution of the radial direction by two to account for the contribution from the non-measured direction. At z=100 mm, the two models overpredict the mean turbulent kinetic energy. At z=500 mm, the predictions are quantitatively better, but the minimum at the centreline shows that the rate of jet development is underpredicted.
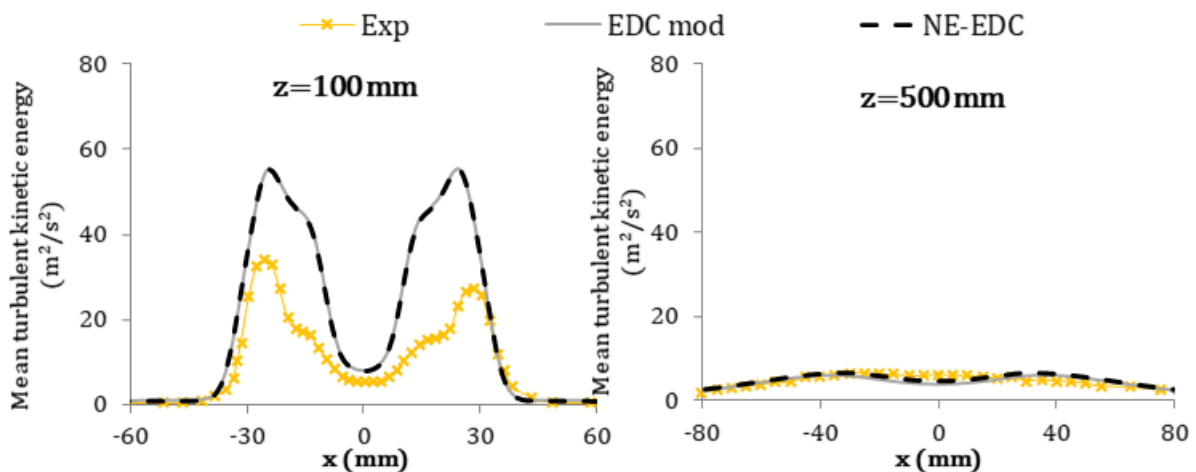
Fig. 3. 6 Comparison between measured and predicted mean turbulence kinetic energy from simulations with EDC model with $C_\xi = 2.9$ and NE-EDC

Next, a comparison is made between the measured and predicted mean temperatures obtained for the extended two turbulence-chemistry interaction models. In Fig. 3. 7, the

mean temperature contour plots are shown for each of the studied extended EDC turbulence-chemistry interaction models.
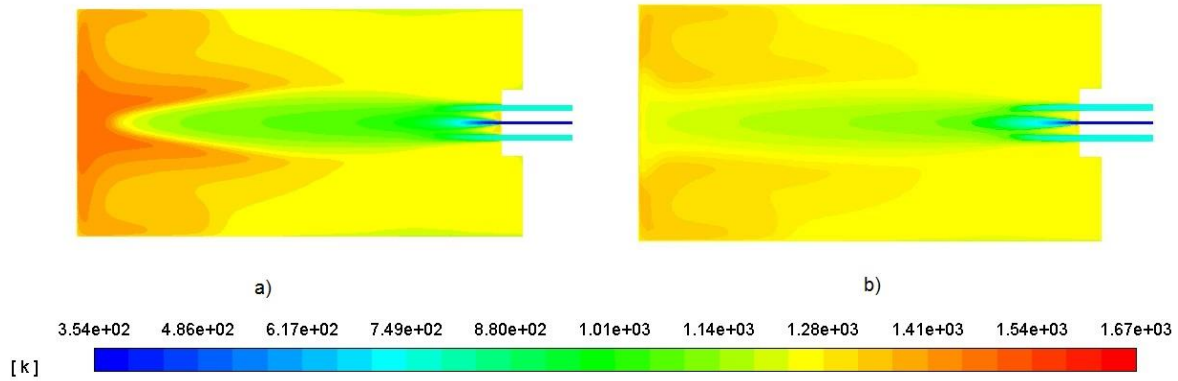
Fig. 3. 7 Temperature contour a) EDC Model Constant $C_\xi = 2.9$ and b) NE-EDC

The EDC model with global change of model constant, C_ξ equal to 2.9 (Fig. 3. 7a)) predicts a quite homogeneous temperature in the area close to the burner (up to z=200 mm), however, in the top zone of the furnace (500 mm< z <400 mm), a maximum temperature of around 1450K is predicted.

In the NE-EDC model, (Fig. 3. 7b), where C_τ and C_ξ are space dependent, since they are calculated directly on the basis of the local Reynolds and the Kolmogorov scale Damköhler numbers, the predicted temperature distribution is very homogeneous along the entire height of the furnace.

Besides, a quantitative comparison with experimental data can be made looking at the mean temperature profiles along horizontal cross sections at different heights above the nozzle exit (shown in Fig. 3. 8).

Analysis of thermofluids in flameless (MILD)
combustion: assessment, improvement and
development of combustion models by CFD
Naiara Romero Anton
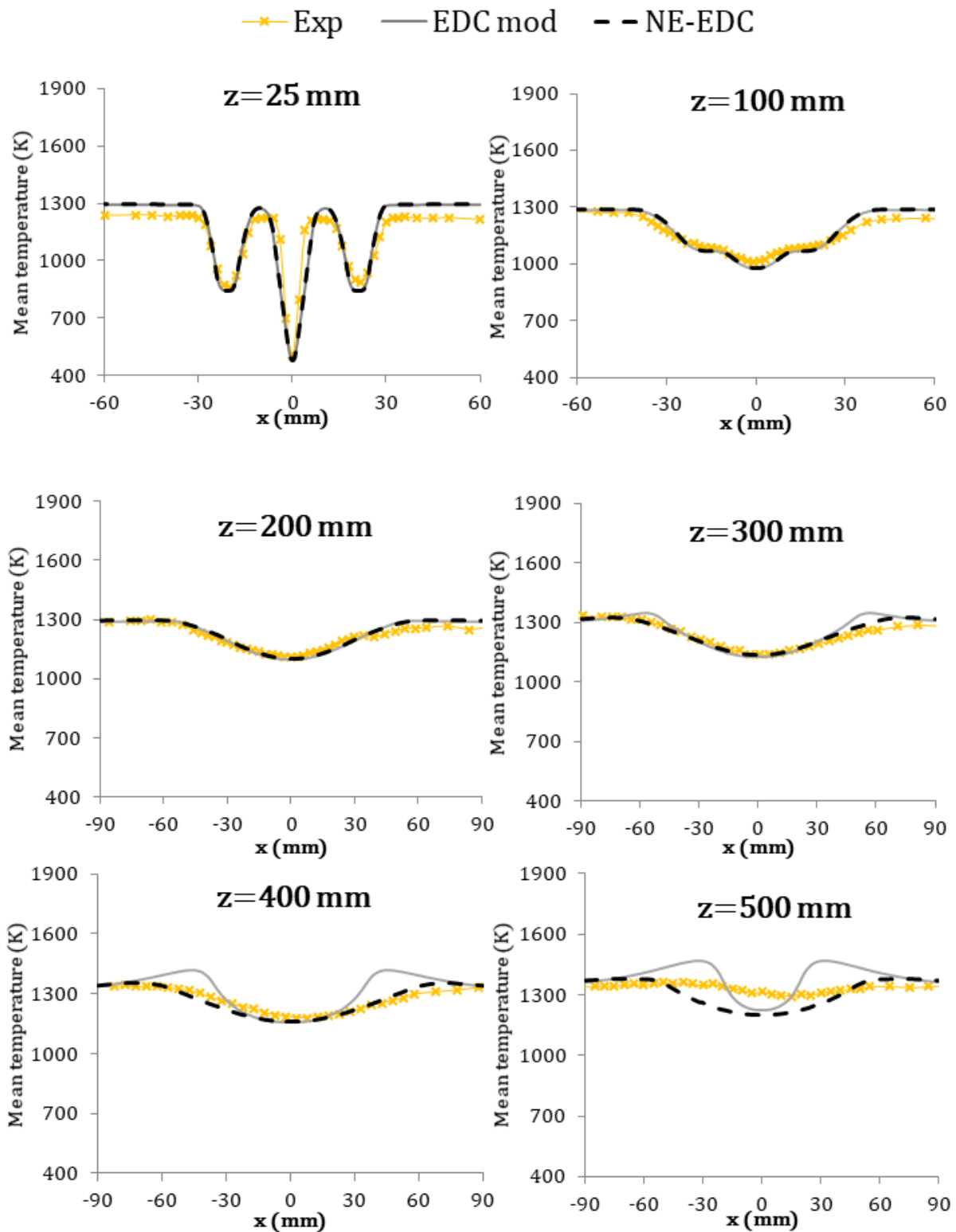
Fig. 3. 8 Comparison of mean temperature from experimental measurements and from simulations with EDC model with $C_\xi = 2.9$ and NE-EDC

The EDC model, with $C_\xi = 2.9$, provides predictions for mean temperatures that are in close agreement with the experimental results in the area close to the burner (z=25 mm, z=100 mm and z=200 mm) and in the middle area (z=300 mm). However, at z=300 mm, there is a slight over prediction by the simulation results far from the centre. At a height of z=400 mm, this deviation is larger in magnitude, but still restricted to the zone far from the centre. In the top zone of the furnace (z=500 mm), there is in addition an under prediction in the central region. In conclusion, the EDC model, with a finite structure constant value equal to 2.9, predicts flameless combustion in the lower and middle parts of the furnace quite accurately, but in the top zone of the furnace the predicted homogeneous temperature distribution is incorrect.

The NE-EDC modelling the lower part of the furnace (z=25 mm, z=100 mm, z=200 mm) gives a temperature prediction that is equally good as that of the EDC model with $C_\xi = 2.9$. In the mid (z=300 mm) and higher (z=400mm) zones of the furnace, the results are in better agreement with the experimental data; in fact, better than the EDC model with globally modified C_ξ. At z=300 and z=400 mm, the temperature over prediction far from the centre is smaller for the NE-EDC. At z=500 mm, the temperature is slightly under predicted in the centre of the furnace, but in the zone close to the furnace walls, the temperature prediction is of the same order as the experimental data. Therefore, it can be concluded that the NE-EDC model is a real improvement compared to the EDC model with constant C_ξ where the EDC mod performs less good than NE-EDC providing the NED-EDC the best prediction.

4.3 NE-EDC vs Generalized NE-EDC

In this section, a comparison is made between measured and predicted mean axial velocity and mean temperatures for each adjusted global mechanism model for chemical time scale calculation. Fig. 3. 9 shows the results of the mean axial velocity for the NE-EDC model in combination with Jones & Lindstedt adjusted global mechanism (JL1), the Westbrook & Dryer adjusted global mechanism (WD1), the Westbrook & Dryer adjusted global mechanism (WD2) and the one-step CH_4 global mechanism. Experimental data at

Analysis of thermofluids in flameless (MILD)
combustion: assessment, improvement and
development of combustion models by CFD
Naiara Romero Anton

different axial locations of the furnace (z=3 mm, z=100 mm, z=300 mm and z=500 mm)
are also displayed.
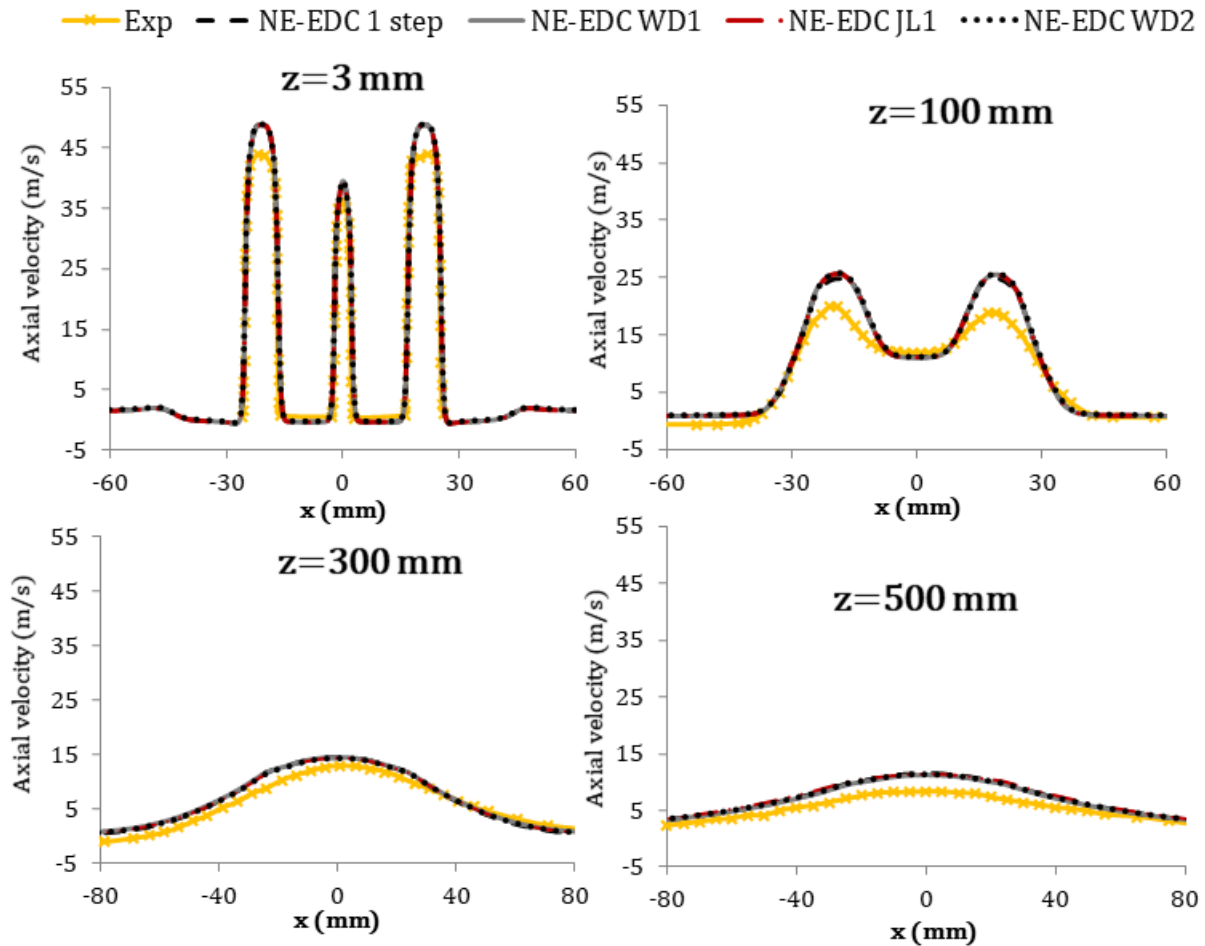
Fig. 3. 9 Comparison between measured and predicted radial profiles of mean axial velocity

There is no difference in mean axial velocity prediction among the four global reaction
mechanisms. This is because the same turbulence-chemistry interaction model, realizable
$k-\varepsilon$ is used. Finally, this model is the cause of velocity prediction, so that it can be said
that this turbulence model is appropriate for this case of study.

Then, the mean temperature contour of the JL1, the WD1, WD2 and the 1-step CH_4 global
mechanisms are shown.

a) JL1   b) WD1

c) WD2   d) 1-step

[k]   3.54e+02   4.86e+02   6.17e+02   7.49e+02   8.80e+02   1.01e+03   1.14e+03   1.28e+03   1.41e+03   1.54e+03   1.67e+03
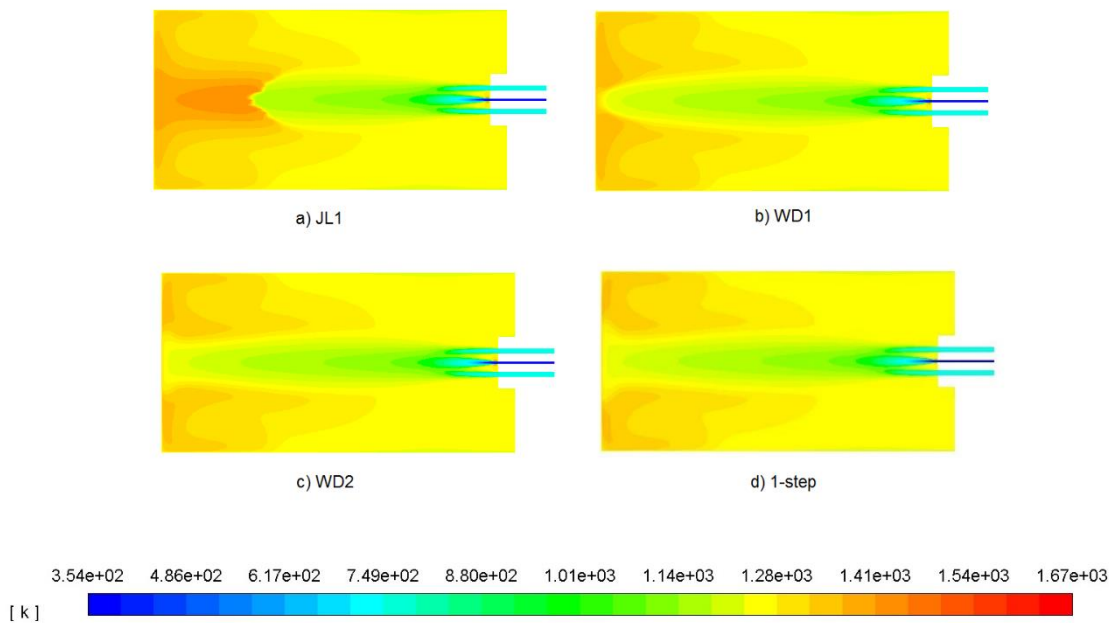
Fig. 3. 10 Mean temperature contour for JL1, WD1, WD2 and 1-steb global mechanisms

At first sight, it can be appreciated that JL1 global mechanism presents greater mean temperature values than the other models, being the only one that exceeds 1400 K in the points away from the flame, while the other global mechanism models provided similar values. For a better viewing, the radial profiles of mean temperature are compared in Fig. 3. 11. In this sense, the NE-EDC model in combination with the JL1, the WD1, WD2, the 1-step CH_4 global mechanism and experimental data are displayed at different axial locations of the furnace (z=25 mm, z=100 mm, z=200 mm, z=300 mm, z=400 mm and z=500 mm).
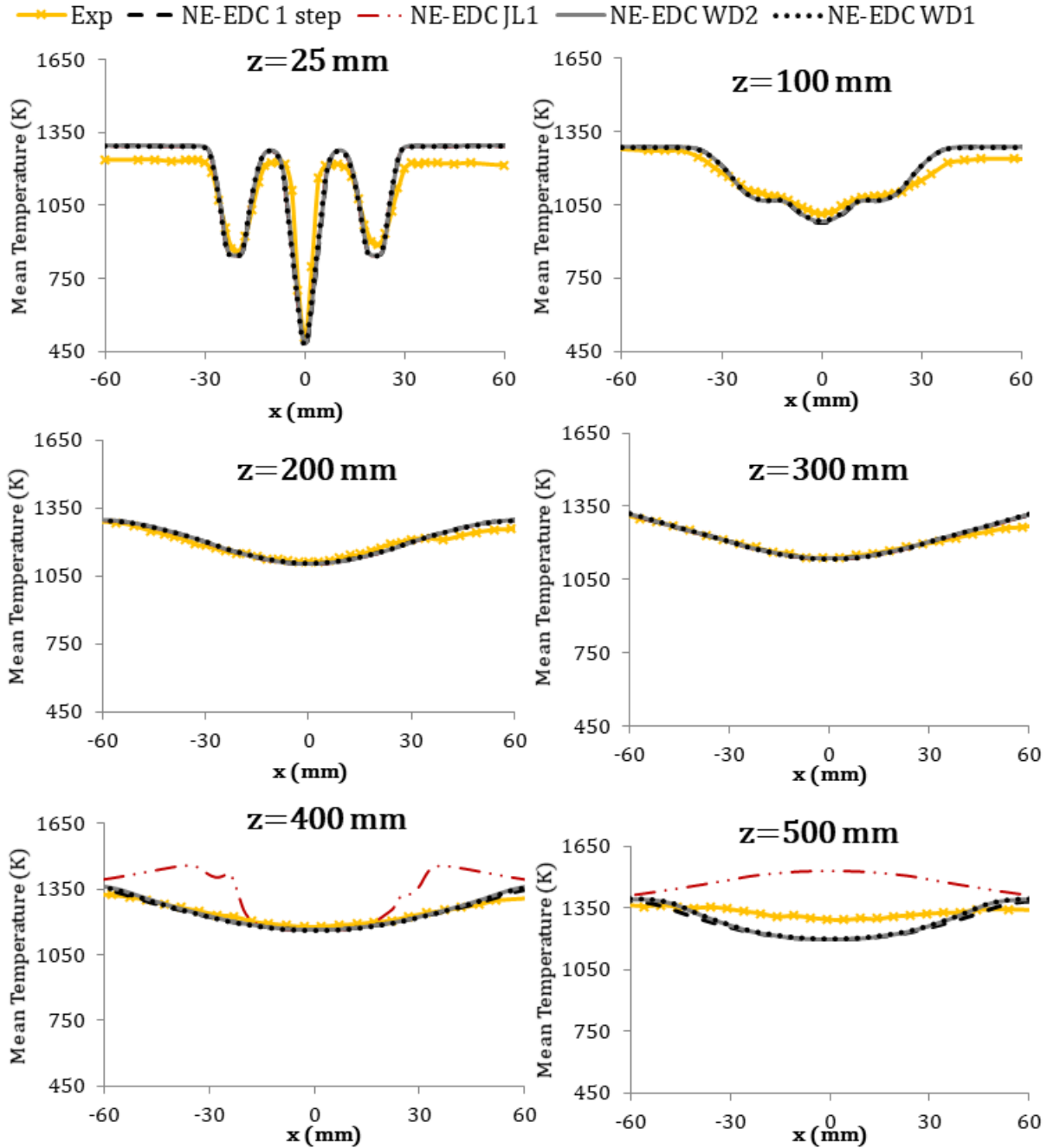
Fig. 3. 11 Comparison of mean temperature from experimental measurements and from simulations with different global mechanisms

The results of the four global mechanism models showed a good agreement with experimental data in the mean temperature predictions at the nozzles exit (z=25 mm) and at the mid-height of the furnace (z=100, z=200 and z=300 mm). At greater heights (z=400 and z=500 mm) JL1 model over predicts mean temperature moving away from experimental data. This deviance is stressed at z=500 mm where the gradient is opposite

from experimental data. This feature can be also appreciated in Fig. 3. 10 where high temperature is displayed close to the furnace top wall. Thus, JL1 global mechanism is discharged for this flameless combustion furnace modelling.

Among the WD1, WD2 and 1-step global mechanism a slight difference is appreciated at z=400 and z=500 mm heights. For a better visualization, Fig. 3. 12 shows these three global mechanisms and experimental data results.
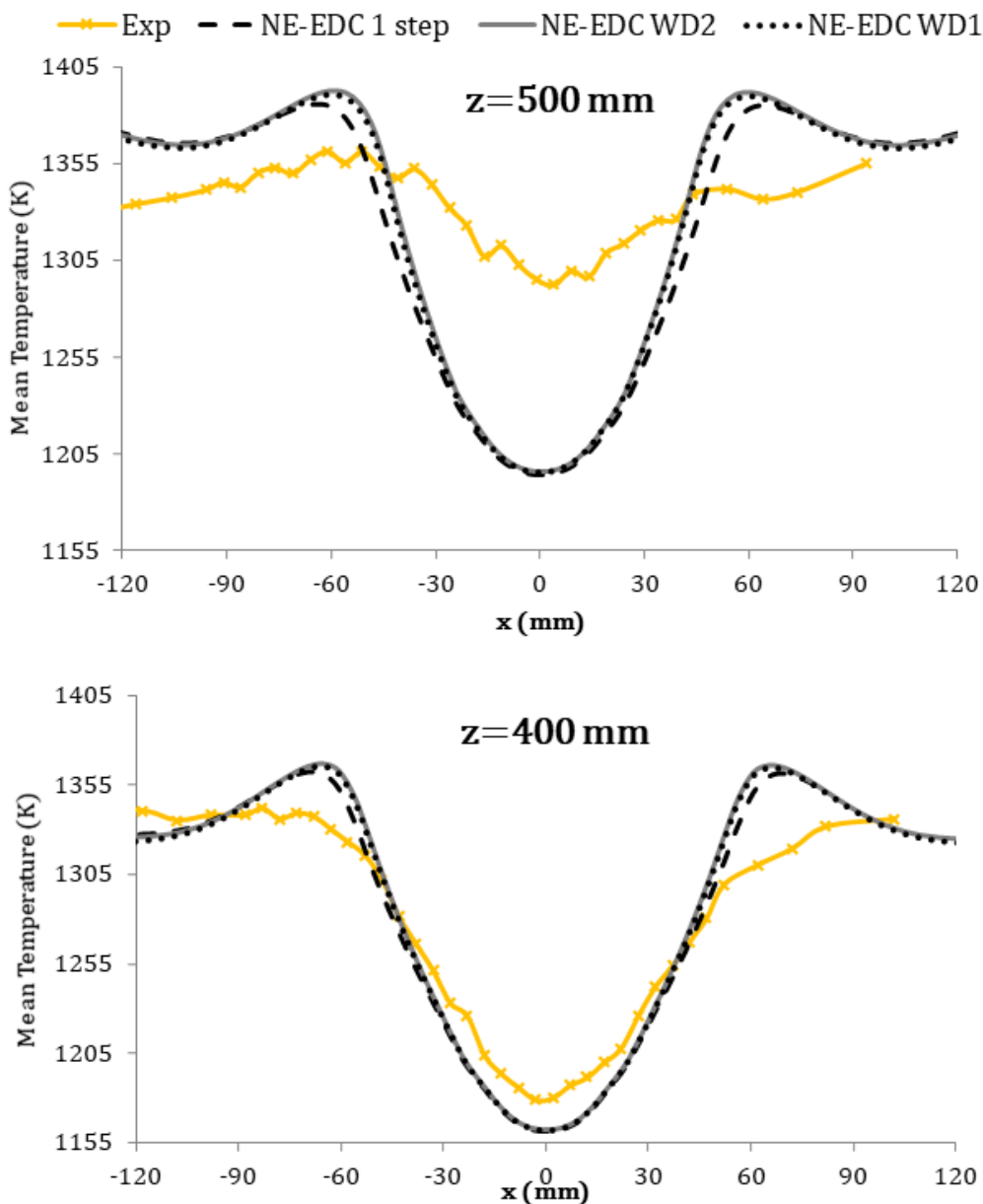
Fig. 3. 12 Comparison of mean temperature from experimental measurements and from NE-EDC –step, NE-EDC WD1 and NE-EDC WD2.

It is appreciated that WD1 and WD2 modelling results are almost the same. Thus, it is concluded that CO oxidations rates does not have a huge impact over the mean temperature in this case. At this point it should be noted that during the modelling, it took more time to converge the WD1 model rather than the WD2 model, so that being the results of both models similar, from a modelling point of view WD2 is recommended. The CPU time for each global mechanism with a 2 cores CPU@ 2.5 GHz is displayed in Table 1. It should be clarified that displayed computational time is starting from a converge reacting flow-field of the NE-EDC model with 1-step reaction mechanism for chemical time calculation:

Table 1 CPU computational time

	Computational time	Convergence of temperature
JL1	23 h	Straight line
WD1	148 h	Sine wave
WD2	22 h	Straight line

Between 1-step global mechanism and WD2 a slight difference is appreciated. At z=400 mm and z=500 mm heights this deviance can be seen clearly. Close to the furnace centre ($|x| < 60$ mm) the WD2 under predicts less the mean temperature than 1-step mechanism at both heights. For example, at $|x|$=36 mm the deviation of WD2 model is 3.5% while 1-step mechanism provides a deviation of 5.5%. Although the WD2 has slight improvements, it does not seem that taking into account CH_4, H_2, O_2, CO and CO_2 species in chemical time scale calculation affects notably the results of the model. This suggests little interaction among reaction zones for this application. The interaction among the reaction zones provides more effect on mean temperature predictions in JHC burner (Evans et al., 2019) than in enclosed furnace. This could be related to the limited height of the enclosed furnace, while on JHC burner there is not volume limitation.

In any case, the NE-EDC model in combination with the WD2 gives better predictions of the radial profiles of the mean temperature as compared to the 1-step global mechanism. For this reason, WD2 is selected as the best global mechanism model to consider the interaction among the reaction zones during flameless modelling, without too much impact on computational time.

4.4 NE-EDC vs E-EDC

The relative performance of the E-EDC and the NE-EDC models is validated by looking at the prediction of mean velocity and temperature. For the velocity fields the differences are very small. For the temperature noticeable differences show up only in the upper part of the furnace, at z=300 mm and higher. In Fig. 3. 13 experimental measurements and the results of the two models are shown.
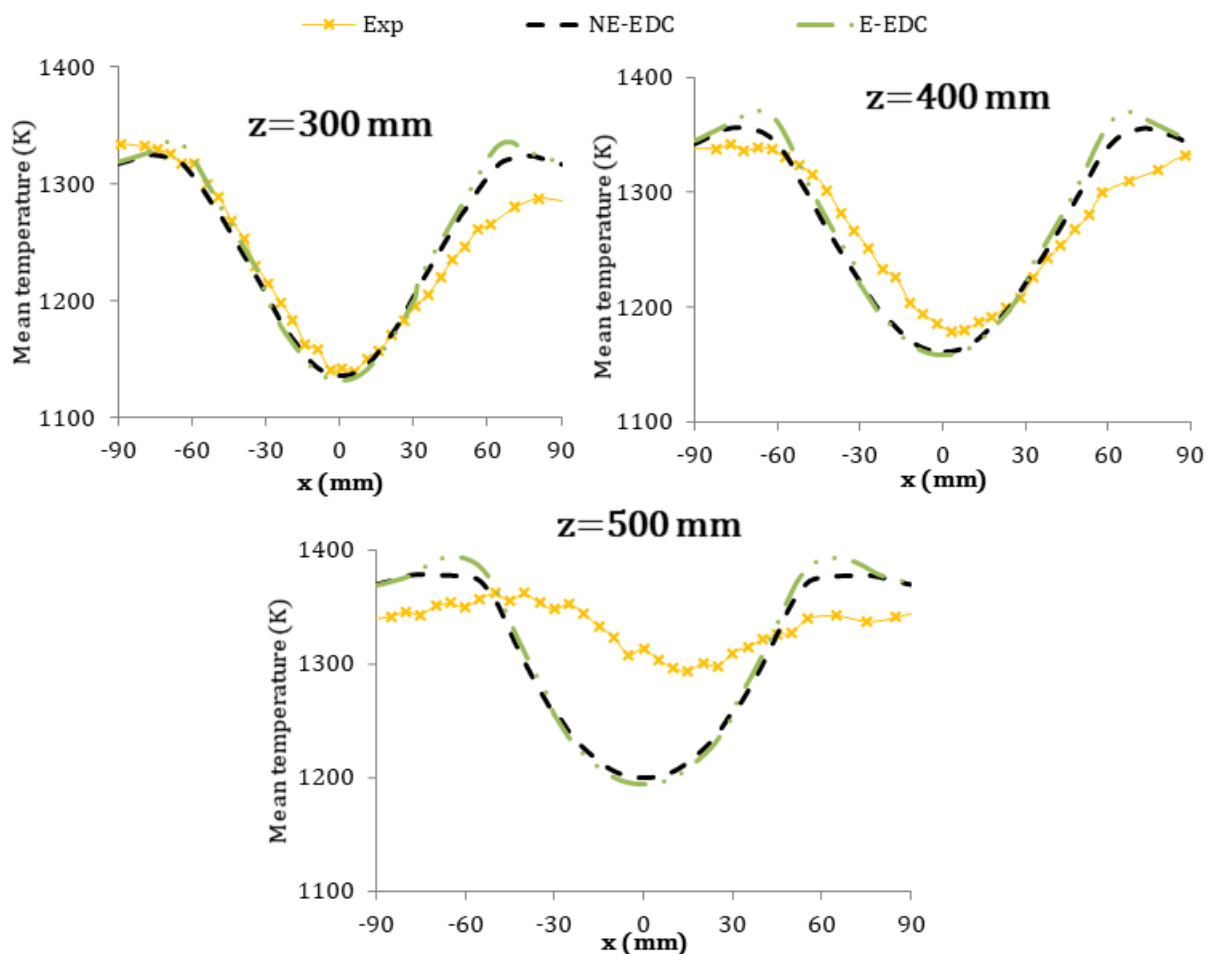
Fig. 3. 13 Comparison between the E-EDC and the NE-EDC mean temperature

The temperature prediction close to the centre (x=0 mm) is essentially the same in both models. However, away from the centre ($|x| > 60$ mm) the temperature is less over predicted by the NE-EDC model for the three heights. Therefore, the NE-EDC gives a better prediction of the radial profiles of the mean temperature as compared to the E-EDC, although it does not exactly reproduce the experimental results.

5 Conclusions

In this chapter, the NE-EDC was derived and its performance studied in comparison with the EDC with calibrated model constants and the E-EDC model developed by Parente et al.. Detailed experimental data available from previous work on a natural gas fired lab-scale furnace were used.

The EDC model with finite constant value set to $C_\xi = 2.9$ provides not as good results as the NE-EDC. The NE-EDC model offer a significant advantage over the EDC model with globally modified C_ξ value. In the latter, there is a need for a parametric calibration in order to optimize the C_ξ value for the case study and this is not needed in the NE-EDC because the C_ξ is evaluated based on local Re and Da numbers. The NE-EDC modelling results and experimental profiles match very well at all heights, although at the highest analysed height (z=500 mm), the mean temperature is a little under predicted. Recently, the DNS modelling results suggest interactions among the reaction zones in flameless combustion. Therefore, the use of more information from a detailed mechanism to calculate the chemical time scale could be a way to improve NE-EDC modelling results. To this goal the Generalized NE-EDC model is proposed in this Thesis which analyses the effect of the interaction among the reaction zones suggested by DNS modelling. The chemical time scale considering CH_4, H_2, O_2, CO and CO_2 species mass fractions is calculated by UDF. The chemical time scale is calculated more accurately but not increasing the computational time during modelling, so that global reaction mechanisms adjusted for flameless combustion are use (note that detail mechanism, smooke-25, is used for temperature and species mass fraction calculation during modelling).

It was found that the WD2 mechanism is the best model for chemical time scale calculation as it under predicts less mean temperature close to the centre of the furnace (|x| < 60 mm) at z=400 and z=500 mm. The WD1 mechanism provided similar results but from a numerical point of view, the numerical convergence takes more time. The JL1 mechanism is neglected as the mean temperature at greater heights is notably over predicted. For this application, the 1-step global mechanism is also a good choice, but it is true that with the WD2 mechanism the results improve slightly. It can be concluded that for this specific

application the interactions among the reaction zones do not have too much impact of mean temperature prediction.

The velocity and turbulence predictions of the NE-EDC and the E-EDC models are very close to each other, also the mean temperature results in the lower part of the furnace are very close. Only in the upper part of the furnace, differences appear. Here the NE-EDC gives a more accurate prediction of the radial profiles of the mean temperature, especially away from the centre. This shows that the differences between the E-EDC and the NE-EDC model assumptions leading to different C_ξ formulation (see Eq. 3. 39 and Eq. 3. 45) and consequently different mean reaction rate is relevant.

It can be concluded that the Generalized NE-EDC model has the most consistent trend with experimental data for the Delft lab-scale furnace modelling.

CHAPTER 4: FGM MODEL APPROACH AND VALIDATION FOR FLAMELESS COMBUSTION

1 Introduction

During the last years computers suffered a huge development allowing engineers to deal with large-scale problems and more complex systems. Due to that, numerical modelling has emerged as a basic tool for engineers in their daily life. The application of CFD leads to savings in time and cost as some experiments could be avoided. Nevertheless, there is still a lack of computation speed and storage capacity to deal with detailed chemistry modelling and complex geometry in turbulence combustion processes (remember that in turbulence combustion there are so many time and length scales). To this goal, a reliable approach is the simplification of chemical mechanisms without too much impact on simulations accuracy. This simplification is trying to describe the reaction rate by a reduce number of species.

The first approach to simplify detailed reaction mechanism is the chemical reduction method (Peters, Norbert, 1991). This method is applied in very fast chemical processes and follows steady state and partial equilibrium approximation. In practice, the variables are calculated "of-line" and stored in a database as a function of some controlling variables and during simulations, only controlling variables are solved, reducing computational time. Nevertheless, the researcher decides which species can be considered in quasi-steady state, so that knowledge of chemical kinetics is required. This issue was resolved with the CSP (Lam & Goussis, 1989) and the ILDM (Maas & Pope, 1992) chemical

reduction methods. They use a mathematical approach to decide quasi-steady state species. The weak point of the CSP and the ILDM models is their low accuracy at low temperatures. In colder part the chemical processes become slower (there are fewer fast reactions), so that less species can be considered in quasi-steady sate. Nevertheless, these models do not make any distinction between low and high temperatures.

The Laminar Flamelet Model (LFM) is another alternative to reduce the computational time (Peters, N., 1986). This model combines the simplicity of laminar flames and detailed chemistry and tabulates the stable branch of the S-curve while the extinction due to quenching is not captured. It is also applied to turbulent flames; in this case it is call Turbulent Flamelet Model (TFM). The TFM assumes that a multidimensional flame (turbulent non-premixed flame in this work) can be considered as a set of one-dimensional stretched laminar flames (flamelets). The model considers that chemical time scales are faster than turbulence time scales, thus the flame is considered locally as a thin laminar interface between fuel and oxidizer (flame front). The turbulent flame is studied in the normal direction of the flame front for stoichiometric flame stretch but considering them locally as a laminar flame, so that LFM concepts are applied (see Fig. 4. 1).
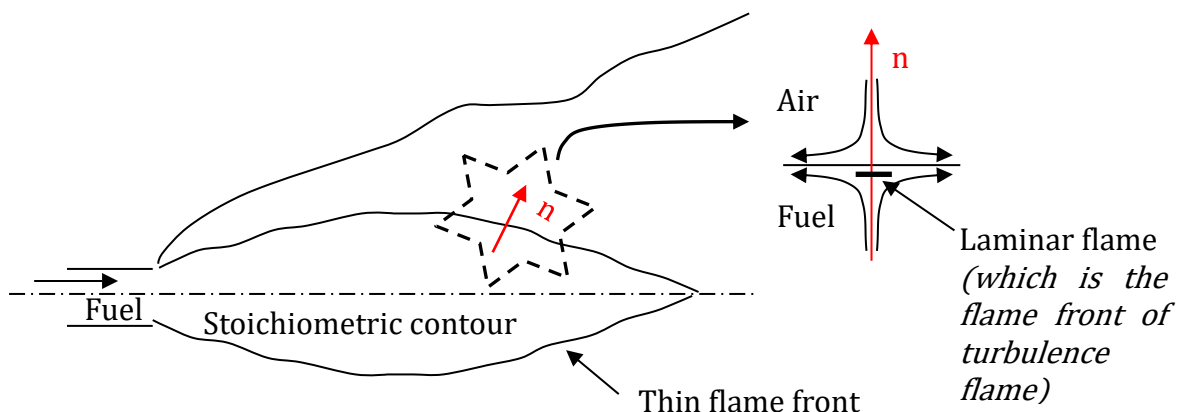
Fig. 4. 1 Flamelet model assumption description

In turbulence flow assumption as flamelets are stretched and wrinkled the scalar dissipation rate (χ) is introduced to consider them. Thus, flamelets equations are defined by Eq. 4. 1 and Eq. 4. 2:

$$\rho \frac{\partial \Phi}{\partial t} = \dot{w}_\Phi + \frac{1}{2} \rho \chi \frac{\partial^2 \Phi}{\partial Z^2}$$

Eq. 4. 1

Φ described species mass fraction and temperature while the scalar dissipation rate is defined as.

$$\chi = 2D \left(\frac{\partial Z}{\partial x_i} \frac{\partial Z}{\partial x_i} \right)$$

Eq. 4. 2

D is the diffusion coefficient which is considered the same for all species. It is appreciated that the only parameter depending on space (x_i) is the scalar dissipation rate, this is because a coordinate change has been made to T and Y_k calculation. For steady laminar flamelet (SLF) assumption, the structure of the flame is considered steady and Eq. 4. 1 is replaced by:

$$\dot{w}_\Phi = -\frac{1}{2} \rho \chi \frac{\partial^2 \Phi}{\partial Z^2}$$

Eq. 4. 3

It is appreciated that the flame structure in turbulent flames can be defined by laminar flamelets with mixture fraction and dissipation rate. Different χ values described different flame structures. Nevertheless, it is of common use the stoichiometric scalar dissipation rate and mixture fraction to define flamelets ($\Phi = \Phi(Z, \chi_{st})$. This approach can be call standard steady laminar flamelet model (SSLF). In the SSLF the internal structure of the flame is considered frozen with a constant flame front thickness as flamelet are characterizes at stoichiometric conditions. Finally, in TFM the mixture fraction and the scalar dissipation rate are statistically distributed, due to that the joint PDF of χ_{st} and Z should be considered.

$$\widetilde{\Phi} = \int_0^{+\infty} \int_0^1 \Phi(Z, \chi_{st}) \tilde{P}(Z, \chi_{st}) dZ d\chi_{st}$$

Eq. 4. 4

$\tilde{P}(Z, \chi_{st})$ is the joint PDF of Z and χ_{st} which are usually supposed statistically independent:

$$\tilde{P}(Z, \chi_{st}) = \tilde{P}(Z)\tilde{P}(\chi_{st})$$

<div align="right">Eq. 4. 5</div>

In order to overcome the deficiencies of the reduction techniques and flamelet models comments above, that is, (1) the low accuracy at low temperatures showed by CSP and ILDM and (2) the weak point of SSLF model that only considers scalar dissipation rate at stoichiometric conditions, the FGM model was developed (van Oijen et al., 2016). This model is a combination of both models but presents some improvement. On the one hand, at low temperatures apart from chemical kinetics, convection and diffusion are considered, increasing model accuracy (Oijen, 2002). As an example, on Fig. 4. 2 the ILDM (dashed line), the FGM (solid line) and detailed chemistry (grey dots) results are compared. It is appreciated that at high temperatures the ILDM, the FGM and detailed chemistry results match perfectly, but at low temperatures the ILDM model loss accuracy while the FGM model shows good agreement with detailed chemistry results.
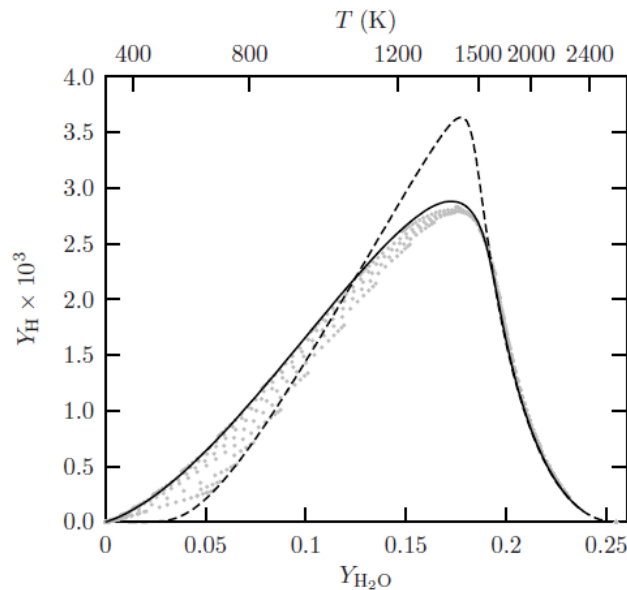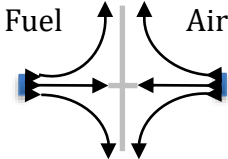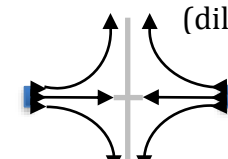
Fig. 4. 2 Projection of 1D FGM (solid line), ILDM (dashed line) and detailed chemistry (grey dots) (Oijen, 2002)

On the other hand, comparing with SSLF model, FGM model's flamelets are generated for several χ values until flame extinction happens. The flame front motion is treated by an un-scaled progress variable (Y_C), so that the transition between fresh to burner gases state is considered.

The FGM model presents lower computational time than the EDC model using detailed chemistry. Therefore, it is an attractive model to be used on flameless combustion. The FGM model available in ANSYS Fluent, where non-premixed flamelets are generated using as boundary condition pure fuel and pure air, does not consider the dilution effect during flamelets generation and modelling. Thus, temperature over predictions are expected when this model is directly used for flameless modelling. The dilution effect on flamelets generation was checked (Abtahizadeh et al., 2012) and the results showed that dilution has impact in the flame structure in laminar counterflow configuration using either diluted and preheated fuel and air, or diluting one of them. Thus, it can be concluded that the use of a dilution variable in flamelet based models is interesting for flameless modelling.

In this Thesis ANSYS Fluent release 19.R2 is used for Delft lab-scale flameless combustion furnace modelling. The performance of two flamelet based models are analysed; on the one hand, the standard version of FGM model based on non-premixed flamelets of fuel and air and on the other hand, the Diluted-Air-FGM (DAFGM) based on non-premixed flamelets of fuel and diluted air with dilution level as an extra independent variable (see Table 4. 1).

Table 4. 1 FGM and DA-FGM flamelet generation description

Model	Flamelet generation description	
FGM (ANSYS Fluent default options)	Pure fuel and air as boundary conditions for flamelets generation	
DA-FGM (first time implemented in ANSYS Fluent)	Pure fuel and DILUTED air as boundary conditions for flamelets generation	

The DA-FGM model so far is only available in OpenFOAM (Huang, Xu, 2018), so in this Thesis it is for the first time implemented in ANSYS Fluent by User Define Functions (UDF), User Defines Memory (UDM) and User Define Scalars (UDS).

Both modelling results are then compared with Delft lab-scale furnace experimental radial profiles of the mean axial velocity ($\widetilde{U}_Z$) and mean temperature distribution at different axial locations.

2   Flamelet Generated Manifold (FGM) model

The flamelet model guess that a turbulent flame is coupled by laminar flames with a frozen internal structure not altered by turbulence. Turbulence flow fluctuations are added to the laminar flamelets by PDF functions (Eq. 4. 4). The FGM model assumes that the local state of the reacting mixture in a turbulent flame evolves in the same way as one of a set of canonical cases of simple laminar flame structures. The relations between all relevant variables and a selected number of variables describing the local state, define a manifold in composition space. In contrast to purely chemical reduction methods, the FGM model also considers the role of diffusion (transport effects) and can also accurately describe states at low temperatures outside the main reaction zone. In contrast to the SSLF model, the selection of the local state is not primarily controlled by the strain rate ($\Phi = \Phi(Z, \chi_{st})$) but by a chemical source term of progress variable, so that flamelet are generated for several progress variable values ($\Phi = \Phi(Z, C)$). This is schematically illustrated in Fig. 4. 3. Selecting a set of non-premixed flamelets for manifold creation the independent variables of the manifold are mixture fraction (Z) and scaled reaction progress variable (C). The progress variable source term ($S_c(Z, C)$) describes the chemical evolution.

The application of the FGM model requires less computational time than the EDC model since detailed chemistry is only used in the manifold creation, whereas relevant quantities in the turbulent flow are retrieved from the lookup tables.
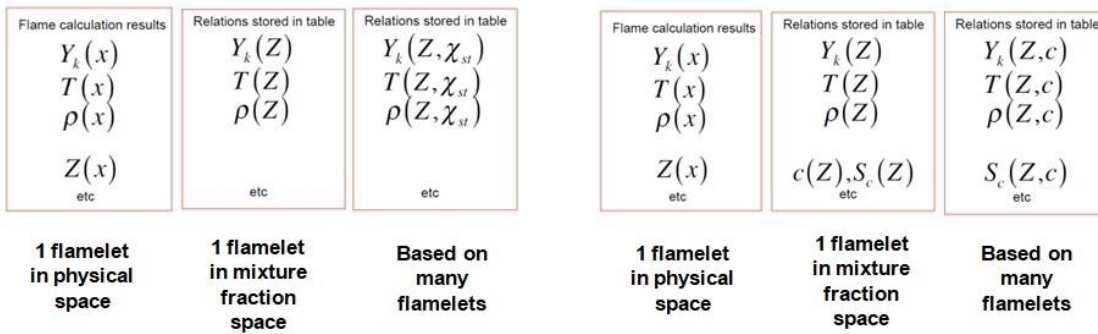
Fig. 4. 3 Comparison of non-premixed Flamelet (left) and FGM (right) models

The scaled progress variable $C(Z)$, describes the reaction progress from a value equal to 0 in the unburnt gases to 1 in the fully burnt gases. In the ANSYS Fluent implementation the un-normalized progress variable is calculated as the sum of the product species mass fraction relative to the species mass fraction in equilibrium and the unburnt state.

$$\tilde{C} = \frac{\sum_k \alpha_k (Y_k - Y_k^u)}{\sum_k (Y_k^{eq} - Y_k^u)}$$

Eq. 4. 6

Note that Y_k^{eq} is a function of local mixture fraction and α_k are constants that are typically zero for reactants and unity for a few products species. Here, $\alpha_{CO_2} = \alpha_{CO} = 1$ is used and zero for the other species. To take into account heat loss local states with heat loss are constructed by reducing the temperature at the boundary of the flamelet computational domain. The maximum enthalpy loss considered in the table generation is determined from the lowest experimentally observed mean temperature of the mixture in the furnace interior, in this case, 951 K. In the implementation of the FGM method in ANSYS Fluent used here the flamelets underlying the manifold are based on fuel and air as the incoming stream. Steady non-premixed flamelets are considered and increasing the scalar dissipation rate in total 64 flamelets are generated until extinction is reached. Therefore, the flamelets are generated until the counterflow diffusion flamelet extinction strain rate is achieved. Then, the final extinguishing unsteady diffusion flamelet is used to model the manifold between the unburnt state and the last steady diffusion flamelet at the highest scalar dissipation rate just before extinction. The generalization of the FGM model

consisting of including the effect of recirculation of products during flamelet creation, that is dilution effect, is not among the default options offered by ANSYS Fluent.

In this chapter RANS approach and non-adiabatic turbulence simulations are studied. The instantaneous relationship between scaled progress variable, mixture fraction and enthalpy are considered for species mass fraction, density and temperature values calculation ($\Phi = \Phi(C, Z, h)$). Nevertheless, RANS approach predicts average values. In order to take into account the influence of turbulent fluctuations, the FGM turbulence-chemistry interaction model relates instantaneous values with average values of this scalars by joint PDF. Fluctuations in the enthalpy loss (relative to the adiabatic conditions) are neglected ($P(Z, h) = p(Z)\delta(h - \bar{h})$). Therefore, in non-adiabatic FGM model average mixture properties are calculated by the joint probability density function:

$$\widetilde{\Phi} = \int_0^1 \int_0^1 \widetilde{\Phi}(C, Z, \tilde{h}) P(C, Z) dC dZ \qquad \text{Eq. 4. 7}$$

where $\tilde{h}$ is the mean enthalpy. It is assumed that the mixture fraction and the scaled progress variable are statistically independent (see Eq. 4. 8) and that both have a presumed β-function PDF fully characterized by the mean and the variance (see Eq. 4. 9, Eq. 4. 10 and Eq. 4. 11 as an example of mixture fraction mean and variance).

$$\widetilde{\Phi} = \int_0^1 \int_0^1 \widetilde{\Phi}(C, Z, \tilde{h}) \tilde{P}(C, Z) dc dZ = \int_0^1 \int_0^1 \widetilde{\Phi}(C, Z, \tilde{h}) \tilde{P}(C) \tilde{P}(Z) dC dZ \qquad \text{Eq. 4. 8}$$

$$\tilde{P} = \frac{Z^{\alpha_1 - 1}(Z - 1)^{\beta - 1}}{\int Z^{\alpha_1 - 1}(Z - 1)^{\beta - 1} dZ} \qquad \text{Eq. 4. 9}$$

where

$$\alpha_1 = \tilde{Z}\left[\frac{\tilde{Z}(1 - \tilde{Z})}{\tilde{Z}''^2} - 1\right] \qquad \text{Eq. 4. 10}$$

$$\beta = \left(1 - \tilde{Z}\right)\left[\frac{\tilde{Z}(1 - \tilde{Z})}{\tilde{Z}''^2} - 1\right] \qquad \text{Eq. 4. 11}$$

Note that this formula can be applied for parameters between 0 and 1 value. This is way scaled progress variable (C) is used for turbulence fluctuations considerations as it is a normalized parameter with values between 0 and 1 while un-scaled progress variable $\widetilde{Y}_c$ is not a normalized variable (Eq. 4. 12). The following transport equations are solved for the mean and variance of mixture fraction and un-scaled progress variable $Y_c = \sum_k \alpha_k Y_k$ calculation:

$$\frac{\partial \bar{\rho}\widetilde{Y}_c}{\partial t} + \frac{\partial}{\partial x_i}\left(\bar{\rho}\tilde{v}_i\widetilde{Y}_c\right) = \frac{\partial}{\partial x_i}\left[\bar{\rho}\left(\frac{k_m}{C_p} + \frac{\mu_t}{Sc_t}\right)\frac{\partial \widetilde{Y}_c}{\partial x_i}\right] + \bar{S}_{Y_c} \qquad \text{Eq. 4. 12}$$

$$\frac{\partial \bar{\rho}\tilde{Z}}{\partial t} + \frac{\partial}{\partial x_i}\left(\bar{\rho}\tilde{v}_i\tilde{Z}\right) = \frac{\partial}{\partial x_i}\left[\bar{\rho}\left(\frac{k_m}{C_p} + \frac{\mu_t}{\sigma_t}\right)\frac{\partial \tilde{Z}}{\partial x_i}\right] \qquad \text{Eq. 4. 13}$$

$$\frac{\partial \bar{\rho}\widetilde{Y_c''^2}}{\partial t} + \frac{\partial}{\partial x_i}\left(\bar{\rho}\tilde{v}_i\widetilde{Y_c''^2}\right)$$
$$= \frac{\partial}{\partial x_i}\left[\left(\frac{k_m}{C_p} + \frac{\mu_t}{Sc_t}\right)\frac{\partial \widetilde{Y_c''^2}}{\partial x_i}\right] + 2\bar{\rho}\frac{\mu_t}{Sc_t}\left(\frac{\widetilde{Y_c''^2}}{\partial x_i}\right)^2 - 2\bar{\rho}\frac{\varepsilon}{k}\widetilde{Y_c''^2} \qquad \text{Eq. 4. 14}$$

$$\frac{\partial \bar{\rho}\widetilde{Z''^2}}{\partial t} + \frac{\partial}{\partial x_i}\left(\bar{\rho}\tilde{v}_i\widetilde{Z''^2}\right) = \frac{\partial}{\partial x_i}\left[\left(\frac{k_m}{C_p} + \frac{\mu_t}{\sigma_t}\right)\frac{\partial \widetilde{Z''^2}}{\partial x_i}\right] + 2.86\mu_t\left(\frac{\partial \tilde{Z}}{\partial x_i}\right)^2 - 2\bar{\rho}\frac{\varepsilon}{k}\widetilde{Z''^2} \qquad \text{Eq. 4. 15}$$

Finally, the resulting FGM table for the mean properties (including the mean chemical source term) has five independent variables and provides relations of the form

$$\tilde{\Phi} = \tilde{\Phi}\left(\tilde{Z}, \widetilde{Z''^2}, \tilde{C}, \widetilde{C''^2}, \tilde{h}\right) \qquad \text{Eq. 4. 16}$$

Where $\tilde{h}$ denotes the enthalpy loss, obtained from the equation for mean enthalpy.

$$\frac{\partial \bar{\rho}\tilde{h}}{\partial t} + \frac{\partial}{\partial x_i}\left(\bar{\rho}\tilde{v}_i\tilde{h}\right) = \frac{\partial}{\partial x_i}\left[\left(\frac{\lambda}{c_p} + \frac{\lambda_t}{c_p}\right)\frac{\partial \tilde{h}}{\partial x_i}\right] + \bar{S}_r \qquad \text{Eq. 4. 17}$$

ANSYS Fluent has implemented the non-adiabatic configurations postulating that species mass fractions are maintained constant with enthalpy variations and that mixture-average properties, excluding species mass fractions, are calculated by average progress

variable. Those assumptions are made in order to increase computation efficiency, so that, ANSYS Fluent release 19.R2 calculates mixture properties, such as, temperature, specific heat and density through 4 independent variables (Eq. 4. 18) while species mass fractions are calculated thought 4 independent variables (Eq. 4. 19):

$$\widetilde{\Phi} = \widetilde{\Phi}\left(\tilde{Z}, \widetilde{Z''^2}, \tilde{C}, \tilde{h}\right)$$

<div align="right">Eq. 4. 18</div>

$$\widetilde{Y_k} = \widetilde{\Phi}\left(\tilde{Z}, \widetilde{Z''^2}, \tilde{C}, \widetilde{C''^2}\right)$$

<div align="right">Eq. 4. 19</div>

3   Diluted air FGM (DAFGM) model

In flameless combustion, fuel and air streams are diluted by aerodynamic recirculation of flue gas producing low mean temperature profiles and low oxygen content mixture. The DA-FGM model was developed to improve FGM model for flameless combustion taking into account the dilution effect. Firstly, local dilution level is accurately calculated by a transport equation. Secondly, pure fuel and diluted air are considered for non-premixed flamelets generation. These improvements can be carried out in the DA-FGM model due to the new chemistry tabulation proposed.

In the literature other extended models including dilution effect can be found, for example, the E-FPV model (Ihme & See, 2011), which includes in its mathematical formulation an additional conserved scalar (oxidizer split) for dilution consideration. Nevertheless, this model is applicable only when reactants dilution is constant. On JHC burners' diluted reactants are controlled by coflow burner, so that the E-FPV model can be applied in these devices. Later, the D-FPV (Lamouroux et al., 2014), the DHR (Locci et al., 2014; Locci et al., 2015) and the DA-FGM models (Huang, X. et al., 2017; Huang, Xu, 2018) were developed. These model's extensions consider the dilution effect when recirculated burn gases quantity is not constant.

The DHR model tabulates auto-ignition trajectories of a diluted homogeneous reactor as a function of mean mixture fraction, dilution, enthalpy loss and un-scaled progress variable. The dilution is considered by a dilution factor (α) which is divided into non-reactive and reactive part. The dilution factor is calculated based on un-scale progress

variable in non-reactive cases, and when reaction happens the dilution factor is defined by the lowest dilution factor leading to autoignition for a given mixture fraction (Z) and heat loss (H'), so that, dilution factor is defined as $\alpha(Z, H') = \min\left[\alpha_{reac}(z, H'), \left(\frac{Y_c}{Y_c^{eq}}\right)\right]$.

The CFD code used was the AVBP, developed in collaboration between CERFACS and the Oxford University Computing Laboratory (Rudgyard et al., 1995; Rudgyard, 1995; Schonfeld & Rudgyard, 1999).

The D-FPV model used the steady flamelet equation for chemistry tabulation considering both dilution and heat loss effect. Flamelets are generated by laminar counterflow flames considering diluted fuel and diluted oxidizer. Nevertheless, this tabulation method does not consider the reactions that happens when the fuel is diluted with burn gases containing O_2 in exceed (typical situation in lean combustion). The dilution variable is calculated by an additional transport equation, while it is defined as $Y_d = Y_{CO_2} + Y_{CO}$. The dilution level is the mass ratio between fresh reactants and diluent, so that finally it is equal to the ratio $\frac{Y_d}{Y_d^{Dil}}$, where Y_d^{Dil} is Y_d value at equilibrium and global equivalence ratio mixing. The finite-volume code used for modelling was YALES2 (Moureau, V. et al., 2011; Moureau, Vincent et al., 2011).

The DA-FGM model is a combination of the DHR and the D-FPV models and improves their weak points. On the one hand, local dilution level is accurately calculated by a transport equation (the DHR model did not use a transport equation) and on the other hand, it does not avoid the reactions between fuel and diluted burn gases at lean conditions when flamelets are generated (like happens in D-FPV model). This improvement is made due to the new chemistry tabulation proposed by the DA-FGM model. The DA-FGM model understand flameless combustion in an enclosed furnace as a diluted environment where the fuel is injected. Therefore, following steady flamelet equation, flamelet tables are generated considering pure fuel and diluted air, so that the reactions between pure fuel and gases with excess air is avoided. The heat loss due to radiation and furnace walls is considered by the dilution, and as the oxidizer is the only one which is diluted, heat loss is only considered in the oxidizer. The local dilution is calculated by a transport equation

and it is defined as $Y_d = Y_{CO_2} + Y_{H_2O}$ The DA-FGM model is implemented in the open access opeanFOAM CFD code (OpenFOAM, 1960).

Among the extension of flamelet based models which consider dilution, the DA-FGM model presents more advantages than others do. In this Thesis, this model is selected for flameless numerical modelling on the Delft-lab-scale furnace. The DA-FGM model so far is only available in OpenFOAM (Huang, Xu, 2018), so that in this Thesis is for the first time implemented in ANSYS Fluent package using User Define Functions (UDF), User Defines Memory (UDM) and User Define Scalars (UDS).

ANSYS Fluent has a user-friendly interface, easy to navigate, use and build models. The user does not need to develop its own code, so that a good knowledge of programming is not necessary. It is a results-oriented code ideal to be used in industrial problems where the goal is to obtain accurate and reliable results. It comes with fully developed models and an excellent technical support. Conversely, in OpenFOAM the user easily can change the code source as well as create a new code itself, but it takes long time to get results and makes various trials during modelling. Additionally, the OpenFOAM mesh offer is poor compared with ANSYS Fluent. The other two CFD codes used with D-FPV and DHR, YALES2 (specialized in two-phase combustion) and AVBP (specialized for LES modelling) respectively, are CFD codes developed by research groups for specific applications. Consequently, it is interesting to implement the DA-FGM in ANSYS Fluent due to both, its advantages to be applied in industrial applications to get results easily and its widely and easier use in combination with the technical support.

3.1 Dilution effect

In the Delft lab-scale furnace, fuel and air streams are injected separately (non-premixed combustion), but due to the furnace technology, internally, combustion gases recirculation is allowed. Therefore, the combustion can be considered as a three-stream problem consisting on fuel, air and recirculated flue gas (see Fig. 4. 5). Burnt gases are the diluents and in this case, they diluted the oxidizer. The dilution consideration in flamelets generation is important, as example go to Fig. 4. 4 where fuel consumption and products formation vary at different dilution levels (γ).
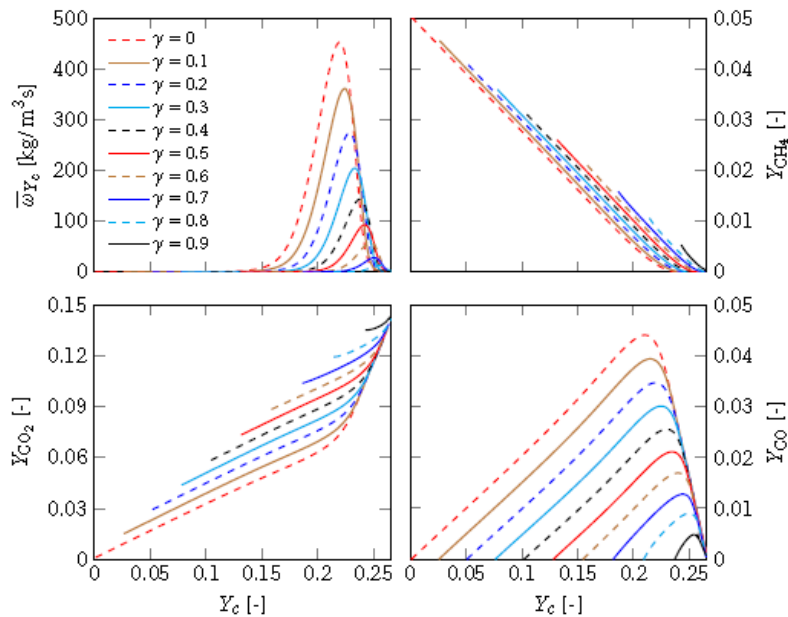
Fig. 4. 4 Properties of counterflow flame of fuel and diluted air at stoichiometric mixture fraction. (Huang, Xu, 2018)

Note that the default FGM model available in ANSYS Fluent tabulates reactions based on pure fuel and pure oxidizer in laminar diffusion counterflow flames, that is, profiles with a dilution value equal to cero ($\gamma = 0$). These flame structures do not represent appropriately recirculated burnt gases effect on chemical reactions. Therefore, in this thesis the Diluted air FGM (DA-FGM) model is implemented in ANSYS Fluent to simulate flameless combustion on an enclosed furnace.

3.2 Flamelets generation considering dilution

A schematic of the three-stream problem is represented in Fig. 4. 5(a). The furnace is operating in lean conditions $\psi < 0,8$, so that burn gases contains diluent and oxidizer. The diluent is considered as the products at stoichiometric mixture fraction Z_{st} and in chemical equilibrium due to long residence time in furnace.

The reactions are treated in the mixture of pure fuel and diluted air, so that, a second mixture fraction (ξ) is defined which describes the mixture between pure fuel and diluted air (it represents the mass fraction of fuel stream in local gas mixture). The mixture before reaction, as it is shown in Fig. 4. 5(b), is divided in three streams; fuel, air (fresh air + excess air) and diluents. Therefore, finally, flamelets are generated using the laminar

diffusion counterflow configuration of Fig. 4. 5(c) where pure fuel and diluted air are used as boundary condition.

a) 3 stream problem   b) mixture before reaction   c) Flamelets generation
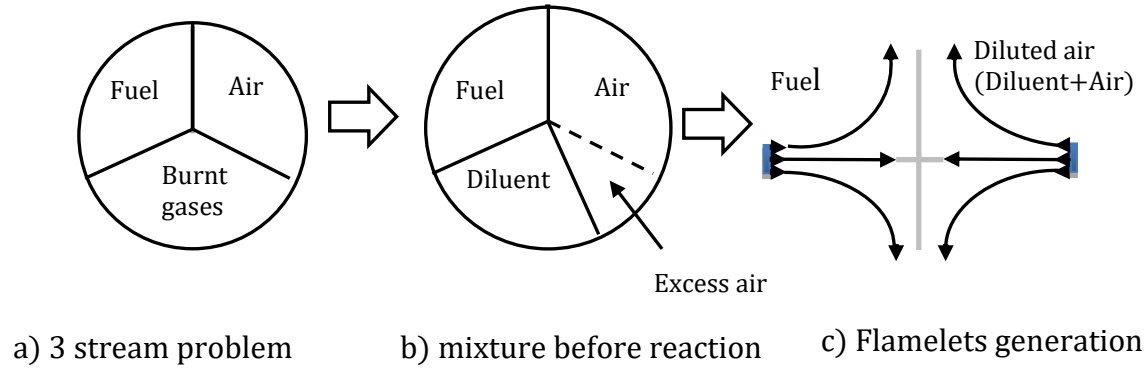
Fig. 4. 5. Three-stream problem scheme

Additionally, a new parameter, air dilution level (γ), is defined and represents the mass fraction of diluent in diluted air. The non-adiabatic effect is considered in the diluent stream by considering that the products generated at stoichiometric conditions have an enthalpy loss. As oxidizer is diluted by the products the heat loss is only considered in the diluted air by the enthalpy loss factor (η). The enthalpy loss factor represents the ratio between enthalpy loss (Δh) and maximum tabulated enthalpy loss (Eq. 4. 36). Finally, the flamelets are generated considering the next boundaries conditions:

$$\Phi(\xi = 1) = \Phi_f \qquad\qquad \text{Eq. 4. 20}$$

$$\Phi(\xi = 0) = \Phi_{ox}(\eta, \gamma) \qquad\qquad \text{Eq. 4. 21}$$

note that Φ_f and Φ_{ox} are pure fuel and diluted air state, respectively. The DA-FGM's flamelets become a four-dimensional (4D) flamelets depending on second mixture fraction (ξ) scaled progress variable (C), enthalpy loss (η) and dilution level (γ).

$$\Phi = \Phi(\xi, C, \eta, \gamma) \qquad\qquad \text{Eq. 4. 22}$$

3.3 Non-premix turbulent combustion model mathematical formulation

The Diluted-Air-FGM (DAFGM) model is a three-stream lean combustion problem defined by injected air, injected fuel and recirculated flue gases. It is based on non-premixed flamelets of fuel and diluted air with dilution level as an extra independent variable. In the non-adiabatic RANS-DA-FGM modelling framework, an additional transport equation is solved for the mean dilution variable, in addition to the usual non-adiabatic RANS-FGM equations, namely:

$$\frac{\partial \bar{\rho}\widetilde{Y_d}}{\partial t} + \frac{\partial}{\partial x_i}\left(\bar{\rho}\tilde{u}_i\widetilde{Y_d}\right) = \frac{\partial}{\partial x_i}\left[\bar{\rho}\left(\widetilde{D} + D_t\right)\frac{\partial \widetilde{Y_d}}{\partial x_i}\right] + \bar{\omega}_{Y_d} \qquad \text{Eq. 4. 23}$$

where source term is defined as

$$\widetilde{\omega}_{Y_d} = \frac{1}{\Delta t}\bar{\rho}\left(Y_d^b - \widetilde{Y_d}\right)H\left(\tilde{C} - 0.99\right) \qquad \text{Eq. 4. 24}$$

Note that Δt is modelling time step, Y_d^b mean dilution variable in in local burnt gases (at C=1 conditions), H is a pulsating function, when $\tilde{C} = 1$ $H = 1$, when $\tilde{C} < 1$ $H = 0$. It is the responsible of activating the source term. The dilution variable is set equal to zero at the inlet boundaries and the source term transform burnt gases to diluent when the reactants are completely burnt. The diffusion term is calculated by $\bar{\rho}\left(\widetilde{D} + D_t\right) = \bar{\rho}\left(\frac{\mu}{S_c} + \frac{\mu_t}{S_{ct}}\right)$ where μ is laminar viscosity, μ_t turbulent viscosity, S_c Schmidt number and S_{ct} turbulent Schmidt number.

This additional transport equation (Eq. 4. 23) is not included in ANSYS Fluent FGM model default options, therefore, on the DA-FGM model implementation methodology the UDS is used to add the local dilution variable.

The local dilution variable is defined by the sum of some species $Y_d = Y_{CO_2} + Y_{H_2O}$ and the mean dilution level is calculated by:

$$\tilde{\alpha} = \frac{\tilde{Y}_d}{\tilde{Y}_d^{Dil}}$$

Eq. 4. 25

$\tilde{Y}_d^{Dil}$ is the mean dilution variable value at stoichiometric mixture conditions (global equivalence ratio equal to one). The un-scale progress variable used in the model is defined as:

$$Y_c = Y_{CO_2} + Y_{CO} + Y_{H_2O} + Y_{H_2}$$

Eq. 4. 26

ANSYS Fluent default options calculated un-scale progress variable by the sum of CO_2 and CO species mass fraction, so that on the DA-FGM implementation a special command must be introduced in the Text User Interface (TUI) to calculate it following Eq. 4. 26, the details are described in section 5.

Apart from continuity and momentum equations, the following Favre-averaged equations for mixture fraction $\tilde{Z}$, un-normalized progress variable $\tilde{Y}_c$, enthalpy $\tilde{h}$, mixture fraction variance $\widetilde{Z''^2}$ and un-scaled progress variable variance $\widetilde{Y''^2}_c$ are solved in the DA-FGM model:

$$\frac{\partial \bar{\rho}\tilde{Z}}{\partial t} + \frac{\partial}{\partial x_i}\left(\bar{\rho}\tilde{u}_i\tilde{Z}\right) = \frac{\partial}{\partial x_i}\left[\bar{\rho}\left(\tilde{D} + D_t\right)\frac{\partial \tilde{Z}}{\partial x_i}\right]$$

Eq. 4. 27

$$\frac{\partial \bar{\rho}\tilde{Y}_c}{\partial t} + \frac{\partial}{\partial x_i}\left(\bar{\rho}\tilde{u}_i\tilde{Y}_c\right) = \frac{\partial}{\partial x_i}\left[\bar{\rho}\left(\tilde{D} + D_t\right)\frac{\partial \tilde{Y}_c}{\partial x_i}\right] + \bar{\dot{\omega}}_{Y_c}$$

Eq. 4. 28

$$\frac{\partial \bar{\rho}\tilde{h}}{\partial t} + \frac{\partial}{\partial x_i}\left(\bar{\rho}\tilde{u}_i\tilde{h}\right) = \frac{\partial}{\partial x_i}\left[\left(\frac{\lambda}{c_p} + \frac{\lambda_t}{c_p}\right)\frac{\partial \tilde{h}}{\partial x_i}\right] + \bar{S}_r$$

Eq. 4. 29

$$\frac{\partial \bar{\rho}\widetilde{Z''^2}}{\partial t} + \frac{\partial}{\partial x_i}\left(\bar{\rho}\tilde{u}_i\widetilde{Z''^2}\right) = \frac{\partial}{\partial x_i}\left[\left(\tilde{D} + D_t\right)\frac{\partial \widetilde{Z''^2}}{\partial x_i}\right] + 2\bar{\rho}D_t\left(\frac{\partial \tilde{Z}}{\partial x_i}\right)^2 - 2\bar{\rho}\frac{\varepsilon}{k}\widetilde{Z''^2}$$

Eq. 4. 30

$$\frac{\partial \bar{\rho} \widetilde{Y_c^{"2}}}{\partial t} + \frac{\partial}{\partial x_i}\left(\bar{\rho} \tilde{u}_i \widetilde{Y_c^{"2}} \right)$$

$$= \frac{\partial}{\partial x_i}\left[(\widetilde{D} + D_t) \frac{\partial \widetilde{Y_c^{"2}}}{\partial x_i} \right] + 2\bar{\rho}D_t \left(\frac{\widetilde{Y_c^{"2}}}{\partial x_i} \right)^2 - 2\bar{\rho}\frac{\varepsilon}{k} \widetilde{Y_c^{"2}}$$

$$+ 2\left(\overline{Y_c \dot{\omega}_{Y_c}} - \widetilde{Y_c}\bar{\dot{\omega}}_{Y_c} \right)$$

Eq. 4. 31

ANSYS Fluent is able to solve the above transport equations (Eq. 4. 27-Eq. 4. 31) but the last term of the right side of Eq. 4. 31, which correspond to the chemical effect, is not considered in ANSYS Fluent default options.

The DA-FGM has a four-dimensional (4D) flamelet table $\Phi = \Phi(\xi, C, \eta, \gamma)$, which depends on second mixture fraction (ξ), scaled progress variable (C), enthalpy loss (η) and dilution (γ) and a six-dimensional (6D) PDF table $\widetilde{\Phi} = \widetilde{\Phi}\left(\tilde{\xi}, S_\xi, \tilde{C}, S_C, \tilde{\eta}, \tilde{\gamma} \right)$, where S_ξ is second mixture fraction variance and S_C scaled progress variable variance. The non-adiabatic effect is considered in the DA-FGM model recalculating temperature at flamelet boundaries according to an enthalpy loss.

In this model statistical independence among the four scaled controlling parameters (ξ, C, η and γ) is considered and the mean values are calculated by the joint PDF of them. A presumed β PDF approach is taken for ξ and C and a δ PDF function for enthalpy loss ($\eta = \tilde{\eta}$) and dilution level ($\gamma = \tilde{\gamma}$). The controlling scaled parameters are defined by:

$$\tilde{\xi} = \tilde{Z} - \tilde{\alpha}Z_{st}$$

Eq. 4. 32

$$S_\xi = \frac{\widetilde{Z^{"2}}}{\tilde{\xi}(1 - \tilde{\xi})}$$

Eq. 4. 33

$$\tilde{C} = \frac{\tilde{Y}_c - \tilde{Y}_c^u}{\tilde{Y}_c^b - \tilde{Y}_c^u}$$

Eq. 4. 34

$$S_C = \frac{\widetilde{C^{"2}}}{\tilde{C}(1 - \tilde{C})}$$

Eq. 4. 35

Analysis of thermofluids in flameless (MILD)
combustion: assessment, improvement and
development of combustion models by CFD
Naiara Romero Anton

$$\tilde{\eta} = \frac{\tilde{h} - \tilde{h}_{ad}}{\tilde{\alpha}(h_{\eta=1}^d - h_{\eta=0}^d)}$$

Eq. 4. 36

$$\tilde{\gamma} = \frac{\tilde{\alpha}}{1 - \tilde{\xi}}$$

Eq. 4. 37

For more detail go to the work of Huang (Huang, Xu, 2018).

The control parameters of the DA-FGM (Eq. 4. 32-Eq. 4. 37) are not calculated in ANSYS Fluent; therefore, they must be calculated using UDF and UDM during the implementation.

4 Implementation methodology in ANSYS Fluent

In the DA-FGM model implementation in ANSYS Fluent, several deviations are found between ANSYS Fluent default options and the DA-FGM model requirements. Next, each deviation and proposed solutions are explained. As it is described in the following subsections, a scheme of the data exchange between ANSYS Fluent and UDF file are shown on Fig. 4. 6.

The UDF is a tool available in ANSYS Fluent to enhance the standard characteristics of the program. The user is responsible for creating, debugging and validating them and by an interface available in ANSYS Fluent they are called by demand or hooked in ANSYS Fluent. The UDF code is written in C languages but uses some macros defined by ANSYS Fluent with a pre-defined code structure that allows modifying or knowing specific information during modelling. Depending on the macros used it is necessary to define at the beginning of the code certain headers, so that those macros can be used. The code needs to be compiled or interpreted when is loaded in ANSYS Fluent and for this work Microsoft Visual Studio compiler has been used.

Table 4. 2 summarizes the ANSYS Fluent default options, the DA-FGM model requirements and the provided solution during the DA-FGM model implementation in ANSYS Fluent. In the next subsections, a detailed description is made.
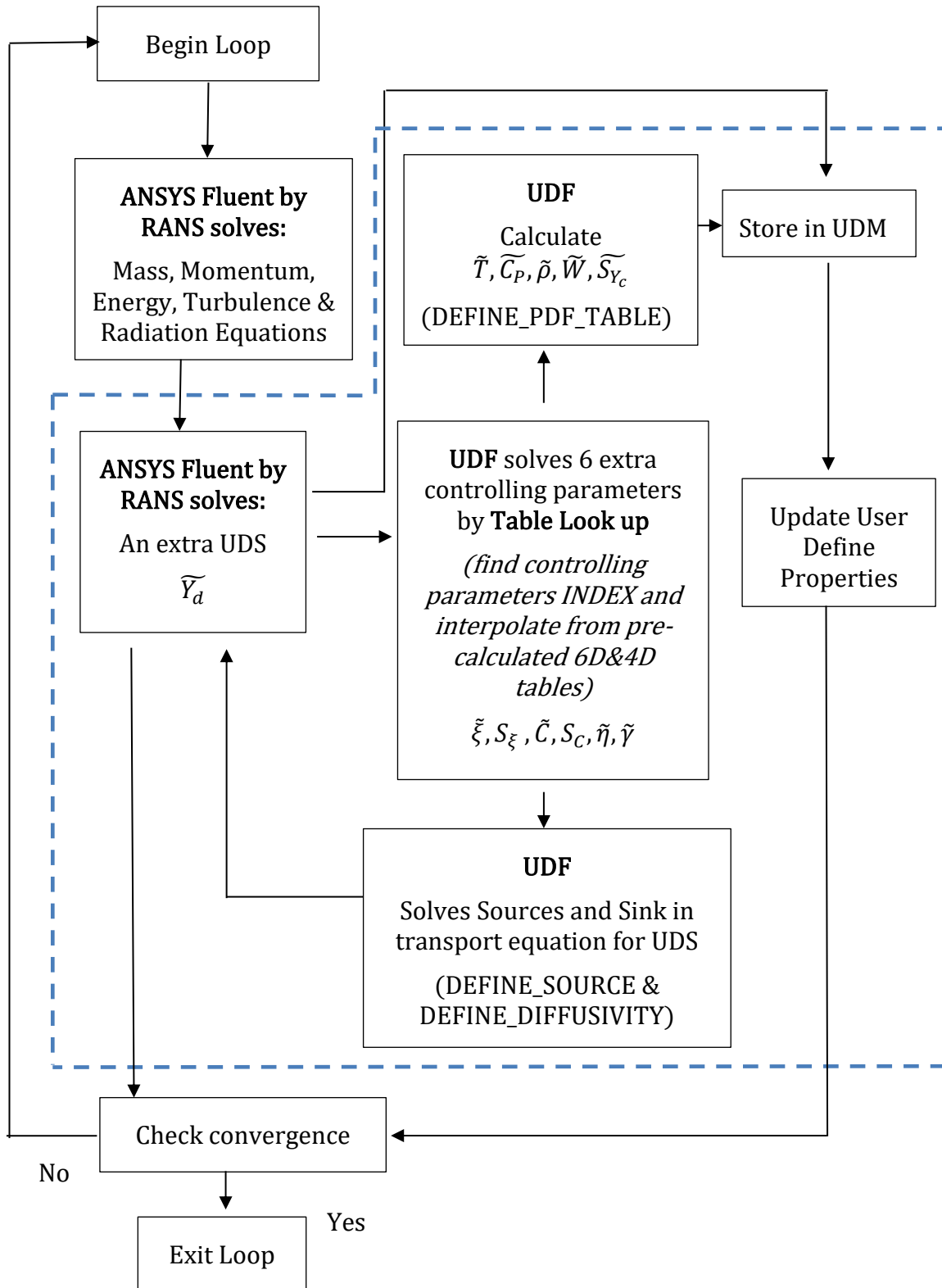
Fig. 4. 6 Flowchart for calculation steps and data exchange scheme between ANSYS Fluent and UDF. The part within the dashed line is developed in this work

Analysis of thermofluids in flameless (MILD) combustion:
assessment, improvement and development of combustion
models by CFD
Naiara Romero Anton

Table 4. 2 ANSYS Fluent FGM model vs DA-FGM model

Point	ANSYS Fluent	DA-FGM	Provided Solution
PDF table	4D Mixture properties $\widetilde{\Phi}' = \widetilde{\Phi}'(\tilde{Z}, \widetilde{Z''^2}, \tilde{C}, \widetilde{H})$ 4D species $\tilde{Y}_k = \tilde{Y}_k(\tilde{Z}, \widetilde{Z''^2}, \tilde{C}, \widetilde{C''^2})$ ❌	6D $\Phi = \widetilde{\Phi}\left(\tilde{\xi}, S_\xi, \tilde{C}, S_C, \tilde{\eta}, \tilde{\gamma}\right)$ ✓	• 6D PDF tables are generated outside ANSYS Fluent • Mixture properties tables depending in 6 controlling parameters are loaded into ANSYS Fluent by UDF (DEFINE_EXECUTE_ON_LOADING). • The 6D scaled controlling parameters are calculated along the UDF code • A 6D interpolation and index finding is programmed into the code. • Mixture properties depending on 6D are calculated and their values are replaced in ANSYS Fluent default PDF table (DEFINE_PDF_TABLE) ✓
Y_d	N.A	$\frac{\partial \bar{\rho}\tilde{Y}_d}{\partial t} + \frac{\partial}{\partial x_i}(\bar{\rho}\tilde{u}_i\tilde{Y}_d) = \frac{\partial}{\partial x_i}\left[\bar{\rho}(\tilde{D} + D_t)\frac{\partial \tilde{Y}_d}{\partial x_i}\right]$ $+ \bar{\dot{\omega}}_{Y_d}$	• An additional transport equation is added in ANSYS Fluent by UDS • UDF are used for dilution and source term definition in UDS; DEFINE_DIFFUSIVITY and DEFINE_SOURCE ✓
Y_c	$Y_c = Y_{CO_2} + Y_{CO}$	$Y_c = Y_{CO_2} + Y_{CO} + Y_{H_2O} + Y_{H_2}$	• Fuel is defined in ANSYS Fluent avoiding CO_2, CO, H_2O and H_2 mass fractions.

ENEDI Research Group
Energy Engineering Department
University of the Basque Country

enedi

FACULTY
OF ENGINEERING
BILBAO

Universidad   Euskal Herriko
del País Vasco   Unibertsitatea

UNIVERSITY
OF THE BASQUE
COUNTRY

			• The following code should be added to the TUI: `rpsetvar 'prepdf/prmx-fla-alpha '(("h2". 1.0) ("h2o" . 1.0) ("co" . 1.0) ("co2" . 1.0)))` • Next, in ANSYS Fluent flamelets and PDF tables should be generated. ✔
Chemical effect	✘	✔	• The following code should be added to the TUI: "(`rpsetvar 'premixc/include-ycvar-rxn-src? #t`) • Nevertheless, this feature is not implemented as there is an incompatibility among this command and the other macros implemented in the code. But its impact has been tested and this is zero, so that it can be avoided ✘
$\tilde{c}$	Y_k are calculating not considering Y_d ✘ and heat loss ✘	Y_k are calculating considering Y_d ✔ and heat loss ✔	• By CHEM1D Y_k is calculated considering Y_d and heat loss, then $\tilde{Y}_c^u$ and $\tilde{Y}_c^b$ tables are generated and loaded in ANSYS Fluent • UDF are used DEFINE_EXECUTE_ON_LOADING for tables loading • The limitations of ANSYS have been overcome except in the calculation of Y_c.. ✔
$\widetilde{C''^2}$	Instantaneous average equilibrium value $Y_{c,eq}(\tilde{Z})$	PDF averaged value	• By CHEM1D $\left(\widetilde{Y_c^u}\right)^2$, $\widetilde{Y_c^u Y_c^b}$, $\left(\widetilde{Y_c^u}\right)^2$ tables are generated $\widetilde{\Phi} = \widetilde{\Phi}\left(\tilde{\xi}, S_\xi, \tilde{\eta}, \tilde{\gamma}\right)$ at $\tilde{C} = 1$ conditions

Analysis of thermofluids in flameless (MILD) combustion:
assessment, improvement and development of combustion
models by CFD
Naiara Romero Anton

			• 4D tables are loaded by DEFINE_EXECUTE_ON_LOADING ✔
Heat losses	Y_k not sensitive to enthalpy change ✘	Y_k sensitive to enthalpy change ✔	• Fluent cannot include the sensitivity of enthalpy change in Y_k calculation • Loading the 4D $\tilde{Y}_c^u$ and $\tilde{Y}_c^b$ tables this issue is reduced ✔

4.1 4D flamelets and 6D PDF table

In the non-adiabatic RANS-DA-FGM modelling framework, the model presents a four-dimensional (4D) flamelet tables $\Phi = \Phi(\xi, C, \eta, \gamma)$ and a six-dimensional (6D) PDF tables $\widetilde{\Phi} = \widetilde{\Phi}\left(\tilde{\xi}, S_\xi, \tilde{C}, S_C, \tilde{\eta}, \tilde{\gamma}\right)$. In ANSYS Fluent it is not possible to create these tables as the maximum flamelet tables dimension is three (3D) $\Phi' = \Phi'(Z, C, H)$ and the maximum PDF tables dimension is five (5D) $\widetilde{\Phi}' = \widetilde{\Phi}'(\tilde{Z}, \widetilde{Z''^2}, \tilde{C}, \widetilde{C''^2}, \tilde{H})$. The average of mixture properties is a function of mean mixture fraction $\tilde{Z}$, mean progress variable $\tilde{C}$, their variances $\widetilde{Z''^2}$ and $\widetilde{C''^2}$ respectively, and mean enthalpy $\tilde{H}$. In order to optimize computational time, the non adiabatic PDF tables of ANSYS Fluent are generated considering that species mass fractions are not sensitive to enthalpy change and that the mixture-averaged properties (except species mass fractions) are modelled by average progress variable. Therefore, temperature, specific heat and density account enthalpy changes and they are estimated by $\widetilde{\Phi}' = \widetilde{\Phi}'(\tilde{Z}, \widetilde{Z''^2}, \tilde{C}, \tilde{H})$ while species mass fractions are calculated not considering the heat loss $\widetilde{\Phi}' = \widetilde{\Phi}'(\tilde{Z}, \widetilde{Z''^2}, \tilde{C}, \widetilde{C''^2})$.

Three main limitations are found on ANSYS Fluent for DA-FGM model implementation: 1) The extra dimension of flamelets and PDF tables (corresponding to dilution) does not exist, 2) species mass fractions are frozen against heat loss $\widetilde{\Phi}' = \widetilde{\Phi}'(\tilde{Z}, \widetilde{Z''^2}, \tilde{C}, \widetilde{C''^2})$ and finally, 3) mixture properties (except species mass fractions) do not consider scaled progress variable variance $\widetilde{C''^2}$ for their calculation. Thus, finally, in RANS Non-Adiabatic FGM model ANSYS Fluent considers 4-dimensions PDF tables.

The extra dimension added in the DA-FGM model and not in the ANSYS Fluent FGM model is the dilution level. This table dimension limitation is solved during the DA-FGM model implementation methodology generating outside ANSYS Fluent the 4D flamelets tables and the 6D PDF tables. These tables are generated using CHEM1D (CHEM1D,) and TU Delft FLAME code (Peeters, 1997). CHEM1D is a one-dimensional laminar flame code where, in this case, steady laminar diffusion counterflow flames are solved in physical space and later they are turn out to mixture fraction space. Boundary conditions for flamelets generation are pure fuel and diluted air, as shown on Fig. 4. 5c). The TU Delft

FLAME code is used for diluted air calculation at the mixture fraction $Z = \gamma Z_{st}$ and for several values of enthalpy losses. The maximum enthalpy loss considered in the table generation is determined from the lowest mean temperature of the mixture in the furnace interior. In this case, it is in the furnace wall and it is 951 K. The enthalpy loss is considered in flamelets generation by decreasing diluent temperature. The way to determine the maximum enthalpy loss is as following; the mixture fraction at wall surface is assumed to be equal to the mixture faction at global equivalence ratio ($Z_\emptyset = \frac{\dot{m}_{fuel}}{\dot{m}_{fuel} + \dot{m}_{air}}$). In the TU Delft FLAME code, enthalpy loss Δh_ø is gradually increased, and the code calculates the equilibrium temperature at Z_ø. This process is repeated until the lowest measured temperature is reached, so that defined enthalpy loss is the maximum enthalpy loss in the system.

Once the 6D PDF tables are generated outside ANSYS Fluent, the mixture properties are extracted from them and new tables are generated. These tables are: mean temperature table ($\widetilde{T}$), mean density table ($\tilde{\rho}$), mean specific heat table ($\widetilde{C_P}$), mean mixture molecular weight table ($\widetilde{W}$) and mean progress variable finite rate source term ($\widetilde{S_{Y_c}}$), table. Note, that this tables were generated outside ANSYS Fluent depending on 6 control parameters $\widetilde{\Phi} = \widetilde{\Phi}\left(\tilde{\xi}, S_\xi, \tilde{C}, S_C, \tilde{\eta}, \tilde{\gamma}\right)$. Then, via UDF mixture properties tables are loaded into ANSYS Fluent (DEFINE_EXECUTE_ON_LOADING).

The ANSYS Fluent default PDF table values, that is, mean temperature, mean density, mean specific heat, mean mixture molecular weight and mean progress variable finite rate source term are substituted by the new values into ANSYS Fluent with UDF (DEFINE_PDF_TABLE). The substitution is made by entering to the loaded mixture properties tables with the 6 control parameters index and doing a 6-dimension interpolation inside each table. Previously the indexes of these controlling parameters are found. This programming has been coded inside the loaded UDF file into ANSYS Fluent. Additionally, scaled controlling parameters (Eq. 4. 32-Eq. 4. 37) are not calculated by ANSYS Fluent, so that they are calculated inside the loaded UDF. The control parameters values are between 0 and 1 and they are saved in arrays of different lengths. The scaled second mixture fraction $\tilde{\xi}$ is divided in 51 values, S_ξ is divided in 11 values, $\tilde{C}$ is divided

in 51 values, S_C is divided in 11 values, $\tilde{\eta}$ has 13 values and finally, $\tilde{\gamma}$ has 11 values. Therefore, mixture properties tables have around 45 million of values. Following this methodology ANSYS Fluent limitation when calculating mixture properties.

For a better understanding among the data exchange between ANSYS Fluent and UDF see Fig. 4. 6.

4.2 Local dilution variable Y_d definition

The transport equation (Eq. 4. 23) defined in the DA-FGM model corresponds to the transport equation of local dilution variable: $\widetilde{Y_d}$. This variable, and consequently, transport equation, is not included in ANSYS Fluent and it must be included by the user. The UDS available in ANSYS Fluent is used to add $\widetilde{Y_d}$ value for modelling. Additionally, the diffusivity and source term of Eq. 4. 23 need to be defined. They are implemented in the modelling by UDF (DEFINE_DIFFUSIVITY and DEFINE_SOURCE respectively).

The source term Eq. 4. 24 is calculated by $\widetilde{Y_d}$ value, which is solved by defined UDS and Y_d^b is obtained from a 4D table $Y_d^b = Y_d^b(\tilde{\xi}, S_\xi, \tilde{\eta}, \tilde{\gamma})$ defined at $\tilde{C} = 1$. This table was generated by CHEM1D and is loaded into ANSYS Fluent by UDF (DEFINE_EXECUTE_ON_LOADING). The 4D Y_d^b table has $\tilde{\xi}, S_\xi, \tilde{\eta}, \tilde{\gamma}$ controlling parameters, so that it stored around 80 thousand of values.

4.3 Un-scale progress variable Y_c

The un-scale progress variable is calculated in ANSYS Fluent by the next expression:

$$Y_c = \alpha_{CO_2}\left(Y_{CO_2} - Y_{CO_2}^u\right) + \alpha_{CO}\left(Y_{CO} - Y_{CO}^u\right) + \alpha_{H_2O}\left(Y_{H_2O} - Y_{H_2O}^u\right) \\ + \alpha_{H_2}\left(Y_{H_2} - Y_{H_2}^u\right)$$

Eq. 4. 38

by default $\alpha_{CO_2} = \alpha_{CO} = 1$ and $\alpha_{H_2O} = \alpha_{H_2} = 0$ are considered, therefore, un-scaled progress variable is calculated as:

$$Y_c = \left(Y_{CO_2} - Y_{CO_2}^u\right) + \left(Y_{CO} - Y_{CO}^u\right)$$

Eq. 4. 39

$Y_{CO_2}^u$ and Y_{CO}^u means unburnt CO_2 and CO mass fraction, respectively, so that the existing CO_2 and CO mass fractions in the fuel composition are considered in un-scale progress variable definition. In order to calculate the un-scale progress variable in ANSYS Fluent like in the DA-FGM model (Eq. 4. 26) two steps must be followed; the first one is to define in ANSYS Fluent a fuel composition run out of CO_2, CO, H_2O and H_2. In the case of study, Dutch natural gas composition does not have those species, therefore this problem is solved. If these species were part of the fuel composition, they should be ignored when defining the fuel composition in ANSYS Fluent and weighting the other values. The second step is adding in the ANSYS Fluent TUI the following code `rpsetvar 'prepdf/prmx-fla-alpha '(("h2". 1.0) ("h2o" . 1.0) ("co" . 1.0) ("co2" . 1.0)))`. This code calculates un-scaled progress variable including H_2O and H_2 species mass fractions. If the user is interested in checking how ANSYS Fluent is considered un-scaled progress variable, the following code should be added to the TUI `(rpgetvar 'prepdf/prmx-fla-alpha '?)`. After these two approaches are implemented, finally ANSYS Fluent is able to calculate un-scale progress variable following Eq. 4. 26 It is important to introduce this command in ANSYS Fluent TUI before generating the default flamelets and PDF tables in ANSYS Fluent. Note that the scaled progress variable, $\tilde{C}$, is calculated based on un-scaled progress variable (Eq. 4. 34) and this value is taken from ANSYS Fluent calculations.

4.4 Chemistry effect of un-scaled progress variable variance, $Y_c^{"2}$

Another deviance found in ANSYS Fluent options comparing with the DA-FGM model is the chemistry effect of un-scaled progress variable variance (the last term of Eq. 4. 31). This term is not considered in $\widetilde{Y_c^{"2}}$ transport equation. In order to consider it a specific code should be introduced in TUI "`(rpsetvar 'premixc/include-ycvar-rxn-src? #t)`". As happens with un-scaled progress variable, once this command is added into ANSYS Fluent TUI then the default PDF table of ANSYS Fluent must be generated. However, it is found that when this command is introduced and the UDF code is loaded, a segmentation fault is found during the modelling. There is an incompatibility among this command and the other macros implemented in the code. The chemistry effect in mean temperature prediction is checked comparing two FGM modelling results, one including chemistry

effect and the another not including it. The results show no deviance between both models (see section 5.1). Therefore, the chemistry effect of un-scaled progress variable variance ($\widetilde{Y_c''^2}$) is not implemented in ANSYS Fluent DA-FGM model as there is no change in mean temperature predictions.

4.5 Scaled progress variable ($\widetilde{C}$) definition

The scaled progress variable ($\tilde{C}$) calculated in ANSYS Fluent does not consider the dilution effect and heat loss as the species mass fractions calculated in ANSYS Fluent are calculated based on pure fuel and pure air boundary conditions and frozen at any heat loss. Additionally, $\tilde{C}$ is calculated based on the instantaneous equilibrium Y_c value $\tilde{C} = \tilde{Y}_c \big/ \widetilde{Y_{ceq}(\tilde{Z})}$ and not on the PDF averaged value.

Therefore, the scaled progress variable ($\tilde{C}$) (used as controlling parameter in loaded tables) is calculated by UDF following Eq. 4. 34. The unburnt species mass fraction ($\tilde{Y}_c^u$) and burnt species mass fraction ($\tilde{Y}_c^b$) values are taken from a table generated by CHEM1D and loaded by UDF (DEFINE_EXECUTE_ON_LOADING). These tables are generated considering both heat loss and dilution $\widetilde{\Phi} = \widetilde{\Phi}\left(\tilde{\xi}, S_\xi, \tilde{\eta}, \tilde{\gamma}\right)$ (improving ANSYS Fluent features). The un-scale progress variable calculated by ANSYS Fluent ($\tilde{Y}_c$) is used to calculate $\tilde{C}$ but unburn ($\tilde{Y}_c^u$) and burn ($\tilde{Y}_c^b$) species mass fractions are taken from loaded tables. By this methodology, the ANSYS Fluent frozen characteristic of species mass fraction at any heat loss is resolved. Data for those tables ($\tilde{Y}_c^u$ and $\tilde{Y}_c^b$) is taken founding the index parameters of the 4 controlling parameters and doing a 4D interpolation inside the table. This programming is also coded inside the loaded UDF file. The 4D $\tilde{Y}_c^u$ and $\tilde{Y}_c^b$ tables are calculated depending on $\tilde{\xi}, S_\xi, \tilde{\eta}, \tilde{\gamma}$ control parameters at $\tilde{C} = 1$. Therefore, these tables stored around 80 thousand of values.

4.6 Scaled progress variable variance ($\widetilde{C''^2}$) definition

The DA-FGM define scaled progress variable variance as:

Analysis of thermofluids in flameless (MILD)
combustion: assessment, improvement and
development of combustion models by CFD
Naiara Romero Anton

$$\widetilde{C''^2} = \frac{\widetilde{Y_c''^2} - \left(\widetilde{Y_c}\right)^2 - \left(\widetilde{Y_c^u}\right)^2 - 2\tilde{C}\left[\widetilde{Y_c^u Y_c^b} - \left(\widetilde{Y_c^u}\right)^2\right]}{\left(\widetilde{Y_c^b} - \widetilde{Y_c^u}\right)^2} - \widetilde{C^2} \qquad \text{Eq. 4. 40}$$

ANSYS Fluent by default calculated it based on the instantaneous equilibrium Y_c value $\widetilde{C''^2} = \frac{\widetilde{Y_c''^2}}{Y_{c,eq}(\tilde{Z}) * Y_{c,eq}(\tilde{Z})}$ and not on the PDF averaged value. Therefore, by CHEM1D $\left(\widetilde{Y_c^u}\right)^2$, $\widetilde{Y_c^u Y_c^b}, \left(\widetilde{Y_c^u}\right)^2$ tables are generated considering heat loss and dilution $\tilde{\Phi} = \tilde{\Phi}\left(\tilde{\xi}, S_\xi, \tilde{\eta}, \tilde{\gamma}\right)$ at $\tilde{C} = 1$ conditions. These tables are loaded into ANSYS Fluent by UDF (DEFINE_EXECUTE_ON_LOADING). Then by index finding and a 4D interpolation methodology their values are calculated and Eq. 4. 40 is solved. All this programming is developed in the code loaded into ANSYS Fluent

5   Results validation and discussions

In this section modelling results and validation are presented. First, some features of the FGM model are studied before proceeding to compare them with the DA-FGM modelling results. Then the radial profiles of the mean axial velocity ($\widetilde{U}_Z$) and mean temperature predictions of both models are compared with experimental data at different heights of the furnace.

5.1   FGM modelling analysis

In ANSYS Fluent there are some characteristics defined as default options when the FGM model is applied. In this section, the default options should be changed to see their impact on mean temperature prediction with the goal of selecting the most accurate FGM model features for flameless combustion modelling.

The first comparison is related to the un-scaled progress variable (Y_c) and the un-scaled progress variable variance ($Y_c''^2$). Three simulations have been carried out; case a), case b) and case c) (see Table 4. 3).

Table 4. 3 Y_c and $Y_c^{"2}$. chemical effect impact on FGM modelling

	Y_c	$Y_c^{"2}$ chemical effect: $2\left(\overline{Y_c \dot{\omega}_{Y_c}} - \widetilde{Y_c} \bar{\dot{\omega}}_{Y_c}\right)$
Case a	$Y_c = Y_{CO_2} + Y_{CO}$	NO
Case b	$Y_c = Y_{CO_2} + Y_{CO} + Y_{H_2O} + Y_{H_2}$	NO
Case c	$Y_c = Y_{CO_2} + Y_{CO} + Y_{H_2O} + Y_{H_2}$	YES

In the case a, default features of ANSYS Fluent are use. Case b improves un-scaled progress variable calculation including H_2O and H_2 species mass fractions (as in the DA-DGM model). Finally, case c incorporates the chemical effect on the un-scaled progress variable calculation.

The mean temperature predictions by the three cases has been compared, and as it is showed on Fig. 4. 7, there are no difference among them; therefore, any option can be suitable for this study.
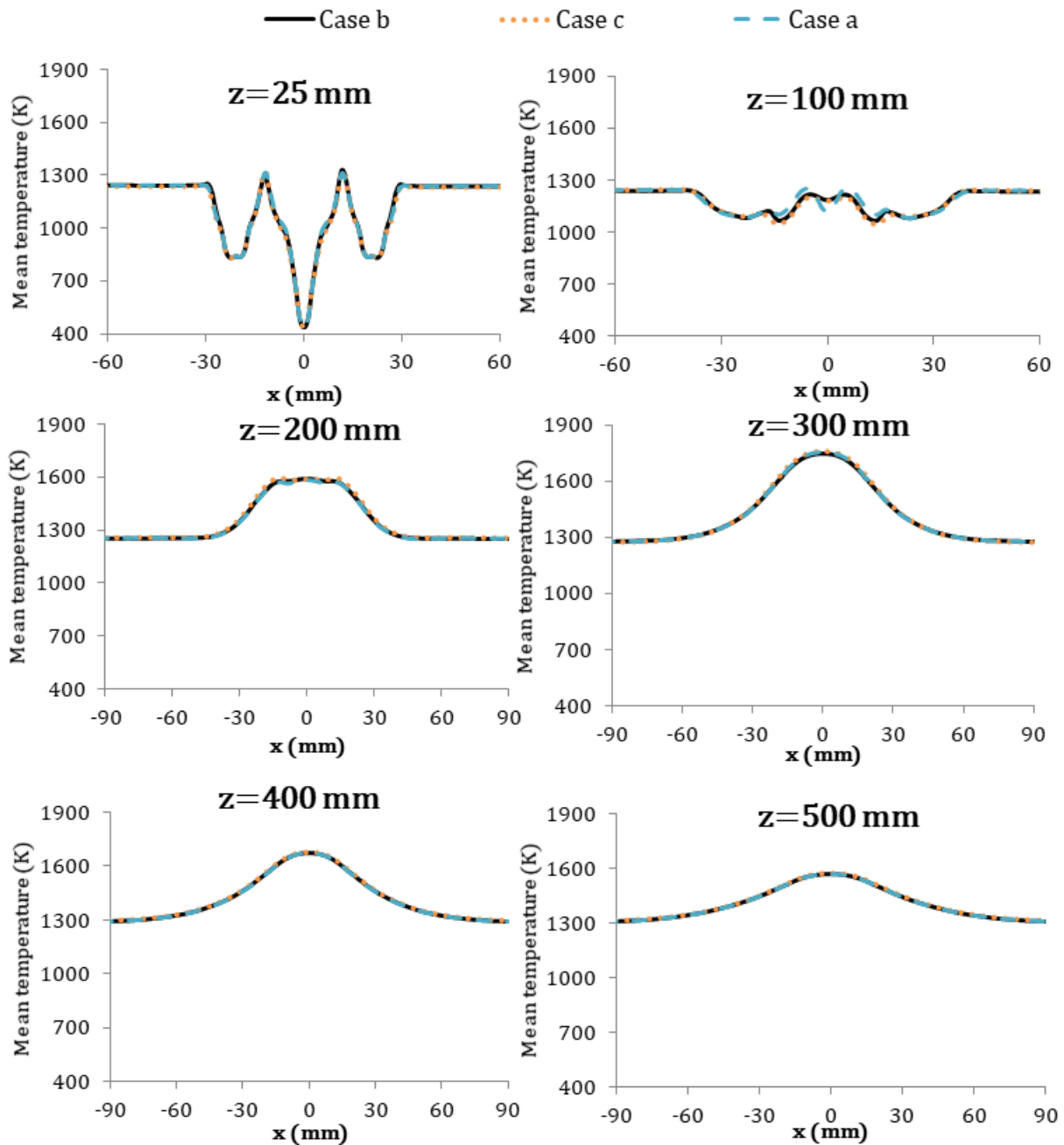
Fig. 4. 7 Y_c and $Y_c^{"2}$. chemical effect impact on FGM modelling mean temperature predictions

As it is explained in section 4.4, the chemistry effect of un-scaled progress variable is considered in the original DA-FGM model but in the implementation in ANSYS Fluent this effect is not considered as a segmentation fault is found during the modelling. It is an incompatibility between the chemistry effect and the macros implemented in the UDF. Nevertheless, Fig. 4. 7 shows the FGM model results considering the chemistry effect on

un-scaled progress variable (orange dots) and not considering it (straight black line and dashed blue line). It is appreciated that there is no change in mean temperature predictions by the three modelling, so that it can be concluded that in this furnace model there is no variation when considering the chemical effect on un-scaled progress variable variance. Thus, it is advisable not to consider it in DA-FGM model implementation methodology to save computational cost and avoid compatibility problems with the developed UDF. Between case a and b, the last case has been chosen as un-scaled progress variable is defined as in the DA-FGM model.

Another important issue for mean temperature prediction is the PDF table generation. During this process, in ANSYS Fluent is necessary to define the minimum temperature of the process. The Fluent Theory manual suggest defining this temperature 30K less than the lowest temperature (in this case fuel inlet 446K). Nevertheless, it has been seen that in many FGM modelling examples, the minimum temperature for PDF table generation was defined as 298K by default. During this work, simulation has been made for this two PDF table generation conditions (see Table 4. 4).

Table 4. 4 PDF Table minimum temperature definition options

	PDF table minimum temperature
Case b	$410\ K$
Case d	$298\ K$

Both cases, b (black straight line) and d (green dot-straight lines) are compared in Fig. 4. 8 with experimental data (yellow line) at different heights of the furnace. Difference between both cases can be appreciated for the height z=100, z=200 and z=300 mm. At z=100 mm case d presents four low points close to the air inlet streams, getting away from experimental data values. Nevertheless, at z=200 and z=300 mm, case d presents lower maximum values than case b at x=0 mm, getting closer to experimental data. Due to that, in this Thesis case d has been chosen as a better alternative for flameless combustion FGM modelling.

Other issue that can change the mean temperature predictions is the turbulence model, as it is related with the FGM turbulence closure. In chapter 4 the realizable two-equation

Analysis of thermofluids in flameless (MILD)
combustion: assessment, improvement and
development of combustion models by CFD
Naiara Romero Anton

$k - \varepsilon$ turbulence model has been used due to its accuracy and efficiency, but in the last year of the Thesis, ANSYS Fluent developed a beta turbulence model within k-omega BSL model called GEKO. Its goal is to consolidate the two-equation model into a formulation. Due to that, the next step is to compare case d, using two-equation $k - \varepsilon$ turbulence model, with case e which used GEKO turbulence model (see Table 4. 5).
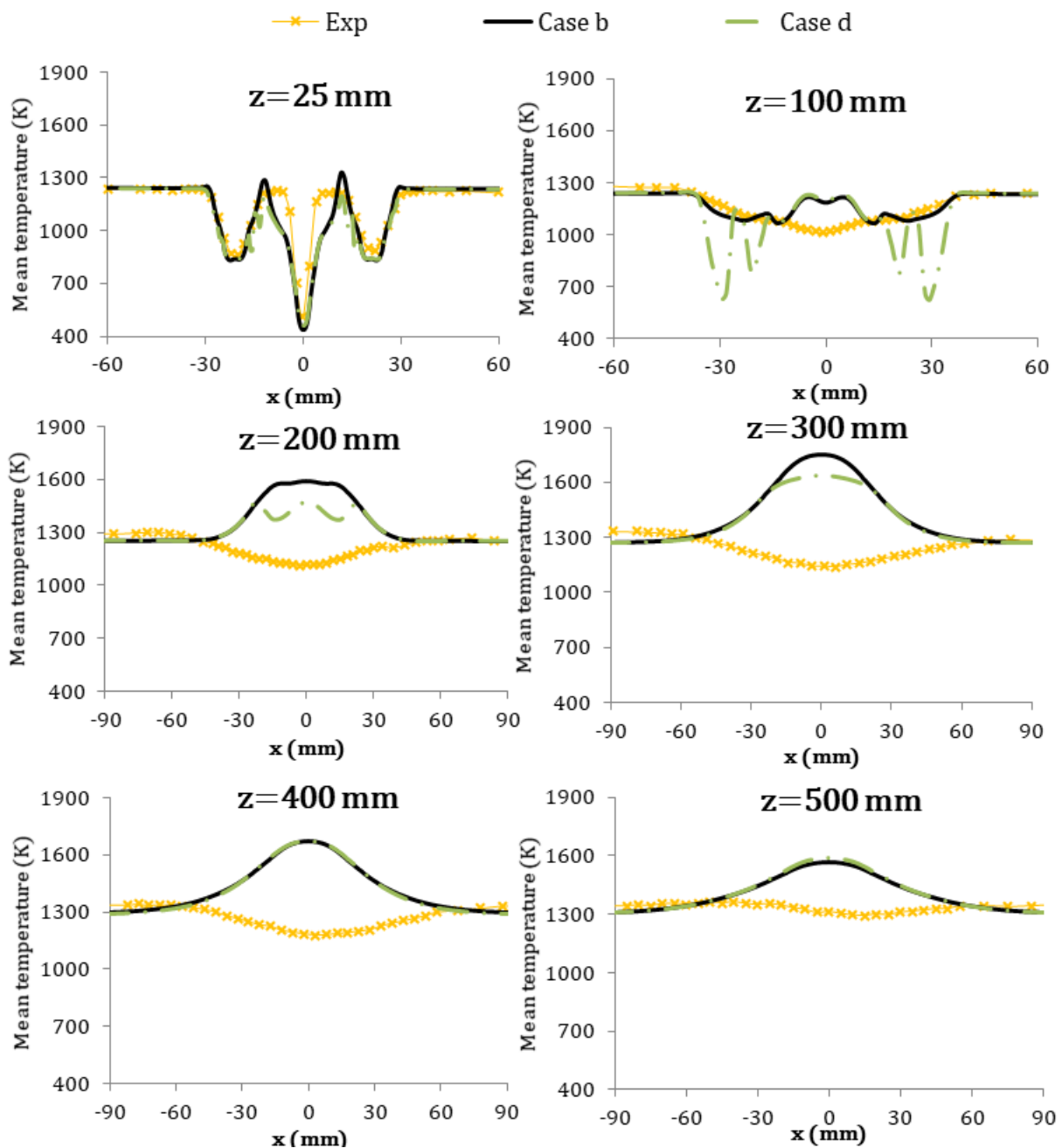
Fig. 4. 8 PDF Table minimum temperature effect of mean temperature predictions

Table 4. 5 Turbulence model options

	Turbulence model
Case d	realizable two-equation $k - \varepsilon$
Case e	k-omega BSL-GEKO

The comparison of case d and case e is made first by radial profiles of the mean axial velocity ($\widetilde{U}_Z$) at different axial locations and heights of the furnace (z=100mm, z=200mm, z=400mm and z=500 mm) (Fig. 4. 9). Note that case e is displayed by red dashed lines, case d by dot-straight green lines and experimental data as yellow lines.
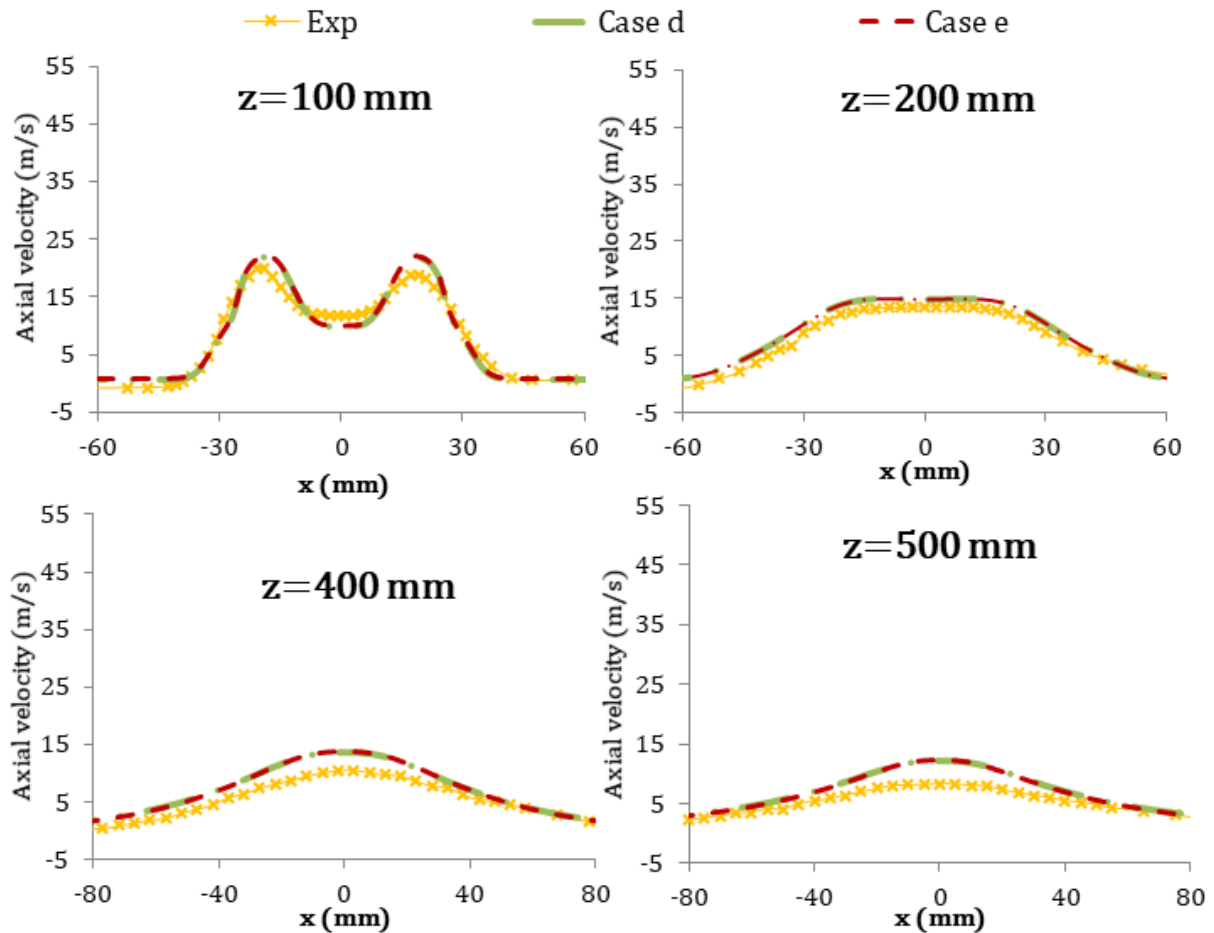
Fig. 4. 9 Comparison between measured and predicted radial profiles of mean axial velocity; case d (realizable two-equation $k - \varepsilon$ turbulence model) and case e (k-omega BSL-GEKO model)

Analysis of thermofluids in flameless (MILD)
combustion: assessment, improvement and
development of combustion models by CFD
Naiara Romero Anton

It can be appreciated that there is no difference between the two tested turbulence models for the mean axial velocity prediction at all heights. As the turbulence closure has effect in FGM model, next step is to compare the mean temperature predicted by both cases.
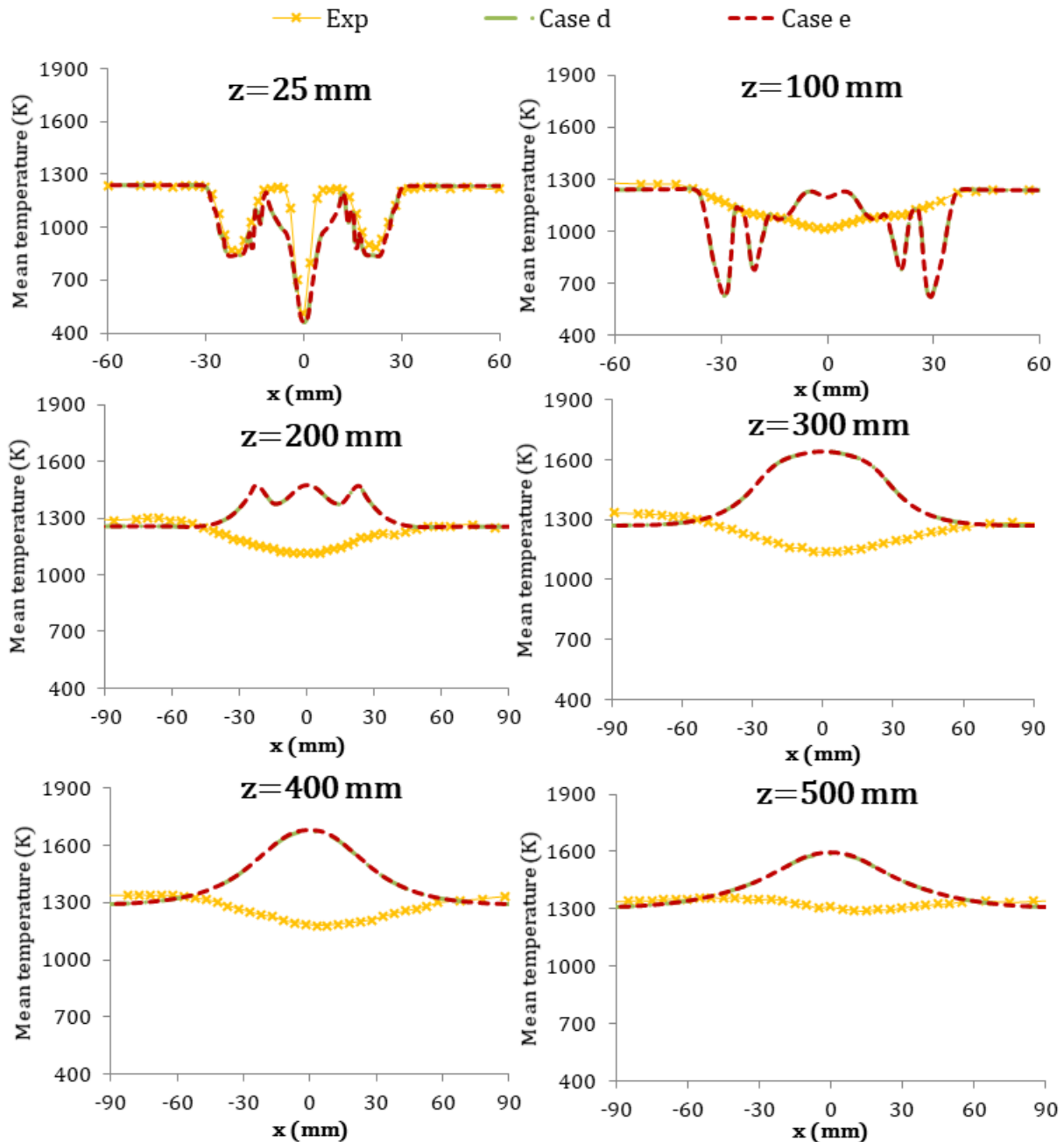
Fig. 4. 10 Comparison between measured and predicted mean temperature profiles; case d (realizable two-equation $k - \varepsilon$ turbulence model) and case e (k-omega BSL-GEKO model)

Fig. 4. 10 shows predicted mean temperatures of case d and case e and they are compared with experimental data at several heights of the furnace above the nozzle exit z=25, 100, 200, 300, 400 and 500 mm. As in the previous figure, the red dashed lines represent case e while the green line&dots line represents case d.

At all heights the same mean temperature is predicted by both turbulence models, due to that in this Thesis the realizable two-equation $k - \varepsilon$ turbulence model is selected, as it is a widen know and used model (case d). It should be noted that comparing the FGM modelling results with experimental data, the predicted mean temperature is over predicted in almost all heights of the furnace.

With the goal of improving the accuracy of the FGM model predictions, the last try in ANSYS Fluent has been based on reaction zone analysis. The product of the formaldehyde (CH_2O) mass fraction and the OH mass fraction, called formylradical (HR), is used to know the reaction zone location in numerical modelling, see Fig. 4. 11 (Medwell et al., 2007).
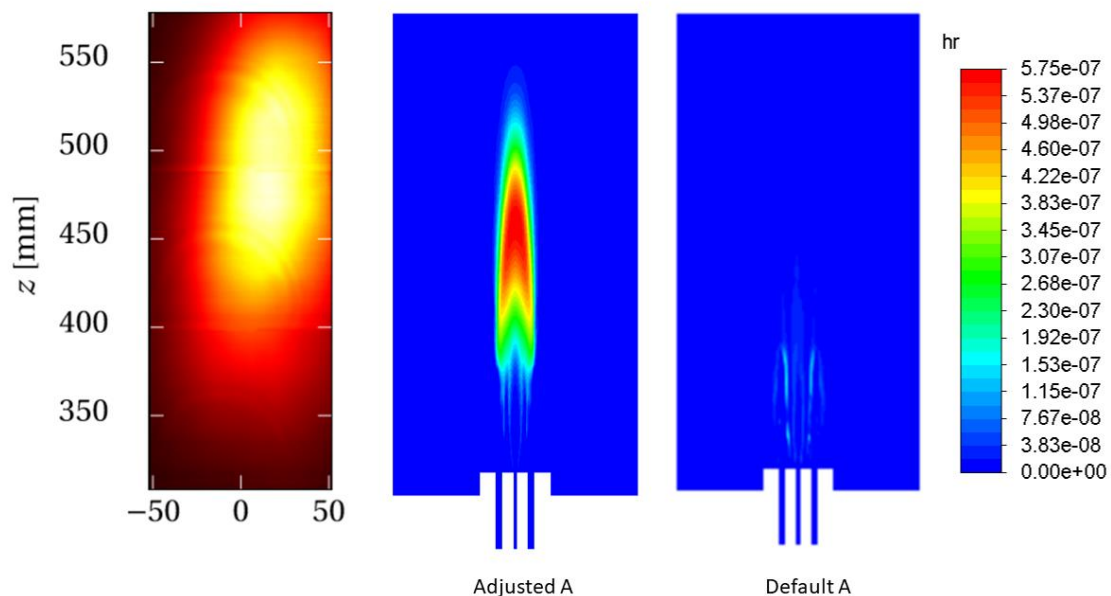
Fig. 4. 11 Reaction zone location comparison between experimental data and modelling

The experimental data shows a reaction zone around 475 mm height, so that there is a detached flame in this flameless configuration. ANSYS Fluent default option (with a turbulent flame speed constant A=0.57) shows a reaction zone attached to the burner,

Fig. 4. 11 Default A. To better model reaction zone, the default value of flame speed has been changed. After calibrating this parameter, a value of A=0.15 has been chosen to obtain a detached flame with a position close to experimental data.

Next, mean temperature contour of case d (default A) and case f (adjusted A) are compared, Fig. 4. 12. The mean temperature peak has been reduced in furnace centre (x=0 mm) with adjusted A modelling. One of the flameless combustion characteristics is a homogeneous temperature distribution along the furnace. At first sight, the modelling results of adjusted A case shows a more homogeneous temperature distribution as the peak temperatures at the centre of the furnace has been reduced.

a) Default A

b) Adjusted A

| 3.54e+02 | 4.86e+02 | 6.17e+02 | 7.49e+02 | 8.80e+02 | 1.01e+03 | 1.14e+03 | 1.28e+03 | 1.41e+03 | 1.54e+03 | 1.67e+03 |

[k]
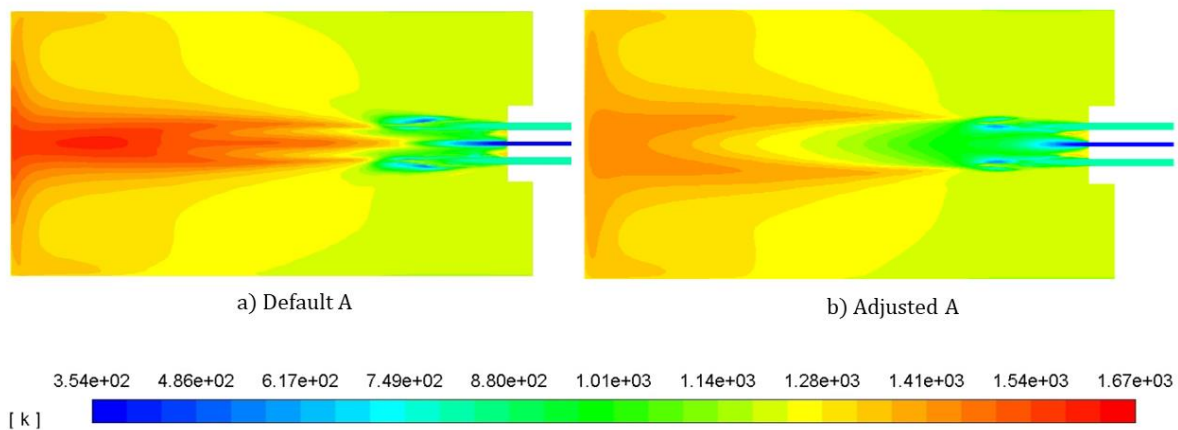
Fig. 4. 12 Temperature contour for several A values

For further analysis, the modelling results of the FGM model with default A and modified A values are compared with experimental data at different heights of the furnace (z=25, 100, 200, 300, 400 and 500 mm), see Fig. 4. 13.

Both modelling cases provide similar results at z=25mm and at z=100 mm. Along z=200, 300, 400 and 500 mm heights, the adjusted A case over predicts less mean temperature at x=0mm getting closer to experimental data and following experimental data profile. It is true that the temperature is still over predicted but the results has been improved as the overprediction has been reduced, and additionally, the gradient opposite to that of experimental data of case d (default A) has been neglected.
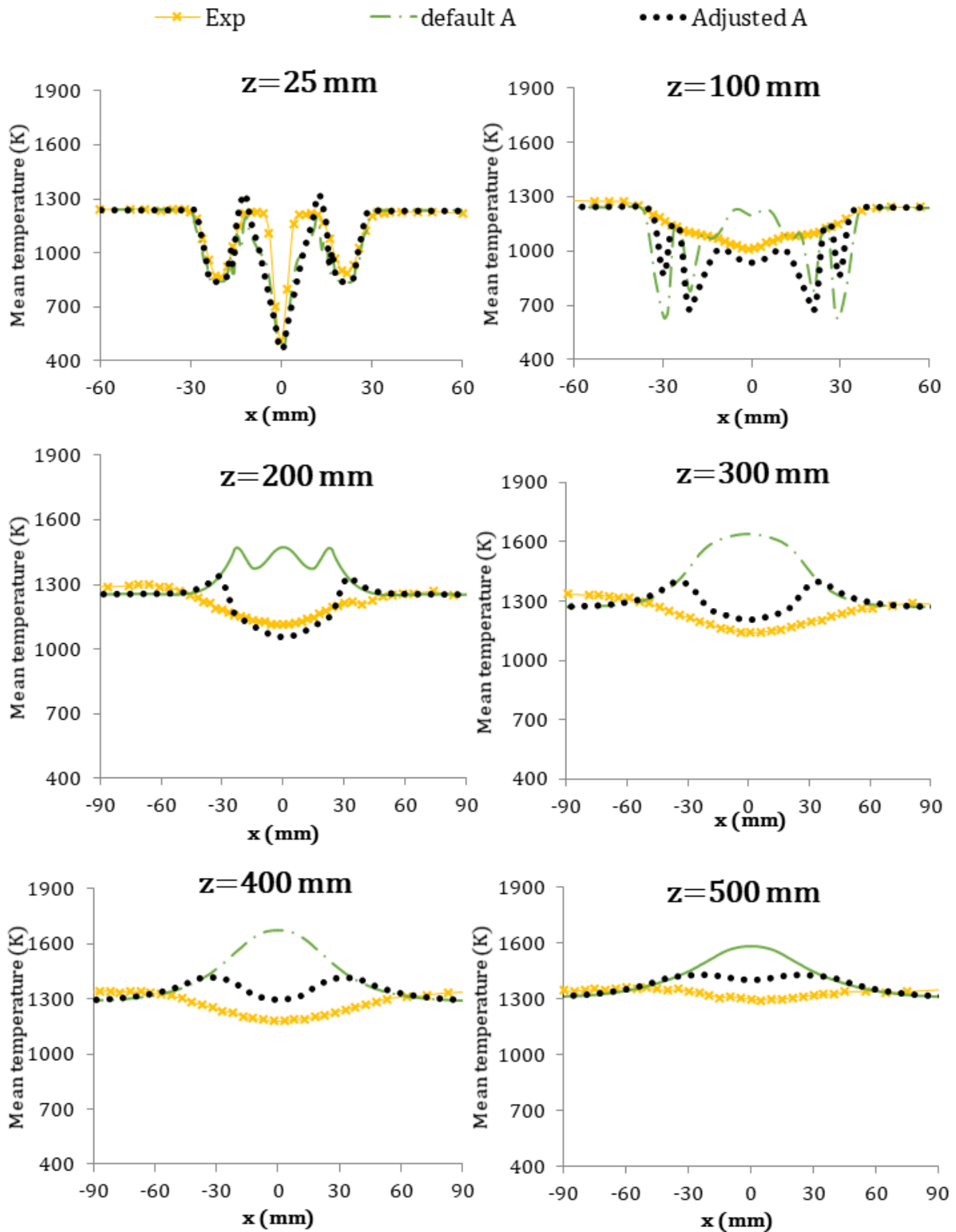
Fig. 4. 13 Comparison of mean temperature from experimental measurements and from simulations with case f (A=0.57, default) and case g (A=0.45)

After analysing the several options available in ANSYS Fluent FGM model in this Thesis the FGM model with adjusted A value, realizable two-equation $k - \varepsilon$ turbulence model, 298K minimum temperature for PDF table generation, $Y_c = Y_{CO_2} + Y_{CO} + Y_{H_2O} + Y_{H_2}$ and without the chemical effect in un-scaled progress variable variance has been chosen as the best FGM model for the present lab-scale application modelling. This model provides a more homogeneous temperature distribution, reduce the peak temperatures and the gradient opposite to that of experimental data has been improved. Nevertheless, estimated mean temperatures by CFD are higher than measured values. This deviance is because the flamelets are generated considering as boundary conditions pure fuel and pure air, so that dilution effect of flameless combustion is not considered during numerical modelling.

5.2   FGM vs DAFGM: mean velocity field

ANSYS Fluent release 19.R2 has been used with the FGM and with the implementation of the DA-FGM turbulence-chemistry interaction models. In both cases, the same sub-models are used: the realizable two-equation $k - \varepsilon$ turbulence model and the Discrete Ordinates (DO) method solving the radiative transfer equation using a grey weighted-sum-of-grey-gases model (WSGGM) for the absorption coefficient. The chemical mechanism used is the GRI 3.0 mechanism (53 species including Ar) (P. Smith et al.,).

Once the FGM model turbulent flame speed constant is selected, the radial profiles of the mean axial velocity ($\widetilde{U}_Z$) at different axial locations are presented for the FGM model with adjusted A, the DA-FGM model and experimental data (see Fig. 4. 14).

Close to the furnace (z=3 mm and z=50 mm) both models show the same radial profiles of mean axial velocity which is close to experimental data. Nevertheless, a slight over prediction is appreciated at air injection. When the flow develops (from z=100 mm to z=500 mm) there is only a slight deviance between the two models close to the furnace top wall, at z=400 and 500 mm, showing the DA-FGM model closer values to experimental data. This deviation can be related to the mean temperature prediction (density under prediction leads to velocity over prediction). Above all, along the entire height of the

furnace both model results are in good agreement with the experimental data, showing an acceptable performance of the realizable $k - \varepsilon$ model.
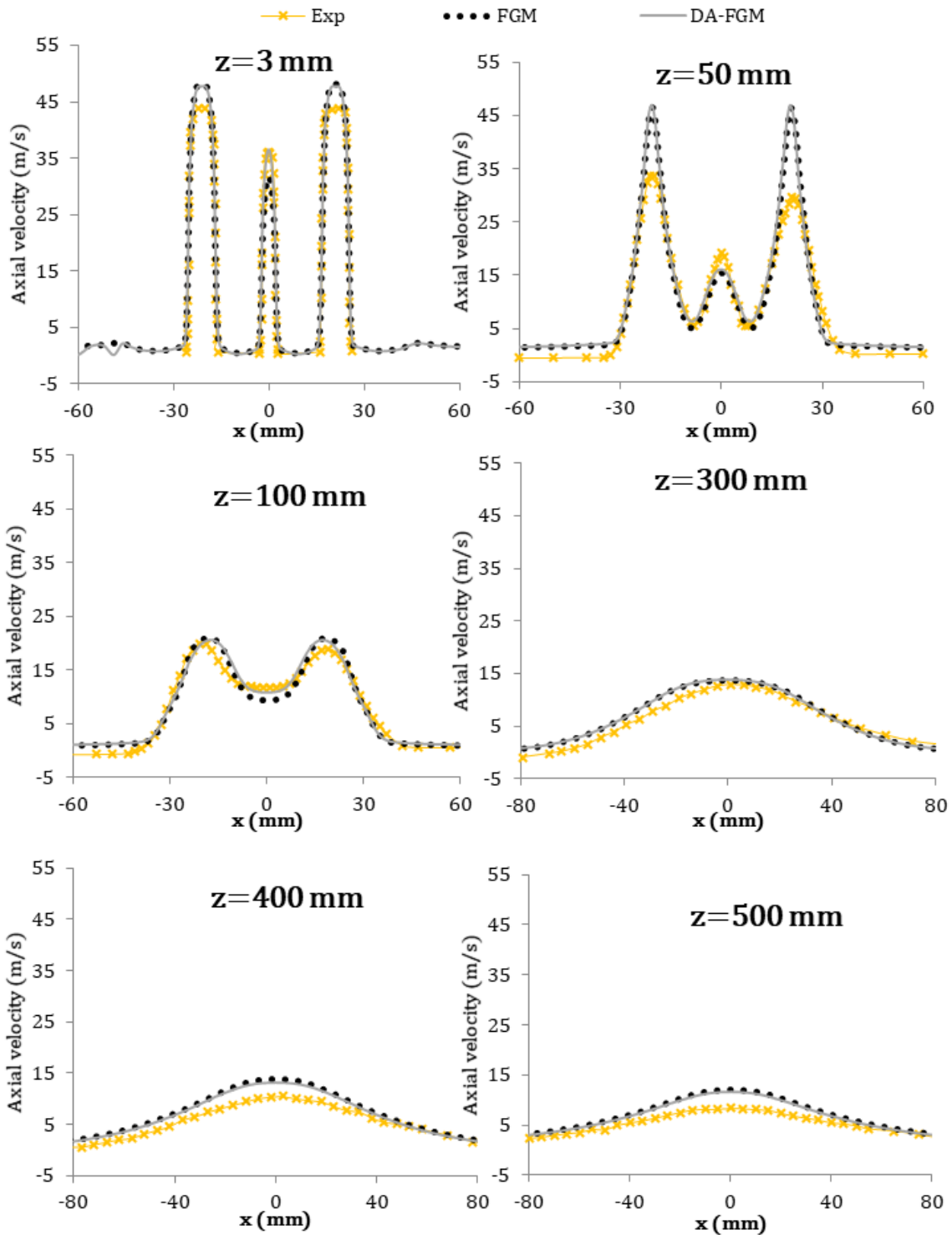
Fig. 4. 14 Comparison between measured and predicted FGM and DA-FGM radial profiles of mean axial velocity.

5.3 FGM vs DA-FGM: mean temperature field

Next, a comparison is made between the measured and predicted mean temperatures obtained for each turbulence-chemistry interaction model. First, the mean temperature contour of the FGM and the DA-DGM models are shown in Fig. 4. 15.

a) FGM   b) DA-FGM

3.54e+02   4.86e+02   6.17e+02   7.49e+02   8.80e+02   1.01e+03   1.14e+03   1.28e+03   1.41e+03   1.54e+03   1.67e+03

[k]
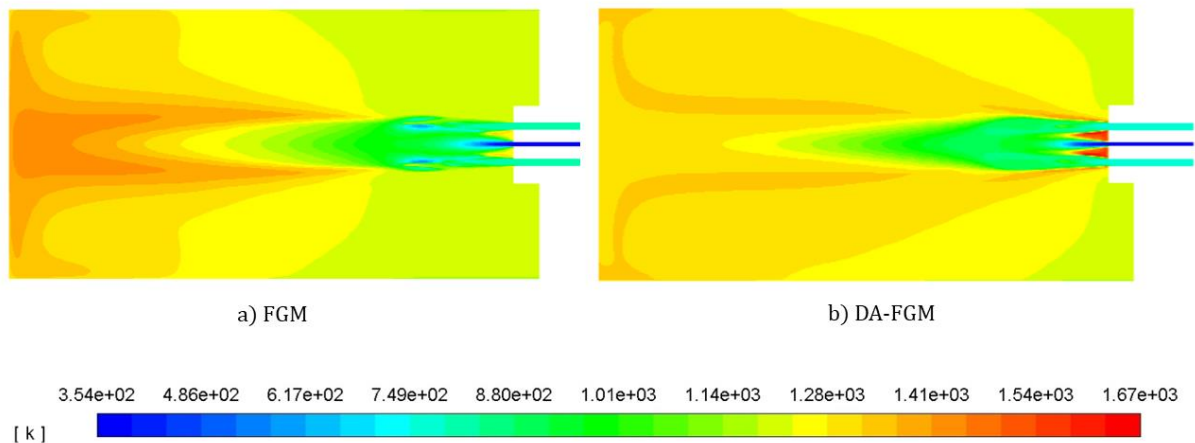
Fig. 4. 15 Comparison of mean temperature from experimental measurements and from simulations with FGM model

The FGM model shows a hot region from 300 mm height to the furnace's top wall while the DA-FGM shows a more homogeneous temperature distribution (also in the area close to the furnace top wall). In flameless combustion, the products recirculation within the furnace act as a heat sink reducing furnace temperature, so that peak temperatures are reduced, and a homogeneous temperature distribution is got. Having a look to Fig. 4. 15 it is appreciated that flameless features are better predicted by the DA-FGM model implemented in ANSYS Fluent than by the FGM model.

Next, the mean temperature fields by the two models and experimental data are compared at several heights of the furnace. As in Fig. 4. 14. the FGM model results, the DA-FGM model results and the experimental data values are represented.
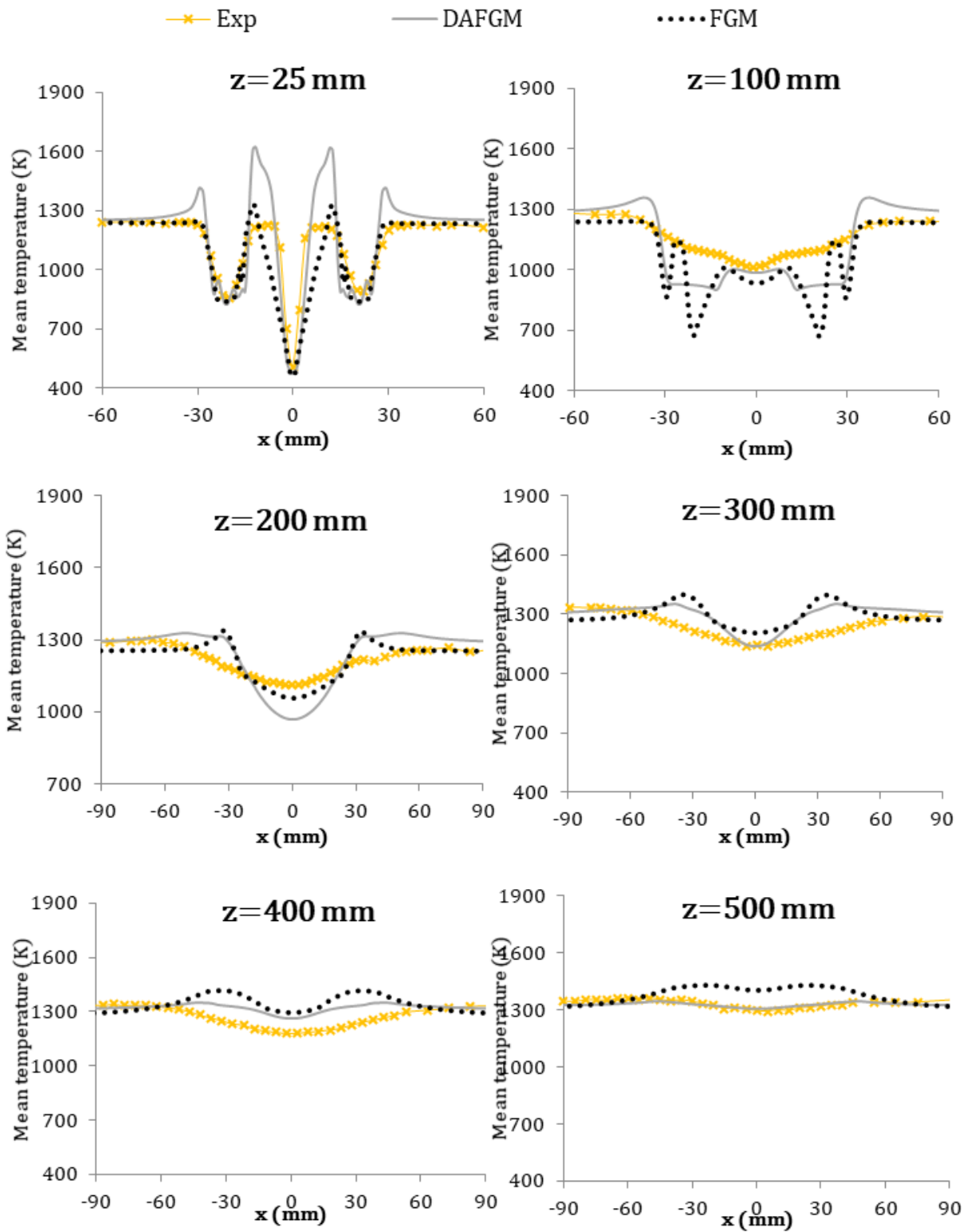
Fig. 4. 16 Temperature contour for the FGM a) and the DA-FGM b) turbulence chemistry interaction models

Close to the burner the FGM model shows better predictions than the DA-FGM model implemented in ANSYS Fluent, as the latter presents some peaks points at |x| = 30 mm and |x| = 10 mm. Nevertheless, in the rest radial locations both modelling results show consistency with experimental data. At z=100 mm the FGM model shows some bottom temperatures at |x| = 10 mm and |x| = 30 mm while the DA-FGM model provides a more homogeneous temperature distribution. The latter slightly underpredict mean temperature but is close to experimental data following the experimental data profile, while the FGM model presents some low values suggesting non-homogeneous mean temperature profile. As the flow develops, the dilution effect within the furnace become more intense. Thus, from z=200 mm to z=500 mm the temperature profiles predicted by the FGM model and DA-FGM model start to differ showing different temperature profiles.

Although in the FGM modelling fuel and air are injected at a distance from each other, the FGM based on counterflow non-premixed flamelets of fuel and air, including the PDF model for the fluctuations of mixture fraction and progress variable, performs well only in the region close to the burner, while the DA-FGM perform better further downstream, where the dilution is dominant. It should be noted that at z=200 mm height the DA-FGM underpredict more the mean temperature at the centre of the furnace. The deviance between DA-FGM model and the experimental data can be attributed to one of the limitations of ANSYS Fluent. Although burnt and unburnt species mass fractions tables, considering heat loss, has been load into ANSYS Fluent by UDF, the un-scaled progress variable $\tilde{Y}_c$ value has been taken from ANSYS Fluent. Thus, the species for $\tilde{Y}_c$ calculation do not consider the heat loss in the furnace (the original DA-FGM model considers heat loss for species calculation). From z=300 to 500 mm, the FGM model starts overpredicting mean temperature while the DA-FGM gets closer to experimental data. The deviance between both models is highly appreciated at z=500 mm where the dilution effect is dominant, there the DA-FGM match perfectly with experimental data.

6 Conclusions

In this chapter, the FGM turbulence-chemistry model and the DA-FGM model implementation in ANSYS Fluent release 19.R2 have been presented. Their advantages comparing to other reduction techniques and flamelet models have been stressed.

Taking advantages of the low computational time required by flamelet based model, the DA-FGM has been implemented in ANSYS Fluent. Flamelets based models with pure fuel and pure air as boundary conditions for flamelets generation are not suitable for this kind of flameless furnace application. The diluted flamelets agree better and that is shown by the DA-FGM modelling results.

The DA-FGM model understand flameless combustion in an enclosed furnace as a diluted environment where the fuel is injected. It is a three-stream problem (pure fuel, pure air and recirculated products) and this model treat the reactions in the mixture of pure fuel and diluted air with a second mixture fraction (ξ) describing the mixture between pure fuel and diluted air. Thus, mixture properties are calculated by a 6-dimensions PDF table

$$\widetilde{\Phi} = \widetilde{\Phi}\left(\tilde{\xi}, S_\xi, \tilde{C}, S_C, \tilde{\eta}, \tilde{\gamma}\right).$$

ANSYS Fluent presents some limitations to implement the DA-FGM model: the diltion effect is not considered in flamelets generation, the species mass fractions are calculated without considering heat loss and mixture properties, except species mass fractions, are calculated not considering scaled progress variable variance. Nevertheless, during DA-FGM model implementation methodology those limitations are corrected. Additionally, ANSYS Fluent release 19.2 or latter should be used for the DA-FGM model implementation, as in previous releases the DEFINE_PDF_TABLE does not allow to change the un-scaled progress variable source term.

After comparing both models resulst with Delft lab-scale furnace experimental data it can be concluded that implemented DA-FGM model predicts mean temperature profile quite accurately and better than the FGM model available in ANSYS Fluent when the dilution effect is dominant (Fluent's FGM model considers pure fuel and pure air for flamelets generation). The DA-FGM model better predict mean temperature in the regions with

more dilution, that is, at z=300, 400 and 500 mm. Thus, it is important to include the dilution effect during flamelets generation for an accurate flameless combustion modelling.

The implementation of the DA-FGM model in ANSYS Fluent is another contribution to take into account. The ANSYS Fluent is one of the most widely used CFD code in the industrial field as it is quite robust and easy to use in CFD applications (easily you can get the result of a problem of interest). On the contrary, the OpenFOAM, for example, is an open CFD code but good knowledge on coding is necessary and it is not a result oriented CFD package. The other two CFD codes commented, the YALES2 (specialized in two-phase combustion) and the AVBP (specialized for LES modelling) are CFD codes developed by research groups for specific applications.

Finally, it is concluded that the DA-FGM can be an alternative for flameless modelling when ANSYS Fluent package is used.

CHAPTER 5: EDC vs FGM APPROACHES IN ANSYS FLUENT

1 Introduction

Climate change is the biggest challenge that the society is dealing with and the burning of fossil fuels to release energy is the main cause of the greenhouse effect. (Wünning & Wünning, 1997). Flameless combustion is a climate-friendly combustion technology able to reduce pollutant emissions (NO_x) and improve energy efficiency. It is an attractive combustion technology to be applied in large-scale furnaces and in non-premix combustion.

In order to gain and in depth understanding of flameless combustion, research has been conducted in Jet-in-hot coflow (JHC) burners as well as in enclosed lab-scale furnaces. With the data of these experimental set-ups flameless RANS modelling studies have been validated. The first conclusion suggests that temperature gradient in the mean profile is lower than in conventional combustion. Thus, the chemical time scale can be longer, thickening reaction zones. Therefore, standard turbulence-chemistry interaction models, like the EDC and flamelet based model, may not be accurate models for flameless combustion modelling as they do not consider this feature, so that they over predict mean temperature profiles.

The EDC model, for example, calculates the reaction rate based on two constants which were empirically chosen for conventional combustion ($C_\xi = 2.1377$ and $C_\tau = 0.4082$), so that they do not take into account the dilution effect of flameless combustion. The FGM

model, for example, generates flamelets tables based on pure fuel and pure air as boundary conditions, not taking into consideration diluted reactants. Therefore, new models or extensions of the existing models should be developed to model flameless combustion.

The EDC model has been widely used for flameless modelling and the first approach to improve its accuracy was to change model constants value (C_ξ and C_τ), in an arbitrary form, calibrating them with experimental data. Later, an Extension of the EDC model was proposed, the E-EDC, where model coefficients are calculated based on local Reynolds and Damköhler numbers, so that the calibration of model coefficients is avoided. To better model flameless combustion, in this Thesis, the NE-EDC model is developed. This model follows a similar strategy to the E-EDC model, that is, model constants are also calculated based on local Reynolds and Damköhler numbers. Nevertheless, the NE-EDC model postulates the fine structure length scale equal to the Kolmogorov scale $L^* = \eta_k$; while the E-EDC model does not follow this assumption. Additionally, the NE-EDC model proposed laminar flame speed calculation as $L^* = \tau_c^* * S_L$ and the proportionality factor for laminar flame speed calculation used in the E-EDC model is omitted. These EDC model extensions show better consistency with experimental data than the standard EDC model. Note that both, the E-EDC and the NE-EDC present important advantages as model coefficients are calculated during modelling and calibration with experimental data is not necessary. Among them, the NE-EDC model seems to provide better radial profiles of the mean temperature on a lab-scale furnace application (see chapter 3 section 4.4). Recently, a review of the proposed changes during the last years to the standard EDC model for flameless modelling with respect to the original ideas of the EDC model proposed by Magnussen et al. was made (Ertesvåg, 2019; Lewandowski & Ertesvåg, 2018).

To better understand reaction zone behaviour under flameless combustion, DNS modelling have been carried out (Minamoto, Y. et al., 2013; Minamoto, Y. & Swaminathan, 2014; Minamoto, Y. et al., 2014; Minamoto, Yuki & Swaminathan, 2014). They suggest interactions among the combustion reaction zones, so that this feature could invalidate the commonly used combustion assumption: infinity fast-chemistry and flamelets modelling. Under this circumstance, a Generalized E-EDC model has been proposed

(Evans et al., 2019) based on the E-EDC model (Parente, Alessandro et al., 2016), but including detailed chemical kinetics in chemical time scale calculation in order to consider the reaction zones interaction. In the Generalized E-EDC, the chemical time scale is calculated considering the reaction rates of CH_4, H_2, O_2, CO and CO_2 and not following the CH_4 one-step mechanism (as was done in the E-EDC and NE-EDC models). Additionally, Generalized E-EDC eliminates the proportionality factor in laminar flame velocity following the NE-EDC suggestion (see chapter 3 section 3.2). The Generalized E-EDC model presents better consistency with experimental data in a JHC furnace than the E-EDC.

In consideration of the recent DNS modelling findings suggesting the interactions among the reaction zones, in this Thesis, chapter 3 section 3.3, presents a revised version of the NE-EDC model, called here Generalized NE-EDC model, in order to include these findings. In this revised version the chemical time scale is calculated considering the reaction rates of CH_4, H_2, O_2, CO and CO_2 and not only the reaction rate of CH_4 (1-step global mechanism) as was made in original NE-EDC. The adjusted global mechanism WD1 has been selected as the best model for chemical time scale calculation for the Delft lab-scale furnace (note that detail chemistry, the smooke-25, is still used for temperature and species mass fractions calculation during modelling). By the UDF the chemical time scale is calculated with the reduced mechanism WD1 and then, in combination with the flow time scale calculated by ANSYS Fluent, the UDF calculates Damköhler number. Finally, Damköhler number is used to calculates the EDC model's constant in each iteration locally considering the dilution effect of flameless combustion. However, it should be noted that for this application there is not a big deference between WD1 and 1-step global mechanism results.

Fig. 5. 1 summarizes the general approach of this study, with the investigations that have been carried out until the moment and those developed in this Thesis.

Analysis of thermofluids in flameless (MILD)
combustion: assessment, improvement and
development of combustion models by CFD
Naiara Romero Anton
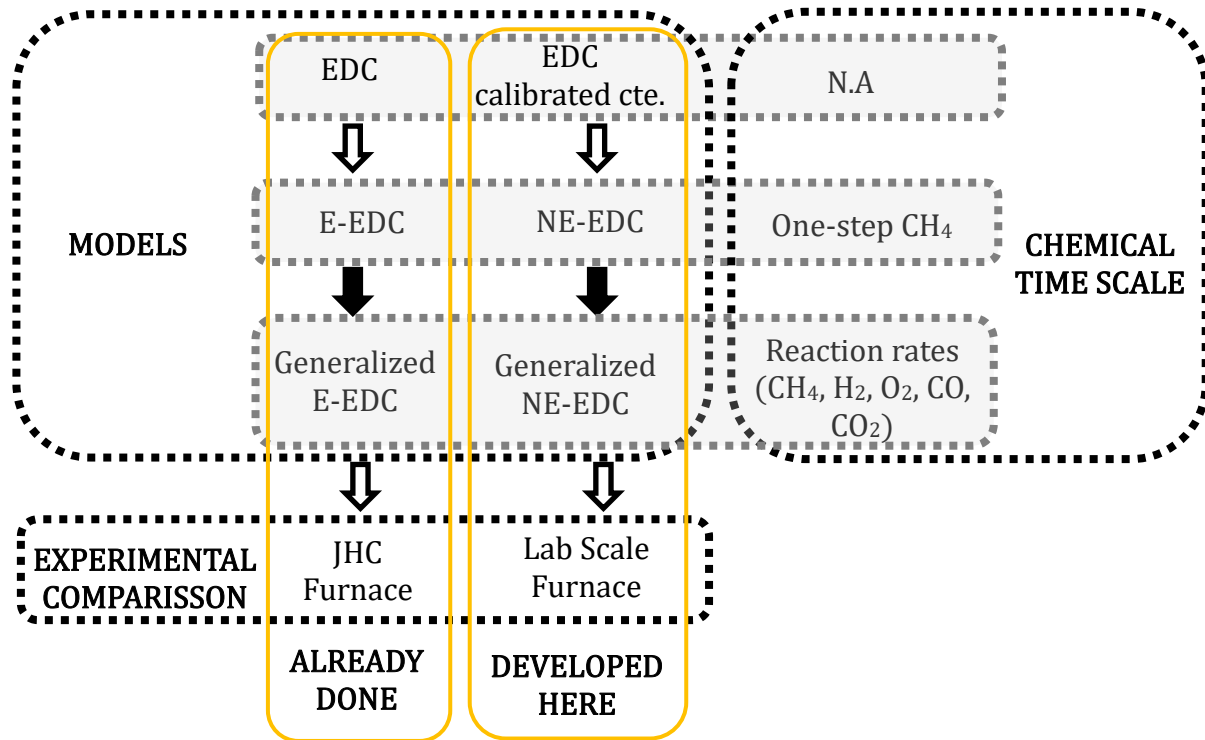
Fig. 5. 1 Summary of extended EDC model situation for flameless modelling

Flamelet based models, like the FGM model, present lower computational time than the EDC model using detailed chemistry. Therefore, it is an attractive model to be used on flameless combustion. It is found that the FGM model described the near burner zone dominated by separate jets of fuel and air quite well but fails to capture the flameless mode further downstream in the furnace. The predicted mean temperature gradients show erroneous trends and the mean temperature is over predicted. The root cause of this appears to be the use of undiluted flamelets (non-premixed flamelets are generated using as boundary condition pure fuel and pure air). The fact that flamelet based models, based on diluted flamelets, perform better than standard undiluted flamelets in flameless combustion agrees with the analysis of DNS simulation results. Thus, flamelet based models should include the dilution effect for flameless modelling. The ANSYS Fluent default FGM option does not allow the inclusion of the dilution on flamelets generation and could not be used for Delft lab-scale flameless furnace modelling.

The DA-FGM model, based on flamelet equations, is an alternative to improve flameless modelling results as included dilution effect. The local dilution level is accurately

calculated by a transport equation ($Y_d = Y_{CO_2} + Y_{H_2O}$) and it does not avoid the reactions between fuel and diluted burn gases at lean conditions when flamelets are generated. The DA-FGM model understands flameless combustion in an enclosed furnace as a diluted environment where the fuel is injected. It follows steady flamelet equations and flamelet tables are generated considering pure fuel and diluted air as boundary conditions. Thus, mixture properties are calculated by a 6-dimensions PDF table $\widetilde{\Phi} = \widetilde{\Phi}\left(\tilde{\xi}, S_{\xi}, \tilde{C}, S_C, \tilde{\eta}, \tilde{\gamma}\right)$. Due to the advantages presented by the DA-FGM model, in this Thesis, it has been selected to implement in ANSYS Fluent, as it is so far only available in OpenFOAM.

ANSYS Fluent has a user-friendly interface, easy to navigate, use and build models. The user does not need to develop its own code, so that a good knowledge of programming is not necessary. It is a results-oriented code ideal to be used in industrial problems where the goal is to obtain accurate and reliable results. It comes with fully developed models and an excellent technical support. Conversely, in OpenFOAM the user easily can change the code source as well as create a new code itself, but it takes long time to get results and makes various trials during modelling. Additionally, the OpenFOAM mesh offer is poor compared with ANSYS Fluent. The other two CFD codes used with D-FPV and DHR, YALES2 (specialized in two-phase combustion) and AVBP (specialized for LES modelling) respectively, are CFD codes developed by research groups for specific applications. Consequently, it is interesting to implement the DA-FGM in ANSYS Fluent due to both, its advantages to be applied in industrial applications to get results easily and its widely and easier use in combination with the technical support.

In this Thesis the DA-FGM model is implemented for the first time in ANSYS Fluent package using User Define Functions (UDF), User Defines Memory (UDM) and User Define Scalars (UDS). Nevertheless, ANSYS Fluent presents three main limitations during DA-FGM model implementation; 1) The extra dimension of flamelets and PDF tables (corresponding to dilution) does not exist, 2) species mass fractions are frozen against heat loss $\widetilde{\Phi}' = \widetilde{\Phi}'\left(\tilde{Z}, \widetilde{Z''^2}, \tilde{C}, \widetilde{C''^2}\right)$ and finally, 3) mixture properties (except species mass fractions) do not consider scaled progress variable variance $\widetilde{C''^2}$ for their calculation. Thus, finally, in RANS Non-Adiabatic FGM model ANSYS Fluent considers 4-dimensions

PDF tables. As explained in chapter 4 section 4, this main limitations has been solved and finally the DA-FGM model implemented in ANSYS Fluent predicts mean temperature profile quite accurately and better than the when the dilution effect is dominant. It is concluded that the DA-FGM implemented in ANSYS Fluent can be an alternative for flameless modelling when ANSYS Fluent package is used.
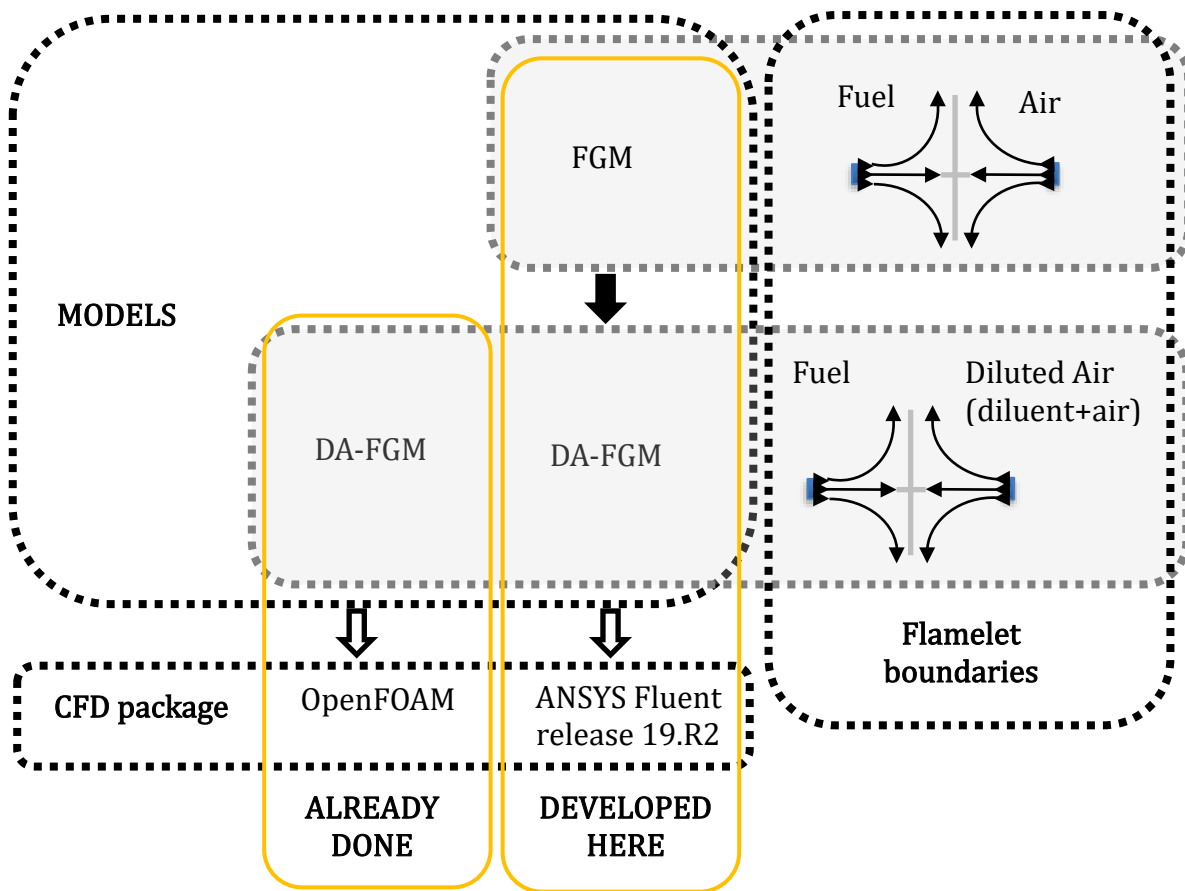
Fig. 5. 2 Summary of flamelet based model approach in this thesis for flameless modelling

In this Thesis the NE-EDC model, Generalized NE-EDC as well as the implementation of DA-FGM in ANSYS Fluent are tested for a new application of flameless lab-scale furnace. The differences between the models are described in detail in chapter 3 and 4 and CFD modelling has been carried out. Modelling results are compared with Delft lab-scale furnace performing in flameless combustion mode at a power input of 9 kW (Huang, X. et al., 2017; Huang, Xu, 2018).

The E-EDC model developed by Parente et al. (Parente, Alessandro et al., 2016) and the FGM model developed by Oijen (van Oijen et al., 2016) has been found as accurate and

efficient turbulence-chemistry interactions models for combustion modelling considering detailed chemical mechanism. In this chapter, first, the modelling results of these two turbulence-chemistry interaction models are compared with experimental data and later the newest extensions proposed in this Thesis, the Generalized NE-EDC model and the DA-FGM model implemented in ANSYS Fluent are compared among them and with experimental data.

2 The E-EDC and the FGM model

In this section the already developed E-EDC and FGM models (with adjusted A value) are compared with experimental data of Delft-lab scale furnace performing in flameless combustion.

First, the radial profiles of the mean axial velocity ($\widetilde{U}_Z$) at different axial locations of both models (dot-straight green line for the E-EDC and black dots the FGM) and experimental data (yellow –x—x line) are shown (see Fig. 5. 3).

There is no difference in mean axial velocity prediction for both turbulence-chemistry interaction models. This is because the same turbulence model, the realizable two-equation $k - \varepsilon$ model, is used and this model is the cause of velocity prediction. Consistency with experimental data is appreciated, so that it can be said that this turbulence model is appropriate for this case of study.

Analysis of thermofluids in flameless (MILD)
combustion: assessment, improvement and
development of combustion models by CFD
Naiara Romero Anton
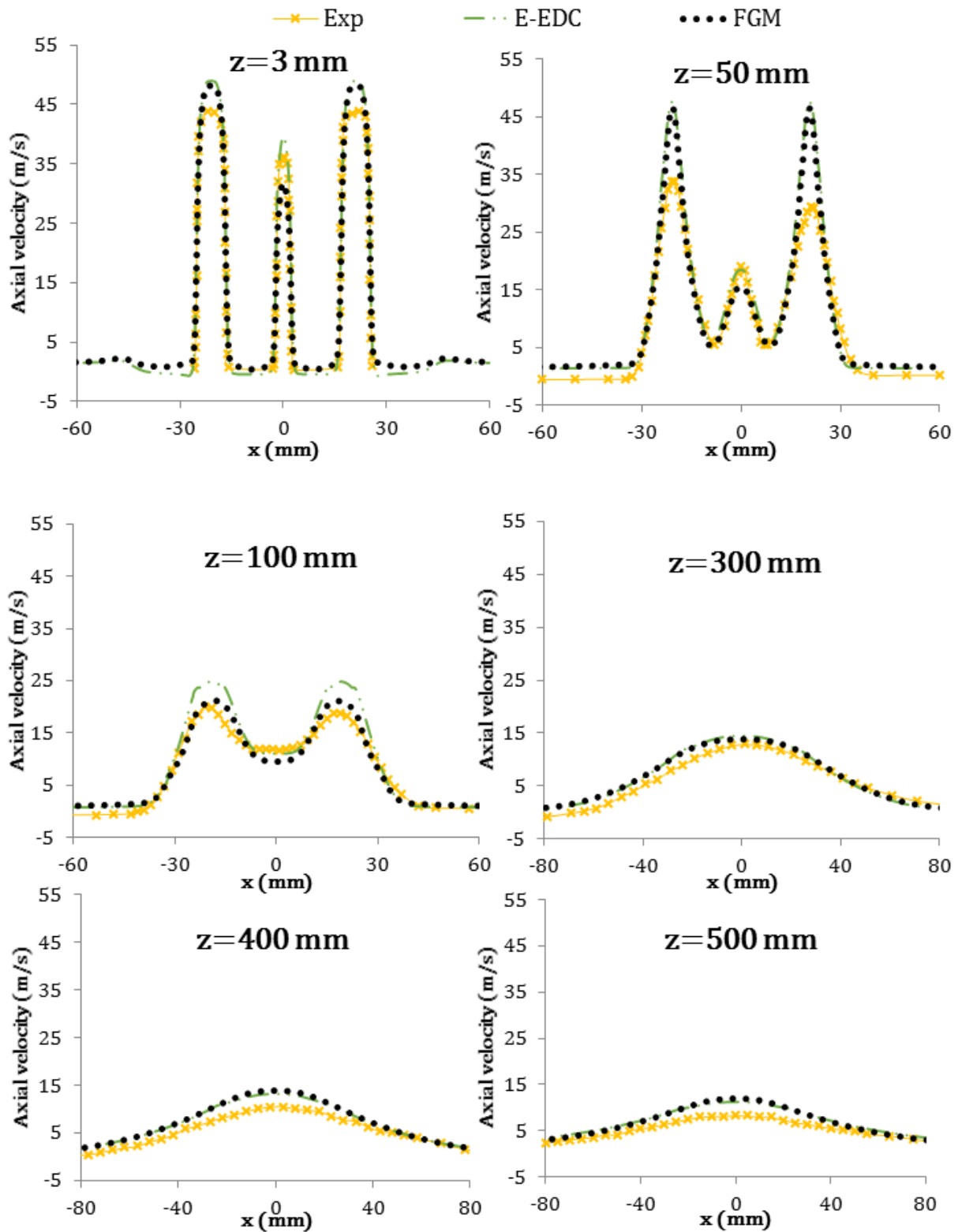
Fig. 5. 3 Comparison between measured and predicted axial mean velocity profiles for FGM
(case f) and E-EDC model

In the next figure, Fig. 5. 4, mean temperature profiles of the E-EDC model, the FGM model (adjusted A) and experimental data are shown. The E-EDC model is selected for comparison and not the Generalized E-EDC model as there is no information about what reduced mechanism was followed and its Arrhenius coefficients.

In general, the E-EDC model results agree better with experimental data than the FGM model considering pure fuel and pure air as boundary conditions for flamelets generation. The FGM model starts to overpredict the mean temperature when the dilution is more noticeable, for example see the z=300-500 mm heights. At z=25 mm both models have good consistency with experimental data. At this height, close to the furnace walls the FGM model shows better accuracy, as the E-EDC model over predicts the mean temperature around 75K close to the furnace walls. Among z=100 mm and z=300 mm, the E-EDC model shows consistency with experimental data. However, in the upper side of the furnace, the mean temperature close to the furnace walls is over predicted (+30 K at z=400 mm and +45K at z=500 mm), while for z=500 mm the mean temperature is under predicted (-115K) in the middle of the furnace. On the other side, the FGM model at z=100 mm close to the air stream injection shows under predicted values; but the rest predicted mean temperatures values at this height agree well with experimental data. Among the other heights (z=200 mm to z=500 mm), the FGM model shows two peak points around air injection and while the flow develops the mean temperature is over predicted. Therefore, it can be concluded that for this application (Delft lab-scale furnace), when the dilution effect is dominant, the ANSYS Fluent default FGM model overpredict mean temperature while the E-EDC model underpredict it (see z=500 mm).

Considering the drawbacks of both models in this Thesis two steps has been followed: 1) develop the NE-EDC model to improve the E-EDC model predictions results at z=400 and z=500 mm height, and 2) include the dilution effect in ANSYS Fluent FGM model (generate flamelets considering the dilution effect of flameless combustion) to better predict mean temperature in high diluted region. In this Thesis, the DA-FGM has been selected to implement in ANSYS Fluent as its accuracy is better than the other models existing in the literature. To the authors known the DA-FGM model has been only implemented in OpenFOAM, therefore it is the first time implemented in ANSYS Fluent.

Analysis of thermofluids in flameless (MILD)
combustion: assessment, improvement and
development of combustion models by CFD
Naiara Romero Anton
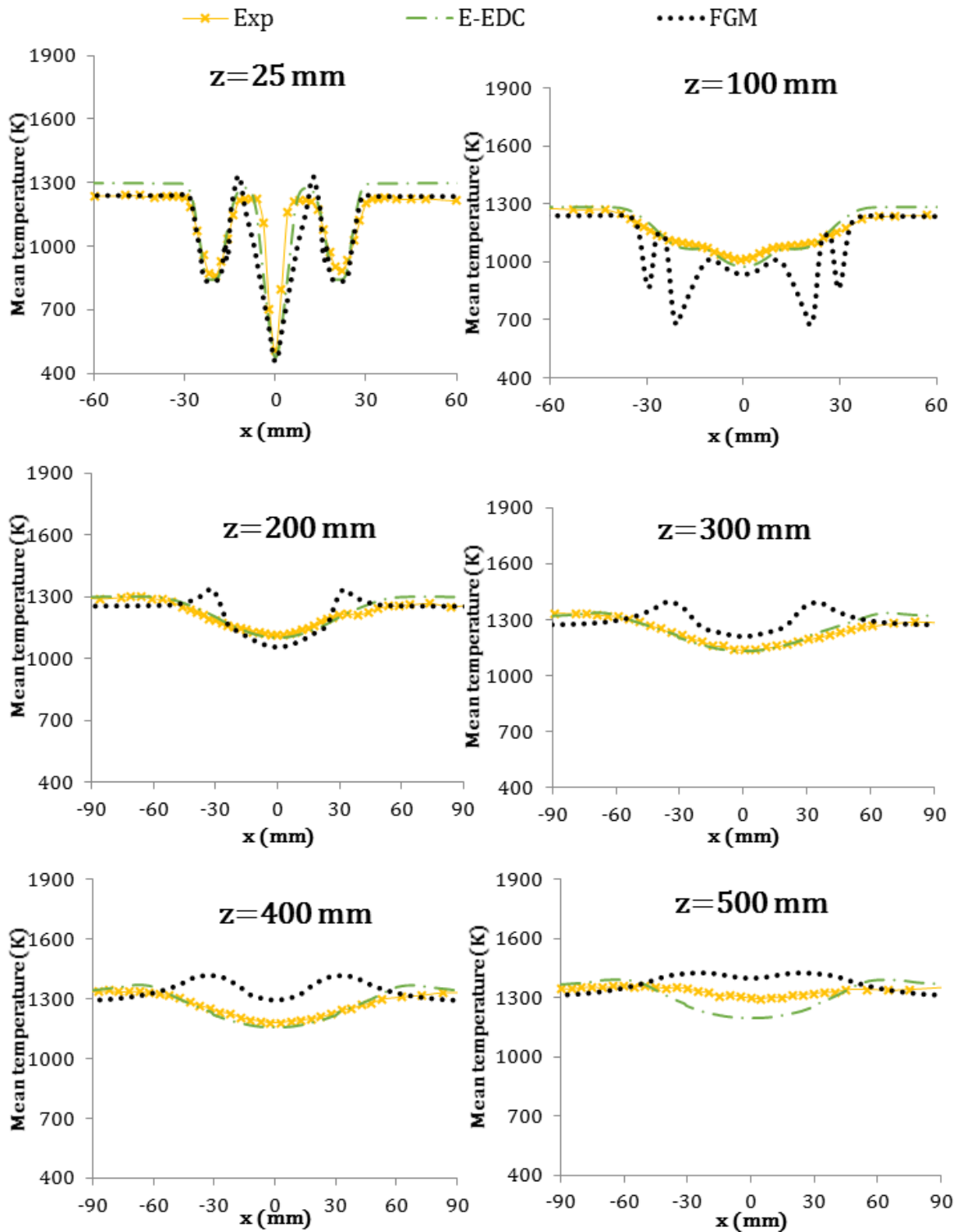
Fig. 5. 4 Comparison between measured and predicted mean temperature profiles for the FGM (adjusted A) and the E-EDC model

3 The Generalized NE-EDC and DA-FGM model

In this section, the turbulence-chemistry interaction models contributed in this Thesis are presented and compared. First, a new model called the New Extended EDC model (NE-EDC) is developed (see chapter 3) and tested with the Delft lab-scale furnace experimental data. Following a similar analysis to that used in the E-EDC model developed by Parente et al. (Parente, Alessandro et al., 2016), in the NE-EDC model, the model coefficients are calculated based on the local Reynolds number and the Kolmogorov scale Damköhler number. The difference between both is that the NE-EDC model postulates that the fine structure length scale (L^*) is equal to the Kolmogorov scale (η_k), following the energy cascade concept; while the E-EDC model is based on the $L^* \neq \eta_k$ idea. In addition, a different description of laminar flame speed is used in each model. The NE-EDC model proposes a laminar flame speed definition based directly on the length and time scales ($L^* = \tau_c^* * S_L$), avoiding a proportionality factor introduced in the E-EDC model ($L^* \propto \tau_c^* * S_L$). Later, the E-EDC model was updated based on the laminar flame speed defined in the NE-EDC model in order to avoid the proportionality factors included in the E-EDC, this updated model is call Generalized E-EDC. Additionally, in the Generalized E- EDC (GE-EDC) model the one-step CH_4 mechanism is not used for chemical time scale calculation, instead, the chemical time scale is calculated considering CH_4, H_2, O_2, CO_2 and CO species. Later, following the approach of Generalized E-EDC model, in this Thesis, the NE-EDC model was updated, called here Generalized NE-EDC, in order to consider also CH_4, H_2, O_2, CO_2 and CO species reaction rates for the chemical time scale. This change is made to consider the interactions among the reactions rates that seems to happen according to the DNS modelling (Minamoto, Y. et al., 2013; Minamoto, Y. & Swaminathan, 2014; Minamoto, Yuki & Swaminathan, 2014). Table 5. 1 shows a summary of extended EDC models development order and characteristics.

Analysis of thermofluids in flameless (MILD)
combustion: assessment, improvement and
development of combustion models by CFD
Naiara Romero Anton

Table 5. 1 Extended EDC models
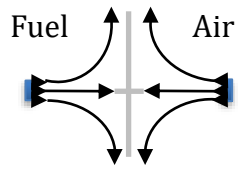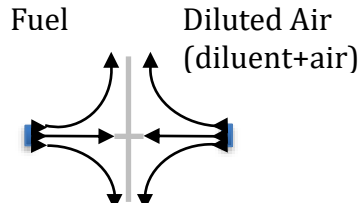
Developed order	Models	Models constants	τ_c
1	EDC	Calibrated model constant C_τ default value $C_\xi=2.9$	1-step global reaction
2	E-EDC Parente et al	$C_\tau = \left(\dfrac{C_{D2}}{3}\right)^{\frac{1}{2}} \propto \dfrac{1}{\sqrt{(Re_T + 1)Da^*}}$ $C_\xi = \left(\dfrac{3C_{D2}}{4C_{D1}^2}\right)^{1/4} \propto \sqrt{(Re_T + 1)Da^*}$	$\tau_c = \dfrac{1}{8.3 \ 10^5 exp\left(-\dfrac{T_A}{T}\right)}$ $T_A = 15,100 \ K$
3	NE-EDC (developed here)	$C_\tau = \left(\dfrac{C_{D2}}{3}\right)^{1/2} = \dfrac{1}{2}\dfrac{1}{\sqrt{(Re_T + 1)Da^*}}$ $C_\xi = \left(\dfrac{3C_{D2}}{4C_{D1}^2}\right)^{1/4} = \sqrt{\dfrac{3}{2}(Re_T + 1)Da^{*3/4}}$	$\tau_c = \dfrac{1}{8.3 \ 10^5 exp\left(-\dfrac{T_A}{T}\right)}$ $T_A = 15,100 \ K$
4	Generalized E-EDC Evans et al	$C_\tau = \left(\dfrac{C_{D2}}{3}\right)^{1/2} = \dfrac{1}{2}\dfrac{1}{\sqrt{(Re_T + 1)Da^*}}$ $C_\xi = \left(\dfrac{3C_{D2}}{4C_{D1}^2}\right)^{1/4} = \left(\dfrac{2}{3}\right)^{1/2}\sqrt{(Re_T + 1)Da^*}$	$\tau_c = \max\left[{Y_k}\Big/\left({|\dot\omega_k|}\big/{\rho}\right)\right]$ $\dot\omega_k$ of CH_4, O_2, CO and CO_2
5	Generalized NE-EDC (developed here)	$C_\tau = \left(\dfrac{C_{D2}}{3}\right)^{1/2} = \dfrac{1}{2}\dfrac{1}{\sqrt{(Re_T + 1)Da^*}}$ $C_\xi = \left(\dfrac{3C_{D2}}{4C_{D1}^2}\right)^{1/4} = \sqrt{\dfrac{3}{2}(Re_T + 1)Da^{*3/4}}$	$\tau_c = \max\left[{Y_k}\Big/\left({|\dot\omega_k|}\big/{\rho}\right)\right]$ $\dot\omega_k$ of CH_4, O_2, CO and CO_2 based on WD-2 constant
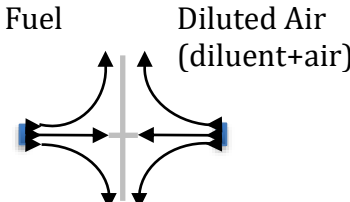
The E-EDC and NE-EDC differ in the postulated length scale of the structures but agree in giving them the turbulent velocity as velocity scale. Chapter 3 describes the differences between the two models in detail and compares their predictions in the application to the Delft lab-scale furnace in flameless combustion mode at 9 kW power (Romero-Anton et al., 2020). The NE-EDC is an accurate and computationally affordable turbulence-chemistry interaction model, which can be suitable for the accurate simulation of flameless combustion without the need for extensive case-by-case model calibration. Modelling results show a slight difference in mean temperature predictions between the Generalized NE-EDC model and the NE-EDC (chapter 3 section 4.3). It does not seem that taking into account CH_4, H_2, O_2, CO and CO_2 species in chemical time scale calculation affects notably the results of the model. This suggests little interaction among reaction

zones for this application. The interaction among the reaction zones provides more effect on mean temperature predictions in JHC burner (Evans et al., 2019) than in enclosed furnace. This could be related to the limited height of the enclosed furnace, while on JHC burner there is not volume limitation.

On the other side, the FGM based models are interesting to apply in flameless combustion due to its reduced computational time compared to the EDC model. Thanks to its efficiency, it is an alternative method to be applied in large-scale furnace configurations, that is, in industrial applications. As it is discussed in chapter 4 the FGM model with pure fuel and pure air as boundary conditions for flamelets generation is not a suitable methodology as dilution effect is not considered. In the literature four models have been found based on flamelets and tabulating chemistry considering the dilution effect; the E-FPV, the D-FPV, the DHR and the DA-FGM model. Among them, the DA-FGM is implement in this Thesis in ANSYS Fluent. The DA-FGM model has been chosen due to its advantages comparing to the others models: its application with constant and no constant reactant dilution, the accurate local dilution level calculation by a transport equation and, at lean conditions, it does not avoid the reactions between fuel and diluted burn gases when flamelets are generated. The DA-FGM model implementation methodology in the ANSYS Fluent commercial CFD package is studied in the Thesis (see chapter 4). Table 5. 2 provides a summary of the FGM model and DA-FGM model differences.

Table 5. 2 FGM and its extensions summary

Model	CFD Package	PDF table	Flamelet generation description
FGM (features selection developed here)	ANSYS Fluent	$\widetilde{\Phi} = \widetilde{\Phi}(\tilde{Z}, \widetilde{Z''^2}, \tilde{C}, \tilde{h})$ $\widetilde{Y_k} = \widetilde{\Phi}(\tilde{Z}, \widetilde{Z''^2}, \tilde{C}, \widetilde{C''^2})$	Fuel — Air
DA-FGM	OpenFOAM	$\widetilde{\Phi} = \widetilde{\Phi}\left(\tilde{\xi}, S_\xi, \tilde{C}, S_C, \tilde{\eta}, \tilde{\gamma}\right)$	Fuel — Diluted Air (diluent+air)

| **DA-FGM**

(developed here) | ANSYS Fluent Release 2019 | $\widetilde{\Phi} = \widetilde{\Phi}\left(\tilde{\xi}, S_{\xi}, \tilde{C}, S_{C}, \tilde{\eta}, \tilde{\gamma}\right)$ | Fuel   Diluted Air (diluent+air) |

First, both models result of the radial profiles of the mean axial velocity ($\widetilde{U}_Z$) at different axial locations are compared with experimental data.
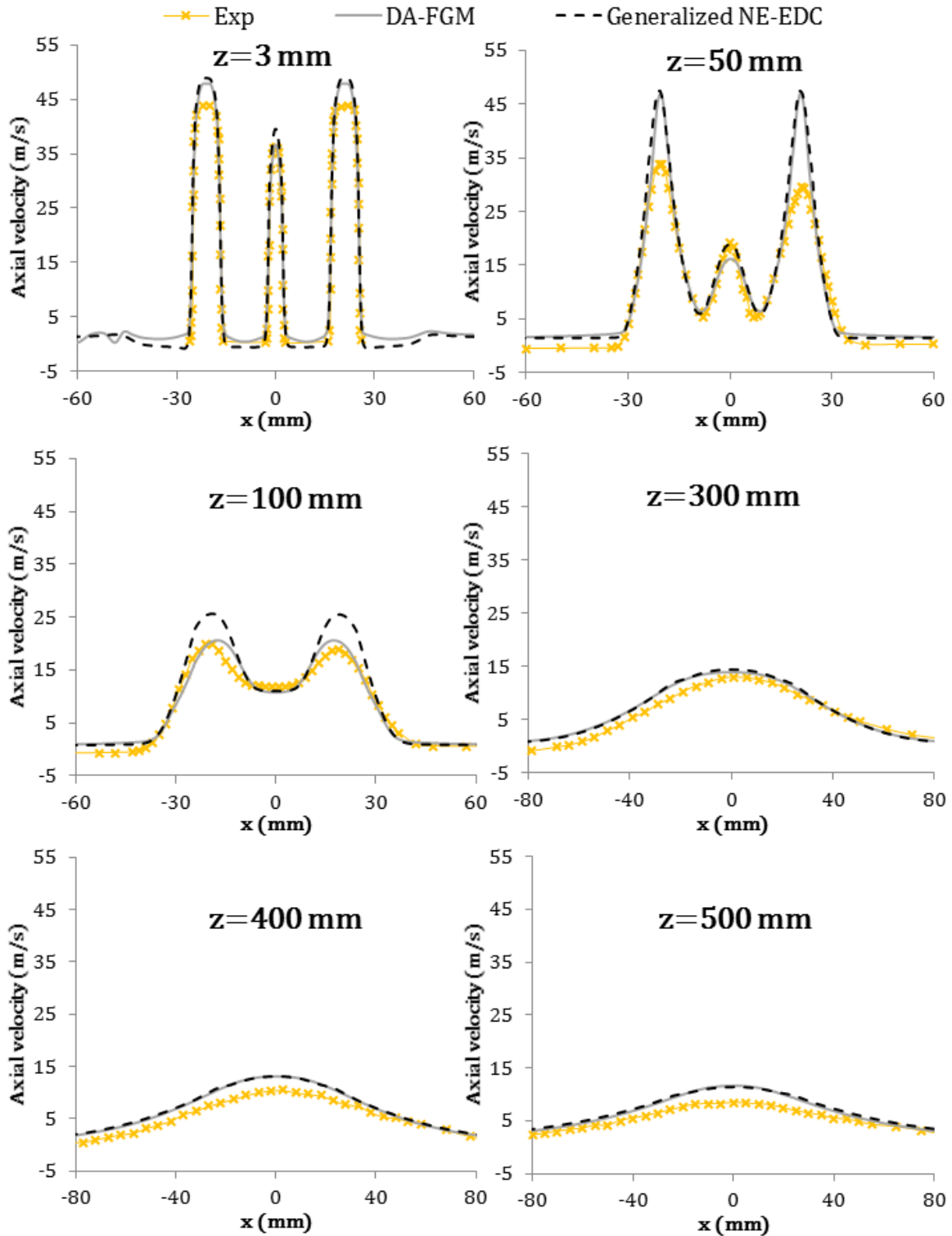
Fig. 5. 5 Comparison between measured and predicted mean velocity profiles for the DA-FGM and the Generalized NE-EDC model

Both models result showed good consistency with experimental data in mean axial velocity ($\widetilde{U}_Z$) prediction. This is directly related with the fact that the same turbulence model has been used during modelling, the realizable two equation $k - \varepsilon$ model. It should be noted that at z=100 mm height the DA-FGM model provides better consistency with experimental data. This is related with the lower mean temperature predicted by the DA-FGM model at this height (Fig. 5. 6). It can be confirmed that this turbulence model is accurate and appropriate for the Delft lab-scale furnace simulations and its interaction with the used turbulence-chemistry interaction models is also appropriate for the case of study.

Next, mean temperature profiles of the both models developed in this Thesis are shown (Fig. 5. 6). At first sight, the Generalized NE-EDC model provides better consistency with experimental data close to the burner and at the medium height of the furnace than the DA-FGM model. At z=25 mm both models show good results but the DA-FGM model shows two peak temperatures at air injection. At z=100 and 200 the DA-FGM model provides good consistency with experimental data, but in the former the mean temperature is underpredicted at air injection radial location and in the later the mean temperature at the centre radial location (x=0) is underpredicted (a 13%). But the Generalized NE-EDC model agree perfectly with experimental data. When the flows develop, at z=300 and 400 height, the DA-FGM model overpredict the mean temperature a maximum of 10% and 8% respectively. At z=500 mm the DA-FGM provides perfect consistency with experimental data while the Generalizer NE-EDC model underpredict the mean temperature at x=0 mm an 8%.

I could be concluded that both models provided consistency with experimental data but the Generalized NE-EDC model gives better results close to the burner and at the middle height of the furnace, while close to the top wall, when the dilution effect is more noticeable, the DA-FGM model provides better results.

From a computational point of view, taking a case from a converge reacting flow-field, the CPU time for a 2 cores CPU@ 2.5 GHz is is %28 lower for the DA-FGM model with 53 species than the Generalized NE-EDC model with 17 species.
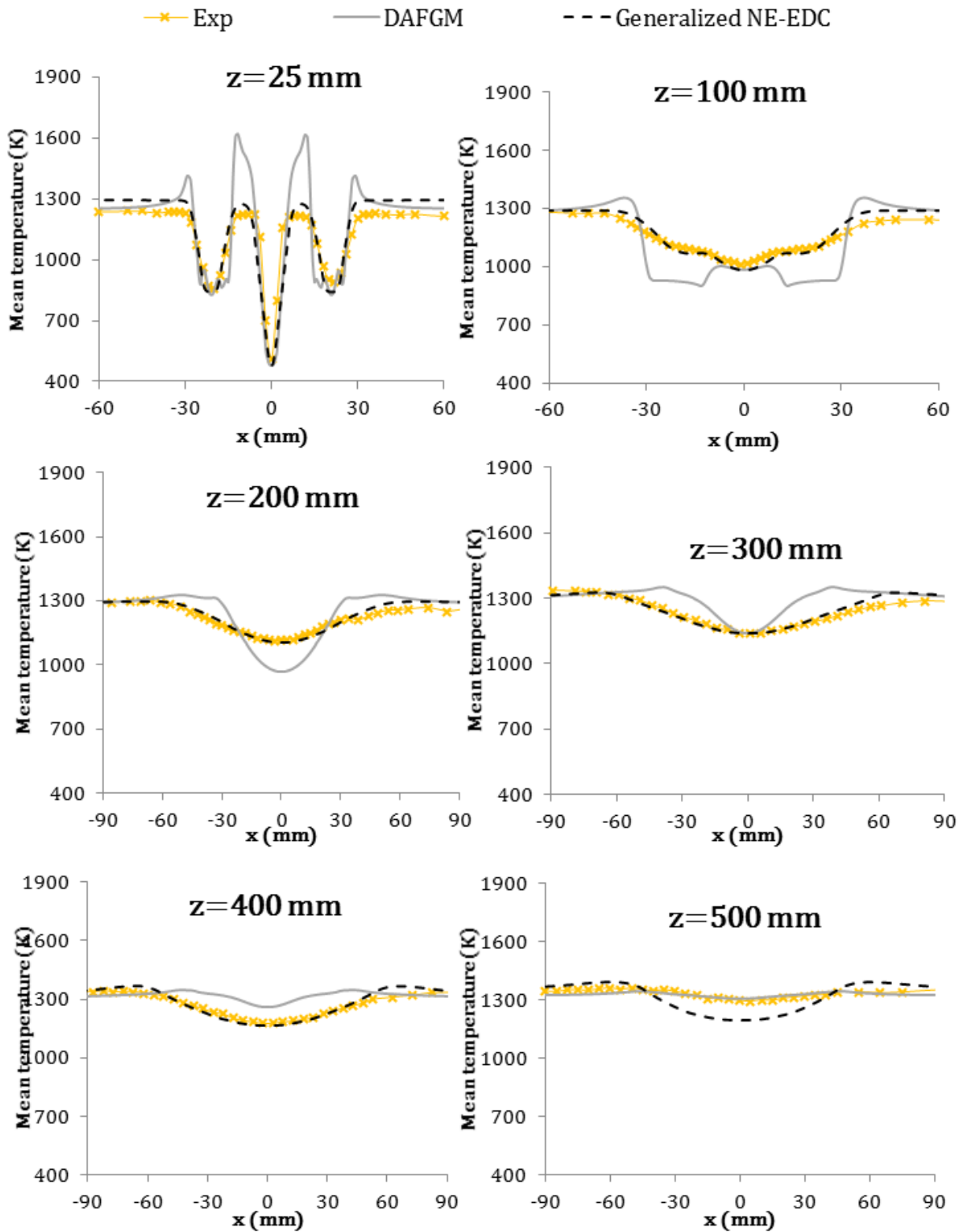
Fig. 5. 6 Comparison between measured and predicted mean temperature profiles for the DA-FGM implemented in ANSYS Fluent and Generalized NE-EDC model

Analysis of thermofluids in flameless (MILD)
combustion: assessment, improvement and
development of combustion models by CFD
Naiara Romero Anton

4 Conclusions

During this work, the NE-EDC model is developed and later, as the DNS modelling results suggest interactions among the reaction zones, the Generalized NE-EDC model is developed in order to include those findings. This model presents several advantages: 1) the model coefficients are calculated based on local Reynolds and Damköhler numbers, so that the calibration of model coefficients is avoided, 2) the laminar flame speed is calculated by no proportionality factor and 3) the chemical time scale is calculated considering CH_4, H_2, O_2, CO and CO_2 species mass fractions, so that the interaction among the reaction zones suggested by DNS modelling are included. After analysing modelling results, it can be concluded that this model provides an acceptable consistency with experimental data for Delft lab-scale furnace modelling.

The DA-FGM implemented in ANSYS Fluent is able to include the dilution effect of flameless combustion by generating the flamelets and PDF tables outside it, something that it is not possible to do with the default options of ANSYS Fluent. Furthermore, ANSYS Fluent simplification in species mass fraction calculation not considering heat loss, even when the modelling of a non-adiabatic case is carried out, has been improved by the used of tables generated outside ANSYS Fluent. Another limitation of ANSYS Fluent is the mixture properties calculation (except species mass fractions) as they are calculated not considering scaled progress variable variance. This limitation is also overcome by generating tables of each mixture properties outside ANSYS Fluent. This model provides improvement comparing with standard FGM model when the dilution effect is noticeable inside the furnace. It shows good consistency with experimental data for Delft lab-scale furnace application.

It could be concluded that both, the Generalized NE-EDC and the DA-FGM models, are a good choice for Delft lab scale furnace modelling. It should be noted that the Generalized NE-EDC model provides better results close to the burner and at the mid height of the furnace while the DA-FGM model shows better consistency close to the top wall of the furnace, where the dilution effect is more noticeable. Finally, the computational time of the DA-FGM model is around %28 lower than the Generalized NE-EDC model.

CHAPTER 6: CONCLUSIONS AND FUTURE RESEARCH

1 Objectives fulfilment

This Thesis aims to contribute to the search for an accurate and computationally affordable turbulence-chemistry interaction model, which can be suitable for the accurate simulation of flameless combustion. In this work, the EDC and the FGM (flamelet based) models have been chosen for flameless combustion modelling taking as reference the cases in the literature with consistency between modelling results and experimental data, at the level of mean properties as targeted in RANS.

The first chapter makes an introduction of current energy target in Europe and fossil fuels paper in that scene. Flameless combustion and its characteristics are defined and the state-of-the-art of flameless combustion regarding experimental test and numerical modelling are shown. During the state-of-the-art analysis the weak points and limitations in the modelling of flameless combustion are detected with respect to the standard EDC and FGM models.

The second chapter presents the lab-scale furnace where ANSYS Fluent modelling are carried out, describing its characteristics, measured techniques and available experimental data to validate later modelling results. Additionally, the turbulent non-premix combustion mathematical modelling, computational domain&grid and modelling boundary conditions are shown.

Analysis of thermofluids in flameless (MILD)
combustion: assessment, improvement and
development of combustion models by CFD
Naiara Romero Anton

In the third chapter main and second objectives of the Thesis have been fulfilled. The applicability of the EDC model in flameless combustion has been studied and in order to overcome existing EDC model extensions limitations, a novel extended version of the EDC model is developed, the Generalized NE-EDC model. This model calculates model coefficients considering flameless combustion dilution effect and chemical time scale is calculated considering interaction among the reaction zones. After comparing modelling mean axial velocity and temperature results with experimental data it is concluded that the Generalized NE-EDC model slightly improves already existing EDC model extension and for this application it is concluded that chemical time scale calculation improvement has not too much impact in mean temperature prediction along different heights of the furnace.

Along the Chapter 4, other main and second objectives of the Thesis are fulfilled. The FGM and DA-FGM flamelet base models implementation methodology in ANSYS Fluent is explained in detail highlighting the limitations of ANSYS Fluent with the implementation of the DAFGM model. The limitations of ANSYS Fluent for DA-FGM model implementation are overcome, so that a flamelet based model considering the dilution effect of flameless combustion has being implemented in ANSYS Fluent. Modelling mean axial velocity and temperature results are compared with Delft lab-scale furnace experimental data and it is concluded that when the dilution effect is dominant, the DA-FGM model improves mean temperature predictions.

Finally, chapter 5 address the improvements and the advantages of the models developed in this Thesis. Both, the Generalized NE-EDC and the DA-FGM model implemented in ANSYS Fluent are suitable turbulence-chemistry interaction models for accurate flameless combustion modelling. It is concluded that the Generalized NE-EDC model provides better results close to the burner and at the mid height of the furnace while the DA-FGM model shows better consistency close to the top wall of the furnace, where the dilution effect is more noticeable. Finally, mention that the computational time of the DA-FGM model is around %28 lower than the Generalized NE-EDC model, using in the DA-FGM model 53 species chemical mechanisim while in the Generalized NE-EDC model it is used a 17 species chemical mechanisim.

2 Contributions

This Thesis contributions are the extension of the EDC model, that is, the EDC model with modified model constant for the Delft lab-scale furnace, the NE-EDC model and the Generalized NE-EDC model, and the implementation of the DA-FGM model in ANSYS Fluent. The Generalized NE-EDC model calculates model coefficients based on local Reynolds and Damköhler numbers, so that the calibration of model coefficients is avoided, the laminar flame speed is calculated by no proportionality factor and chemical time scale is calculated considering CH_4, H_2, O_2, CO and CO_2 species mass fractions (interaction among the reaction zones is considered). The implemented DA-FGM model calculates flamelets and PDF tables considering the dilution of flameless combustion. Those tables are generated outside ANSYS Fluent and later, by UDF they are implemented in Fluent. Due to that species mass fractions are calculated considering both dilution and heat loss, while ANSYS Fluent default option does not consider them. Additionally, as mixture properties are also calculates outside Fluent, they consider scaled progress variable variance, while ANSYS Fluent´s FGM default model does not consider it.

The author contributes to the scientific community publishing the following works:

- Articles

    1) N. Romero-Anton, K. Martin-Escudero, L.A. Portillo-Valdés, I. Gómez-Elvira, E. Salazar-Herran **Improvement of auxiliary BI-DRUM boiler operation by dynamic simulation.** *Energy,* 2018; 148, 676 - 686

    2) N. Romero-Anton, X. Huang, H. Bao, K. Martin-Escudero, E. Salazar-Herran, D.J.E.M. Roekaerts **New extended eddy dissipation concept model for flameless combustion in furnaces.** *Combustion and Flame*, 2020;220, 49-62.

    3) N. Romero, K. Martin, L. del Portillo. **Europar Batasuneko Energia-testuingurua. Eraginkortasun Energetikoa Industrian** *Ekaia*, 2019;36,191 - 207-0214-9001

    4) N. Romero, K. Martin, L. del Portillo. **Flameless errekuntzak klima aldaketaren aurka**. *Ekaia, 2020.* https://doi.org/10.1387/ekaia.21753

- Under review

1) N. Romero-Anton, K. Martin-Escudero, M. Ren, Z. Azkorra-Larrinaga. **Consideration of the Interactions Among Reaction Zones in the New Extended Eddy Dissipation Concept model.** *Energy.*

On going

2) N. Romero, X. Huang, K. Martin, D.J.E.M. Roekaerts. **Diluted-Air-FGM Turbulent-Combustion Model for flameless combustion.** *xxxxx*

- International Conferences

    1) M. Ren, N. Romero, S. Wang, D. Roekaerts **Numerical study of a turbulent methanol hydrothermal flame using EDC and FGM models**. *International Workshop on "Clean Combustion Principles and Application"*, Darmstadt, 2019

    2) M. Ren, N. Romero, S. Wang, D. Roekaerts **Application of EDC and FGM models to hydrothermal flames** *Combura Symposium*, Soesterberg, 2019

    3) N. Romero, H. Bao, X. Huang, K. Martin, D.J.E.M. Roekaerts **Simulation of Flameless Combustion in Delft Lab-Scale Furnace using EDC Model** *9th European Combustion Meeting*, Lisboa, 2019

    4) N. Romero, K. Martin, E. Salazar, L. A. del Portillo, D.J.E.M. Roekaerts **Flameless combustion numerical simulation in Labscale furnace by Eddy Dissipation Concept Model with modified constants** *XI National and II International Engineering Thermodynamics Congress,* Albacete, 2019

    5) N. Romero, K. Martin, E. Salazar, L.A. del Portillo and D.J.E.M. Roekaerts **On the implementation of Diluted-Air-FGM Turbulent combustion model in Ansys-Fluent** *11th Mediterranean Combustion Symposium,* , Tenerife, 2019

    6) N Romero, K. Martin, L.A. del Portillo, **Standby mode and fast hot start-up in auxiliary bi-drum boiler**, *10 CNIT,* Lleida, 2017.

3   Future research lines

One of the future researching lines is the calculation of the absorption coefficient through a more accurate model. During the modelling in this Thesis the WSGMM model is used, it is a simple model which considers the whole gases spectrum as a grey gas, so that this model could be improved. In ANSYS Fluent there is not available other options for absorption coefficient modelling, thus it should be implemented by UDF.

The next step should be to analyse the capability of the DA-FGM and the Generalized NE-EDC models in LES modelling. The computational time required in LES is greater than in RANS, so that it can be expected that the computational time saved by the DA-FGM should be more notable than in RANS modelling.

The last step should be the application of these models in industrial scales furnace, for example, in bi-drum boilers furnace where flameless burners has been started to be used due to its NO_x emissions reductions.

REFERENCES

References

[1]Horizon 2020-the framework programme for research and innovation (2014-2020), (2013). Retrieved from
https://ec.europa.eu/research/participants/data/ref/h2020/legal_basis/rules_particip
ation/h2020-rules-participation_en.pdf

[2]Industrial emissions (integrated pollution prevention and control), (2010). Retrieved from https://eur-lex.europa.eu/LexUriServ/LexUriServ.do?uri=OJ:L:2010:334:0017:0119:en:PDF

[3]The regulation on the governance of the energy union and climate action, (2018). Retrieved from https://eur-lex.europa.eu/legal-content/EN/TXT/?uri=uriserv:OJ.L_.2018.328.01.0001.01.ENG&toc=OJ:L:2018:328:TOC

[4]Abtahizadeh, E., de Goey, P., & van Oijen, J. (2017). LES of delft jet-in-hot coflow burner to investigate the effect of preferential diffusion on autoignition of CH4/H2 flames. *Fuel, 191*, 36-45. doi://doi.org/10.1016/j.fuel.2016.11.054

[5]Abtahizadeh, E., van Oijen, J., & de Goey, P. (2012). Numerical study of mild combustion with entrainment of burned gas into oxidizer and/or fuel streams. *Combustion and Flame, 159*(6), 2155-2165.

[6]Agarwal, A. K. (2007). Biofuels (alcohols and biodiesel) applications as fuels for internal combustion engines. *Progress in Energy and Combustion Science, 33*(3), 233-271. doi://doi.org/10.1016/j.pecs.2006.08.003

[7]Agreement, P. (2015). (2015). Paris agreement. Paper presented at the *United Nations. Http://Unfccc. Int/Files/Essential_background/Convention/Application/Pdf/English_paris_agr Eement. Pdf,*

[8]Aminian, J., Galletti, C., Shahhosseini, S., & Tognotti, L. (2012). Numerical investigation of a MILD combustion burner: Analysis of mixing field, chemical kinetics and turbulence-chemistry interaction. *Flow, Turbulence and Combustion, 88*(4), 597-623. doi:10.1007/s10494-012-9386-z

[9]Aminian, J., Galletti, C., & Tognotti, L. (2016). Extended EDC local extinction model accounting finite-rate chemistry for MILD combustion. *Fuel, 165*, 123-133. doi://doi.org/10.1016/j.fuel.2015.10.041

Analysis of thermofluids in flameless (MILD)
combustion: assessment, improvement and
development of combustion models by CFD
Naiara Romero Anton

[10]Andersen, J., Rasmussen, C. L., Giselsson, T., & Glarborg, P. (2009). Global combustion mechanisms for use in CFD modeling under oxy-fuel conditions. *Energy & Fuels, 23*(3), 1379-1389.

[11]Arrhenius, S. (1896). On the influence of carbonic acid in the air upon the temperature of the ground. *Philosophical Magazine and Journal of Science, 41*, 237–275. Retrieved from https://www.rsc.org/images/Arrhenius1896_tcm18-173546.pdf

[12]B. B. Dally, A.N Karpetis, & R.S. Barlow. (2002). Structured of turbulent non-premixed jet flames in a diluted hot flow.*27*, 2255-2265.

[13]Barbir, F. (2005). PEM electrolysis for production of hydrogen from renewable energy sources. *Solar Energy, 78*(5), 661-669. doi://doi.org/10.1016/j.solener.2004.09.003

[14]Baroutaji, A., Wilberforce, T., Ramadan, M., & Olabi, A. G. (2019). Comprehensive investigation on hydrogen and fuel cell technology in the aviation and aerospace sectors. *Renewable and Sustainable Energy Reviews, 106*, 31-40. doi://doi.org/10.1016/j.rser.2019.02.022

[15]Beér, J. M. (1994). Minimizing NOx emissions from stationary combustion; reaction engineering methodology. *Chemical Engineering Science, 49*(24, Part A), 4067-4083. doi://doi.org/10.1016/S0009-2509(05)80006-5

[16]Bilger, R. W., Stårner, S. H., & Kee, R. J. (1990). On reduced mechanisms for methane-air combustion in nonpremixed flames. *Combustion and Flame, 80*(2), 135-149. doi:https://doi.org/10.1016/0010-2180(90)90122-8

[17]Bongers, H., Van Oijen, J. A., & De Goey, L. P. H. (2002). Intrinsic low-dimensional manifold method extended with diffusion. *Proceedings of the Combustion Institute, 29*(1), 1371-1378. doi://doi.org/10.1016/S1540-7489(02)80168-7

[18]Buhre, B. J. P., Elliott, L. K., Sheng, C. D., Gupta, R. P., & Wall, T. F. (2005). Oxy-fuel combustion technology for coal-fired power generation. *Progress in Energy and Combustion Science, 31*(4), 283-307. doi://doi.org/10.1016/j.pecs.2005.07.001

[19]Bykov, V., & Maas, U. (2007). The extension of the ILDM concept to reaction–diffusion manifolds. *Combustion Theory and Modelling, 11*(6), 839-862. doi:10.1080/13647830701242531

[20]Cabra, R., Myhrvold, T., Chen, J. Y., Dibble, R. W., Karpetis, A. N., & Barlow, R. S. (2002). Simultaneous laser raman-rayleigh-lif measurements and numerical modeling results of a lifted turbulent H2/N2 jet flame in a vitiated coflow. *Proceedings of the Combustion Institute, 29*(2), 1881-1888. doi://doi.org/10.1016/S1540-7489(02)80228-0

ENEDI Research Group
Energy Engineering Department
University of the Basque Country

FACULTY
OF ENGINEERING
BILBAO
UNIVERSITY
OF THE BASQUE
COUNTRY

Universidad
del País Vasco
Euskal Herriko
Unibertsitatea

[21]Cavaliere, & de Joannon. (2004). Mild combustion. *Progress in Energy and Combustion Science, 30*(4)

[22]Cavigiolo, A., Galbiati, M. A., Effuggi, A., Gelosa, D., & Rota, R. (2003). Mild combustion in a laboratory-scale apparatus. *Combustion Science and Technology, 175*(8), 1347-1367. doi:10.1080/00102200302356

[23]Celik, I., Ghia, U., Roache, P. J., Freitas, C., Coloman, H., & Raad, P. (2008). *Procedure of estimation and reporting of uncertainty due to discretization in CFD applications* doi:10.1115/1.2960953

[24]CHEM1D.A one-dimensional laminar flame code [computer software]. Eindhoven Universityn of Technology:

[25]Cherubini, F., Bird, N. D., Cowie, A., Jungmeier, G., Schlamadinger, B., & Woess-Gallasch, S. (2009). Energy- and greenhouse gas-based LCA of biofuel and bioenergy systems: Key issues, ranges and recommendations. *Resources, Conservation and Recycling, 53*(8), 434-447. doi://doi.org/10.1016/j.resconrec.2009.03.013

[26]Cho, E. -., Danon, B., de Jong, W., & Roekaerts, D. J. E. M. (2011). Behavior of a 300kWth regenerative multi-burner flameless oxidation furnace. *Applied Energy, 88*(12), 4952-4959. doi://doi.org/10.1016/j.apenergy.2011.06.039

[27]Christo, F. C., & Dally, B. B. (2005). Modeling turbulent reacting jets issuing into a hot and diluted coflow. *Combustion and Flame, 142*(1), 117-129. doi://doi.org/10.1016/j.combustflame.2005.03.002

[28]Christo, F. C., & Dally, B. (2004). *Application of transport PDF approach for modelling MILD combustion*

[29]Coelho, P. J. (2007). Numerical simulation of the interaction between turbulence and radiation in reactive flows. *Progress in Energy and Combustion Science, 33*(4), 311-383. doi:https://doi.org/10.1016/j.pecs.2006.11.002

[30]A policy framework for climate and energy in the period from 2020 to 2030, (2014). Retrieved from https://eur-lex.europa.eu/legal-content/EN/ALL/?uri=CELEX%3A52014DC0015

[31]Cormos, C. (2012). Integrated assessment of IGCC power generation technology with carbon capture and storage (CCS). *Energy, 42*(1), 434-445. doi://doi.org/10.1016/j.energy.2012.03.025

[32]Dally, B. B., Riesmeier, E., & Peters, N. (2004). Effect of fuel mixture on moderate and intense low oxygen dilution combustion. *Combustion and Flame, 137*(4), 418-431. doi:https://doi.org/10.1016/j.combustflame.2004.02.011

Analysis of thermofluids in flameless (MILD)
combustion: assessment, improvement and
development of combustion models by CFD
Naiara Romero Anton

[33] Danon, B., Cho, E. -., de Jong, W., & Roekaerts, D. J. E. M. (2011a). Numerical investigation of burner positioning effects in a multi-burner flameless combustion furnace. *Applied Thermal Engineering, 31*(17), 3885-3896. doi://doi.org/10.1016/j.applthermaleng.2011.07.036

[34] Danon, B., Cho, E. -., de Jong, W., & Roekaerts, D. J. E. M. (2011b). Parametric optimization study of a multi-burner flameless combustion furnace. *Applied Thermal Engineering, 31*(14), 3000-3008. doi://doi.org/10.1016/j.applthermaleng.2011.05.033

[35] De, A., Oldenhof, E., Sathiah, P., & Roekaerts, D. (2011). Numerical simulation of delft-jet-in-hot-coflow (DJHC) flames using the eddy dissipation concept model for Turbulence–Chemistry interaction. *Flow, Turbulence and Combustion, 87*(4), 537-567. doi:10.1007/s10494-011-9337-0

[36] Descamps, C., Bouallou, C., & Kanniche, M. (2008). Efficiency of an integrated gasification combined cycle (IGCC) power plant including CO2 removal. *Energy, 33*(6), 874-881. doi://doi.org/10.1016/j.energy.2007.07.013

[37] Driscoll, J. F., Chen, J. H., Skiba, A. W., Carter, C. D., Hawkes, E. R., & Wang, H. (2020). Premixed flames subjected to extreme turbulence: Some questions and recent answers. *Progress in Energy and Combustion Science, 76*, 100802.

[38] Duwig, C., Li, B., Li, Z. S., & Aldén, M. (2012). High resolution imaging of flameless and distributed turbulent combustion. *Combustion and Flame, 159*(1), 306-316. doi://doi.org/10.1016/j.combustflame.2011.06.018

[39] Eckbreth, A. C. (1978). BOXCARS: Crossed-beam phase-matched CARS generation in gases. *Applied Physics Letters, 32* doi:10.1063/1.90070

[40] Eckbreth, A. C. (1998). *Laser diagnostic for combustion temperature and species*. Amsterdam, The Netherlands: Gordon and Breach Publishers.

[41] EIA. (2016). International energy outlook 2016. Retrieved from https://www.eia.gov/outlooks/ieo/pdf/0484(2016).pdf

[42] EIA. (2018). International energy outlook 2018. Retrieved from https://www.eia.gov/outlooks/aeo/

[43] Ertesvag, I. S., & Magnussen, B. F. (2000). The eddy dissipation turbulence energy cascade model. *Combustion Science and Technology, 159*, 213-235.

[44] Ertesvåg, I. S. (2019). Analysis of some recently proposed modifications to the eddy dissipation concept (EDC). *Combustion Science and Technology, *, 1-29. doi:10.1080/00102202.2019.1611565

[45]Evans, M. J., Medwell, P. R., & Tian, Z. F. (2015). Modeling lifted jet flames in a heated coflow using an optimized eddy dissipation concept model. *Combustion Science and Technology, 187*(7), 1093-1109. doi:10.1080/00102202.2014.1002836

[46]Evans, M. J., Petre, C., Medwell, P. R., & Parente, A. (2019). Generalisation of the eddy-dissipation concept for jet flames with low turbulence and low damköhler number. *Proceedings of the Combustion Institute, 37*(4), 4497-4505. doi:https://doi.org/10.1016/j.proci.2018.06.017

[47]Favre, A. (1969). Statistical equations of turbulent gases. *Problems of Hydrodynamics and Continuum Mechanics,* , 231-266.

[48]Favre, E. (2007). Carbon dioxide recovery from post-combustion processes: Can gas permeation membranes compete with absorption? *Journal of Membrane Science, 294*(1), 50-59. doi://doi.org/10.1016/j.memsci.2007.02.007

[49]Ferrarotti, M., Li, Z., & Parente, A. (2019). On the role of mixing models in the simulation of MILD combustion using finite-rate chemistry combustion models. *Proceedings of the Combustion Institute, 37*(4), 4531-4538. doi://doi.org/10.1016/j.proci.2018.07.043

[50]Flamme, M. (2001). Low NOx combustion technologies for high temperature applications. *Energy Conversion and Management, 42*(15), 1919-1935. doi://doi.org/10.1016/S0196-8904(01)00051-6

[51]Fluent Manual. (2017). *Ansys fluent theory guide 18.2*. Canonsburg PA: ANSYS lnc.

[52]Fox, R. O. (2003). *Computational models for turbulent reacting flows* Cambridge university press.

[53]Franco, A., & Diaz, A. R. (2009). The future challenges for "clean coal technologies": Joining efficiency increase and pollutant emission control. *Energy, 34*(3), 348-354. doi://doi.org/10.1016/j.energy.2008.09.012

[54]Galletti, C., Parente, A., & Tognotti, L. (2007). Numerical and experimental investigation of a mild combustion burner. *Combustion and Flame, 151*(4), 649-664. doi://doi.org/10.1016/j.combustflame.2007.07.016

[55]Gicquel, O., Darabiha, N., & Thévenin, D. (2000). Laminar premixed hydrogen/air counterflow flame simulations using flame prolongation of ILDM with differential diffusion. *Proceedings of the Combustion Institute, 28*(2), 1901-1908. doi://doi.org/10.1016/S0082-0784(00)80594-9

[56]Göktolga, M. U., van Oijen, J. A., & de Goey, L. Philip H. (2017). Modeling MILD combustion using a novel multistage FGM method. *Proceedings of the Combustion Institute, 36*(3), 4269-4277. doi://doi.org/10.1016/j.proci.2016.06.004

Analysis of thermofluids in flameless (MILD)
combustion: assessment, improvement and
development of combustion models by CFD
Naiara Romero Anton

[57]Graça, M., Duarte, A., Coelho, P. J., & Costa, M. (2013). Numerical simulation of a reversed flow small-scale combustor. *Fuel Processing Technology, 107*, 126-137. doi://doi.org/10.1016/j.fuproc.2012.06.028

[58]Gran, I. R. (1994). *Mathematical modeling and numerical simulation of chemical kinetics in turbulent combustion* Norwegian Institute of Technology, Trondheim

[59]Gran, I. R., & Magnussen, B. F. (1996). A numerical study of a bluff-body stabilized diffusion flame. part 2. influence of combustion modeling and finite-rate chemistry. *Combustion Science and Technology, 119*(1-6), 191-217. doi:10.1080/00102209608951999

[60]Hekkens, R., & Mancini, M. (2004). Non-isothermal CFD model of HEC burner and furnace. *Tech. Rep. G108/2. IRFR Research Station,*

[61]Hiroshi Tsuji, Ashwani K. Gupta, Toshiaki Hasegawa, Masashi Katsuki, Ken Kishimoto, & Mitsunobu Morita. (2002). *High temperature air combustion: From energy conservation to pollution reduction*. New York: CRC Press.

[62]Huang, X., Tummers, M. J., & Roekaerts, D. J. E. M. (2017). Experimental and numerical study of MILD combustion in a lab-scale furnace. *Energy Procedia, 120*, 395-402. doi://doi.org/10.1016/j.egypro.2017.07.231

[63]Huang, X. (2018). *Measurements and model development for flameless combustion in a lab-scale furnace* Delft University of Technology

[64]Ihme, M., & See, Y. C. (2010). Prediction of autoignition in a lifted methane/air flame using an unsteady flamelet/progress variable model. *Combustion and Flame, 157*(10), 1850-1862. doi:https://doi.org/10.1016/j.combustflame.2010.07.015

[65]Ihme, M., & See, Y. C. (2011). LES flamelet modeling of a three-stream MILD combustor: Analysis of flame sensitivity to scalar inflow conditions. *Proceedings of the Combustion Institute, 33*(1), 1309-1317. doi://doi.org/10.1016/j.proci.2010.05.019

[66]Ishii, T., Zhang, C., & Hino, Y. (2002). Numerical study of the performance of a regenerative furnace. *Heat Transfer Engineering, 23*(4), 23-33. doi:10.1080/01457630290090473

[67]Jerzy Chomiak. (1987). *Combustion: A study in theory, fact and application*

[68]Jones, W. P., & Lindstedt, R. P. (1988). Global reaction schemes for hydrocarbon combustion. *Combustion and Flame, 73*(3), 233-249.

[69] Khalil, A. E. E., & Gupta, A. K. (2014). (2014). Mixture preparation effects on distributed combustion for gas turbine application. Paper presented at the *Novel Combustion Concepts for Sustainable Energy Development,* 277-296.

[70] Kim, J. P., Schnell, U., & Scheffknecht, G. (2008). Comparison of different global reaction mechanisms for MILD combustion of natural gas. *Combustion Science and Technology, 180*(4), 565-592.

[71] Kumar, S., Paul, P. J., & Mukunda, H. S. (2002). Studies on a new high-intensity low-emission burner. *Proceedings of the Combustion Institute, 29*(1), 1131-1137. doi://doi.org/10.1016/S1540-7489(02)80143-2

[72] Kuo, K. K. (2005). *Principles of combustion*. New Jersey: John Wiley & Sons, Inc., Hoboken.

[73] Kuo, K. K., & Acharya, R. (2012). *Fundamentals of turbulent and multiphase combustion* John Wiley & Sons.

[74] Kyoto 2nd commitment period (2013–20). Retrieved from https://ec.europa.eu/clima/policies/strategies/progress/kyoto_2_en

[75] Lai, J. Y. W., Lin, K. C., & Violi, A. (2011). Biodiesel combustion: Advances in chemical kinetic modeling. *Progress in Energy and Combustion Science, 37*(1), 1-14. doi://doi.org/10.1016/j.pecs.2010.03.001

[76] Lam, S. H., & Goussis, D. A. (1989). (1989). Understanding complex chemical kinetics with computational singular perturbation. Paper presented at the *Symposium (International) on Combustion, , 22*(1) 931-941.

[77] Lamouroux, J., Ihme, M., Fiorina, B., & Gicquel, O. (2014). Tabulated chemistry approach for diluted combustion regimes with internal recirculation and heat losses. *Combustion and Flame, 161*(8), 2120-2136. doi://doi.org/10.1016/j.combustflame.2014.01.015

[78] Lewandowski, M. T., & Ertesvåg, I. S. (2018). Analysis of the eddy dissipation concept formulation for MILD combustion modelling. *Fuel, 224*, 687-700. doi://doi.org/10.1016/j.fuel.2018.03.110

[79] Li, Z., Cuoci, A., Sadiki, A., & Parente, A. (2017). Comprehensive numerical study of the adelaide jet in hot-coflow burner by means of RANS and detailed chemistry. *Energy, 139*, 555-570. doi://doi.org/10.1016/j.energy.2017.07.132

[80] Li, Z., Ferrarotti, M., Cuoci, A., & Parente, A. (2018). Finite-rate chemistry modelling of non-conventional combustion regimes using a partially-stirred reactor closure: Combustion model formulation and implementation details. *Applied Energy, 225*, 637-655. doi://doi.org/10.1016/j.apenergy.2018.04.085

Analysis of thermofluids in flameless (MILD)
combustion: assessment, improvement and
development of combustion models by CFD
Naiara Romero Anton

[81]Locci, C., Colin, O., & Michel, J. (2014). Large eddy simulations of a small-scale flameless combustor by means of diluted homogeneous reactors. *Flow, Turbulence and Combustion, 93*(2), 305-347. doi:10.1007/s10494-014-9548-2

[82]Locci, C., Colin, O., Poitou, D., & Mauss, F. (2015). A tabulated, flamelet based no model for large eddy simulations of non premixed turbulent jets with enthalpy loss. *Flow, Turbulence and Combustion, 94*(4), 691-729. doi:10.1007/s10494-014-9591-z

[83]Lopez-Ruiz, G., Fernandez-Akarregi, A. R., Diaz, L., Urresti, I., Alava, I., & Blanco, J. M. (2019). Numerical study of a laminar hydrogen diffusion flame based on the non-premixed finite-rate chemistry model; thermal NOx assessment. *International Journal of Hydrogen Energy, 44*(36), 20426-20439.

[84]Lupant, D., Pesenti, B., Evrard, P., & Lybaert, P. (2007). Numerical and experimental characterization of a self-regenerative flameless oxidation burner operation in a pilot-scale furnace. *Combustion Science and Technology, 179*(1-2), 437-453. doi:10.1080/00102200600837275

[85]Lupant, D., & Lybaert, P. (2015). Assessment of the EDC combustion model in MILD conditions with in-furnace experimental data. *Applied Thermal Engineering, 75*, 93-102. doi://doi.org/10.1016/j.applthermaleng.2014.10.027

[86]Lupant, D., Pesenti, B., & Lybaert, P. (2006). *Assessment of combustion models of a self-regenerative flameless oxidation burner*

[87]Maas, U., & Pope, S. B. (1992). Simplifying chemical kinetics: Intrinsic low-dimensional manifolds in composition space. *Combustion and Flame, 88*(3-4), 239-264.

[88]Magnussen, B. F.Modeling of NOx and soot formation by the eddy dissipation concept. Paper presented at the

[89]Magnussen, B. F.The eddy dissipation concept a bridge between science and technology. Paper presented at the *ECCOMAS Thematic Conference on Computational Combustion, Lisbon, Portugal,*

[90]Magnussen, B. F., & Hjertager, B.On the structure of turbulence and a generalized eddy dissipation concept for chemical reaction in turbulent flow. Paper presented at the *19th AIAA Aerospace Meeting St. Louis,*

[91]Magnussen, B. F., & Hjertager, B. H. (1977). On mathematical modeling of turbulent combustion with special emphasis on soot formation and combustion. *Symposium (International) on Combustion, 16*(1), 719-729. doi://doi.org/10.1016/S0082-0784(77)80366-4

[92]Mardani, A. (2017). Optimization of the eddy dissipation concept (EDC) model for turbulence-chemistry interactions under hot diluted combustion of CH4/H2. *Fuel, 191*, 114-129. doi://doi.org/10.1016/j.fuel.2016.11.056

[93]Marinov, N. M., Westbrook, C. K., & Pitz, W. J. (1995). No title. *Detailed and Global Chemical Kinetics Model for Hydrogen,*

[94]Medwell, P. R., Kalt, P. A. M., & Dally, B. B. (2007). Simultaneous imaging of OH, formaldehyde, and temperature of turbulent nonpremixed jet flames in a heated and diluted coflow. *Combustion and Flame, 148*(1), 48-61. doi://doi.org/10.1016/j.combustflame.2006.10.002

[95]Minamoto, Y., Swaminathan, N., Cant, R. S., & Leung, T. (2014). Reaction zones and their structure in MILD combustion. *Combustion Science and Technology, 186*(8), 1075-1096. doi:10.1080/00102202.2014.902814

[96]Minamoto, Y., Dunstan, T. D., Swaminathan, N., & Cant, R. S. (2013). DNS of EGR-type turbulent flame in MILD condition. *Proceedings of the Combustion Institute, 34*(2), 3231-3238.

[97]Minamoto, Y., & Swaminathan, N. (2014). Modelling paradigms for MILD combustion. *International Journal of Advances in Engineering Sciences and Applied Mathematics, 6*(1-2), 65-75.

[98]Minamoto, Y., & Swaminathan, N. (2014). Scalar gradient behaviour in MILD combustion. *Combustion and Flame, 161*(4), 1063-1075.

[99]Minamoto, Y., Swaminathan, N., Cant, S. R., & Leung, T. (2014). Morphological and statistical features of reaction zones in MILD and premixed combustion. *Combustion and Flame, 161*(11), 2801-2814.

[100]Moureau, V., Domingo, P., & Vervisch, L. (2011). From large-eddy simulation to direct numerical simulation of a lean premixed swirl flame: Filtered laminar flame-pdf modeling. *Combustion and Flame, 158*(7), 1340-1357.

[101]Moureau, V., Domingo, P., & Vervisch, L. (2011). Design of a massively parallel CFD code for complex geometries. *Comptes Rendus Mécanique, 339*(2-3), 141-148.

[102]N. A. Chigier. (1981). *Energy, combustion and environment*. US: McGraw-Hill Inc.

[103]NREL.Renewable electrolysis. Retrieved from https://www.nrel.gov/hydrogen/renewable-electrolysis.html

[104]Oijen, J. A. v. (2002). *Flamelet-generated manifolds : Development and application to premixed laminar flames* Eindhoven: Technische Universiteit Eindhoven

Analysis of thermofluids in flameless (MILD)
combustion: assessment, improvement and
development of combustion models by CFD
Naiara Romero Anton

[105]Oldenhof, E., Tummers, M. J., van Veen, E. H., & Roekaerts, D. J. E. M. (2010). Ignition kernel formation and lift-off behaviour of jet-in-hot-coflow flames. *Combustion and Flame, 157*(6), 1167-1178. doi://doi.org/10.1016/j.combustflame.2010.01.002

[106]Oldenhof, E., Tummers, M. J., van Veen, E. H., & Roekaerts, D. J. E. M. (2011). Role of entrainment in the stabilisation of jet-in-hot-coflow flames. *Combustion and Flame, 158*(8), 1553-1563. doi://doi.org/10.1016/j.combustflame.2010.12.018

[107]Oldenhof, E., Tummers, M. J., van Veen, E. H., & Roekaerts, Dirk J. E. M. (2013). Conditional flow field statistics of jet-in-hot-coflow flames. *Combustion and Flame, 160*(8), 1428-1440. doi://doi.org/10.1016/j.combustflame.2013.03.003

[108]OpenFOAM. (1960). The open source CFD toolbox [computer software]. https://www.openfoam.com/:

[109]P. Glarborg, R.J. Kee, J.F. Grcar, & J.A. Miller. (1986). PSR: A fortran program for modeling well-stirred reactors. *Sandia Report,* , 8186-8209.

[110]P. Smith, G., M. Golden, D., Frenklach, M., W. Moriarty, N., Eiteneer, B., Goldenberg, M., . . . Qin, Z.GRI-mech 3.0. Retrieved from http://www.me.berkeley.edu/gri_mech/

[111]Parente, A., Galletti, C., & Tognotti, L. (2008). Effect of the combustion model and kinetic mechanism on the MILD combustion in an industrial burner fed with hydrogen enriched fuels. *International Journal of Hydrogen Energy, 33*(24), 7553-7564. doi://doi.org/10.1016/j.ijhydene.2008.09.058

[112]Parente, A., Malik, M. R., Contino, F., Cuoci, A., & Dally, B. B. (2016). Extension of the eddy dissipation concept for turbulence/chemistry interactions to MILD combustion. *Fuel, 163*, 98-111. doi://doi.org/10.1016/j.fuel.2015.09.020

[113]Peeters, T. W. (1997). Numerical modeling of turbulent natural gas diffusion flames.

[114]Perpignan, A. A. V., Gangoli Rao, A., & Roekaerts, Dirk J. E. M. (2018). Flameless combustion and its potential towards gas turbines. *Progress in Energy and Combustion Science, 69*, 28-62. doi://doi.org/10.1016/j.pecs.2018.06.002

[115]Peters, N. (1985). Numerical and asymptotic analysis of systematically reduced reaction schemes for hydrocarbon flames. *Numerical simulation of combustion phenomena* (pp. 90-109) Springer.

[116]Peters, N. (1986). Laminar flamelet concepts in turbulent combustion.*21*(1), 1231-1250.

[117]Peters, N., & Williams, F. A. (1987). The asymptotic structure of stoichiometric methane-air flames. *Combustion and Flame, 68*(2), 185-207.

[118]Peters, N. (1991). *Reducing mechanisms. in: Smooke M.D. (eds) reduced kinetic mechanisms and asymptotic approximations for methane-air flames. lecture notes in physics, vol 384*. Berlin, Heidelberg: Springer. doi:https://doi.org/10.1007/BFb0035365

[119]Pierce, C. D., & Moin, P. (2004). Progress-variable approach for large-eddy simulation of non-premixed turbulent combustion. *Journal of Fluid Mechanics, 504*, 73-97. doi:10.1017/S0022112004008213

[120]Pitsch, H. (2000). Unsteady flamelet modeling of differential diffusion in turbulent jet diffusion flames. *Combustion and Flame, 123*(3), 358-374. doi:https://doi.org/10.1016/S0010-2180(00)00135-8

[121]Pitsch, H., & Ihme, M. (2005). (2005). An unsteady/flamelet progress variable method for LES of nonpremixed turbulent combustion. Paper presented at the *43rd AIAA Aerospace Sciences Meeting and Exhibit,* 557.

[122]Plessing, T., Peters, N., & Wünning, J. G. (1998a). *Laseroptical investigation of highly preheated combustion with strong exhaust gas recirculation*

[123]Plessing, T., Peters, N., & Wünning, J. G. (1998b). Laseroptical investigation of highly preheated combustion with strong exhaust gas recirculation. *Symposium (International) on Combustion, 27*(2), 3197-3204. doi://doi.org/10.1016/S0082-0784(98)80183-5

[124]Poinsot, T., & Veynante, D. (2005). *Theoretical and numerical combustion* RT Edwards.

[125]Pope, S. B. (2000). *Turbulent flows*. Cambridge: Cambridge University Press. doi:10.1017/CBO9780511840531 Retrieved from https://www.cambridge.org/core/books/turbulent-flows/C58EFF59AF9B81AE6CFAC9ED16486B3A

[126]Rebola, A., Costa, M., & Coelho, P. J. (2013). Experimental evaluation of the performance of a flameless combustor. *Applied Thermal Engineering, 50*(1), 805-815. doi://doi.org/10.1016/j.applthermaleng.2012.07.027

[127]Rehm, M., Seifert, P., & Meyer, B. (2009). Theoretical and numerical investigation on the EDC-model for turbulence–chemistry interaction at gasification conditions. *Computers & Chemical Engineering, 33*(2), 402-407. doi://doi.org/10.1016/j.compchemeng.2008.11.006

[128]Roache, P. J. (1997). Quantification of uncertainty in computational fluid dynamics. *Annual Review of Fluid Mechanics, 29*(1), 123-160. doi:10.1146/annurev.fluid.29.1.123

[129]Romero Anton, N., Martin-Escudero, K., & del-Portillo-Valdés, L. A. (2019). Europar batasuneko energia-testuingurua.

eraginkortasun energetikoa industrian. *Ekaia, 36*, 189-205. doi:https://doi.org/10.1387/ekaia.19698

[130]Romero-Anton, N., Martin-Escudero, K., Portillo-Valdés, L. A., Gómez-Elvira, I., & Salazar-Herran, E. (2018). Improvement of auxiliary BI-DRUM boiler operation by dynamic simulation. *Energy, 148*, 676-686. doi://doi.org/10.1016/j.energy.2018.01.160

[131]Romero-Anton, N., Huang, X., Bao, H., Martin-Eskudero, K., Salazar-Herran, E., & Roekaerts, D. (2020). New extended eddy dissipation concept model for flameless combustion in furnaces. *Combustion and Flame, 220*, 49-62. doi:https://doi.org/10.1016/j.combustflame.2020.06.025

[132]Rudgyard, M. (1995). Integrated preprocessing tools for unstructured parallel CFD applications. *CERFACS Report,*

[133]Rudgyard, M., Schoenfeld, T., Struijs, R., Audemar, G., & Leyland, P. (1995). A modular approach for computational fluid dynamics. *A Modular Approach for Computational Fluid Dynamics.Rapport Technique TR,* , 25.

[134]Sabia, P., Sorrentino, G., Bozza, P., Ceriello, G., Ragucci, R., & de Joannon, M. (2019). Fuel and thermal load flexibility of a MILD burner. *Proceedings of the Combustion Institute, 37*(4), 4547-4554. doi://doi.org/10.1016/j.proci.2018.09.003

[135]Sawyer, R. F. (2009). Science based policy for addressing energy and environmental problems. *Proceedings of the Combustion Institute, 32*(1), 45-56. doi://doi.org/10.1016/j.proci.2008.07.003

[136]Schonfeld, T., & Rudgyard, M. (1999). Steady and unsteady flow simulations using the hybrid flow solver AVBP. *AIAA Journal, 37*(11), 1378-1385.

[137]Shabanian, S. R., Medwell, P. R., Rahimi, M., Frassoldati, A., & Cuoci, A. (2013). Kinetic and fluid dynamic modeling of ethylene jet flames in diluted and heated oxidant stream combustion conditions. *Applied Thermal Engineering, 52*(2), 538-554. doi://doi.org/10.1016/j.applthermaleng.2012.12.024

[138]Shin, J., Hwang, W., & Choi, H. (2019). Can hydrogen fuel vehicles be a sustainable alternative on vehicle market?: Comparison of electric and hydrogen fuel cell vehicles. *Technological Forecasting and Social Change, 143*, 239-248. doi://doi.org/10.1016/j.techfore.2019.02.001

[139]Sorrentino, G., Göktolga, U., de Joannon, M., van Oijen, J., Cavaliere, A., & de Goey, P. (2017). An experimental and numerical study of MILD combustion in a cyclonic burner. *Energy Procedia, 120*, 649-656. doi://doi.org/10.1016/j.egypro.2017.07.173

[140]Sorrentino, G., Sabia, P., de Joannon, M., Cavaliere, A., & Ragucci, R. (2016). The effect of diluent on the sustainability of MILD combustion in a cyclonic burner. *Flow, Turbulence and Combustion, 96*(2), 449-468. doi:10.1007/s10494-015-9668-3

[141]Sorrentino, G., Sabia, P., de Joannon, M., Ragucci, R., Cavaliere, A., Göktolga, U., . . . de Goey, P. (2015). Development of a novel cyclonic flow combustion chamber for achieving MILD/flameless combustion. *Energy Procedia, 66*, 141-144. doi://doi.org/10.1016/j.egypro.2015.02.079

[142]Spalding, D. B. (1971). Mixing and chemical reaction in steady confined turbulent flames. *Symposium (International) on Combustion, 13*(1), 649-657. doi://doi.org/10.1016/S0082-0784(71)80067-X

[143]Swaminathan, N. (2019). Physical insights on mild combustion from dns. *Frontiers in Mechanical Engineering, 5*, 59.

[144]Szegö, G. G., Dally, B. B., & Nathan, G. J. (2008). Scaling of NOx emissions from a laboratory-scale mild combustion furnace. *Combustion and Flame, 154*(1), 281-295. doi://doi.org/10.1016/j.combustflame.2008.02.001

[145]Tabacco, D., Innarella, C., & Bruno, C. (2002). Theoretical and numerical investigation on flameless combustion. *Combustion Science and Technology, 174*(7), 1-35. doi:10.1080/00102200208984086

[146]Tacina, Wey, Laing, & Mansour, A. (2002). A low NO(x) lean-direct injection, multipoint integrated module combuster concept for advanced aircraft gas turbines.

[147]Tomasch, S., & Ertesvag, I. S.The influence of the reactor model on EDC's mean reaction rate-A study on the relevance of choice. Paper presented at the *European Combustion Meeting 2019, Lisbon,*

[148]van Oijen, J. A., Donini, A., Bastiaans, R. J. M., ten Thije Boonkkamp, J. H. M., & de Goey, L. P. H. (2016). State-of-the-art in premixed combustion modeling using flamelet generated manifolds. *Progress in Energy and Combustion Science, 57*, 30-74. doi://doi.org/10.1016/j.pecs.2016.07.001

[149]Veríssimo, A. S., Rocha, A. M. A., Coelho, P. J., & Costa, M. (2015). Experimental and numerical investigation of the influence of the air preheating temperature on the performance of a small-scale mild combustor. *Combustion Science and Technology, 187*(11), 1724-1741. doi:10.1080/00102202.2015.1059330

[150]Veríssimo, A. S., Rocha, A. M. A., & Costa, M. (2011). Operational, combustion, and emission characteristics of a small-scale combustor. *Energy Fuels, 25*(6), 2469-2480. doi:10.1021/ef200258t

[151]Veríssimo, A. S., Rocha, A. M. A., & Costa, M. (2013a). Experimental study on the influence of the thermal input on the reaction zone under flameless oxidation conditions. *Fuel Processing Technology, 106*, 423-428. doi://doi.org/10.1016/j.fuproc.2012.09.008

[152]Veríssimo, A. S., Rocha, A. M. A., & Costa, M. (2013b). Importance of the inlet air velocity on the establishment of flameless combustion in a laboratory combustor. *Experimental Thermal and Fluid Science, 44*, 75-81. doi://doi.org/10.1016/j.expthermflusci.2012.05.015

[153]Wall, T., Liu, Y., Spero, C., Elliott, L., Khare, S., Rathnam, R., . . . Yu, J. (2009). An overview on oxyfuel coal combustion—State of the art research and technology development. *Chemical Engineering Research and Design, 87*(8), 1003-1016. doi://doi.org/10.1016/j.cherd.2009.02.005

[154]Wang, L., Liu, Z., Chen, S., & Zheng, C. (2012). Comparison of different global combustion mechanisms under hot and diluted oxidation conditions. *Combustion Science and Technology, 184*(2), 259-276.

[155]Wartha, E., Bösenhofer, M., & Harasek, M. (2020). Characteristic chemical time scales for reactive flow modeling. *Combustion Science and Technology,* , 1-26.

[156]Weihong, Y., & Wlodzimierz, B. (2006). CFD as applied to high temperature air combustion in industrial furnaces. *IFRF Combust J,* (200603)

[157]Westbrook, C. K., & Dryer, F. L. (1984). Chemical kinetic modeling of hydrocarbon combustion. *Progress in Energy and Combustion Science, 10*(1), 1-57.

[158]Wünning, J. A., & Wünning, J. G. (1997). Flameless oxidation to reduce thermal no-formation. *Progress in Energy and Combustion Science, 23*(1), 81-94. doi://doi.org/10.1016/S0360-1285(97)00006-3

[159]Yao, M., Zheng, Z., & Liu, H. (2009). Progress and recent trends in homogeneous charge compression ignition (HCCI) engines. *Progress in Energy and Combustion Science, 35*(5), 398-437. doi://doi.org/10.1016/j.pecs.2009.05.001

[160]Yeh, Y., & Cummins, H. (1964). Localized fluid flow measurements with an he-ne laser spectrometer. *Applied Physics Letters, 4*, 176-178. doi:10.1063/1.1753925

ATTACHMENTS

Annex A. Generalized NE-EDC model's UDF

```
#include "udf.h"
#include "prop.h"
#include "pdf_transport.h"
#include "flamelet.h"
#include "materials.h"

/* This UDF will reproduce the steady EDC model when run unsteady,
as in Fluent 14:

 * To use:
 * 1) set up Fluent just like EDC model (import Chemkin mechanism)
 * 2) disable reactions in fluid BC panel
 * 3) set yk_source terms in fluid BC panel for
 *    all species, and energy_source for energy
 * 4) allocate n_spe UDMs
 * 5) hook up adjust function */
/*recordar definir las variables al principio, sino da error*/


/* ----------------------- start user input ---------------------
--- */
#define C1          2.1377
#define C2          0.4083
#define EDC_ACC     0    /* acceleration factor: 0=slow+stable ->
1=fast+unstable */
#define VERBOSITY   0
/* -----------------------  end user input  ---------------------
--- */

#define max_time_scale 1000

static real flow_time_step=0.;
static real udf_time=-1;

static void *lib_isat=NULL;
ISAT_Functions *isat_fcns = NULL;
static char *isat_dir = NULL;

static void Open_ISAT_library(char *dir);

static real
calc_tau(cell_t c, Thread *t, real time_step)
{
  real ted, tau;
  if( LES_IN_CELL_THREAD_P(t) )
    {
      real t_scale = MAX(TRB_TIM_SCAL(c,t),SMALL);
```

Analysis of thermofluids in flameless (MILD)
combustion: assessment, improvement and
development of combustion models by CFD
Naiara Romero Anton

```
      real V_scale = MAX(TRB_VEL_SCAL(c,t),SMALL);
      ted = SQR(V_scale) / t_scale;
    }
  else if( M_turb_model==K_OMEGA ||
        M_turb_model==K_OMEGA_EASM ||
        M_turb_model==WJ_BSL_EARSM ||
        M_turb_model==SST ||
        M_turb_model==TRANS_SST ||
        M_turb_model==DES_SST ||
        M_turb_model==SAS_SST ||
        M_turb_model==RSM_K_OMEGA)
    {
      real Cmu = (rp_kw_easm || rp_kw_wj_bsl_earsm) ? M_kw_easm_Cmu
: M_kw_beta_star_inf;
      ted = MAX( Cmu*C_K(c,t)*C_O(c,t), 1.e-3);
    }
  else
    ted = C_D(c,t);

  tau = C_UDMI(c,t,n_spe+1)*sqrt( C_MU_L(c,t)/(ted*C_R(c,t)) );
  /*tau = C2*sqrt( C_MU_L(c,t)/(ted*C_R(c,t)) );*/

  return tau;
}

static real
calc_mdot(cell_t c, Thread *t, real tau)
{
  real mdot, gamma, gamma2;
  if( LES_IN_CELL_THREAD_P(t) )
    {
      gamma = C_UDMI(c,t,n_spe+2)*pow( C_MU_L(c,t) /
MAX(C_MU_T(c,t),SMALL), 0.25);
      /*gamma = C1*pow( C_MU_L(c,t) / MAX(C_MU_T(c,t),SMALL),
0.25);*/
    }
  else
    {
      real ted;
      if( M_turb_model==K_OMEGA ||
        M_turb_model==K_OMEGA_EASM ||
        M_turb_model==WJ_BSL_EARSM ||
        M_turb_model==SST ||
        M_turb_model==TRANS_SST ||
        M_turb_model==DES_SST ||
        M_turb_model==SAS_SST ||
        M_turb_model==RSM_K_OMEGA)
      {
        real Cmu = (rp_kw_easm || rp_kw_wj_bsl_earsm) ? M_kw_easm_Cmu
: M_kw_beta_star_inf;
        ted = Cmu*C_K(c,t)*C_O(c,t);
      }
```

```
     else
      ted = C_D(c,t);
      gamma = C_UDMI(c,t,n_spe+2)*pow(
C_MU_L(c,t)*ted/(C_R(c,t)*SQR(C_K(c,t))), 0.25);
      /* gamma = C1*pow( C_MU_L(c,t)*ted/(C_R(c,t)*SQR(C_K(c,t))),
0.25);*/
     }
gamma = MIN( gamma, 0.99999);
  gamma2 = gamma*gamma;
  mdot = gamma2/((1.-gamma2*gamma)*tau);
  return C_R(c,t)*mdot;
}

DEFINE_ADJUST(edc_adjust, domain)
{
  Thread *t;
  cell_t c;
  int ns, nspm=n_spe-1;
  int subtract_p_work = M_compressible || M_pressure_work;
  Material *m=mixture_material(domain), *sp;
  real solver_time = RP_Get_Real("flow-time");
  int const current_iter = (nres == 0) ? (0) : ((int) count2[nres -
1]);

#if !RP_HOST
  if(rp_unsteady)
    {
      if(ABS(udf_time-solver_time)<SMALL)
     return;
      else
     {
       flow_time_step = RP_Get_Real("physical-time-step");
       udf_time = solver_time;
     }
    }
  else
    {
      int n_iter_chem = RP_Get_Integer("species/edc-niter");
      if(current_iter%n_iter_chem!=0)
     return;
    }

  if( n_udm < n_spe )
    Error("Increase UDMs to at least %i\n",n_spe);

  if( NULLP(isat_fcns) )
    {
      if( NULLP(isat_dir) )
     isat_dir = get_isat_dir_name();
      Open_ISAT_library(isat_dir);
      isat_fcns->isat_init();
```

Analysis of thermofluids in flameless (MILD)
combustion: assessment, improvement and
development of combustion models by CFD
Naiara Romero Anton

```
      }

   thread_loop_c(t,domain)
     if(FLUID_THREAD_P(t))
       {
      if( !THREAD_VAR(t).cell.sources )
        Error("Set the cell species and energy sources");

         Message("Integrating chemistry on zone %d\n", t->id);

       begin_c_loop_int(c,t)
         {
           double dtd, pd, rhod, phi0[MAX_SPE_EQNS+1],
phit[MAX_SPE_EQNS+1];
           real E_after, rho, hk[MAX_SPE_EQNS], yk[MAX_SPE_EQNS],
temp;
           int rp_energy_save = rp_energy, sg_enthalpy_save =
sg_enthalpy;

           if( MATERIAL_PROP_METHOD(m,PROP_rho) == RHO_IDEAL_GAS )
             pd = (double)ABS_P(C_P(c,t),op_pres);
           else
             pd = (double)op_pres;
           dtd = (double)calc_tau(c,t,flow_time_step);
           rhod = (double)C_R(c,t);


           temp = C_T(c,t);
           yk[nspm] = 1.;
           spe_loop(ns,nspm)
             yk[nspm] -= yk[ns] = C_YI(c,t,ns);

           rp_energy = sg_enthalpy = FALSE; /* use sensible enthalpy
*/

           mixture_species_loop(m,sp,ns)
             phi0[ns] = (double)( yk[ns] / MATERIAL_PROP(sp,PROP_mwi)
);
           phi0[n_spe] = (double) Enthalpy(m, temp, 0., 0., yk, hk);

           /*isat_fcns->isat_step(c, t, NULL, dtd, pd, rhod, phi0,
phit); version 14.5*/
              isat_fcns->isat_step(c, t,NULL, dtd, pd, rhod, phi0,
phit,THREAD_ID(t));



           mixture_species_loop(m,sp,ns)
             yk[ns] = (real)phit[ns] * MATERIAL_PROP(sp,PROP_mwi);
           if( !rp_seg || VERBOSITY)
             temp = Temperature(m, (real)phit[n_spe], 0., 0., temp,
yk, hk);
```

```
                E_after = phit[n_spe];

                rp_energy = rp_energy_save;
                sg_enthalpy = sg_enthalpy_save;

                if( VERBOSITY==2 )
                   Message("c=%i    dt=%7.4es     T0=%6.1fK
T1=%6.1f\n",c,dtd,C_T(c,t),temp);

                if(subtract_p_work)
                   E_after -= ABS_P(C_P(c,t),op_pres)/C_R(c,t);

                    spe_loop(ns,nspm)
                      C_UDMI(c,t,ns) = yk[ns];
                    C_UDMI(c,t,nspm) = E_after;
           }
       end_c_loop_int(c,t)
        }
#endif /* !RP_HOST */
}

DEFINE_SOURCE(yk_source,c,t,dS,eqn)
{
  real tau  = calc_tau(c,t,flow_time_step);
  real mdot = calc_mdot(c,t,tau);
  int ns = eqn-EQ_SPECIES;
  dS[eqn] = -(1.-EDC_ACC)*mdot;
  return mdot*(C_UDMI(c,t,ns)-C_YI(c,t,ns));
}

DEFINE_SOURCE(energy_source,c,t,dS,eqn)
{
  real tau  = calc_tau(c,t,flow_time_step);
  real mdot = calc_mdot(c,t,tau);
  real E = C_H(c,t);
  int subtract_p_work = M_compressible || M_pressure_work;
  if(subtract_p_work)
    E -= ABS_P(C_P(c,t),op_pres)/C_R(c,t);
  dS[eqn] = -(1.-EDC_ACC)*mdot*C_CP(c,t);
  return mdot*(C_UDMI(c,t,n_spe-1) - E);
}

static void
Open_ISAT_library(char *dir)
{
  char libname[4096]; /* for modification by CX_DLL_OpenLib */

  /* close library if already open. */
  if (NNULLP(lib_isat))
    {
      CX_DLL_CloseLib(lib_isat);
```

Analysis of thermofluids in flameless (MILD)
combustion: assessment, improvement and
development of combustion models by CFD
Naiara Romero Anton

```
      lib_isat = NULL;
      isat_fcns = NULL;
    }

  /* Open ISAT library. */
  strcpy(libname,dir);
  lib_isat=CX_DLL_OpenLib(libname,libname,0);

  if (!lib_isat)
    {
      Message("\n\"%s\"",libname);
      Error("open_isat_library: %s", CX_DLL_GetError());
    }
  else
    Message("EDC UDF: Successfully opened ISAT library\n");

  /* Get ISAT functions from library. */
  isat_fcns=CX_DLL_GetData(lib_isat,"ISATFunctionList");
  if (!isat_fcns)
    Error("open_isat_library: couldn't get isat_fcns\n%s",
CX_DLL_GetError());
}


DEFINE_ADJUST(constants, domain)
{
  Thread *t;
  cell_t c;
  real Ret=0.0;
  real tau_c=0.0;
  real tau_c2 = 0.0;
  real tau_c_single=0.0;
  real tau_c_all=0.0;
  real tau_m=0.0;
  real Da=0.0;
  real C_tau=0.0;
  real CD2=0.0;
  real C_gamma=0.0;
  real nu=0.0;
  real C_gamma_coeff=1.22474;
  real C_tau_coeff=0.75;
  real C_gamma_std=2.1377;
  real C_tau_std=0.4083;
  real C_gamma_ns=0.0;
  real C_tau_ns=0.0;
  real delta_scal=0.0;
  real n_exp=1.00;
  /*real Da_min=0.20;
  real Da_max=0.25;*/
  real Da_min=0.00002;
  real Da_max=0.068;
  real Da_all=0.0;
```

```
   real Da_single=0.0;
   real Da_single2 = 0.0;
   real delta=Da_max-Da_min;
   real C_tau_all=0.0;
   real C_gamma_all=0.0;

   thread_loop_c(t,domain)
     if(FLUID_THREAD_P(t))
       {
               Material *m = THREAD_MATERIAL(t);

                   int ich4 = mixture_specie_index(m, "ch4");
                   int io2 = mixture_specie_index(m, "o2");
                   int ih2o = mixture_specie_index(m, "h2o");
                   int ico = mixture_specie_index(m, "co");
                   int ico2 = mixture_specie_index(m, "co2");
                   int ih2 = mixture_specie_index(m, "h2");
       begin_c_loop_int(c,t)
         {
                   real Ych4, Yo2, Yh2o, Yco, Yco2, Yh2;
                   double w_3, w_6f, w_6r, w_8f, w_8r;
                   double R_ch4, R_h2o, R_o2, R_co, R_co2, R_h2;
                   double w_ch4, w_h2o, w_o2, w_co, w_co2, w_h2;
                   double tau_c_ch4, tau_c_h2o, tau_c_o2,
tau_c_co, tau_c_co2, tau_c_h2;
                   double w_array[6];
                   double tau_c_array[6];
                   double max = tau_c_array[0];
                   int i;

                   Ych4 = C_YI(c, t, ich4); /* ch4 mass fraction*/
                   Yo2 = C_YI(c, t, io2);
                   Yh2o = C_YI(c, t, ih2o);
                   Yco = C_YI(c, t, ico);
                   Yco2 = C_YI(c, t, ico2);
                   Yh2 = C_YI(c, t, ih2);

                   if (c == 333)
                   {
                           Message("1-Testing value of Ych4 %lf, Yo2
%lf, Yh2o %lf, Yco %lf, Yco2 %lf,Yh2 %lf\n", Ych4, Yo2, Yh2o, Yco,
Yco2, Yh2);
                   }
                   /* each reaction reaction-rate, units-->
kmol/m^3/s  */
                   w_3 = 5.3 * 1e11 * exp(-24056 / C_T(c,
t))*pow((C_R(c, t)*Ych4 / 16),0.7)*pow((C_R(c, t)*Yo2 / 32),0.8);
                   w_6f = 2.24 * 1e06 * exp(-5032 / C_T(c,
t))*(C_R(c, t)*Yco / 28)*pow((C_R(c, t)*Yo2 / 32),0.25)*pow((C_R(c,
t)*Yh2o / 18), 0.5);
```

Analysis of thermofluids in flameless (MILD)
combustion: assessment, improvement and
development of combustion models by CFD
Naiara Romero Anton

```
                w_6r = 1.10 * 1e13 *pow(C_T(c, t),-0.97)* exp(-
39452 / C_T(c, t))*(C_R(c, t)*Yco / 28)*pow((C_R(c, t)*Yo2 / 32), -
0.25)*pow((C_R(c, t)*Yh2o / 18), 0.5);
                w_8f = 7.91 * 1e10 * exp(-17609 / C_T(c,
t))*(C_R(c, t)*Yh2 / 2)*pow((C_R(c, t)*Yo2 / 32), 0.5);
                w_8r = 3.48 * 1e13 * exp(-47907 / C_T(c,
t))*(C_R(c, t)*Yh2o / 18);
                if (c == 333)
                {
                        Message("2-Testing value of w_3 %lf, w_6f
%lf, w_6r %lf, w_8f %lf, w_8r %lf\n", w_3, w_6f, w_6r, w_8f, w_8r);
                }
                /*species product rate as a function of
temperature */
                R_ch4 = -1 * w_3;
                R_o2 = -1.5*w_3 - 0.5*w_6f + 0.5*w_6r-0.5*w_8f
+0.5*w_8r ;

                R_h2o = 2 * w_3 + w_8f - w_8r;
                R_co = w_3- w_6f + w_6r;
                R_co2 = w_6f - w_6r;
                R_h2 = -w_8f + w_8r;
                if (c == 333)
                {
                        Message("3-Testing value of R_ch4 %lf,
R_o2 %lf, R_h2o %lf, R_co %lf, R_co2 %lf, R_h2 %lf\n", R_ch4, R_o2,
R_h2o, R_co, R_co2, R_h2);
                }
                /*species reaction rate units-->  kg/m^3/s*/
                w_ch4 = R_ch4 * 16;
                w_o2 = R_o2 * 32;
                w_h2o = R_h2o * 18;
                w_co = R_co * 28;
                w_co2 = R_co2 * 44;
                w_h2 = R_h2 * 2;
                if (c == 333)
                {
                        Message("4-Testing value of w_ch4 %lf,
w_o2 %lf, w_h2o %lf, w_co %lf, w_co2 %lf, w_h2 %lf\n", w_ch4, w_o2,
w_h2o, w_co, w_co2, w_h2);
                }

                w_array[0] = w_ch4;
                w_array[1] = w_o2;
                w_array[2] = w_h2o;
                w_array[3] = w_co;
                w_array[4] = w_co2;
                w_array[5] = w_h2;

                for (i = 0; i < 6; i++)

                {
                        if (w_array[i] < 0)
```

```
                        {
                                w_array[i] = -1 * w_array[i];
                        }
                }


                for (i = 0; i < 6; i++)
                {
                        if (w_array[i] <= 0.0000000000000001)
                        {
                        w_array[i] = 1;

                        }
                }
                if (c == 333)
                {
                        Message("5-Testing value of w_array[ch4]
%lf, w_array[o2] %lf, w_array[h2o] %lf, w_array[co] %lf,
w_array[co2] %lf, w_array[h2] %lf\n", w_array[0], w_array[1],
w_array[2], w_array[3], w_array[4], w_array[5]);
                }
                /*each species chemical time scale*/
                tau_c_ch4 = Ych4 / w_array[0]; /* / C_R(c,
t));*/
                tau_c_o2 = Yo2 / w_array[1]; /* / C_R(c, t));*/
                tau_c_h2o = Yh2o / w_array[2]; /* / C_R(c,
t));*/
                tau_c_co = Yco / w_array[3]; /* / C_R(c, t));*/
                tau_c_co2 = Yco2 / w_array[4]; /* / C_R(c,
t));*/
                tau_c_h2 = Yh2 / w_array[5]; /* / C_R(c, t));*/
                if (c == 333)
                {
                        Message("x rho %lf\n", C_R(c, t));
                }


                tau_c_array[0] = tau_c_ch4 * C_R(c, t);
                tau_c_array[1] = tau_c_o2 * C_R(c, t);
                tau_c_array[2] = tau_c_h2o * C_R(c, t);
                tau_c_array[3] = tau_c_co * C_R(c, t);
                tau_c_array[4] = tau_c_co2 * C_R(c, t);
                tau_c_array[5] = tau_c_h2 * C_R(c, t);
                if (c == 333)
                {
                        Message("6-Testing value of  tau_c[ch4]
%lf,  tau_c[o2] %lf,  tau_c[h2o] %lf,  tau_c[co] %lf,  tau_c[co2]
%lf,  tau_cm[h2] %lf\n", tau_c_array[0], tau_c_array[1],
tau_c_array[2], tau_c_array[3], tau_c_array[4], tau_c_array[5]);
                }
```

Analysis of thermofluids in flameless (MILD)
combustion: assessment, improvement and
development of combustion models by CFD
Naiara Romero Anton

```c
                    for (i = 1; i < 6; i++)
                    {
                            if (tau_c_array[i] > max)
                            {
                                    max = tau_c_array[i];
                            }
                    }

                    tau_c = max;
                    tau_c2 = 1 / (8.3*1e05*exp(-15100 / C_T(c,
t)));

                    if (c == 333)
                    {
                            Message("7-Testing value of  tau_c_max
%lf, tau_c_needc %lf \n", tau_c, tau_c2);
                    }

                    nu=C_MU_L(c,t)/C_R(c,t);
            Ret=pow(C_K(c,t),2)/(nu*C_D(c,t));
        /* Ret=C_MU_T(c,t)/(0.09*C_MU_L(c,t));*/
        /* tau_c=1/(8.3*1e05*exp(-15100/C_T(c,t)));*/
        tau_m = pow(nu/C_D(c,t), 0.5);

        /* Da calculation */
        Da_single=tau_m/tau_c;
        Da=Da_single;
            Da_single2 = tau_m / tau_c2;

        CD2=C_tau_coeff/((Ret+1.)*pow(Da,2.0));
        C_tau_ns=sqrt(CD2/3.0);

        delta_scal=(Da-Da_min)/delta;

        /* C_gamma definition*/
        C_gamma_ns=C_gamma_coeff*(pow((Ret+1.), 0.5)*pow(Da,
0.75));

        C_gamma=C_gamma_ns;
        C_tau=C_tau_ns;

        /* Min/Max value of C_gamma*/
        if (C_gamma<C_gamma_std)
        {C_gamma=C_gamma_std;}
        if (C_gamma>13)
        {C_gamma=13;}

        /*Min/Max value of Ctau*/
        if (C_tau<0.2)
```

```
            {C_tau=0.2;}
            if (C_tau>C_tau_std)
            {C_tau=C_tau_std;}


            C_UDMI(c,t,100) = C_tau;
            C_UDMI(c,t,101) = C_gamma;
            C_UDMI(c,t,102) = Da_all;
            C_UDMI(c,t,103) =
2.0/3.0*CD2/sqrt(3.0/4.0*CD2/pow(C_gamma, 2));
            C_UDMI(c,t,104) = Ret;
            C_UDMI(c,t,105) = Da_single;
                C_UDMI(c,t,106) = C_tau_ns;
                C_UDMI(c,t,107) = C_gamma_ns;
                C_UDMI(c,t,108) = tau_c;
                C_UDMI(c, t, 109) = tau_c2;
                C_UDMI(c, t, 110) = Da_single;
                C_UDMI(c, t, 111) = Da_single2;


        }
    end_c_loop_int(c,t)
     }
}
```

Annex B. DA-FGM model's UDF

```
#include "udf.h"
#include "sg_mem.h" /*neccesary for scaled progress variable*/
#include "pdf_props.h"
#include "pdf_table.h"
#include "mem.h"
#include "materials.h"


/*****************************************************/
/* This UDF will implement DAFGM 6D model in FLUENT

* To use :
*1) Write the following commands in Flunet TUI in order to calculate
Yc=Yco2+Yco+Yh2+Yh2o:
1.1) (rpsetvar 'prepdf/prmx-fla-alpha '(("h2". 1.0) ("h2o" . 1.0)
("co" . 1.0) ("co2" . 1.0)))
[un normalized progrss variable is calculated considering co, co2,
h2, h2o]
1.2)(rpgetvar 'prepdf/prmx-fla-alpha '?)

1.3)

(rpsetvar 'premixc/include-ycvar-rxn-src? #t)
(rpgetvar 'premixc/include-ycvar-rxn-src?)
```

Analysis of thermofluids in flameless (MILD)
combustion: assessment, improvement and
development of combustion models by CFD
Naiara Romero Anton

[chemical effects of un - normalized progress varable is considered]

1.4) (rpsetvar 'premixc/use-inst-yceq? #f)
    [When normalizing C Yceq value is calculated considering PDF averaged value(turbulence)]
* 2) Define UDS = 1
* 3) UDM 20
* 3) Add + Build + Load programmed UDF
* 4) Hook - VISCOUS + wALL TEMP
* 5) RUN
* 6) Hook PDF TABLE
* 7) RUN
* 8) HOOK SOURCE
* 9) RUN
* 5) EXECUTE on_demand the following tables :

Note1 : Make sure that the.data and .case files are save in the same folder as.c file
Note2 : LOAD UDF BEFORE CASE AND DATA ARE READING WHEN YOU ARE OPENING A SAVE CASE.* /

/***/

```
#define DVZstC1 0.2719 /*YdDil */
#define Zst 0.071077 /*stoichiometric mixture fraction Zst*/
#define HadF -3339580.0 /*J/kg*/
#define HadO 545469.0 /*J/kg*/
#define Hmaxloss 2341000.0 /*J/kg*/
#define Hminloss 0.0 /*J/kg*/

#define verySmall 0.000001

/*------------DEFINITIONS 6D------------------*/
#define N1 11
#define N2 11
#define N3 51
#define N4 51
#define N5 13
#define N6 11

/*------------DEFINITIONS 4D------------------*/
#define N7 11
#define N8 51
#define N9 13
#define N10 11

/*-----------6D Variables definitions-----------*/
real  SPV[N1];
real  SE[N2]; /*second mixture fraction variance*/
```

ENEDI Research Group
Energy Engineering Department
University of the Basque Country

FACULTY
OF ENGINEERING
BILBAO
UNIVERSITY
OF THE BASQUE
COUNTRY

```
real  PV[N3]; /*normalized progress variable C*/
real  E[N4]; /*E= second mixture fraction*/
real  sDH[N5]; /*enthalpy loss*/
real  sDV[N6]; /*air diluent*/

real *vector_Temp;

real *vector_wPV;

real *vector_Alpha;

real *vector_Density;

/*-----------4D Variables definitions------------*/
real  SE4D[N7]; /*second mixture fraction variance*/
real  E4D[N8];/*E= second mixture fraction*/
real  sDH4D[N9]; /*enthalpy loss*/
real  sDV4D[N10]; /*air diluent*/

real *vector_ydb;
real *vector_Ycb;
real *vector_Ycu;
real *vector_Ycb2;
real *vector_Ycu2;
real *vector_YcuYcb;


/*******************************************************************
**/
  /*            FIND INDEX for LINEAR INTERPOLATION          */

/*******************************************************************/


void find_index(int i0[2], real *x0, real *x, int n)
{

     /*check if index in inbounds*/
     if (*x0 < x[0])
     {
          printf("Out of Lower bounds!! The number of points is %d
%le %le\n", n, *x0, x[0]);
          *x0 = x[0];
          i0[0] = 0;
          i0[1] = 1;
          return;
     }
     if (*x0 > x[n - 1])
     {
```

```
        /*printf("Out of Higher bounds!! The number of points is
%d %le %le\n", n, *x0, x[n - 1]);*/
        *x0 = x[n - 1];
        i0[0] = n - 2;
        i0[1] = n - 1;
        return;
    }

    /*if (*x0 = 1)
    {
    i0[0] = n - 2;
    i0[1] = n - 1;
    return;
    }*/


    /*bisection search of index*/
    int i = 0;
    int w = n - 1;
    while (w > i + 1)
    {
        int d = (i + w) / 2;
        if (*x0 <  x[d])
            w = d;
        else
            i = d;
    }

    i0[0] = i;
    i0[1] = i + 1;

    return;
}

/*index for interpolation with a singel pointer*/

int idx_n66D(int i, int j, int k, int q, int p, int t, int n1, int
n2, int n3, int n4, int n5)
{
    return t + n1*(p + n2*(q + n3*(k + n4*(j + n5*i))));
}

int idx_n55D(int i, int j, int k, int q, int p, int n2, int n3, int
n4, int n5)
{
    return p + n2*(q + n3*(k + n4*(j + n5*i)));
}

int idx_n44D(int i, int j, int k, int q, int n7, int n8, int n9)
{
    return q + n7*(k + n8*(j + n9*i));
}
```

```c
int idx_n33D(int i, int j, int k, int n4, int n5)
{
      return k + n4*(j + n5*i);
}

int idx_n22D(int i, int j, int n5)
{
      return j + n5*i;
}
```

```
/********************************************************************
**/
/*          LINEAR INTERPOLATION
*/
/********************************************************************
*/
```

```c
real lin_interp(real x0, real x1, real x2, real y1, real y2)
{
      return (y2 - y1) / (x2 - x1) * (x0 - x1) + y1;
}


real interp_matricLinear6D(int *i0, int *j0, int *k0, int *q0, int
*p0, int *t0, real *I, real *J, real *K, real *Q, real *P, real *T,
real I0, real J0, real K0, real Q0, real P0, real T0, real *M6D)
{
      real M1[2][2][2][2][2], M2[2][2][2][2], M3[2][2][2], M4[2][2],
M5[2];
      real value;
      int i, j, k, q, p, n1, n2;

      for (i = 0; i <= 1; i++)
      {
            for (j = 0; j <= 1; j++)
            {
                  for (k = 0; k <= 1; k++)
                  {
                        for (q = 0; q <= 1; q++)
                        {
                              for (p = 0; p <= 1; p++)
                              {
                                    n1 = idx_n66D(i0[i], j0[j], k0[k],
q0[q], p0[p], t0[0], N1, N2, N3, N4, N5);
                                    n2 = idx_n66D(i0[i], j0[j], k0[k],
q0[q], p0[p], t0[1], N1, N2, N3, N4, N5);
```

Analysis of thermofluids in flameless (MILD)
combustion: assessment, improvement and
development of combustion models by CFD
Naiara Romero Anton

```
                                M1[i][j][k][q][p] = lin_interp(T0,
T[t0[0]], T[t0[1]], M6D[n1], M6D[n2]);


                        }
                        M2[i][j][k][q] = lin_interp(P0, P[p0[0]],
P[p0[1]], M1[i][j][k][q][0], M1[i][j][k][q][1]);
                }

                M3[i][j][k] = lin_interp(Q0, Q[q0[0]],
Q[q0[1]], M2[i][j][k][0], M2[i][j][k][1]);
                }

            M4[i][j] = lin_interp(K0, K[k0[0]], K[k0[1]],
M3[i][j][0], M3[i][j][1]);
            }


        M5[i] = lin_interp(J0, J[j0[0]], J[j0[1]], M4[i][0],
M4[i][1]);

    }
    value = lin_interp(I0, I[i0[0]], I[i0[1]], M5[0], M5[1]);

    return value;
}

real interp_matricLinear4D(int *i0, int *j0, int *k0, int *q0, real
*I, real *J, real *K, real *Q, real I0, real J0, real K0, real Q0,
real *M4D)
{
    real M1[2][2][2], M2[2][2], M3[2];
    real value;
    int i, j, k, n1, n2;

    for (i = 0; i <= 1; i++)
    {
        for (j = 0; j <= 1; j++)
        {
            for (k = 0; k <= 1; k++)
            {
                n1 = idx_n44D(i0[i], j0[j], k0[k], q0[0], N7,
N8, N9);
                n2 = idx_n44D(i0[i], j0[j], k0[k], q0[1], N7,
N8, N9);
                M1[i][j][k] = lin_interp(Q0, Q[q0[0]],
Q[q0[1]], M4D[n1], M4D[n2]);
                }
                M2[i][j] = lin_interp(K0, K[k0[0]], K[k0[1]],
M1[i][j][0], M1[i][j][1]);
            }
        M3[i] = lin_interp(J0, J[j0[0]], J[j0[1]], M2[i][0],
M2[i][1]);
```

```
                    /*printf("i: %d Temperature: %lf \n",i, M5[i]);*/
        }
        value = lin_interp(I0, I[i0[0]], I[i0[1]], M3[0], M3[1]);

        return value;
}

/************************************************************/
/*          READING 6D TABLES                             */
/************************************************************/

/*------------READ tableproperties (6D table controlling
parameters)---------*/

DEFINE_EXECUTE_ON_LOADING(read_tableProperties6D,
udfTableProperties6D)
{
        int i, j, k, q, p, t;

        FILE *rfile1; /*declare FILE name as pointer*/

        char dummyCS[30]; /*to read a sentence*/
        char dummyCS1[30]; /*to read a sentence*/
        char dummyC; /*to read a single word, character*/

        rfile1 = fopen("tableProperties6D", "r"); /*open file for
reading*/

        fscanf(rfile1, "%s\n", dummyCS1); /*read "tableLookupParaNames"
and throw */
        fscanf(rfile1, "%s\n", dummyCS); /*read "PV_Vars" and throw */
        fscanf(rfile1, "%c\n", &dummyC); /*read "(" and throw, & symbol
mean to find the adress of the variable*/

        for (t = 0; t<N1; t++)
        {
             fscanf(rfile1, "%le\n", &SPV[t]); /*read "N3" elements
and save, l letter means that it is a real variable */
                                                    /*printf("PV:
%le\n", PV[q]);*/
        }

        fscanf(rfile1, "%c\n", &dummyC); /*read ")" and throw*/
        fscanf(rfile1, "%s\n", dummyCS); /*read "Mixfrac_Vars" and
throw*/
        fscanf(rfile1, "%c\n", &dummyC); /*read "(" and throw*/

        for (p = 0; p<N2; p++)
        {
             fscanf(rfile1, "%le\n", &SE[p]); /*read "N3" elements and
save, l letter means that it is a real variable */
```

```
                                            /*printf("PV:
%le\n", PV[q]);*/
      }

      fscanf(rfile1, "%c\n", &dummyC); /*read ")" and throw*/
      fscanf(rfile1, "%s\n", dummyCS); /*read "PV" and throw*/
      fscanf(rfile1, "%c\n", &dummyC); /*read "(" and throw*/


      for (q = 0; q<N3; q++)
      {
            fscanf(rfile1, "%le\n", &PV[q]); /*read "N3" elements and
save, l letter means that it is a real variable */
                                            /*printf("PV:
%le\n", PV[q]);*/
      }

      fscanf(rfile1, "%c\n", &dummyC); /*read ")" and throw*/
      fscanf(rfile1, "%s\n", dummyCS); /*read "Mixfrac" and throw*/
      fscanf(rfile1, "%c\n", &dummyC); /*read "(" and throw*/

      for (k = 0; k<N4; k++)
      {
            fscanf(rfile1, "%le\n", &E[k]); /*read "N4" elements and
save, l letter means that it is a real variable */
                                            /*printf("E:
%le\n", E[k]);*/
      }

      fscanf(rfile1, "%c\n", &dummyC); /*read ")" and throw*/
      fscanf(rfile1, "%s\n", dummyCS); /*read "sDH" and throw*/
      fscanf(rfile1, "%c\n", &dummyC); /*read "(" and throw*/

      for (j = 0; j<N5; j++)
      {
            fscanf(rfile1, "%le\n", &sDH[j]); /*read "N2" elements
and save */

/*printf("sDH: %le\n", sDH[j]);*/
      }
      fscanf(rfile1, "%c\n", &dummyC); /*read "(" and throw*/
      fscanf(rfile1, "%s\n", dummyCS); /*read "sDV" and throw*/
      fscanf(rfile1, "%c\n", &dummyC); /*read "(" and throw*/

      for (i = 0; i<N6; i++)
      {
            fscanf(rfile1, "%le\n", &sDV[i]); /*read "N6" elements
and save */

/*printf("sDV: %le\n", sDV[i]);*/
      }
```

```
        fscanf(rfile1, "%c\n", &dummyC); /*read "(" and throw*/
        fclose(rfile1);

}

/*-------------READ Temperature_table----------------------------
----------*/

DEFINE_EXECUTE_ON_LOADING(read_Temperature_table, udfT)
{
    int i, j, k, q, p, t, n;

    vector_Temp = (real *)malloc(N6*N5*N4*N3*N2*N1 * sizeof(real));

    FILE *rfile; /*declare FILE name as pointer*/

    char dummyCS[20]; /*to read a sentence*/
    char dummyC; /*to read a character*/
    int  dummyI; /*to read an integer*/

    rfile = fopen("Temperature_table", "r"); /*open file for
reading*/
    n = 0;

    fscanf(rfile, "%s\n", dummyCS); /*read "Temperature_table and
throw */
    fscanf(rfile, "%d\n", &dummyI); /*read "11" and throw*/
    fscanf(rfile, "%c\n", &dummyC); /*read "(" and throw*/

    for (i = 0; i < N6; i++)
    {
        fscanf(rfile, "%d\n", &dummyI); /*read "13" and throw*/
        fscanf(rfile, "%c\n", &dummyC); /*read "(" and throw*/

        for (j = 0; j < N5; j++)
        {
            fscanf(rfile, "%d\n", &dummyI); /*read "51" and
throw*/
            fscanf(rfile, "%c\n", &dummyC); /*read "(" and
throw*/

            for (k = 0; k < N4; k++)
            {
                fscanf(rfile, "%d\n", &dummyI); /*read "51" and
throw*/
                fscanf(rfile, "%c\n", &dummyC); /*read "(" and
throw*/

                for (q = 0; q < N3; q++)
                {
```

Analysis of thermofluids in flameless (MILD)
combustion: assessment, improvement and
development of combustion models by CFD
Naiara Romero Anton

```c
                                fscanf(rfile, "%d\n", &dummyI); /*read
"11" and throw*/
                                fscanf(rfile, "%c\n", &dummyC); /*read
"(" and throw*/

                                for (p = 0; p < N2; p++)
                                {
                                        fscanf(rfile, "%d\n", &dummyI);
/*read "11" and throw*/
                                        fscanf(rfile, "%c\n", &dummyC);
/*read "(" and throw*/

                                        for (t = 0; t < N1; t++)
                                        {
                                                /*fscanf(rfile, "%le\n",
&matric_T[i][j][k][q][p][t]); */
                                                fscanf(rfile, "%le\n",
&vector_Temp[n]); /*read "11" elements and save */
                                                n += 1;
                                        }
                                        fscanf(rfile, "%c\n", &dummyC);
/*read "(" and throw*/
                                }
                                fscanf(rfile, "%c\n", &dummyC); /*read
"(" and throw*/
                        }

                        fscanf(rfile, "%c\n", &dummyC); /*read "(" and
throw*/

                }
                fscanf(rfile, "%c\n", &dummyC); /*read "(" and
throw*/
        }
        fscanf(rfile, "%c\n", &dummyC); /*read "(" and throw*/
    }
    fscanf(rfile, "%c\n", &dummyC); /*read "(" and throw*/
    fclose(rfile);

    /*real temperature;

    real PV0, E0, sDH0, sDV0, SPV0, SE0;

    PV0 = 0.1;
    E0 = 0.028;
    sDH0 = 0.582657;
    sDV0 = 0.5;
    SPV0 = 0.5;
    SE0 = 0.4;


    int i0[2], j0[2], k0[2], q0[2], p0[2], t0[2];
```

ENEDI Research Group
Energy Engineering Department
University of the Basque Country

FACULTY
OF ENGINEERING
BILBAO
UNIVERSITY
OF THE BASQUE
COUNTRY

```c
        find_index(t0, &SPV0, SPV, N1);
        find_index(p0, &SE0, SE, N2);
        find_index(q0, &PV0, PV, N3);
        find_index(k0, &E0, E, N4);
        find_index(j0, &sDH0, sDH, N5);
        find_index(i0, &sDV0, sDV, N6);

        printf("index definition i0[0] %d i0[1]%d j0[0] %d j0[1] %d
k0[0] %d k0[1] %d  q0[0] %d q0[1] %d p0[0] %d p0[1] %d t0[0] %d
t0[1] %d \n", i0[0], i0[1], j0[0], j0[1], k0[0], k0[1], q0[0],
q0[1], p0[0], p0[1], t0[0], t0[1]);

        temperature = interp_matricLinear6D(i0, j0, k0, q0, p0, t0,
sDV, sDH, E, PV, SE, SPV, sDV0, sDH0, E0, PV0, SE0, SPV0,
vector_Temp);
        printf("Temperature Final result: %le\n", temperature);


        printf("Temperature INDEX[0] Final result: %le\n",
vector_Temp[5 + N1 * (4 + N2 * (5 + N3 * (5 + N4 * (5 + N5 *
5)))))]);
        printf("Temperature INDEX[1] Final result: %le\n",
vector_Temp[5 + N1 * (4 + N2 * (5 + N3 * (6 + N4 * (5 + N5 *
5)))))]);*/




}


DEFINE_EXECUTE_ON_LOADING(read_alpha_table, udfT)
{
        int i, j, k, q, p, t, n;

        vector_Alpha = (real *)malloc(N6*N5*N4*N3*N2*N1 *
sizeof(real));

        FILE *rfile; /*declare FILE name as pointer*/

        char dummyCS[20]; /*to read a sentence*/
        char dummyC; /*to read a character*/
        int  dummyI; /*to read an integer*/

        rfile = fopen("alpha_table", "r"); /*open file for reading*/
        n = 0;

        fscanf(rfile, "%s\n", dummyCS); /*read "Temperature_table and
throw */
        fscanf(rfile, "%d\n", &dummyI); /*read "11" and throw*/
        fscanf(rfile, "%c\n", &dummyC); /*read "(" and throw*/
```

```
for (i = 0; i < N6; i++)
{
        fscanf(rfile, "%d\n", &dummyI); /*read "13" and throw*/
        fscanf(rfile, "%c\n", &dummyC); /*read "(" and throw*/

        for (j = 0; j < N5; j++)
        {
                fscanf(rfile, "%d\n", &dummyI); /*read "51" and
throw*/
                fscanf(rfile, "%c\n", &dummyC); /*read "(" and
throw*/

                for (k = 0; k < N4; k++)
                {
                    fscanf(rfile, "%d\n", &dummyI); /*read "51" and
throw*/
                    fscanf(rfile, "%c\n", &dummyC); /*read "(" and
throw*/

                    for (q = 0; q < N3; q++)
                    {
                        fscanf(rfile, "%d\n", &dummyI); /*read
"11" and throw*/
                        fscanf(rfile, "%c\n", &dummyC); /*read
"(" and throw*/

                        for (p = 0; p < N2; p++)
                        {
                            fscanf(rfile, "%d\n", &dummyI);
/*read "11" and throw*/
                            fscanf(rfile, "%c\n", &dummyC);
/*read "(" and throw*/

                            for (t = 0; t < N1; t++)
                            {
                                /*fscanf(rfile, "%le\n",
&matric_T[i][j][k][q][p][t]); */
                                fscanf(rfile, "%le\n",
&vector_Alpha[n]); /*read "11" elements and save */
                                n += 1;
                            }
                            fscanf(rfile, "%c\n", &dummyC);
/*read "(" and throw*/
                        }
                        fscanf(rfile, "%c\n", &dummyC); /*read
"(" and throw*/
                    }

                    fscanf(rfile, "%c\n", &dummyC); /*read "(" and
throw*/
```

```
                }
                fscanf(rfile, "%c\n", &dummyC); /*read "(" and
throw*/
            }
            fscanf(rfile, "%c\n", &dummyC); /*read "(" and throw*/
        }
        fscanf(rfile, "%c\n", &dummyC); /*read "(" and throw*/
        fclose(rfile);

        /*real alpha;

        real PV0, E0, sDH0, sDV0, SPV0, SE0;

        PV0 = 0.1;
        E0 = 0.028;
        sDH0 = 0.582657;
        sDV0 = 0.5;
        SPV0 = 0.5;
        SE0 = 0.4;


        int i0[2], j0[2], k0[2], q0[2], p0[2], t0[2];

        find_index(t0, &SPV0, SPV, N1);
        find_index(p0, &SE0, SE, N2);
        find_index(q0, &PV0, PV, N3);
        find_index(k0, &E0, E, N4);
        find_index(j0, &sDH0, sDH, N5);
        find_index(i0, &sDV0, sDV, N6);

        printf("index definition i0[0] %d i0[1]%d j0[0] %d j0[1] %d
k0[0] %d k0[1] %d  q0[0] %d q0[1] %d p0[0] %d p0[1] %d t0[0] %d
t0[1] %d \n", i0[0], i0[1], j0[0], j0[1], k0[0], k0[1], q0[0],
q0[1], p0[0], p0[1], t0[0], t0[1]);

        alpha = interp_matricLinear6D(i0, j0, k0, q0, p0, t0, sDV, sDH,
E, PV, SE, SPV, sDV0, sDH0, E0, PV0, SE0, SPV0, vector_Alpha);
        printf("alpha Final result: %le\n", alpha);


        printf("alpha INDEX[0] Final result: %le\n", vector_Alpha[5 +
N1 * (4 + N2 * (5 + N3 * (5 + N4 * (5 + N5 * 5)))))]);
        printf("alpha INDEX[1] Final result: %le\n", vector_Alpha[5 +
N1 * (4 + N2 * (5 + N3 * (6 + N4 * (5 + N5 * 5)))))]);*/



    }
```

Analysis of thermofluids in flameless (MILD)
combustion: assessment, improvement and
development of combustion models by CFD
Naiara Romero Anton

```c
/*-------------READ Source term table of un-normalized progress
variable-------------------------------------*/

DEFINE_EXECUTE_ON_LOADING(read_wPV_table, udfwPV)
{
    int i, j, k, q, p, t, n;

    vector_wPV = (real *)malloc(N6*N5*N4*N3*N2*N1 * sizeof(real));

    FILE *rfile4; /*declare FILE name as pointer*/

    char dummyCS[20]; /*to read a sentence*/
    char dummyC; /*to read a character*/
    int  dummyI; /*to read an integer*/

    rfile4 = fopen("SourcePV_table", "r"); /*open file for
reading*/
    n = 0;

    fscanf(rfile4, "%s\n", dummyCS); /*read "SourcePV_table and
throw */
    fscanf(rfile4, "%d\n", &dummyI); /*read "11" and throw*/
    fscanf(rfile4, "%c\n", &dummyC); /*read "(" and throw*/

    for (i = 0; i < N6; i++)
    {
        fscanf(rfile4, "%d\n", &dummyI); /*read "13" and throw*/
        fscanf(rfile4, "%c\n", &dummyC); /*read "(" and throw*/

        for (j = 0; j < N5; j++)
        {
            fscanf(rfile4, "%d\n", &dummyI); /*read "51" and
throw*/
            fscanf(rfile4, "%c\n", &dummyC); /*read "(" and
throw*/

            for (k = 0; k < N4; k++)
            {
                fscanf(rfile4, "%d\n", &dummyI); /*read "51"
and throw*/
                fscanf(rfile4, "%c\n", &dummyC); /*read "(" and
throw*/

                for (q = 0; q < N3; q++)
                {
                    fscanf(rfile4, "%d\n", &dummyI); /*read
"11" and throw*/
                    fscanf(rfile4, "%c\n", &dummyC); /*read
"(" and throw*/

                    for (p = 0; p < N2; p++)
                    {
```

```
                                     fscanf(rfile4, "%d\n", &dummyI);
/*read "11" and throw*/
                                     fscanf(rfile4, "%c\n", &dummyC);
/*read "(" and throw*/

                                     for (t = 0; t < N1; t++)
                                     {
                                            fscanf(rfile4, "%le\n",
&vector_wPV[n]); /*read "11" elements and save */
                                            n += 1;
                                     }
                                     fscanf(rfile4, "%c\n", &dummyC);
/*read "(" and throw*/
                              }
                              fscanf(rfile4, "%c\n", &dummyC); /*read
"(" and throw*/
                       }

                       fscanf(rfile4, "%c\n", &dummyC); /*read "(" and
throw*/
                }
                fscanf(rfile4, "%c\n", &dummyC); /*read "(" and
throw*/
         }
         fscanf(rfile4, "%c\n", &dummyC); /*read "(" and throw*/
     }
     fscanf(rfile4, "%c\n", &dummyC); /*read "(" and throw*/
     fclose(rfile4);

/*    real yc_source;

      real PV0, E0, sDH0, sDV0, SPV0, SE0;*/ /*fluent output result*/

      /*PV0 = 0.1;
      E0 = 0.028;
      sDH0 = 0.582657;
      sDV0 = 0.5;
      SPV0 = 0.5;
      SE0 = 0.4;


      int i0[2], j0[2], k0[2], q0[2], p0[2], t0[2];

      find_index(t0, &SPV0, SPV, N1);
      find_index(p0, &SE0, SE, N2);
      find_index(q0, &PV0, PV, N3);
      find_index(k0, &E0, E, N4);
      find_index(j0, &sDH0, sDH, N5);
      find_index(i0, &sDV0, sDV, N6);
```

Analysis of thermofluids in flameless (MILD)
combustion: assessment, improvement and
development of combustion models by CFD
Naiara Romero Anton

```
    printf("index definition i0[0] %d i0[1]%d j0[0] %d j0[1] %d
k0[0] %d k0[1] %d  q0[0] %d q0[1] %d p0[0] %d p0[1] %d t0[0] %d
t0[1] %d \n", i0[0], i0[1], j0[0], j0[1], k0[0], k0[1], q0[0],
q0[1], p0[0], p0[1], t0[0], t0[1]);

    yc_source = interp_matricLinear6D(i0, j0, k0, q0, p0, t0, sDV,
sDH, E, PV, SE, SPV, sDV0, sDH0, E0, PV0, SE0, SPV0, vector_wPV);
    printf("yc_source Final result: %le\n", yc_source);


    printf("yc_source INDEX[0] Final result: %le\n", vector_wPV[5 +
N1 * (4 + N2 * (5 + N3 * (5 + N4 * (5 + N5 * 5)))))]);
    printf("yc_source INDEX[1] Final result: %le\n", vector_wPV[5 +
N1 * (4 + N2 * (5 + N3 * (6 + N4 * (5 + N5 * 5)))))]);*/

}

DEFINE_EXECUTE_ON_LOADING(read_Density, udfT)
{
    int i, j, k, q, p, t, n;

    vector_Density = (real *)malloc(N6*N5*N4*N3*N2*N1 *
sizeof(real));

    FILE *rfile12; /*declare FILE name as pointer*/

    char dummyCS[20]; /*to read a sentence*/
    char dummyC; /*to read a character*/
    int  dummyI; /*to read an integer*/

    rfile12 = fopen("psi_table", "r"); /*open file for reading*/
    n = 0;

    fscanf(rfile12, "%s\n", dummyCS); /*read "psi_table and throw
*/
    fscanf(rfile12, "%d\n", &dummyI); /*read "11" and throw*/
    fscanf(rfile12, "%c\n", &dummyC); /*read "(" and throw*/

    for (i = 0; i < N6; i++)
    {
        fscanf(rfile12, "%d\n", &dummyI); /*read "13" and throw*/
        fscanf(rfile12, "%c\n", &dummyC); /*read "(" and throw*/

        for (j = 0; j < N5; j++)
        {
            fscanf(rfile12, "%d\n", &dummyI); /*read "51" and
throw*/
            fscanf(rfile12, "%c\n", &dummyC); /*read "(" and
throw*/

            for (k = 0; k < N4; k++)
            {
```

```
                        fscanf(rfile12, "%d\n", &dummyI); /*read "51"
and throw*/
                        fscanf(rfile12, "%c\n", &dummyC); /*read "("
and throw*/

                        for (q = 0; q < N3; q++)
                        {
                             fscanf(rfile12, "%d\n", &dummyI); /*read
"11" and throw*/
                             fscanf(rfile12, "%c\n", &dummyC); /*read
"(" and throw*/

                             for (p = 0; p < N2; p++)
                             {
                                  fscanf(rfile12, "%d\n", &dummyI);
/*read "11" and throw*/
                                  fscanf(rfile12, "%c\n", &dummyC);
/*read "(" and throw*/

                                  for (t = 0; t < N1; t++)
                                  {
                                       /*fscanf(rfile, "%le\n",
&matric_T[i][j][k][q][p][t]); */
                                       fscanf(rfile12, "%le\n",
&vector_Density[n]); /*read "11" elements and save */
                                       n += 1;
                                  }
                                  fscanf(rfile12, "%c\n", &dummyC);
/*read "(" and throw*/
                             }
                             fscanf(rfile12, "%c\n", &dummyC); /*read
"(" and throw*/
                        }

                        fscanf(rfile12, "%c\n", &dummyC); /*read "("
and throw*/

                   }
              fscanf(rfile12, "%c\n", &dummyC); /*read "(" and
throw*/
         }
         fscanf(rfile12, "%c\n", &dummyC); /*read "(" and throw*/
    }
    fscanf(rfile12, "%c\n", &dummyC); /*read "(" and throw*/
    fclose(rfile12);

    /*real density;

    real PV0, E0, sDH0, sDV0, SPV0, SE0; */ /*fluent output
result*/
```

Analysis of thermofluids in flameless (MILD)
combustion: assessment, improvement and
development of combustion models by CFD
Naiara Romero Anton

```c
/*PV0 = 0.1;
E0 = 0.028;
sDH0 = 0.582657;
sDV0 = 0.5;
SPV0 = 0.5;
SE0 = 0.4;


int i0[2], j0[2], k0[2], q0[2], p0[2], t0[2];

find_index(t0, &SPV0, SPV, N1);
find_index(p0, &SE0, SE, N2);
find_index(q0, &PV0, PV, N3);
find_index(k0, &E0, E, N4);
find_index(j0, &sDH0, sDH, N5);
find_index(i0, &sDV0, sDV, N6);

printf("index definition i0[0] %d i0[1]%d j0[0] %d j0[1] %d
k0[0] %d k0[1] %d  q0[0] %d q0[1] %d p0[0] %d p0[1] %d t0[0] %d
t0[1] %d \n", i0[0], i0[1], j0[0], j0[1], k0[0], k0[1], q0[0],
q0[1], p0[0], p0[1], t0[0], t0[1]);

density = interp_matricLinear6D(i0, j0, k0, q0, p0, t0, sDV,
sDH, E, PV, SE, SPV, sDV0, sDH0, E0, PV0, SE0, SPV0,
vector_Density);
printf("vector_Density Final result: %le\n", density);


printf("density INDEX[0] Final result: %le\n", vector_Density[5
+ N1 * (4 + N2 * (5 + N3 * (5 + N4 * (5 + N5 * 5))))]);
printf("density INDEX[1] Final result: %le\n", vector_Density[5
+ N1 * (4 + N2 * (5 + N3 * (6 + N4 * (5 + N5 * 5))))]);*/




}




/****************************************************************
**************/
/*        READING 4D TABLES
*/
/****************************************************************
**************/
```

```
/*-------------READ 4D PVtableProperties---------*/

DEFINE_EXECUTE_ON_LOADING(read_PVtableProperties, udfPV)
{

      int i4, j4, k4, q4;

      FILE *rfile5; /*declare FILE name as pointer*/

      char dummyCS1[30]; /*to read a sentence*/
      char dummyCS[20]; /*to read a sentence*/
      char dummyC; /*to read a single word*/

      rfile5 = fopen("PVtableProperties", "r"); /*open file for
reading*/

      fscanf(rfile5, "%c\n", &dummyC); /*read "(" and throw*/
      fscanf(rfile5, "%s\n", dummyCS1); /*read
"PVtableLookupParaNames" and throw */
      fscanf(rfile5, "%s\n", dummyCS); /*read "Mixfrac_Vars" and
throw, & symbol mean to find the adress of the variable*/
      fscanf(rfile5, "%c\n", &dummyC); /*read "(" and throw*/

      for (q4 = 0; q4<N7; q4++)
      {
            fscanf(rfile5, "%le\n", &SE4D[q4]); /*read "N1" elements
and save */
      }
      fscanf(rfile5, "%c\n", &dummyC); /*read "(" and throw*/
      fscanf(rfile5, "%s\n", dummyCS); /*read "Mixfrac" and throw*/
      fscanf(rfile5, "%c\n", &dummyC); /*read "(" and throw*/

      for (k4 = 0; k4<N8; k4++)
      {
            fscanf(rfile5, "%le\n", &E4D[k4]); /*read "N8" elements
and save, l letter means that it is a real variable */
            /*printf("E4D: %le\n", E4D[k4]);*/
      }
      fscanf(rfile5, "%c\n", &dummyC); /*read "(" and throw*/
      fscanf(rfile5, "%s\n", dummyCS); /*read "sDH and throw*/
      fscanf(rfile5, "%c\n", &dummyC); /*read "(" and throw*/

      for (j4 = 0; j4<N9; j4++)
      {
            fscanf(rfile5, "%le\n", &sDH4D[j4]); /*read "N2" elements
and save */
            /*printf("sDH4D: %le\n", sDH4D[j4]);*/
      }
      fscanf(rfile5, "%c\n", &dummyC); /*read "(" and throw*/
      fscanf(rfile5, "%s\n", dummyCS); /*read "sDV and throw*/
      fscanf(rfile5, "%c\n", &dummyC); /*read "(" and throw*/
```

Analysis of thermofluids in flameless (MILD)
combustion: assessment, improvement and
development of combustion models by CFD
Naiara Romero Anton

```
        for (i4 = 0; i4<N10; i4++)
        {
                fscanf(rfile5, "%le\n", &sDV4D[i4]); /*read "N2" elements
and save */
                /*printf("sDV4D: %le\n", sDV4D[i4]);*/
        }

        fscanf(rfile5, "%c\n", &dummyC); /*read "(" and throw*/
        fclose(rfile5);
}

/*-------------READ 4D DVDIL_CO2_H2O_table---------*/

DEFINE_EXECUTE_ON_LOADING(read_DVDIL_CO2_H2O_table, udfDVDIL)
{
        int i4, j4, k4, q4, n;

        vector_ydb = (real *)malloc(N10*N9*N8*N7*sizeof(real));

        FILE *rfile6; /*declare FILE name as pointer*/

        char dummyCS1[30]; /*to read a sentence*/
        char dummyC; /*la traduccion de dummy es como muneco*/
        int  dummyI; /*la traduccion de dummy es como muneco*/

        rfile6 = fopen("DVDil_CO2_H2O_table", "r"); /*open file for
reading*/
        n=0;

        fscanf(rfile6, "%s\n", dummyCS1); /*read "DVDil_CO2_H2O_table"
and throw */
        fscanf(rfile6, "%d\n", &dummyI); /*read "11" and throw*/
        fscanf(rfile6, "%c\n", &dummyC); /*read "C" and throw*/

        for (i4 = 0; i4 < N10; i4++)
        {
                fscanf(rfile6, "%d\n", &dummyI); /*read "13" and throw*/
                fscanf(rfile6, "%c\n", &dummyC); /*read "C" and throw*/

                for (j4 = 0; j4 < N9; j4++)
                {
                        fscanf(rfile6, "%d\n", &dummyI); /*read "51" and
throw*/
                        fscanf(rfile6, "%c\n", &dummyC); /*read "C" and
throw*/

                        for (k4 = 0; k4 < N8; k4++)
                        {
                                fscanf(rfile6, "%d\n", &dummyI); /*read "11"
and throw*/
```

```
                         fscanf(rfile6, "%c\n", &dummyC); /*read "C" and
throw*/

                         for (q4 = 0; q4 < N7; q4++)
                         {
                                 fscanf(rfile6, "%le\n", &vector_ydb[n]);
/*read "11" elements and save */
                                 n += 1;
                         }
                         fscanf(rfile6, "%c\n", &dummyC); /*read "(" and
throw*/
                 }
                 fscanf(rfile6, "%c\n", &dummyC); /*read "(" and
throw*/
         }
         fscanf(rfile6, "%c\n", &dummyC); /*read "(" and throw*/
     }
     fscanf(rfile6, "%c\n", &dummyC); /*read "(" and throw*/
     fclose(rfile6);

/*    real Ydb_p;

     real SE0, E0, sDH0, sDV0;*/  /*fluent output result*/

     /*SE0=0.4;
     E0=0.028;
     sDH0=0.582657;
     sDV0=0.5;



     int i04[2], j04[2], k04[2], q04[2];

     find_index(q04, &SE0, SE4D, N7);
     find_index(k04, &E0, E4D, N8);
     find_index(j04, &sDH0, sDH4D, N9);
     find_index(i04, &sDV0, sDV4D, N10);



     printf("index definition i04[0] %d i04[1]%d j04[0] %d j04[1] %d
k04[0] %d k04[1] %d  q04[0] %d q04[1] %d \n", i04[0], i04[1],
j04[0], j04[1], k04[0], k04[1], q04[0], q04[1]);

     Ydb_p = interp_matricLinear4D(i04, j04, k04, q04, sDV4D, sDH4D,
E4D, SE4D, sDV0, sDH0, E0, SE0, vector_ydb);
     printf("Ydb_p Final result: %le\n", Ydb_p);


     printf("Ydb_p INDEX[0] Final result: %le\n",
vector_ydb[5+N7*(5+N8*(5+N9*5))]);
```

Analysis of thermofluids in flameless (MILD)
combustion: assessment, improvement and
development of combustion models by CFD
Naiara Romero Anton

```
        printf("Ydb_p INDEX[1] Final result: %le\n",
vector_ydb[5+N7*(6+N8*(5+N9*5))]);*/



}

/*-------------READ PVmax_table (Ycb)---------*/

DEFINE_EXECUTE_ON_LOADING(read_Ycb_table, udfYcb)
{
        int i4, j4, k4, q4, n;

        vector_Ycb = (real *)malloc(N10*N9*N8*N7*sizeof(real));

        FILE *rfile7; /*declare FILE name as pointer*/

        char dummyCS[20]; /*to read a sentence*/
        char dummyC; /*la traduccion de dummy es como muneco*/
        int  dummyI; /*la traduccion de dummy es como muneco*/

        rfile7 = fopen("PVmax_table", "r"); /*open file for reading*/
        n=0;

        fscanf(rfile7, "%s\n", dummyCS); /*read "PV_max and throw, &
symbol mean to find the adress of the variable*/
        fscanf(rfile7, "%d\n", &dummyI); /*read "11" and throw*/
        fscanf(rfile7, "%c\n", &dummyC); /*read "C" and throw*/

        for (i4 = 0; i4 < N10; i4++)
        {
                fscanf(rfile7, "%d\n", &dummyI); /*read "13" and throw*/
                fscanf(rfile7, "%c\n", &dummyC); /*read "C" and throw*/

                for (j4 = 0; j4 < N9; j4++)
                {
                        fscanf(rfile7, "%d\n", &dummyI); /*read "51" and
throw*/
                        fscanf(rfile7, "%c\n", &dummyC); /*read "C" and
throw*/

                        for (k4 = 0; k4 < N8; k4++)
                        {
                                fscanf(rfile7, "%d\n", &dummyI); /*read "11"
and throw*/
                                fscanf(rfile7, "%c\n", &dummyC); /*read "C" and
throw*/

                                for (q4 = 0; q4 < N7; q4++)
                                {
                                        fscanf(rfile7, "%le\n", &vector_Ycb[n]);
/*read "11" elements and save */
                                        n += 1;
```

```
                }
                fscanf(rfile7, "%c\n", &dummyC); /*read "(" and
throw*/
            }
            fscanf(rfile7, "%c\n", &dummyC); /*read "(" and
throw*/
        }
        fscanf(rfile7, "%c\n", &dummyC); /*read "(" and throw*/
    }
    fscanf(rfile7, "%c\n", &dummyC); /*read "(" and throw*/
    fclose(rfile7);

    /*real Ycb_p;

    real SE0, E0, sDH0, sDV0;*/  /*fluent output result*/

/*   SE0 = 0.4;
    E0 = 0.028;
    sDH0 = 0.582657;
    sDV0 = 0.5;


    int i04[2], j04[2], k04[2], q04[2];

    find_index(q04, &SE0, SE4D, N7);
    find_index(k04, &E0, E4D, N8);
    find_index(j04, &sDH0, sDH4D, N9);
    find_index(i04, &sDV0, sDV4D, N10);



    printf("index definition i04[0] %d i04[1]%d j04[0] %d j04[1] %d
k04[0] %d k04[1] %d  q04[0] %d q04[1] %d \n", i04[0], i04[1],
j04[0], j04[1], k04[0], k04[1], q04[0], q04[1]);

    Ycb_p = interp_matricLinear4D(i04, j04, k04, q04, sDV4D, sDH4D,
E4D, SE4D, sDV0, sDH0, E0, SE0, vector_Ycb);
    printf("Ycb_p Final result: %le\n", Ycb_p);


    printf("Ycb_p INDEX[0] Final result: %le\n", vector_Ycb[5 + N7
* (5 + N8 * (5 + N9 * 5))]);
    printf("Ycb_p INDEX[1] Final result: %le\n", vector_Ycb[5 + N7
* (6 + N8 * (5 + N9 * 5))]);*/



}

/*-------------READ PVmin_table (Ycu)---------*/
```

Analysis of thermofluids in flameless (MILD)
combustion: assessment, improvement and
development of combustion models by CFD
Naiara Romero Anton

```
DEFINE_EXECUTE_ON_LOADING(read_Ycu_table, udfYcu)
{
     int i4, j4, k4, q4, n;

     vector_Ycu = (real *)malloc(N10*N9*N8*N7*sizeof(real));

     FILE *rfile8; /*declare FILE name as pointer*/

     char dummyCS[20]; /*to read a sentence*/
     char dummyC; /*la traduccion de dummy es como muneco*/
     int  dummyI; /*la traduccion de dummy es como muneco*/

     rfile8 = fopen("PVmin_table", "r"); /*open file for reading*/
     n = 0;

     fscanf(rfile8, "%s\n", dummyCS); /*read "PV_min and throw, &
symbol mean to find the adress of the variable*/
     fscanf(rfile8, "%d\n", &dummyI); /*read "11" and throw*/
     fscanf(rfile8, "%c\n", &dummyC); /*read "C" and throw*/

     for (i4 = 0; i4 < N10; i4++)
     {
          fscanf(rfile8, "%d\n", &dummyI); /*read "13" and throw*/
          fscanf(rfile8, "%c\n", &dummyC); /*read "C" and throw*/

          for (j4 = 0; j4 < N9; j4++)
          {
               fscanf(rfile8, "%d\n", &dummyI); /*read "51" and
throw*/
               fscanf(rfile8, "%c\n", &dummyC); /*read "C" and
throw*/

               for (k4 = 0; k4 < N8; k4++)
               {
                    fscanf(rfile8, "%d\n", &dummyI);/*read "11" and
throw*/
                    fscanf(rfile8, "%c\n", &dummyC); /*read "C" and
throw*/

                    for (q4 = 0; q4 < N7; q4++)
                    {
                         fscanf(rfile8, "%le\n", &vector_Ycu[n]);
/*read "11" elements and save */
                         n += 1;
                    }
                    fscanf(rfile8, "%c\n", &dummyC); /*read "(" and
throw*/
               }
               fscanf(rfile8, "%c\n", &dummyC); /*read "(" and
throw*/
          }
          fscanf(rfile8, "%c\n", &dummyC); /*read "(" and throw*/
```

```
        }
        fscanf(rfile8, "%c\n", &dummyC); /*read "(" and throw*/
        fclose(rfile8);


        /*real Ycu_p;

        real SE0, E0, sDH0, sDV0; */ /*fluent output result*/

        /*SE0 = 0.4;
        E0 = 0.028;
        sDH0 = 0.582657;
        sDV0 = 0.5;


        int i04[2], j04[2], k04[2], q04[2];

        find_index(q04, &SE0, SE4D, N7);
        find_index(k04, &E0, E4D, N8);
        find_index(j04, &sDH0, sDH4D, N9);
        find_index(i04, &sDV0, sDV4D, N10);



    printf("index definition i04[0] %d i04[1]%d j04[0] %d j04[1] %d
k04[0] %d k04[1] %d  q04[0] %d q04[1] %d \n", i04[0], i04[1],
j04[0], j04[1], k04[0], k04[1], q04[0], q04[1]);

    Ycu_p = interp_matricLinear4D(i04, j04, k04, q04, sDV4D, sDH4D,
E4D, SE4D, sDV0, sDH0, E0, SE0, vector_Ycu);
    printf("Ycu_p Final result: %le\n", Ycu_p);


    printf("Ycu_p INDEX[0] Final result: %le\n", vector_Ycu[5 + N7
* (5 + N8 * (5 + N9 * 5))]);
    printf("Ycu_p INDEX[1] Final result: %le\n", vector_Ycu[5 + N7
* (6 + N8 * (5 + N9 * 5))]);*/


}

DEFINE_EXECUTE_ON_LOADING(read_Ycb2_table, udfYcb2)
{
        int i4, j4, k4, q4, n;

        vector_Ycb2 = (real *)malloc(N10*N9*N8*N7 * sizeof(real));

        FILE *rfile9; /*declare FILE name as pointer*/

        char dummyCS[20]; /*to read a sentence*/
        char dummyC; /*la traduccion de dummy es como muneco*/
        int  dummyI; /*la traduccion de dummy es como muneco*/
```

```
    rfile9 = fopen("Yb2I_table", "r"); /*open file for reading*/
    n = 0;

    fscanf(rfile9, "%s\n", dummyCS); /*read "Yb2I_table and throw,
& symbol mean to find the adress of the variable*/
    fscanf(rfile9, "%d\n", &dummyI); /*read "11" and throw*/
    fscanf(rfile9, "%c\n", &dummyC); /*read "C" and throw*/

    for (i4 = 0; i4 < N10; i4++)
    {
        fscanf(rfile9, "%d\n", &dummyI); /*read "13" and throw*/
        fscanf(rfile9, "%c\n", &dummyC); /*read "C" and throw*/

        for (j4 = 0; j4 < N9; j4++)
        {
            fscanf(rfile9, "%d\n", &dummyI); /*read "51" and
throw*/
            fscanf(rfile9, "%c\n", &dummyC); /*read "C" and
throw*/

            for (k4 = 0; k4 < N8; k4++)
            {
                fscanf(rfile9, "%d\n", &dummyI);/*read "11" and
throw*/
                fscanf(rfile9, "%c\n", &dummyC); /*read "C" and
throw*/

                for (q4 = 0; q4 < N7; q4++)
                {
                    fscanf(rfile9, "%le\n", &vector_Ycb2[n]);
/*read "11" elements and save */
                    n += 1;
                }
                fscanf(rfile9, "%c\n", &dummyC); /*read "(" and
throw*/
            }
            fscanf(rfile9, "%c\n", &dummyC); /*read "(" and
throw*/
        }
        fscanf(rfile9, "%c\n", &dummyC); /*read "(" and throw*/
    }
    fscanf(rfile9, "%c\n", &dummyC); /*read "(" and throw*/
    fclose(rfile9);
}

DEFINE_EXECUTE_ON_LOADING(read_Ycu2_table, udfYcu2)
{
    int i4, j4, k4, q4, n;

    vector_Ycu2 = (real *)malloc(N10*N9*N8*N7 * sizeof(real));
```

```
        FILE *rfile10; /*declare FILE name as pointer*/

        char dummyCS[20]; /*to read a sentence*/
        char dummyC; /*la traduccion de dummy es como muneco*/
        int  dummyI; /*la traduccion de dummy es como muneco*/

        rfile10 = fopen("Yu2I_table", "r"); /*open file for reading*/
        n = 0;

        fscanf(rfile10, "%s\n", dummyCS); /*read "PV_min and throw, &
symbol mean to find the adress of the variable*/
        fscanf(rfile10, "%d\n", &dummyI); /*read "11" and throw*/
        fscanf(rfile10, "%c\n", &dummyC); /*read "C" and throw*/

        for (i4 = 0; i4 < N10; i4++)
        {
            fscanf(rfile10, "%d\n", &dummyI); /*read "13" and throw*/
            fscanf(rfile10, "%c\n", &dummyC); /*read "C" and throw*/

            for (j4 = 0; j4 < N9; j4++)
            {
                fscanf(rfile10, "%d\n", &dummyI); /*read "51" and
throw*/
                fscanf(rfile10, "%c\n", &dummyC); /*read "C" and
throw*/

                for (k4 = 0; k4 < N8; k4++)
                {
                    fscanf(rfile10, "%d\n", &dummyI);/*read "11"
and throw*/
                    fscanf(rfile10, "%c\n", &dummyC); /*read "C"
and throw*/

                    for (q4 = 0; q4 < N7; q4++)
                    {
                        fscanf(rfile10, "%le\n",
&vector_Ycu2[n]); /*read "11" elements and save */
                        n += 1;
                    }
                    fscanf(rfile10, "%c\n", &dummyC); /*read "("
and throw*/
                }
                fscanf(rfile10, "%c\n", &dummyC); /*read "(" and
throw*/
            }
            fscanf(rfile10, "%c\n", &dummyC); /*read "(" and throw*/
        }
        fscanf(rfile10, "%c\n", &dummyC); /*read "(" and throw*/
        fclose(rfile10);
}
```

Analysis of thermofluids in flameless (MILD)
combustion: assessment, improvement and
development of combustion models by CFD
Naiara Romero Anton

```
DEFINE_EXECUTE_ON_LOADING(read_YcuYcb_table, udfYcu2)
{
      int i4, j4, k4, q4, n;

      vector_YcuYcb = (real *)malloc(N10*N9*N8*N7 * sizeof(real));

      FILE *rfile11; /*declare FILE name as pointer*/

      char dummyCS[20]; /*to read a sentence*/
      char dummyC; /*la traduccion de dummy es como muneco*/
      int  dummyI; /*la traduccion de dummy es como muneco*/

      rfile11 = fopen("YuYbI_table", "r"); /*open file for reading*/
      n = 0;

      fscanf(rfile11, "%s\n", dummyCS); /*read "PV_min and throw, &
symbol mean to find the adress of the variable*/
      fscanf(rfile11, "%d\n", &dummyI); /*read "11" and throw*/
      fscanf(rfile11, "%c\n", &dummyC); /*read "C" and throw*/

      for (i4 = 0; i4 < N10; i4++)
      {
            fscanf(rfile11, "%d\n", &dummyI); /*read "13" and throw*/
            fscanf(rfile11, "%c\n", &dummyC); /*read "C" and throw*/

            for (j4 = 0; j4 < N9; j4++)
            {
                  fscanf(rfile11, "%d\n", &dummyI); /*read "51" and
throw*/
                  fscanf(rfile11, "%c\n", &dummyC); /*read "C" and
throw*/

                  for (k4 = 0; k4 < N8; k4++)
                  {
                        fscanf(rfile11, "%d\n", &dummyI);/*read "11"
and throw*/
                        fscanf(rfile11, "%c\n", &dummyC); /*read "C"
and throw*/

                        for (q4 = 0; q4 < N7; q4++)
                        {
                              fscanf(rfile11, "%le\n",
&vector_YcuYcb[n]); /*read "11" elements and save */
                              n += 1;
                        }
                        fscanf(rfile11, "%c\n", &dummyC); /*read "("
and throw*/
                  }
                  fscanf(rfile11, "%c\n", &dummyC); /*read "(" and
throw*/
            }
            fscanf(rfile11, "%c\n", &dummyC); /*read "(" and throw*/
```

```
    }
    fscanf(rfile11, "%c\n", &dummyC); /*read "(" and throw*/
    fclose(rfile11);
}


DEFINE_PDF_TABLE(pdf_table, m, c, t, fmean, fvar, fmean2, fvar2,
cmean, cvar, h, what, prop, x, s_pollut)
{
    real Yc, Yd, psi_table, wPV, Ycb, Ycu, Yc_eq;
    real PV0, E0, sDH0, sDV0, SE0, SPV0, PV01, PV02;  /*fluent
output result*/
    real alfa, h_adiab, mf, tZ, talfa;
    real fc, gc, hc, varPV0, Yc_var, Ycb2, Ycu2, YcuYcb;
    real temperature, Cp, density, alpha_table;

    int i04[2], j04[2], k04[2], q04[2];

    /* Calculate Dilution level*/
    Yd = C_UDSI(c, t, 0);/*dilution variable*/
    /*Yd = MAX(MIN(Yd, 1.0), 0.0);*/ /*Xu did not consider*/
    alfa = Yd / DVZstC1;
    alfa = MAX(MIN(alfa, 1.0), 0.0);

    /*Calculate THREE STREAMS scaled mixture fraction (second) and
its variance*/

    mf = fmean; /*mixture fraction*/

    if (mf < verySmall)
    {
        mf = 0;
        /*temperature = 816;*/
    }
    else if ((1 - mf) < verySmall)
    {
        mf = 1;
        /*temperature = 416;*/
    }

    E0 = mf - alfa * Zst; /*second mixture fraction*/
    E0 = MAX(MIN(E0, 1.0), 0.0);

    if (E0 < verySmall)
    {
        E0 = 0;
        /*temperature = 816;*/
    }
    else if ((1 - E0) < verySmall)
    {
        E0 = 1;
```

Analysis of thermofluids in flameless (MILD)
combustion: assessment, improvement and
development of combustion models by CFD
Naiara Romero Anton

```
        /*temperature = 416;*/
    }
    C_UDMI(c, t, 1) = E0;

    SE0 = fvar / MAX(E0*(1 - E0), verySmall);
    SE0 = MAX(MIN(SE0, 0.99), 0.0);
    C_UDMI(c, t, 16) = SE0;

    if (mf > 0.9999)
    {
        sDV0 = 0;
    }

    /*else if (mf < 0.0001)/* /*Xu did not consider*/
    /*{
        sDV0 = 0;
    }*/
    else
    {
        sDV0 = alfa / MAX((1 - E0), verySmall);/*normalized
dilution level */
        sDV0 = MAX(MIN(sDV0, 1.0), 0.0);
    }

    C_UDMI(c, t, 2) = sDV0;

    /*Calculate Enthlapy loss*/
    if (sDV0 < 0.00001)
    {
        sDH0 = 0;
    }
    else
    {
        tZ = E0 + (1 - E0)*sDV0*Zst;
        talfa = (1 - E0)*sDV0;
        sDH0 = (tZ*(HadF - HadO) + HadO - h) /
MAX(talfa*Hmaxloss, verySmall); /*enthalpy loss */
    }

    sDH0 = MAX(MIN(sDH0, 1.0), 0.0);
    C_UDMI(c, t, 3) = sDH0;

    /*Calculate unscaled progress variable*/
    if (NNULLP(THREAD_STORAGE(t, SV_PREMIXC))) /* this means
C_PREMIXC is available in memory */
    {
        Yc = C_PREMIXC(c, t); /*un-normalized progress variable*/
        if (Yc < verySmall)
        {
            Yc = 0;
            /*temperature = 816;*/
        }
```

```
            C_UDMI(c, t, 0) = Yc; /* adapt the UDM index
appropriately */
      }
      else    /* C_PRMEMIXC not available in memory -> recover it
from the UDM */
      {
            Yc = C_UDMI(c, t, 0); /* adapt the UDM index
appropriately */
      }

      if (c == 333)
            Message0("PDF1 E0 %lf,  SE0 %lf, sDV0 %lf, sDH0 %lf\n",
E0, SE0, sDV0, sDH0);
      /*Update minimum and maximum unscaled progress variable*/

      find_index(q04, &SE0, SE4D, N7);
      find_index(k04, &E0, E4D, N8);
      find_index(j04, &sDH0, sDH4D, N9);
      find_index(i04, &sDV0, sDV4D, N10);

      if (c == 333)
            Message0("PDF2 k04[0] %d k04[1]%d q04[0]%d q04[1]%d
i04[0]%d i04[1]%d  j04[0]%d j04[1]%d \n", k04[0], k04[1], q04[0],
q04[1], i04[0], i04[1], j04[0], j04[1]);
      Ycb = interp_matricLinear4D(i04, j04, k04, q04, sDV4D, sDH4D,
E4D, SE4D, sDV0, sDH0, E0, SE0, vector_Ycb);
      Ycu = interp_matricLinear4D(i04, j04, k04, q04, sDV4D, sDH4D,
E4D, SE4D, sDV0, sDH0, E0, SE0, vector_Ycu);

      /*if Yc = 0
      {
            Ycb = 0;
      }*/
      C_UDMI(c, t, 4) = Ycb;
      C_UDMI(c, t, 5) = Ycu;


      if (c == 333)
            Message0("PDF3 Ycb %lf, Ycu %lf, Yc %lf\n", Ycb, Ycu,
Yc);

      /*Update scaled progress variable C*/
      /*if ((Ycb - Ycu)<1e-8)
      {
            PV0 = 0.0;
      }
      else
      {*/ /*Xu no lo hace*/
      PV0 = (Yc - Ycu) / MAX((Ycb - Ycu), verySmall); /*scaled-
normalized progress variable==C*/
      Yc_eq = Get_Yc_eq(fmean, fvar);
```

Analysis of thermofluids in flameless (MILD)
combustion: assessment, improvement and
development of combustion models by CFD
Naiara Romero Anton

```
    PV01 = Yc / Yc_eq;
    PV02 = cmean;
    /*}*/

    PV0 = MAX(MIN(PV0, 1.0), 0.0);
    PV01 = MAX(MIN(PV01, 1.0), 0.0);


    C_UDMI(c, t, 6) = PV0;
    C_UDMI(c, t, 15) = PV01;
    C_UDMI(c, t, 19) = PV02;
    if (c == 333)
        Message0("PDF4 PV0 %lf, PV01 %lf, PV02 %lf\n", PV0, PV01,
PV02);

    /*Calculate scaled progress variable VARIANCE from unscaled
progress variance*/
    if (NNULLP(THREAD_STORAGE(t, SV_GVAR))) /* this means C_GVAR is
available in memory */
    {
        Yc_var = C_GVAR(c, t); /*un-normalized progress variable
variance*/

        C_UDMI(c, t, 9) = Yc_var; /* adapt the UDM index
appropriately */
    }
    else    /* C_GVAR not available in memory -> recover it from
the UDM */
    {
        Yc_var = C_UDMI(c, t, 9); /* adapt the UDM index
appropriately */
    }

    Ycb2 = interp_matricLinear4D(i04, j04, k04, q04, sDV4D, sDH4D,
E4D, SE4D, sDV0, sDH0, E0, SE0, vector_Ycb2);
    Ycu2 = interp_matricLinear4D(i04, j04, k04, q04, sDV4D, sDH4D,
E4D, SE4D, sDV0, sDH0, E0, SE0, vector_Ycu2);
    YcuYcb = interp_matricLinear4D(i04, j04, k04, q04, sDV4D,
sDH4D, E4D, SE4D, sDV0, sDH0, E0, SE0, vector_YcuYcb);

    C_UDMI(c, t, 10) = Ycb2;
    C_UDMI(c, t, 11) = Ycu2;
    C_UDMI(c, t, 12) = YcuYcb;

    fc = Ycu2;
    gc = YcuYcb - Ycu2;
    hc = Ycb2 - 2.0 *YcuYcb + Ycu2;

    varPV0 = (Yc_var + Yc*Yc - fc - 2.0*gc*PV0) / MAX(hc,
verySmall) - PV0*PV0;
    if (hc < verySmall)
    {
```

```
            varPV0 = 0.0;
      }

      else
      {
            varPV0 = MAX(varPV0, 0.0); /*así lo tiene Xu*/
            /*varPV0 = MAX(MIN(varPV0, 1), 0.0); *//*poner coo maximo
0.25*/
      }

      C_UDMI(c, t, 13) = varPV0;

/*     varPV0 = cvar;*/

      SPV0=MAX(MIN(varPV0/MAX(PV0*(1-PV0), verySmall),0.99),0.0);
      C_UDMI(c, t, 14) = SPV0;

      if (c == 333)
            Message0("PDF4-2 varPV0 %lf, SPV0 %lf\n", varPV0, SPV0);


      int i0[2], j0[2], k0[2], q0[2], p0[2], t0[2];

      find_index(t0, &SPV0, SPV, N1);
      find_index(p0, &SE0, SE, N2);
      find_index(q0, &PV0, PV, N3);
      find_index(k0, &E0, E, N4);
      find_index(j0, &sDH0, sDH, N5);
      find_index(i0, &sDV0, sDV, N6);

      if (c == 333)
            Message0("PDF5 i0[0] %d i0[1]%d j0[0] %d j0[1] %d  k0[0]
%d k0[1] %d  q0[0] %d q0[1] %d p0[0] %d p0[1] %d t0[0] %d t0[1] %d
\n", i0[0], i0[1], j0[0], j0[1], k0[0], k0[1], q0[0], q0[1], p0[0],
p0[1], t0[0], t0[1]);


      if NULLP(pf)
            Error("Please generate or read a Fluent PDF file
first\n");

      /*Update internal field dilution variable source term*/
      if (what < 0)
      {
            if (PV0>0.9999) /* When C=1 Yc_source_term should be 0,
when the source is provided by UDF the user needs to impose source
term to 0*/
            {
                  prop[TEMP_UDF] = 0.000001; /* un-normalized progress
variable source term*/
```

Analysis of thermofluids in flameless (MILD)
combustion: assessment, improvement and
development of combustion models by CFD
Naiara Romero Anton

```
                                                    /*C_UDMI(c, t, 8)
= 0.000001;*/ /* un-normalized progress variable source term*/
            wPV = 0.000001;
        }
        else
        {
            wPV = interp_matricLinear6D(i0, j0, k0, q0, p0, t0,
sDV, sDH, E, PV, SE, SPV, sDV0, sDH0, E0, PV0, SE0, SPV0,
vector_wPV);
            prop[TEMP_UDF] = wPV;
        }

        C_UDMI(c, t, 8) = wPV;
        if (c == 333)
        {
            Message0("PDF6 source Yc=%lf l/s\n", wPV);
        }

    }


    if (what == 1)
    {
        temperature= interp_matricLinear6D(i0, j0, k0, q0, p0,
t0, sDV, sDH, E, PV, SE, SPV, sDV0, sDH0, E0, PV0, SE0, SPV0,
vector_Temp);
        prop[TEMP_UDF] = temperature;
        C_UDMI(c, t, 7) = temperature;

        alpha_table= interp_matricLinear6D(i0, j0, k0, q0, p0,
t0, sDV, sDH, E, PV, SE, SPV, sDV0, sDH0, E0, PV0, SE0, SPV0,
vector_Alpha);
        Cp = 0.0454/ alpha_table;
        prop[CP_UDF] = Cp;
        C_UDMI(c, t, 20) = Cp;

        psi_table = interp_matricLinear6D(i0, j0, k0, q0, p0, t0,
sDV, sDH, E, PV, SE, SPV, sDV0, sDH0, E0, PV0, SE0, SPV0,
vector_Density);
        density=100000* psi_table;
        prop[DEN_UDF] = density; /*C_P(c, t) *psi_table;*/
        C_UDMI(c, t, 22) = prop[DEN_UDF];

        prop[MOL_WT_MIX_UDF] = 8314 * prop[TEMP_UDF] * psi_table;
        C_UDMI(c, t, 21) = prop[MOL_WT_MIX_UDF];


        if (c == 333)
        {
            Message0("PDF7 temperature=%lf K, CP=%lf J/kg*K,
ro=%lf kg/m3, WT%lf kg/kmol \n", temperature, Cp, prop[DEN_UDF],
prop[MOL_WT_MIX_UDF]);
```

```
            }

        }

}

DEFINE_TURB_SCHMIDT(udf_sct, c, t, i)
{
        return 0.7;
}

/*DEFINE_DIFFUSIVITY(Yd_diff, c, t, i)
{
        real D;

        D = C_R(c, t) * (C_MU_L(c, t) / 0.7 + C_MU_T(c, t) / 0.7);*/
/*0.7 is the value of scmidt(S) number and 0.7 turbulent(St) schmidt
number Fluent by default use St_0.85, but we decide to use St_0.7 in
burner area */

        /*return D;
}*/

DEFINE_SOURCE(source_wyd, c, t, dS, eqn)

{
        real wyd, source, Yc, mf, Ycb, Ycu, Ycb2, Ycu2, Yd, tZ, talfa,
Ydb;
        real sDV0, sDH0, E0, PV0, SE0;   /*output result*/
        real alfa, h_adiab;
        real fmean, fvar, Yc_eq, PV01, SPV0, wPV;
        real fc, gc, hc, varPV0, Yc_var, YcuYcb, temperature;

        PV0 = C_UDMI(c, t, 6);

        if (c == 333)
                Message0("SOURCE0 PV0 %lf \n", PV0);

        /*fmean = C_FMEAN(c, t);*/ /* mean mixture fraction */
        /*fvar = C_FVAR(c, t);*/ /* mean mixture fraction variance
varZ*/


        if (PV0 > 0.99)
        {

                Yd = C_UDSI(c, t, 0);/*dilution variable*/
                E0 = C_UDMI(c, t, 1);
                sDV0 = C_UDMI(c, t, 2);
                sDH0 = C_UDMI(c, t, 3);
                /*mfvar = C_FVAR(c, t);*/
```

Analysis of thermofluids in flameless (MILD)
combustion: assessment, improvement and
development of combustion models by CFD
Naiara Romero Anton

```
        SE0 = C_UDMI(c, t, 16);


        if (c == 333)
            Message0("SOURCE1 E0 %lf,  SE0 %lf, sDV0 %lf, sDH0
%lf \n", E0, SE0, sDV0, sDH0);

        int i04[2], j04[2], k04[2], q04[2];

        find_index(q04, &SE0, SE4D, N7);
        find_index(k04, &E0, E4D, N8);
        find_index(j04, &sDH0, sDH4D, N9);
        find_index(i04, &sDV0, sDV4D, N10);

        if (c == 333)
            Message0("SOURCE2 k04[0] %d k04[1]%d q04[0]%d
q04[1]%d  i04[0]%d i04[1]%d  j04[0]%d j04[1]%d \n", k04[0], k04[1],
q04[0], q04[1], i04[0], i04[1], j04[0], j04[1]);

        Ydb = interp_matricLinear4D(i04, j04, k04, q04, sDV4D,
sDH4D, E4D, SE4D, sDV0, sDH0, E0, SE0, vector_ydb);
        C_UDMI(c, t, 17)=Ydb;

        if (Ydb > DVZstC1)
        {
            Ydb = DVZstC1;
            C_UDMI(c, t, 17) = Ydb;
        }
        source = (1 / CURRENT_TIMESTEP)*C_R(c, t)*(Ydb - Yd);
/*first 0 value is Ydb */

        if (c == 333)
        {
            Message0("SOURCE3 Ydb= %lf\n", Ydb);
        }
    }

    else
    {
        source = 0;
    }

    /*source = MAX(MIN(source, 1.0), 0.0);*/ /*Xu no tiene esto*/


    if (c == 333)
    {
        Message0("SOURCE4 source= %lf\n", source);

    }
    C_UDMI(c, t, 18) = source;
```

```
            dS[eqn] = (1 / CURRENT_TIMESTEP)*C_R(c, t);



        /*wyd = MAX(MIN(Ydb, 1.0), 0.0);*/
        /*source = 0.001;

        if (c == 333)
        {
                Message0("SOURCE9 source= %lf \n", source);

        }*/

        return source;
}

DEFINE_PROFILE(temSideWall_profile, t, i)
{
        real x[ND_ND]; /* this will hold the position vector */
        real z;
        face_t f;

        begin_f_loop(f, t)
        {
                F_CENTROID(x, f, t);
                z = x[2];

                if (z <= 0.3)
                        F_PROFILE(f, t, i) = 300 * z + 1150;
                else if (z <= 0.4)
                        F_PROFILE(f, t, i) = 400 * z + 1120;
                else
                        F_PROFILE(f, t, i) = 1280;
        }
        end_f_loop(f, t)
}


DEFINE_DIFFUSIVITY(Yd_diff, c, t, i)
{
        real D;

        D = (C_MU_L(c, t) / 0.7 + C_MU_T(c, t) / 0.7) / C_R(c, t);
/*0.7 is the value of scmidt(S) number and 0.7 turbulent(St) schmidt
number Fluent by default use St_0.85, but we decide to use St_0.7 in
burner area */

        return D;
}
```